Spectroscopic Studies on the Transport Properties of Ionic Liquids

Mohd Azizi Nawawi

Department of Chemistry

Imperial College London

This dissertation is submitted for the degree of

Doctor of Philosophy

JULY 2019

I would like to dedicate this thesis to my late loving parents and my family members …

Declaration

The work described in this thesis was, unless clearly stated and referenced, under taken by me during January 2015 – June 2018.

Copyright

Acknowledgements

Firstly, I would like to express my sincere gratitude to my supervisory team, Prof. Tom Welton, Prof. Joshua Edel and Dr Alastair McIntosh for their continuous support throughout my PhD study. Thanks for your patience, motivation, immense knowledge and all the guidance since the first day I embarked to my PhD journey. Without their precious support it would not possible to conduct this research.

My sincere thanks also goes to Dr. Alex Ivanov and Dr Marina Kuimova for your help, useful discussions and advice regarding the fluorescence lifetime experiments. I also would like to express sincere thank Mr Ryan Clark for helping me in writing the MATLAB code and analysing the fluorescence lifetime data. I would like to thank my 'fluorescence friends', Jane, Shenglin, Victoria and Marketa for being very helpful and considerate while we are sharing the instrument.

To all Welton research group members (past and present), thank you guys for making the lab a wonderful place to work over the three and half years. Jay, Raquel, Liyana, Gilly, Rafiq, Hanim Eduards, Nik, Ryan and Qing Shan, it has been a great pleasure to share the space and the scientific thought of ionic liquids with you guys!

To all my Malaysian buddies in the UK, too many of you to list here! Thank you for the friendship and the great experience we had here. I will be missing (a lot!) the good cooks from Vellacottish people and of course the smashes and screams from the badminton buddies!

A very special thanks to my late mother for the never-ending pray and support, I love you and you will always be in my every pray! To my brothers, sisters and nieces and nephews, thank you very much for your kind understanding and help throughout my PhD journey.

Lastly, I would like to thank Universiti Teknologi MARA and Ministry of Education Malaysia for funding my study at Imperial College London.

Azizi
18th July 2019
London

Abstract

Ionic liquids are liquids composed entirely of ions. These ions are in constant motion. Ionic liquids have found use in a wide range of electrochemical applications, such as batteries, fuel cells and solar cells. In these applications they are exposed to various external forces including magnetic and electric fields. Gaining a thorough understanding of how these external forces affect the physical and chemical properties of ionic liquids is important; and it remains a fundamental challenge. In this study, fluorescence lifetime spectroscopy was utilised as a technique to gain an insight into the behaviour of the ions when experiencing electric fields. To enable the fluorescence measurements, synthetic processes were explored and developed to produce good quality ionic liquids with low fluorescence backgrounds. The physical and chemical properties of the ionic liquids were characterised by various established techniques such as nuclear magnetic resonance spectroscopy, mass spectrometry, impedance spectroscopy, cyclic voltammetry and elemental analysis. Upon the successful production of low fluorescence background ionic liquids, fluorescence lifetime experiments were conducted to monitor their local viscosities. In this study, molecular rotors were used as probes to estimate local viscosity of the ionic liquids. The fluorescence lifetimes were derived from a molecular rotor, 3,3'-diethylthiacarbocyanine (Cy3) which was dissolved in the ionic liquids (*ca.* 100 nM). The local viscosities were then estimated from a calibration curve developed from various ionic liquids and these values were also compared to those estimated from a calibration curve usually used for molecular solvent systems. Further to this, attempts to use the obtained correlation between fluorescence lifetime of Cy3 and viscosity to estimate the local viscosities of the ionic liquid under application of +2V potential were conducted. Even though the change of viscosity of ionic liquids was observed upon application of the +2V potential, the explanation to the observation is rather complicated due to many factors that can contribute to the viscosity change. Based on analysis and support data from the literature, the observed change in viscosity could be either attributed to change in molecular dynamics of ionic liquids as the potential is applied or it may be affected by instability of the indium-tin oxide (ITO) electrode over the applied potential which has the potential to cause dissolution of ITO components into ionic liquid system.

Contents

List of Figures

List of Tables

Chapter 1 Introduction

1.1 Motivation of study

Room temperature ionic liquids are low melting point salts that usually exist in liquid states at, or close to, room temperature, and therefore they are being extensively studied as possible electrolytes.[1] Their excellent properties, such as being non-flammable, having very low volatility, relatively high conductivity and wide electrochemical windows, have attract interest in academia as well as industry. Currently ionic liquids have been studied as electrolytes for a wide range electrochemical devices and processes, such as energy generation and storage,[2,3] metals deposition[4,5] and electrochemical sensors.[6] This has stimulate the need for a deeper understanding of transport properties of ionic liquids such as conductivities, ion mobilities and viscosities,[7] and the relationships between these.[8] In real electrochemical devices, the electrolytes like ionic liquids are often exposed to various external forces including the electric field. In electrochemical devices, the electric field usually arises from the application of a voltage between electrodes. Therefore, there has been considerable current interest in understanding behaviour of ions in ionic liquids at charged surfaces.[9] Although this has been a controversial subject, but it can be generalised that ions will form charge-ordered layers on the electrode surface and these layers could extend to a few nanometres depending on the characteristics of both the surface and the particular ion and that beyond this to a few tens of

nanometres longer range forces, about the origin of which there is no consensus, can be detected.[10] In this project, the effects of electric fields on the viscosities of ionic liquids was investigated using fluorescence molecular rotors as probes. Molecular rotors are a group of fluorescence molecules for which their fluorescence emission is sensitive to the viscosity of the surrounding environment.[11,12] A number of studies of different molecular rotors being used to measure the viscosities of a number of different ionic liquids have recently been reported.[13–16] In spite of their differences, they generally reach similar conclusions of there being a disparity between the ionic liquid viscosities reported by the molecular rotors and the bulk viscosities measured by conventional viscometer, and that the results were strongly influenced by their microheterogeneity and the availability of free volume in the ionic liquids.

1.2 Outline of work

The main objective of this work is to investigate the effects of electric field on the viscosity of ionic liquids under the influence of electric fields utilising fluorescent molecular rotors as a probe. In this study, the local viscosity of ionic liquids was predicted by measuring the fluorescence lifetime of the molecular rotors. In order to achieve that objective, the development of synthetic procedures for producing good quality and low fluorescence background ionic liquids are needed and the behaviour of molecular rotors in ionic liquids need to be carefully understood. The establishment of correlation between the fluorescence lifetime of the molecular rotors and viscosity of ionic liquids is important and it serves as the basis for estimation of viscosity of ionic liquids under influence of electric fields. This thesis is divided into six main chapters as the following:

Chapter 1 outlines the motivation of this study and the overview of this thesis. The history and applications of ionic liquids also presented in this chapter. These include the review of electrochemical aspects of ionic liquids and their potential applications for electrochemical devices. The successful story of applications of ionic liquids in industry was also included in this chapter.

Chapter 2 consists of the reviews of methods for preparation and purification of ionic liquids and the theoretical aspect of fluorescence spectroscopy. In the first part, the methods for purification of starting materials and final products of ionic liquids were reviewed. The second part consists of the basic principle of fluorescence spectroscopy which include the explanation of fluorescence phenomena and the method for the measurement of fluorescence lifetime. This

chapter also describes the properties of fluorescent molecular rotors and their application as viscosity sensor.

Chapter 3 details the procedures used for the preparation of low fluorescence background ionic liquids. These include the procedures for preparation of highly clean glassware and purifications of the starting materials, intermediates and final products. This is followed by the detailed procedures for the preparation and the characterisation ionic liquids used in this study. The analytical results for the characterization of ionic liquids were also included.

Chapter 4 undertakes to characterise the physical properties of ionic liquids. This involves the measurements of density, viscosity, conductivity and diffusivity of ionic liquids. The measured values of these properties were compared to those in the literature and these serve as the preliminary evaluation to the purity of ionic liquids. The correlations between these properties are discussed using various type of equations and models.

Chapter 5 is an investigation into the local viscosity of ionic liquids under the influence of electric fields using fluorescence spectroscopy. The behaviour of molecular rotors in ionic liquids was studied using the steady state fluorescence spectroscopy. The fluorescence lifetime of molecular rotors obtained from the time resolved fluorescence spectroscopy experiments were used to derive the local viscosity in ionic liquids.

Chapter 6 summarises the overall conclusions from this project and suggests the future works for possible improvements and expansion of this work.

1.3 Introduction to ionic liquids

Ionic liquids have been the subject of significant research since the discovery of the first ionic liquid that can be dated back to the early 20th century. The first ionic liquid, ethyl ammonium nitrate ([$EtNH_3$][NO_3]), was formed from the neutralisation reaction between ethylamine and concentrated nitric acid which led to the formation of the liquid salt which had a low melting point of 13-14°C. It was first reported by Paul Walden in 1914.[17] Two decades after this discovery, the first patent related to ionic liquids appeared. The patent related to the ability of liquified quaternary ammonium salts to dissolve cellulose-based materials to produce solutions with varying viscosities.[18] This invention enabled, and eased, the process of conversion of cellulose based materials to other products either via chemical or mechanical methods. The revolution continued, and another patent was granted in 1948 relating to the use of ionic liquid mixtures *i.e.* aluminium (III) chloride and 1-ethylpyridinium bromide for the electrodeposition of aluminium.[19] In 1992, Wilkes and Zaworotko reported the discovery of more air and water stable ionic liquids *i.e.* 1-ethyl-3-methylimidazoilum tetrafluoroborate [C_2C_1im][BF_4] and 1-ethyl-3-methylimidazoilum acetate [C_2C_1im][CH_3COO]. This was an important milestone for the application of ionic liquids as most of the previously reported ionic liquids were highly moisture sensitive. Since then a wide variety of ionic liquids have been synthesized and many synthetic techniques have been developed.

More than 1000 ionic liquids have been synthesised to date and theoretically millions could be synthesised by solely varying the anion or cation constituents of the ionic liquids. This provides a high degree of tunability and thus allows for precise control of their physical and chemical properties to meet the characteristics needed for a specific application. This represents the most

notable advantage of ILs over the traditional molecular solvents. For this reason, ILs can be termed as 'designer solvents'.[20–22] Many ionic liquids have low melting points[23] and most of them exist in the liquid state at room temperature. They are composed exclusively of free moving anions and cations while they are in the liquid state. Ionic liquids generally consist of an organic, or inorganic, anion paired with a bulky organic cation. Among the cations used in ionic liquids are imidazolium, pyridinium, pyrolidinium, ammonium, phosphonium and sulfonium (**Figure 1**). The counter ions are normally made up of species such as: halides, hexafluorophosphate, tetrafluoroborate, *bis*(trifluoromethylsulfonyl)imide, tetrachloroaluminate, and alkylsulfate (**Figure 2**). The combinations of the anions and cations produce ionic liquids with different degrees of solubility in water. The solubility of ionic liquids in water is primarily governed by the identity of the anions. The more basic the anion, the greater the solubility in water.[24] The shorter length of alkyl chain length or presence of hydrophilic functional group attach to the cation also contribute to the greater water solubility. Some ionic liquids are even decomposed in water e.g. ionic liquids containing $[AlCl_4]^-$.[25]

The wide range of excellent properties of ionic liquids with the high degree of tunability have made ionic liquids relevant for use in a wide spectrum of applications including:

a) Solvents – organic reactions, bio-catalysis, separations and extractions, and polymerisations
b) Electrolytes – Fuel cells, batteries, supercapacitors and sensors
c) Lubricants and fuel additives
d) Liquid crystals – displays, ion conductive materials
e) Heat storage – thermal storage fluids and heat transfer fluids

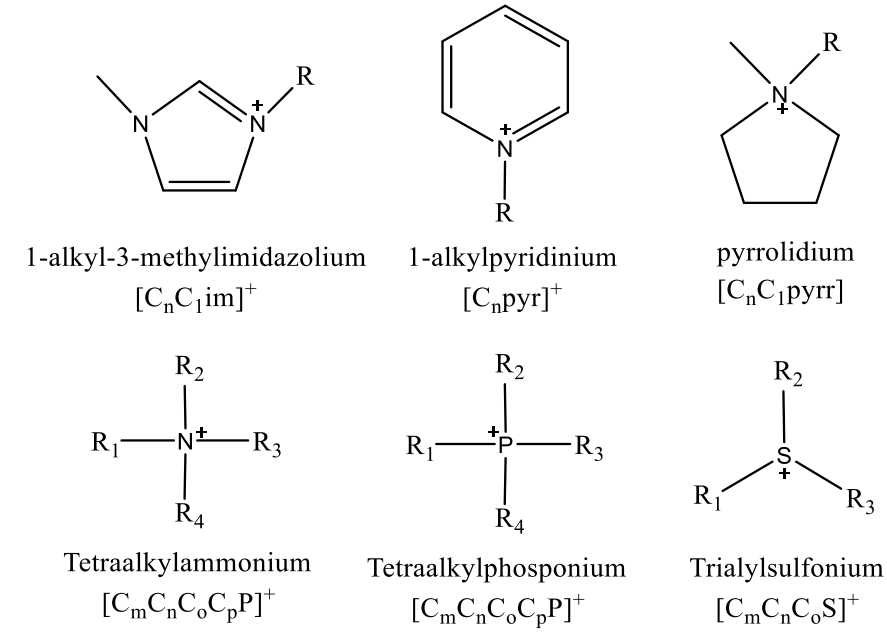

Figure 1: Commonly used cations in ionic liquids.

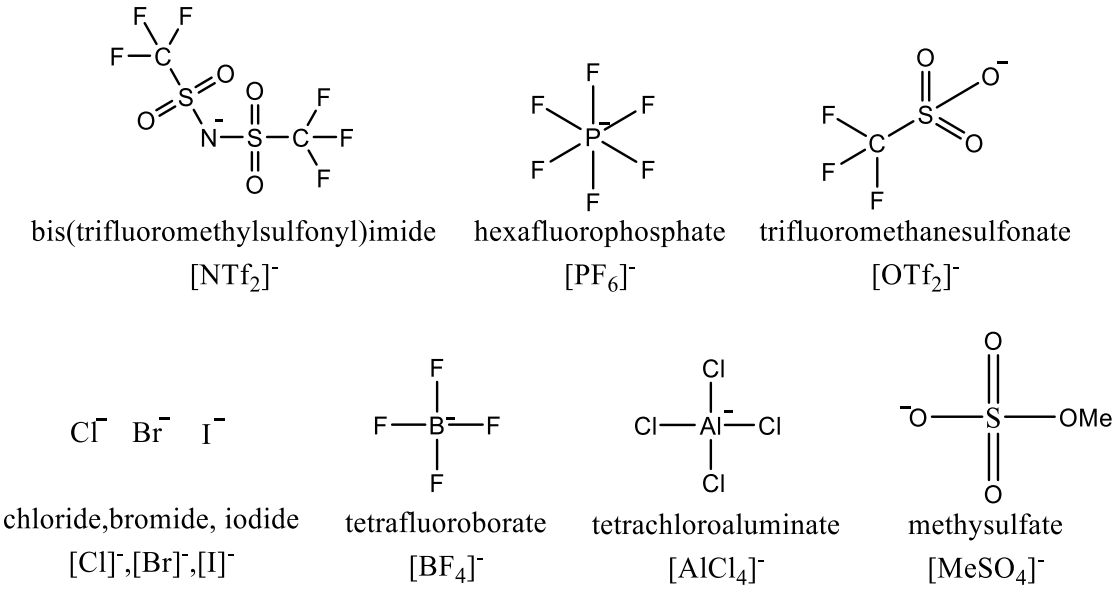

Figure 2: Commonly used anions in ionic liquids.

The ions in ionic liquids are held together by Coulombic forces by virtue of their positive and negative charges. However, the Coulombic forces in ionic liquids are relatively weak compared to those forces found in salts comprised of relatively small ions such as NaCl , $LiNO_3$, KBr, Cs_2CO_3 *etc*.[26] This is due the nature of the ions in ionic liquids that are comprised of bulky and highly asymmetric ions, which reduce the effective electrostatic attraction forces between the oppositely charge ions. Therefore, ionic liquids generally exist in a liquid state at moderate temperatures, making them suitable candidate materials for use as a solvent for synthesis,[24,27] catalysis[28–30] and other various chemical processes.[19,31,32] In contrast, the small and simple inorganic salts exist in a solid state at ambient temperature due to their high melting point (see **Table 1**) and this limits the possibility of their use as electrolytes and solvents for chemical reactions.

Table 1: Melting point of selected Group 1 salts.

System	Melting point (°C)
Sodium chloride (NaCl)	803
Potassium nitrate (KNO_3)	334
Lithium nitrate ($LiNO_3$)	255
Cesium carbonate (Cs_2CO_3)	610

1.5 Electrochemistry of ionic liquids

Electrochemistry is a field in chemistry that studies the oxidation and reduction reactions that occur at the surface of electrodes. The oxidation and reduction that occurred at the anode and cathode are collectively known as redox reactions. In general, the direction of a half-reaction is determined by the electrical potential difference of the electrodes and thus an electrochemical reaction can be controlled by manipulating the potential. The potential of an electrochemical cell when the two half reactions are at equilibrium is known as equilibrium potential (E_{cell}). If the conditions of electrochemical cell are the standard states, the potential difference is called as standard potential (E^{o}_{cell}). Apart from the temperature must be at 298.15K, the standard conditions of an electrochemical cell are also defined by the concentration of electrolyte of 1.0 M for a solution and pressure of 1.013 bar for a gas. The relationship between E_{cell} and E^{o}_{cell} can be expressed by the Nernst equation (equation **(1)**).

$$E_{cell} = E^{\circ}_{cell} \quad \frac{RT}{nF} \ln Q \qquad \textbf{(1)}$$

In the equation **(1)**, R = universal gas constant, T = temperature, n = number of electrons involved in the redox reaction, F = Faraday constant and Q = reaction quotient.

The widely used standard reduction potential tables are constructed using the standard hydrogen electrode (SHE) as a reference cell. This is because hydrogen has been universally recognized to have oxidation and reduction potentials of zero. All the potential values in the table are corresponding measurements in aqueous solutions of chemical species (water as solvent) that has activity of ions = 1. However, in ionic liquids the standard states have not

been well defined and thus the determination of standard potentials in ionic liquids are not usually reported. This is due to the different solvation environment of redox species would have in each different ionic liquid. For example, the potential of $Co^{3+} + 2e^- \rightarrow Co^{2+}$ is strongly affected by the medium in which it is dissolved. The potential of redox couple of $Co(bpy)_3^{2+/3+}$ varies as much as 20mV as the medium changes from $[C_2mim][NTf_2]$ to $[C_4mpyr][NTf_2]$.[33] This observation suggests that the redox process is dependent on the nature of medium and ionic liquids produced quite different redox potentials compared to molecular solvents.

The proper setup to study a reaction occurring at an electrode surface is using a three-electrode setup as illustrated in **Figure 3**. The reaction of interest occurs on the working electrode and the potential of the working is measured against a reference electrode. The reference electrode usually uses a reversible process such as Ag/Ag^+ which have a well-known and stable potential. The potential of the reference is usually measured using a high impedance circuit to avoid polarizing effects that might occur if a substantial amount of current passes through it.

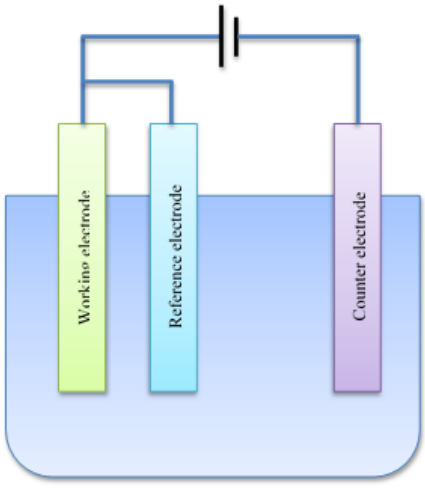

Figure 3: Typical setup of a three-electrode electrochemical cell.

The standard hydrogen electrode (SHE) is the primary reference electrode for measuring a redox potential for reactions in aqueous electrolytes. Other examples of reference electrodes are saturated calomel electrode (SCE) ([Hg | Hg_2Cl_2 | KCl], E = +0.242V versus SHE), silver-silver chloride ([Ag | AgCl | KCl], E = +0.197V versus SHE) and copper-copper (II) sulfate ([Cu | $CuSO_4$], E = +0.314V versus SHE). These are the examples of aqueous based reference electrodes in which the electrodes are usually constructed with a frit that connectsto the bulk electrolytes. However, the aqueous based reference electrodes are not the best reference electrodes for electrochemical measurements involving ionic liquids. This is because the difference in ion activity between the electrolyte in the electrode system and the bulk electrolyte will result in a junction potential. Moreover, the presence of water in the aqueous based reference electrode may lead to contamination of bulk electrolytes and therefore is not suitable to be used for measurement involving ionic liquids as electrolytes. To overcome this problem, a reference electrode made up of similar ionic liquids can be used such as Ag wire in solution of 10nM Ag[OTf] in [C_3mpyr][NTf_2]. This approach will minimize the junction potential. **Figure 4** shows the schematic illustration of reference electrodes for aqueous and non-aqueous systems. Another alternative to avoid the contamination problem is through the use of inert metals such as silver and platinum reference electrodes. These electrodes are called quasi-reference electrodes or pseudo-reference electrodes.

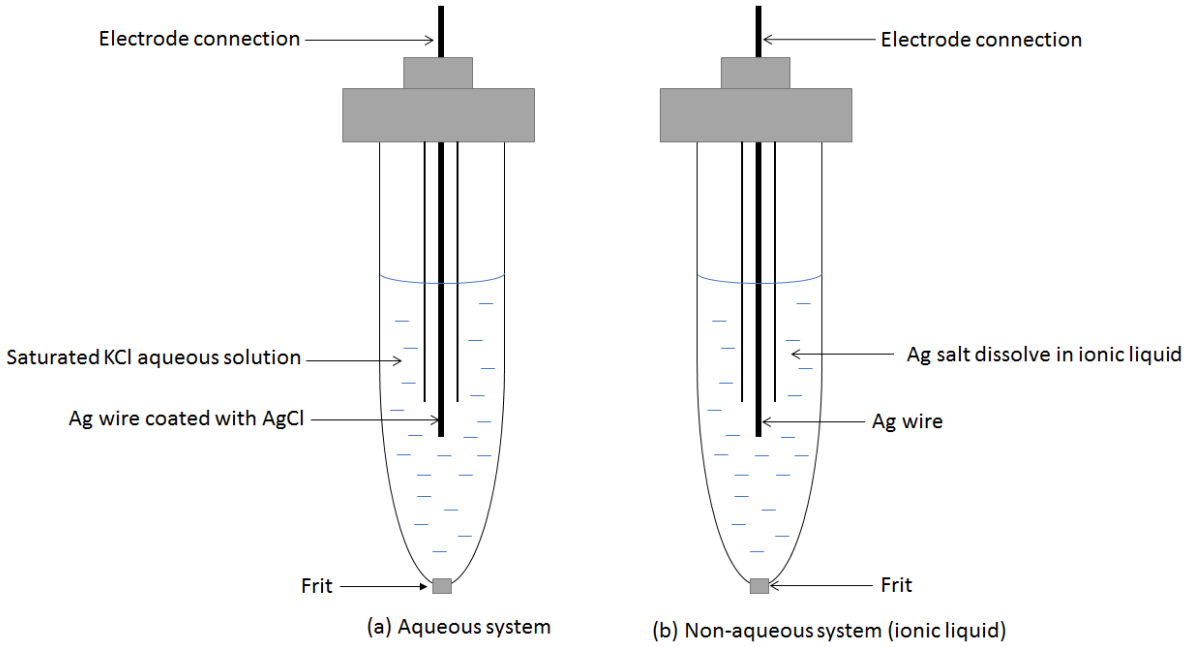

Figure 4: Comparison between aqueous reference electrode and non-aqueous reference electrode.

The electrochemical window of an ionic liquid can be defined as the potential over which the electrolyte is electrochemically inert or stable. It depends on both the oxidative and reductive stability of the electrolyte. Typically, the electrochemical window of an ionic liquid depends on the resistance of the anion to oxidation and the cation to reduction. The electrochemical window is usually calculated from the difference between the potential limits of the oxidation and reduction process. There are many factors that affect the electrochemical window of ionic liquids. The presence of impurities such as water, unreacted starting materials and trace of solvent residue may reduce the potential window of an ionic liquid.[34] The well-known method used to determine the electrochemical window of an electrolyte is cyclic voltammetry. Cyclic voltammetry measurements are normally conducted using a three-electrode setup which

consists of a reference electrode, a working electrode and a counter electrode (see **Figure 3**). During the cyclic voltammetry measurements, the potential of the inert working electrode is scanned out to a greater positive (anodic) and negative (cathodic) potential until the background current rise dramatically this is due to the oxidation and reduction of ionic liquid's ions.

The electrochemical windows of common ionic liquids are well established in the literature. In general, the electrochemical stabilities of the cations of ionic liquids are as follows: pyridinium < pyrrolidinium < imidazolium ≤ sulfonium ≤ ammonium.[23] The order of stabilities of the anion are: halides (Cl^-, Br^-, I^-) < chloroaluminates ($[AlCl_4]^-$, $[Al_2Cl_7]^-$) ≤ fluorinated ions ($[BF_4]^-$, $[PF_6]^-$, $[AsF_6]^-$) ≤ triflate/triflyl ions $[CF_3SO_3]^-$, $[(CF_3SO_2)_2N]^-$, $[(C_2F_5SO_2)_2N]^-$, $[(CF_3SO_2)_3C]^-$). The main source of impurities in ionic liquids are unreacted starting materials. The presence of water will affect both the anodic and cathodic potential limits as water can be both reduced and oxidised within the potential limits of ionic liquids.[35] In some cases, water can also react with the anion or cation to produce a product that is electro-active in the potential window of an ionic liquid. For example $AlCl_3$ in chloroaluminate ionic liquids reacts with water to form HCl and $[HCl_2]^-$ which both are electroactive active proton-containing species.[36] Hexafluorophosphate $[PF_6]^-$ and tetrafluoroborate $[BF_4]^-$ react with water to produce HF. The presence of halide ions in ionic liquids, such as chloride (Cl^-), bromide (Br^-) and iodide (I^-), will generally reduce the anodic potential limit of ionic liquids. These ions are easier to oxidise than fluoride (F^-) ion.

1.6 Electrical double layer in aqueous electrolytes and ionic liquids

A huge number of researches has been done with intentions of using ionic liquids in electrochemistry and its applications. Most of the applications of ionic liquids in the electrochemistry field will involve the interaction of ionic liquids at electrified interfaces. Thus, understanding the basic structure and properties of ionic liquids at the interfaces seems crucial before ionic liquids can be realized in any electrochemical devices. The electrical double layer model is often used to visualize the ionic environment in the vicinity of charged surface. There are several models that have been proposed to explain the interfacial structure such as the Helmholtz model, the Gouy-Chapman model and Stern's modification model. These models have been widely used to explain the electrical double layer in aqueous electrolytes, in which the concentration of ions are low and thus electrostatic interactions are very weak due to the high dielectric constant of the solvent (water).[37] However, the concentration of ions in electrolyte systems like molten salts and ionic liquids is very high and thus strong electrostatic interaction is assumed to exist in such solventless systems.

A simple and classic model that can be used to explain the formation of the double layer at the electrode surface is presented in **Figure 5**. The liquid solution in the vicinity of charged metal is thought to be made up of several layers. The species that are directly adsorbed on the charged surface of electrode are either solvent molecules (*e.g.* water molecules for aqueous electrolytes) or other molecules or ions that are called "specifically adsorbed" species and they form the first layer. The plane located just behind first this layer of adsorbed molecules is called inner Helmholtz plane (IHP), which is at distance X_1 relative to the charged metal. On the top of the inner layer, solvated ions will be absorbed on it and this will form the second layer and the

locus centre of these solvated ions forms the outer Helmholtz plane (OHP). The solvated ions can approach the metal to a distance X_2. The interaction between solvated ions with the charged metal involve long-range electrostatic forces and they are considered as non-specifically adsorbed species. Due to the thermal agitation in the solution, the non-specifically adsorbed species are scattered in a three-dimensional region called the diffuse layer, which cover the area from the OHP to the bulk solution.[38] **Figure 5** illustrates the model of the double layer region in which anions are specifically absorbed on a negatively charged metal surface and the potential profile across the double layer region. The thickness of the diffuse layer depends on the total ionic concentration in the solution. As can be seen from **Figure 5**, the potential decays exponentially as the distance from electrode is increased.

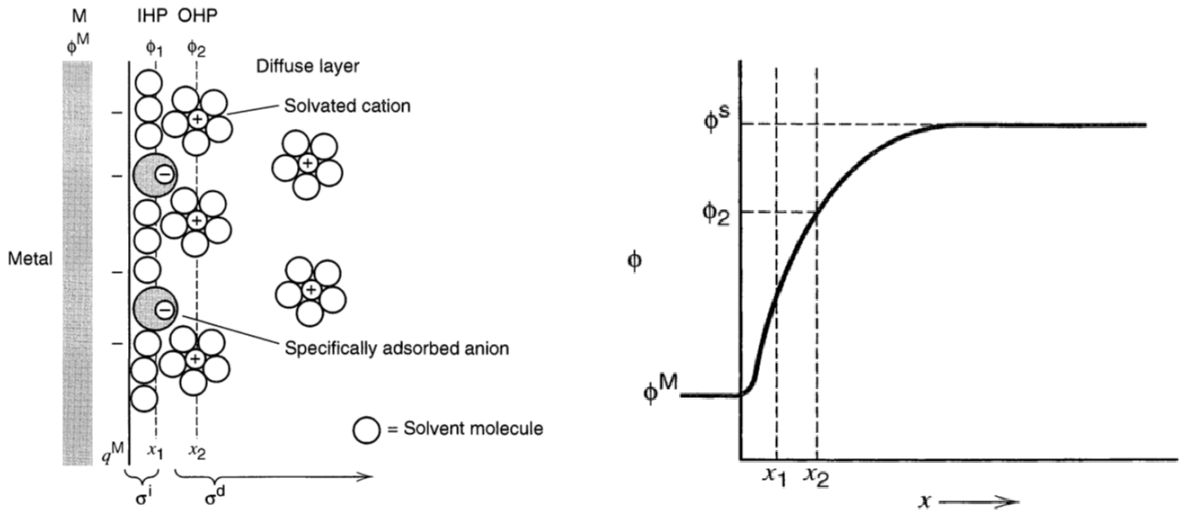

Figure 5: The double-layer model of an electrolyte solution and potential profile across the double-layer region. This figure is adopted from other reference.[38]

The thickness of the double layer is about $1.5\kappa^{-1}$, where κ^{-1} is the Debye-Huckle length which can be calculated using the following equation **(2)**.

$$\kappa^{-1} = (\varepsilon\varepsilon_o kT / 2c^0 z_i^2 e_0^2)^{1/2} \quad \textbf{(2)}$$

In the equation **(2)**, c^0 is the bulk $z{:}z$ electrolyte concentration, ε is the relative dielectric permittivity of the solvent, ε_0 is permittivity of vacuum, k is the Boltzmann constant, T is absolute temperature, z is the charge of ion and e_0 is the elementary charge.[39] Apart from the concentration, the thickness of the double layer is also affected by potential difference between electrode potential and the potential of zero charge.

The study on double layer structure in a solventless electrolyte systems like molten salts and ionic liquids is still lagging compared to diluted electrolytes. The controversy that arises from the interpretation of the double layer structure in the solventless electrolyte system using the existing models that were developed for aqueous electrolytes is due the inability to apply the dilute-solution approximation, on which most of the models rely, to systems composed of highly concentrated ions. If this factor is considered, the Gouy-Chapman theory is no longer valid to explain the electrical double layer in concentrated electrolytes. Compared to the molten salt systems, room temperature ionic liquids which composed of large, asymmetric polyatomic ions ionic radii are about 5-10 bigger than those monoatomic ion like Li^+ and K^+. This will increase the separation distance between cation and anion charge centers and thus decreasing the electrostatic interaction.[10] To date, the electrical double layer in solventless systems has been studied by both experimentally and theoretically.[40–42] The experimental studies include the measurement of macroscopic quantities, such as surface tension and capacitance while theoretically it can be studied using mathematical models or using computer simulations. The

examples of these studies include the use of density functional theory,[37] molecular dynamics,[43] Monte Carlo simulations[41] and lattice-gas model.[40]

The common experimental method that is used for exploring double layer structure in aqueous electrolytes is based on Gouy-Chapman (GC) theory which assumes the ions as point charges that interact only via Columbic interactions. The double layer structure of electrolytes is usually studied by measuring the differential capacitance (C_d) as a function of surface potential (ϕ_0). In ionic liquids the large size of the ions and strong ion correlations should be considered in determining their electrical double layer structure. The high ion density becomes oscillatory at the charged surface and this produces a different structure of double layer in ionic liquids.[37] Kornyshev has conducted theoretical studies using a modified Poisson-Boltzmann lattice-gas model which considers for the excluded volume effects in determining double layer capacitance at planar metal-ionic liquids interface.[40] The commonly used GC theory predicts a parabolic or U-shaped capacitance curve with minimum point at the potential of zero charge (pzc).[37] However, the capacitance curve produced by the modified Poisson-Boltzmann lattice-gas model has a bell-shaped with maximum point at pzc.[40] These observations indicate the double layer structure of ionic liquids is different from the aqueous electrolyte. Using the modified Poisson-Boltzmann lattice-gas model, the curve showing variation of electric potential as function of the distance shows a less steep curve compared to the one produced using GC theory.

There is consensus that pure liquid salt systems like molten salts and ionic liquids have exceedingly high ionic strengths and very short Debye lengths. However, a growing number of experimental measurements have suggested the presence of a longer range force than

anticipated when an ionic liquid is exposed to a charged surface. Gebbie and co-workers have measured forces experienced by two surfaces (positive charged gold and negatively charged mica) separated by the $[C_4C_1im][NTf_2]$ ionic liquid, using surface force apparatus (SFA).[10,44] The force distance profile between the two surfaces showed an exponentially decaying force as the distance increases. The double layer attraction and total interaction forces were observed for over 30nm distance.[10,44] Similar observations were reported by Smith *et al.* after they measured the interaction force between two negatively charge mica sheets across ionic liquids and concentrated electrolytes.[45] They found that decay lengths for these electrolytes are greater than the theoretical Debye length. For $[C_4C_1Pyrr][NTf_2]$ the decay length is extended to up to about 19 nm compared to 2M aqueous of NaCl which has a decay length of only about 6 nm. In the Debye-Huckel regime (diluted electrolytes), it is expected that decay length decreases with concentration. They showed that if the concentration of an electrolyte is increased beyond 0.5M, the experimental decay length starts to deviate from theoretical Debye length by up to 120 times.

The measurements of forces experienced by an atomic force microscopy (AFM) tip as it approaches an Au(111) surface in contact with 1-butyl-1-methyl-pyrrolidinium tris(pentafluoroethyl)trifluorophosphate $[C_4C_1Pyrr][FAP]$ ionic liquid have been conducted by Atkin *et al*.[46] The results showed that no force is recorded beyond 5nm which indicates that AFM measurement is insensitive to any structure beyond this distance but it gives valuable information regarding the possibility of having more than one layer structure near to the surface of electrode (<4nm). They observed a few stepwise increases of force as the AFM tip approached the surface. The number of steps is believed due to the formation of nanostructure of ions near the charged surface.

In general, the trends of variation of potential against distance that were observed in ionic liquids is similar to the trend observed for aqueous electrolytes (see **Figure 5**) *i.e.* both show exponential decay of potential trend as the distance from the surface is increases. This observation suggests that although the trend is similar the mechanism of formation of the double layer in ionic liquids and diluted aqueous electrolytes might be different due to the differences in physical (size of ions and strength of electrostatic force) and chemical (charge) nature of constituents in the electrolytes. For ionic liquids, the decay length is also believed to depend on the nanostructure of the ionic liquids. For ionic liquids with homogeneous bulk nanostructure (*i.e.* ionic liquids with shorter alkyl chain length) the ions arrange into solvation layer and those with sponge-like nanostructure (*i.e.* ionic liquids with alkyl chain length longer than 3 carbon units), the surface flattens the sponge into a more layered order.[10,47] Based all of these observations, Gebbie and co-workers come up with the illustration of the short range nanostructure forces and long range double layer forces for ionic liquids in contact with charged surfaces is shown in **Figure 6**.

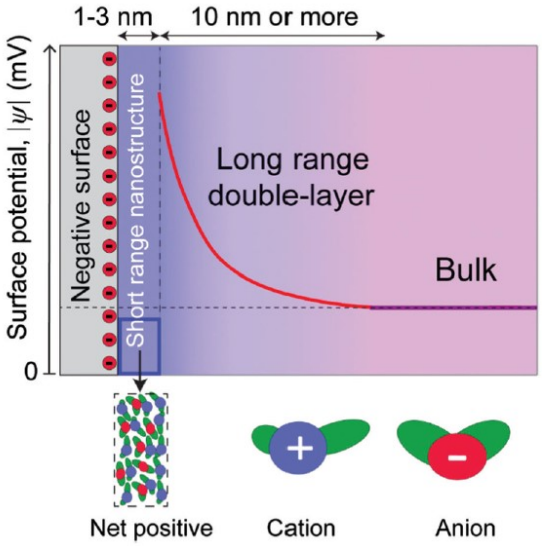

Figure 6: Schematic illustration of short-range nanostructure forces and long-range double layer forces for ionic liquids in contact with a charged surface. Reproduced from other reference paper.[10]

1.8 Potential applications of ionic liquids in electrochemical devices

Ionic liquids possess several properties that make them suitable for electrochemical applications. The key property of ionic liquids, that they consist entirely of ions, implies that these materials should have high ionic conductivities. Apart from this, they also show relatively wider electrochemical windows compared to conventional electrolyte system, which usually comprise of inorganic salt dissolved in molecular solvents. However, in most cases, the determined ionic conductivities are not as high as expected and do not reflect the number of ionic species presence. The ionic conductivity of ionic liquids is not as high as the salt solution used in metal-air batteries or the organic carbonate liquid-based electrolytes that are currently used in most of lithium-ion batteries. For these reasons, there is much effort focusing on understanding and improving the transport properties of/in ionic liquids so that they will achieve reliable performance for real applications.

The real problem with current electrolyte systems that are used in lithium batteries is their weak thermal properties. The solvent based electrolytes are relatively volatile which expose them the risk of drying out and risk of explosion due to the production of gases from the volatile solvents. The flammability of many of organic solvents further give a bad impression to these electrolyte systems and some of them have high toxicities as well. In comparison, ionic liquids prevail over conventional electrolytes as they are thermally more stable *i.e.* their constituents are non-volatile. The use of an ionic liquid system as an electrolyte appear to offer a much safer and cost-effective alternative for large electrochemical devices such as batteries for electric vehicles. The batteries for large devices usually evolve a lot of heat during their charging-discharging process. For this reason, additional thermal management unit such as liquid coolant

circuits need to be incorporated into the battery which incurs additional cost to the manufacturer. Similar concern arises for other energy related devices such as dye-sensitised solar cells and supercapacitors. In some cases, exposing the electrolytes to the heat is unavoidable. For example, thermo-cells and advance fuel cells are usually requires to operate at elevated temperature as high as 150°C.[33]

Ionic liquids have been used as an ion conductive solvent in lithium ion batteries. The species that are involved in the electrochemical reactions *i.e.* lithium ions (Li^+) usually originate from lithium salt such as $Li[NTf_2]$ and usually have been dissolved in another ionic liquid containing a common anion to the lithium salt. The $[NTf_2]$-based ionic liquids are preferred for this application due to the fact that this family of ionic liquids usually has wide electrochemical windows.[48] Another advantage of using these ionic liquids as ion conductive solvents is that the most negative reduction potential of Li^+ falls within potential window of these ionic liquids.[33] Another family of ionic liquids that has been extensively studied for lithium ion battery applications is those containing bis(fluorosulfonyl)imide [NTf] or also abbreviated as FSI. The FSI ions are relatively smaller than the TFSI ions. The Li[NTf] based salt is preferred over the $Li[NTf_2]$ salt due to their higher solubility which means more Li[NTf] can be dissolved in the salt mixture.[33] However, the greater presence of Li^+ in the mixture lead to a higher viscosity which correspond to a lower conductivity. Girard *et al.* studied an electrolyte system consisting of trimethyl(isobutyl)phosphonium (P_{111i4}) bis(fluorosulfonyl)imide (FSI) and lithium bis(fluorosulfonyl)imide (LiFSI) salt mixtures. They found that even though the viscosity increased, and conductivity decreased with the addition of Li^+ to the mixture, the transport number of lithium ions increased as shown by the increase in the transport number of lithium ions $t(Li^+)$ due to the high concentration of Li^+.[49] The continuous interest in high content Li^+ electrolytes has led the Watanabe

group to develop electrolyte systems based on 'solvate' ionic liquids. The mixing of equimolar chelating agent such as tetraglyme with Li[NTf_2] has been reported to produce a liquid electrolyte that exhibits high thermal and electrochemical stabilities.[50] Addition of an excess of Li[NTf_2] to the system (non-equimolar system) has produced a electrolyte system with improved charge-discharge reactions and leads to longer cycle life of the batteries, even though the viscosity is increased. [51]

Ionic liquids also have a potential to be used as electrolyte for supercapacitors. Supercapacitors are electronic devices that store charge in the double layer at the surface of electrodes. The energy capacity of supercapacitor is generally lower than those of batteries, but it can deliver a higher power over many cycles.[33] The advantages of using ionic liquids as electrolytes in supercapacitor are (1) the wide electrochemical window of ionic liquids allows for extended operating voltages of the supercapacitor, (2) the high concentration of ions in ionic liquids means low volumes of ionic liquids are needed to satisfy the charge requirements, (3) the ability of ionic liquids to act as electrolyte without any solvent allow for denser packing of ions at the electrode interface. However, conductivity of pure ionic liquids is still relatively lower to meet the requirements for this application. The large size of the ions in ionic liquids means they have no access to the small channels and cavities of porous electrode and hence reduces the efficiency of the electrode to conduct electricity.[52,53] Among the common ionic liquids being studied for supercapacitors are imidazolium or pyrrolidinium cations paired with fluorinated anions owing to their good conductivity and electrochemical stability.[54,55]

The low volatility with a good thermal stability of many ionic liquids at elevated temperature have made them suitable candidate to be used as electrolytes in fuel cells. This is because the oxygen reduction reaction (ORR) in fuel cells is more efficient if it is conducted at a relatively high temperature *i.e.* >100 ^{O}C than it is at room temperature.[33] Protic ionic liquids are among the ionic

liquids that has been intensively studied as proton carriers for fuel cell application. This is due to the presence of the chemically active and exchangeable protons in the protic ionic liquids. The protic ionic liquids are usually synthesized by the reaction between Bronsted acids and bases (see **section 2.1** for details). The use of protic ionic liquids can avoid the problem of solvent loss or drying when the cell operated at such high temperature. The typical electrolytes that have been used in fuel cells includes the aqueous solution of potassium hydroxide, phosphoric acid, molten salts and solid oxide of calcium and zincornium. The plausible chemical reactions that occur in a fuel cell that consist of protic ionic liquids are as the following:

$2RNH_3^+ + ½\ O_2 + 2e^- \leftrightharpoons 2RNH_2 + H_2O$	Oxygen reduction reaction (ORR)
$2RNH_2 + H_2 \rightleftharpoons 2RNH_3^+ + 2e^-$	Hydrogen oxidation reaction (HOR)
$½\ O_2 + H_2 \rightleftharpoons H_2O$	Overall reaction

The water formed from the reduction process will accumulate at the surface of the electrode, but it will eventually be removed by the gas stream flowing across the cathode. For real application of ionic liquids in fuel cell system, fabrication of the electrolytes into solid thin films is usually essential[56] and several methods for solidification of ionic liquids has been developed.[57–59] The solid thin film fuel cells that consist of protic ionic liquids also susceptible to the risk of drying due to the reversible equilibrium.

$$HA + B \rightleftharpoons HB^+ + A^-$$

At higher temperatures, the loss of amine from the electrolytes system is possible and this raises concern over the effect of the released amine to the environment and their inherent toxicity. To

counter this problem, explorations of high molecular weight and multifunctional amines and the use of relatively non-volatile acid are currently being undertaken.[33]

The high ionic concentration in ionic liquids has made them become a good solvent which are able to screen the interionic interactions of solutes dissolved in them. The charge transport between I^-/I_3^- redox reactions in ionic liquids have been intensively studied for application in dye-sensitized solar cells. Alkylimidazolium iodides are one of the most studies ionic liquids for application in dye sensitised solar cells because they can improve the photovoltaic performance of the system.[60–62] Kawano and Watanabe have highlighted the advantages of using ionic liquids as solvents in dye sensitised solar cells over molecular solvent. They have compared the performance of 1-ethyl-3-methylimidazolium bis(trifluoromethanesulfonyl)imide ionic liquid with a molecular solvent that have similar viscosity, that is polyethylene glycol dimethylether, They observed a faster charge transport between I^-/I_3^- redox reaction in the ionic liquid medium and believed this is due to the ionic strength, an effect that cannot occur in molecular solvent system.[56,63]

1.9 Applications of ionic liquids in the industry

One of the most notable applications of ionic liquids in industry is the Biphasic Acid Scavenging Utilising Ionic Liquids (BASIL^{TM}) process that was introduced by BASF in 2002.[21,64] Traditionally, triethylamine had been used as an acid scavenger in the production process of photo-initiator alkoxyphenylphosphines. However, the reaction leads to the formation of a thick slurry by-product that is difficult to handle and to separate. In the BASIL process, the function of the triethylamine is replaced by 1-methylimidazole and the reaction leads to the formation of two discrete phase products that consist of the main product and the side product, 1-methylimidazolium chloride, which is an ionic liquid.[65] In this way, the ionic liquid can be recovered, and it can be recycled to back to 1-methylimidazole. The recycled product can be reused making the BASIL process more sustainable and cost effective. **Figure 7** shows the chemical reaction that is involved in the BASIL process. The efficiency of the process is increased from 8 kg m^{-3} h^{-1} to 690000 kg m^{-3} h^{-1} and the yield of the reaction improved from 50% to 98% by using the BASIL process compared to the traditional process. This work has received an Innovation for Growth Award by Electronic Component News (ECN) in 2004.

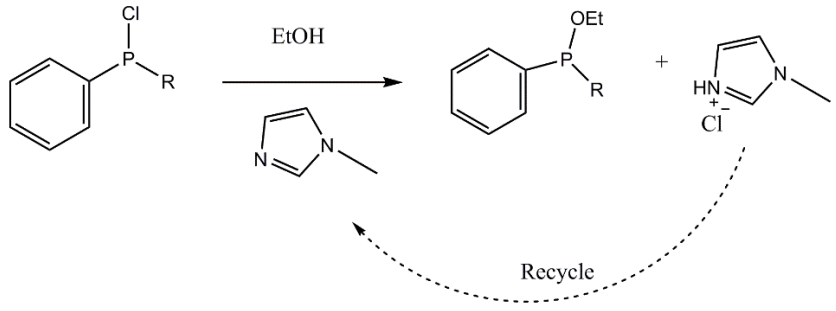

Figure 7 : The BASIL^{TM} process.

An ionic liquid has also been used by the Eastman Chemical Company as a catalyst in the isomerisation of 3,4-epoxybut-1-ene to 2,5-dihydrofuran.[19,66] The isomerisation reaction was discovered by a research team lead by Dr Stephen N. Falling in 1988. The isomerisation reaction needs both a Lewis acid and a Lewis base catalyst. In the isomerisation process, phosphonium ionic liquid $[P_{888\ 18}]I$ acts as a Lewis basic catalyst and the reaction led to the production of the 2,5-dihydrofuran isomer with a yield of 97%.[66] In this particular reaction, the phosphonium ionic liquid is preferable over ammonium based ionic liquids due to its high thermal stability. The reaction was conducted in three continuous stirred tank reactors that perform evaporation, distillation and extraction processes. The catalyst was recovered at the end of the processes by liquid-liquid extraction. The reaction scheme of this isomerisation process is shown in **Figure 8**.

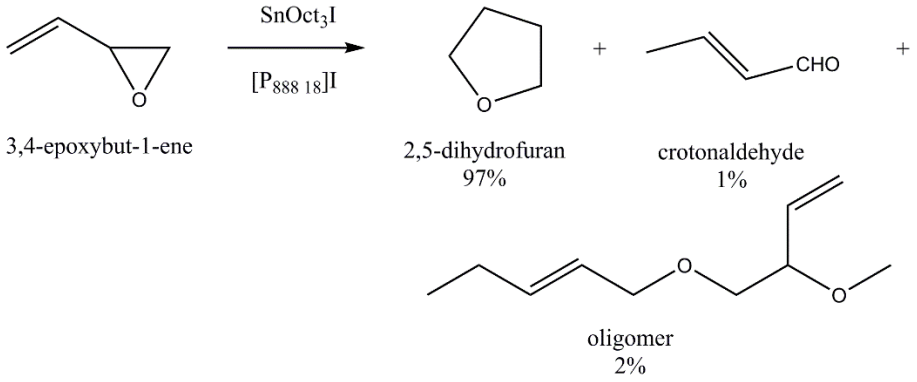

Figure 8 : The isomerisation of 3,4-epoxybut-1-ene to 2,5-dihydrofuran.

The Central Glass Company based in Japan has developed and commercialised the production of pharmaceutical intermediates using ionic liquids as solvents.[19] The production of the intermediates is based on the Sonogashira coupling reaction which produced alkyl-, aryl- and

diaryl-substituted alkynes and is usually carried out in organic solvents such as tetrahydrofuran and toluene.[66] Replacing the organic solvent with a tetraalkylphosphonium ionic liquid led to faster and higher yielding reactions. The reaction is shown in **Figure 9**.

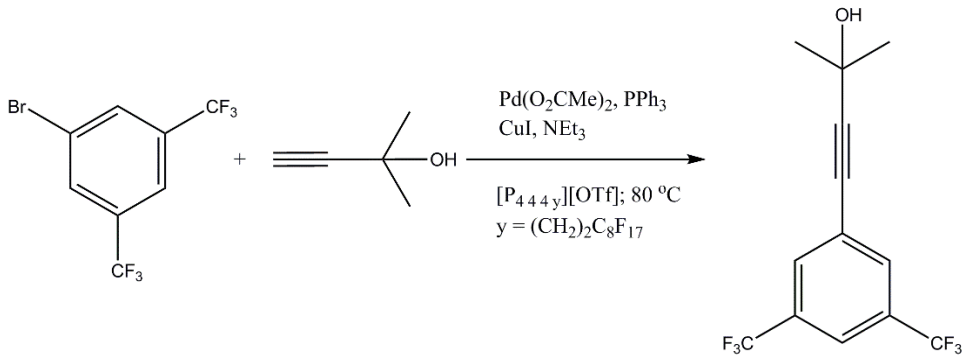

Figure 9 : The Sonogashira coupling reaction in the presence of ionic liquid.

The product of the reaction is collected from the ionic liquid phase by extraction using hexane and the side product salt $[HNEt_3]Br$ is removed from the system using a counter-current flow of water. The remaining ionic liquid-catalyst solution usually can be recycled and reused even with little reduction in catalytic activity.

Degussa is another company that utilised ionic liquids for three different applications – hydrosilylation, paint additives and lithium ion batteries.[19] The hydrosilylation reaction is usually performed in the presence of a homogeneous Pt catalyst. The problem with this procedure is that the catalyst cannot easily be removed or recovered at the end of the process. To overcome this problem, ionic liquid is added to the system and to turn the catalyst system from homogeneous to heterogeneous system.[67] The ionic liquid acts as a solvent for the reaction and as nanoparticle stabiliser. The reaction can be described as an one-pot biphasic synthesis.

The example of the hydrosilylation reaction of a compound containing a carbon double bond with Si-H functional polydimethylsiloxanes is shown in **Figure 10**.

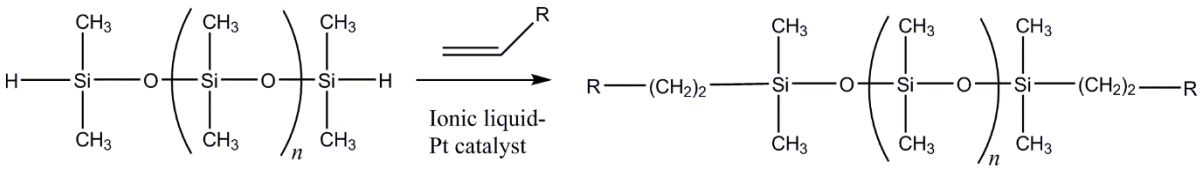

Figure 10 : Synthesis of polydimethysiloxane.

Degussa have also developed paint formulations with ionic liquids as performance additives to improve the appearance, surface and drying properties of the paint.[68,69] They have used five different ionic liquids in their formulations, four of which are commercial ionic liquids. The commercial ionic liquids that were used are distributed in the market under the name TEGO® Dispers and these ionic liquids were added to the solvent-based coatings marketed under the Pliolite® paint range. The addition of ionic liquids to the paint system also helps to reduce the use of volatile organic solvents in the paints and coatings formulations. Additionally, the potential of ionic liquids as electrolytes for lithium ion batteries which can substitute the volatile and flammable organic solvents i.e. ethylene carbonate and dialkyl carbonates that traditionally used in the lithium-ion batteries were investigated.[19]

More recently, on 22nd September 2016, Honeywell UOP announced another successful use of ionic liquid in industry.[70] They used ionic liquids as a catalyst in a liquid alkylation process to produce cleaner, high-octane motor fuels.[71] This new technology has been patented under the name ISOALKYL™. This new technology has been patented under the name ISOALKYL™.

Traditional liquid alkylation uses hydrofluoric or sulfuric acids as an alkylation catalyst which was introduced in between 1938 and 1942. Ionic liquids have replaced the role of the conventional acids to perform the acid catalysis reaction and are able to produce same yields with high levels of octane with lower volume of the catalyst being used. In addition, the low vapour pressure properties of ionic liquids are preferable than the conventional acids for this process as it make them easier to handle. The non-volatility properties of ionic liquids and the ability to regenerate the catalyst on-site helps to reduce the impact of the process to the environment. The company is currently converting its hydrofluoric acid (HF) alkylation unit located in Salt Lake City USA to the ISOALKYL^{TM} technology and the site is expected to fully run with this new technology in 2020. This work won the Platts Breakthrough Solution Award in 2017.

Chapter 2 Literature Review

2.1 Preparation of ionic liquids

Over the past two decades, there has been rapid growth in the number of ionic liquids prepared via a wide variety of methods. Nowadays most of the common ionic liquids are sold commercially and they have found to be used in various applications. For industrial application, it is more economical to buy the ionic liquids from the supplier as the cost and supply is a concern in this field. There are many suppliers of ionic liquids in the market nowadays including: Merck, BASF, Fluka Analytical, Sigma-Aldrich, Iolitec, ACROS, Kanto Chemical Co. etc. However, for analytical work involving fundamental research it is always preferable to synthesise the ionic liquids yourself. This is because purity is an important consideration in most analytical research and high purity ionic liquids can only be produced through careful and controlled synthetic procedures. **Figure 11** shows the comparison of the physical appearance of 1-butyl-3-methylimidazolium methyl sulphate [C_4C_1im][$MeSO_4$] synthesised by a member of the Welton research group member and a commercially purchased version.

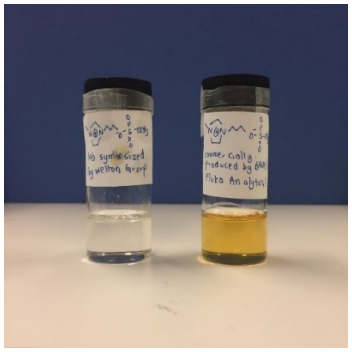

Figure 11: The physical appearance of laboratory synthesised ionic liquid (left) and commercial ionic liquids(right).

The acid-base reaction can be used to produce protic ionic liquids. The ionic liquid is formed from the neutralisation reaction of an acid and a base. The protonation of the base by the acid makes the base positively charged and hence it acts as the cation of the ionic liquid. Meanwhile the produced negatively charged conjugate base acts as the anion of the ionic liquid. The acid-base reaction is a spontaneous reaction in which the reaction occurs very quickly. A specific example of an ionic liquid that can be prepared using this method is 1-butylimidazolium hydrogensulfate [HC_4im][HSO_4]. This ionic liquid is produced via the reaction of 1-butylimidazole with H_2SO_4 as shown by reaction scheme in **Figure 12**. Water is often used as solvent for this exothermic reaction as it helps to dissipate the heat from the reaction. The limitation of this method is that it is not safe to be used to prepare ionic liquids with anions contain of highly delocalised electrons such as $[NTf_2]^-$ and $[OTf]^-$, as the reaction is too exothermic and hard to control.

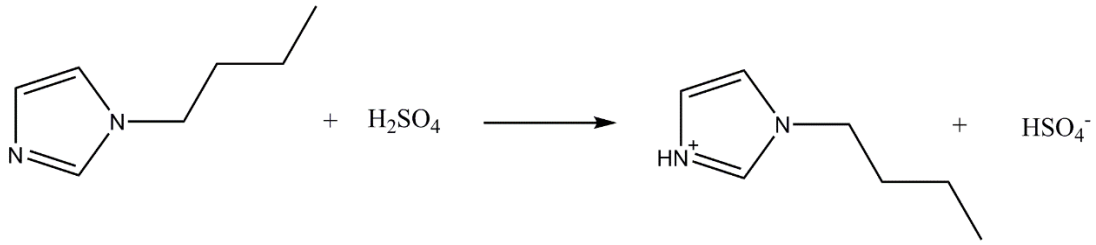

Figure 12 : The synthesis of 1-butylimidazolium hydrogensulfate [HC_4im][HSO_4] by acid-base reaction.

In contrast to the acid-base method, the direct alkylation method can be used to prepare aprotic ionic liquids. The reaction of 1-butylimidazole with the appropriate alkylating agents such as dimethyl sulfate (Me_2SO_4) and trimethyl phosphate (Me_3PO_4) will produce corresponding

ionic liquids *i.e.* 1-butyl-3-methylimidazolium methylsulphate [C_4C_1im][$MeSO_4$] and 1-butyl-3-methylimidazolium dimethylphosphate [C_4C_1im][Me_2PO_4].[72] The reaction schemes showing the formation of these two ionic liquids are illustrate in **Figure 13**. This method can be used to prepare halide free ionic liquids. Contamination with halide salts not only change the physical properties of ionic liquids,[25] but it can cause catalyst poisoning and lead to catalyst deactivation.[72]

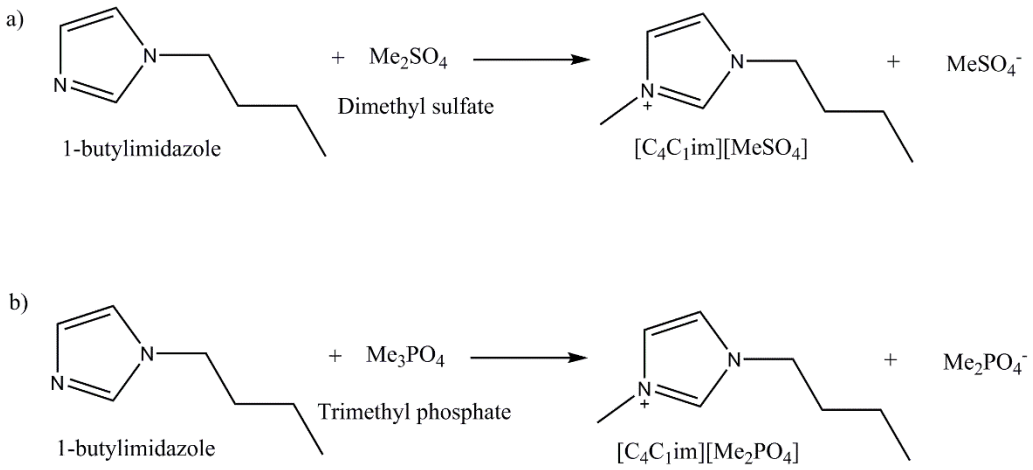

Figure 13: The direct alkylation reaction of 1-butylimidazole with a) dimethyl sulfate and b) trimethyl phosphate.

The ionic liquids obtained from the direct alkylation method can also be used as intermediates to prepare other ionic liquids. For example, the alkylation of 1-ethylimidazole with dimethyl carbonate will produce 1-ethyl-3-methylimizolium carbonate [C_2C_1im][$MeCO_3$]. The product of the alkylation can react with ammonium fluoride (NH_4F) to produce another ionic liquid, 1-ethyl-3-methylimidazolium fluoride [C_2C_1im]F via the evolution of ammonia, carbon dioxide

and methanol as by-products.[73] The reaction schemes representing these reactions is shown in **Figure 14**.

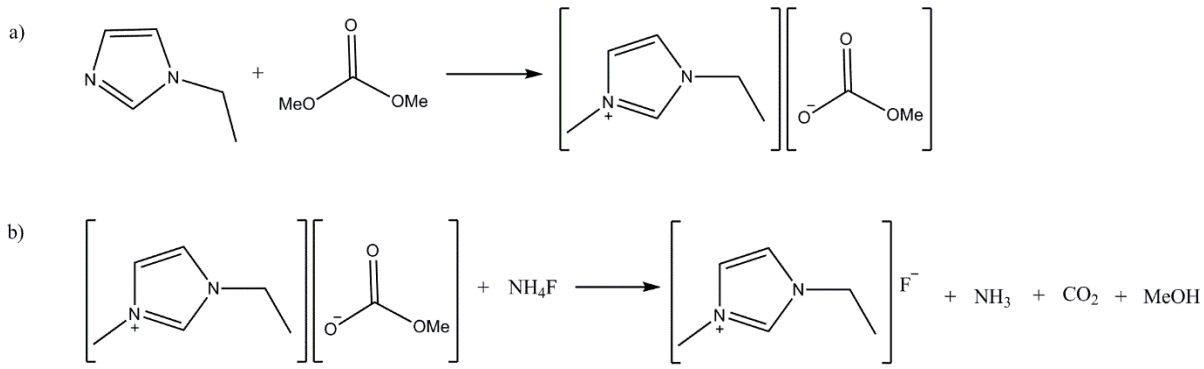

Figure 14: The direct alkylation reaction of 1-ethylimidazole with dimethyl carbonate and subsequent reaction to produce other ionic liquid.

Another alternative to route to prepare aprotic ionic liquids is via halide intermediates. In general, the preparation of ionic liquids via this method involves a two-stage procedure. The first stage involves the making of the halide intermediates via the alkylation of a tertiary amine or phosphine to form the halide salt of the cation. Haloalkanes (bromide, chloride or iodide) are the preferred alkylating agents as they are commercially available and relatively cheap. However, fluoride salts cannot be synthesised using this technique. The ease of alkylation follows the order: I > Br > Cl. The reactivity of the haloalkane decreases with increasing alkyl chain length.[23] The alkylation process takes place via a nucleophilic substitution reaction. The reaction is usually carried out in ethyl acetate as solvent and the reaction should be conducted in inert environment due to hygroscopic nature of halide intermediates. The second stage

involves the metathesis of the synthesised halide intermediate with a sodium or lithium salt of the desired anion. For ease of separation, the metathesis reaction is either carried out in dichloromethane for preparing hydrophilic ionic liquids or in water for preparing hydrophobic ionic liquids. The halide intermediate method is considered as one of the most versatile methods for producing ionic liquids as it can be used to prepare various types of ionic liquids and is able to produce good quality ionic liquids. The drawbacks of this route are that it requires long procedures and it also uses a huge volume of molecular solvents. The ionic liquids prepared for this project were all synthesised via the halide intermediate route. Details of the preparation of ionic liquids via halide intermediates is discussed in **Section 3.2**.

It is worth to mention that there are a lot of other methods which have been developed to prepare ionic liquids. These include the use of ion-exchange columns, use of methyl carbonate intermediates and metathesis of hydroxide. Research on the synthesis of ionic liquids is currently focused on various methods to produce ionic liquids using less solvent and energy, with faster reaction rates, while still being able to produce a relatively good purity ionic liquid.

2.2 Purity and purification of ionic liquids

2.2.1 Purification of chemicals

Production of a pure compound always starts with the use of pure reagents and/or solvents. Common sources of contamination of solvents come from the corrosion of metal storage containers and leaching of monomer or plasticisers of plastics containers, as well as unreacted starting materials.[74] It can also arise from direct contact with the grease and screw caps from apparatus (*e.g.* separating funnel) used for solvent extraction and chemical manipulation.[75] The exposure of the solvent to oxygen present in the air can lead to production of various oxidation products. Usually a reagent/solvent needs to undergo at least two methods of purification before it achieves acceptable level of purity. Common methods that are usually used to purify reagents and solvents are solvent extraction, distillation, recrystallisation and sublimation. The principles of separation for each method are explained below:

a) solvent extraction – usually used for separating a substance from a matrix which either involves liquid-liquid phase or solid-liquid phase extraction. This technique employs two immiscible phases to separate a solute from one phase to another.

b) Distillation – this technique is applicable to liquids or low melting point solids. This physical process exploits the difference in boiling temperature of the constituents to separate them from one another.

c) Recrystallisation – the impure material is dissolved in a suitable solvent and allowed to crystallise out from the solvent. This method utilises the difference in solubility to remove the impurities.

d) Sublimation – this method can be used to purify compounds that can change their state from solid to gas directly upon heating. The volatile compound will sublime when heated under vacuum which will then deposit on a cool surface yielding the pure compound. The non-sublimable compounds or impurities will remained in the evaporating dish.

e) Filtration – this can be used to remove or collect insoluble solids from a liquid.

f) Drying – the removal of trace solvent from a chemical either by application of heat, vacuum or for water using drying agent. The traces of organic solvent remaining in a chemical is easily removed by heating it above its boiling point. Unlike organic solvents, the boiling point of water is relatively high, and it is usually removed using drying agents (desiccants). The drying agents can either react chemically with water or they act as molecular sieves. Some desiccants react with water reversibly and form hydrates. Another group of desiccants react irreversibly with water. These include alkali metals, metal hydrides and calcium carbide. The suitability, intensity and capacity of the desiccants to remove the water varies from one another.

The purity of level of the chemicals depends on their intended use. Even though it is the best practice to use the absolute pure chemicals, they are often not attainable. Various high-grade chemicals are commercially available such as spectroscopic and chromatographic grades. Several methods are available to assess the purity of chemicals as listed below.

a) Assessing the physical properties such as melting point, boiling point, density, refractive index and specific conductivity.
b) Analytical testing such as elemental analysis.
c) Chemical and physical tests for a particular type of impurity such as silver nitrate test for

chloride ion.

d) Spectroscopic and electrochemical methods.

Impurities could also originate from the glassware and plasticware that were used to contain the chemicals and perform the reactions. In order to make sure that the glassware is clean and safe to be used, the following actions become necessary.

a) Cleaning practices – intensive cleaning of glassware and Teflon equipment can be done through careful immersion in a suitable solution followed by draining and rinsing copiously with distilled water. Glassware usually needs to be soaked or rinsed with strong oxidative solution such as sodium dichromate in concentrated sulphuric acid, a 1:1 mixture of concentrated sulphuric acid and nitric acid, or 3:1 mixture of concentrated sulphuric acid and hydrogen peroxide. Glassware should then be heated to a high temperature of 200 – 300 °C overnight after which they can be rinsed with distilled water. Teflon equipment can be cleaned through soaking with acetone followed by petroleum ether before being dried in vacuum before use.[75]

b) Silylation of surface of glassware – silylation agents can be used to coat the walls of glassware making it either repellent to water and hydrophilic materials depending on the type of silylation agents used. Surface silylation can minimise adsorption of solutes onto the walls of the glassware and therefore help prevents contamination.[75–77]

2.2.2 Purification of ionic liquids

Although purity of ionic liquids is not the main concern for every purpose, it increasingly gains more attention from the ionic liquids community due to the growing number of publications reporting the adverse effects of water, halide ions and unreacted starting materials (*e.g.* 1-methyimidazole) on the rate and selectivity of reactions conducted in ionic liquid as a medium and their physical properties.[25,27,34,78] There are also an increasing number of new methods which have been developed to identify and quantify these impurities in ionic liquids.[79–83] The properties of ionic liquids do limit the purification techniques which can be used. Most of the ionic liquids are expected to appear as white solids or colourless liquids when they are in their pure form. However, it is common to observe the discoloration of ionic liquids when they are prepared. They often appear as yellowish or brownish solids or liquids, and this is a clear indication of the presence of impurities. Based on our experience in the laboratory, extreme and prolonged heating will lead to the discoloration of ionic liquids. However, the exact reaction and identity of species that are responsible for the discoloration remained unknown. Possible contaminants and their removal procedures are discussed below:

a) Excess starting materials – these species usually originate from incomplete an alkylation reaction during the production of the halide intermediates and from the non-stochiometric mixing of reactants at the beginning of a metathesis reaction. The starting materials presence in the halide intermediates can usually be removed through recrystallisation and washing with a suitable solvent. Halide impurities from the metathesis reaction can be removed by washing with distilled water followed by vacuum drying at 65°C for 24 hours to remove any traces of water remaining in the ionic liquid.[84] A small amount of ionic liquid will be

lost in every washing step. This purification technique is efficient for removing halide ions from hydrophobic ionic liquids. For hydrophilic ionic liquids, the washing needs to be done with care using the minimum amount of water to prevent the large losses of the ionic liquid. These include the ionic liquids containing $[CF_3SO_3]^-$, $[BF_4]^-$, $[CF_3COO]^-$, $[NO_3]^-$ and halide anions.[25] Even washing of some hydrophobic ionic liquids, such as those containing a hexafluorophosphate $[PF_6]^-$ anion, could be problematic as the anion can undergo partial hydrolytic decomposition upon heating to release hydrofluoric acid and form oxo- and hydroxophosphates complexes.[84–86] Ionic liquids containing $[BF_4]^-$ and $[SbF_4]^-$ anions are also prone to this hydrolysis.[87]

b) Colour contaminant – discolouration of ionic liquids mainly occurs due to excessive heating during the synthesis *i.e.* alkylation reaction and during purifications.[84] The excessive heating is believed to cause the decomposition of ionic liquids. The discolouration of ionic liquids might also be caused by improper purification of starting materials or the presence of trace amount solvents or halides. Trace amounts of coloured impurities present in the ionic liquids is not detectable by NMR spectroscopy or by any other analytical technique other than UV-Vis spectroscopy.[23] Thus, the chemical nature of the coloured impurities is difficult to identify. In general, for solid crystal ionic liquid precursors, repetitive washing and recrystallisation with a suitable solvent might help to remove the coloured impurities and be able to lead to colourless ionic liquids. Treatment with activated charcoal followed by filtration is the most effective way to remove coloured contaminants from ionic liquids themselves.[84,88]

c) Acid or base contaminants – traces of acid or base that remain in the ionic liquids can be removed by passing through the liquids over a short alumina plug. Then, the liquid needs to be filtered through a pad of celite or a PTFE filter to ensure a complete removal of alumina particulates from the liquid. it is important to remove the traces of acid in ionic liquids because it can cause decomposition of ionic liquid over time.[23]

2.3 Fluorescence phenomena

Emission of light from a substance in an electronically excited state is called luminescence. The emission of the light occurs when an electron in the excited state returns to the ground state. The timescale of this process depends on the multiplicity of the electron in the excited state. If the spin orientation (*i.e.* multiplicity) of the electron in the excited state is opposite to the one in the ground state, the emission process will occur at a rapid rate typically at about 10^8 s^{-1}.[89] This emission process is called fluorescence. On the other hand, if the spin orientation of the electron in the excited state is same as the spin of electron in the ground state, relaxation from the excited state is hindered, and hence the emission rate is slower, typically in the range of 10^3-10^0 s^{-1}.[89] This emission process is formally called phosphorescence. Consequently, the lifetimes observed in the fluorescence process are shorter, usually in the nanoseconds range compared to the lifetimes for phosphorescence process which range from milliseconds to seconds.

Fluorescence phenomena are commonly observed in aromatic, planar and/or cyclic molecules containing several alternate single and double bonds. These types of molecules can absorb invisible ultra-violet (UV) light and re-emit longer wavelength, visible, light upon relaxation back to the ground state. The first fluorescence phenomenon was described by Sir George Gabriel Stokes in 1852 when he noticed the ability of fluorspar and uranium glass to convert invisible UV light in to visible light. The process which describes the conversion is now known as the Stokes shift. A Jablonski diagram is normally used to illustrate the fluorescence process. A typical Jablonski diagram is shown in **Figure 15**.

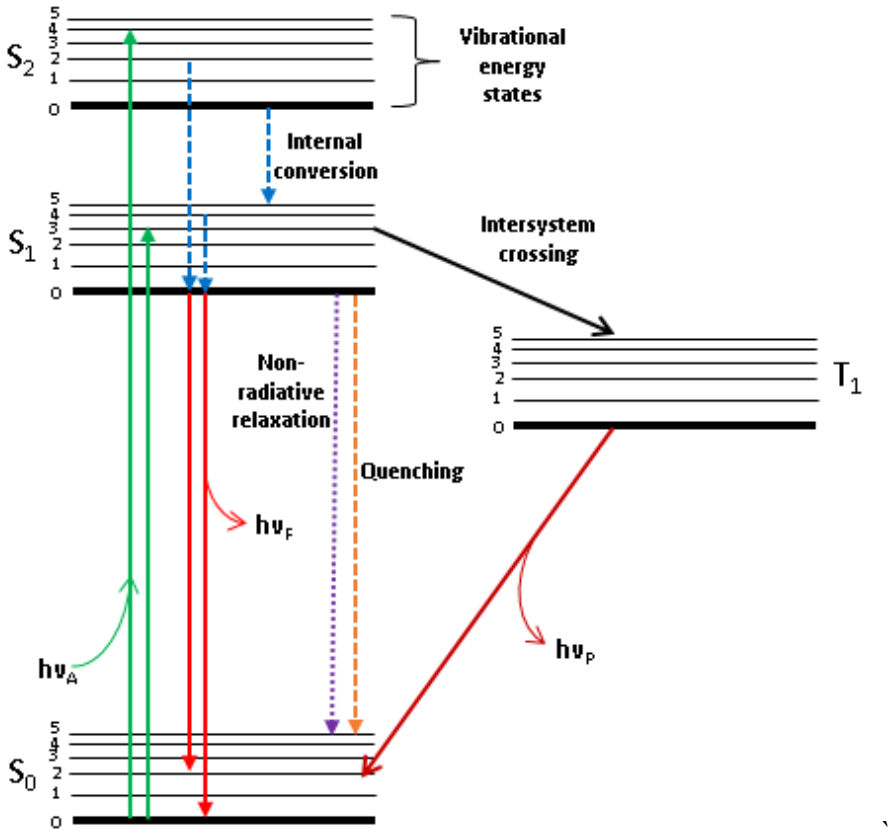

Figure 15: A typical representation of a Jablonski diagram.

In the Jablonski diagram, S_0, S_1, and S_2 denote the singlet ground, first and second electronic states respectively. In each electronic state, the energy is further divided into a few energy levels, which are marked with the integers 0,1,2,3,4 and 5. Upon photo excitation (green arrows), a fluorophore is promoted to a higher vibrational level, *i.e.* S_1 or S_2. The excited molecules in the vibrational level will undergo a very fast relaxation process to the lowest vibrational level of S_1; a process called internal conversion. This process occurs in the timescale of less than 10^{-12} s, which is much faster than the fluorescence lifetime timescale (10^{-8} s). Therefore, the internal conversion process will generally complete before the emission process takes place. From the thermally equilibrated excited state of S_1, the excited molecules will

return the ground state (red arrows) accompanied by the emission of fluorescence light ($h\nu_F$). The molecules at ground state are then quickly reach thermal equilibrium at the timescale of 10^{-12} s.

It is also possible for the excited molecules at S_1 level to undergo intersystem crossing to the lower energy triplet state (T_1). The emission of light results from the relaxation of molecules in the triplet state to the ground state (S_0) is known as phosphorescence ($h\nu_P$). However, the relaxation from T_1 to S_0 is forbidden because of the electron spin is parallel to the electron in the ground state.[89] Thus, phosphorescence process occurs at a slow rate and has a rate constant that is several magnitudes smaller compared to the rate constant for fluorescence process. The excited molecules at S_1 can also undergo intermolecular interactions and results in quenching that will generally cause the fluorescence intensity to decrease. Intermolecular interactions include: excited-state reactions, molecular rearrangements, energy transfer, ground state complex formation and collisional quenching. Additionally, the optical properties of the sample such as high optical densities or turbidity also can lead to quenching. The quenching process can be generally categorised into two types, either static or dynamic (collisional) quenching. In static quenching, the fluorophore interacts with quencher and formed a new non-fluorescent complex during the lifetime of the excited state and returns to the ground state without emission of fluorescence light. In dynamic quenching, the quenchers diffuse to fluorophore molecule and cause a non-fluorescence relaxation. However, the quenching process does not involve any photochemical reaction which can cause a permanent change to the fluorophores. Apart from quenching, it also possible for the excited molecules to relax to the ground state without emission of a photon (light). This process is called non-radiative relaxation. In the non-radiative process, energy is generally released to solvent in form of heat.

2.4 Fluorescence lifetime

The steady-state measurement of fluorescence intensity is a well-known, conventional method to gain information about the distribution of fluorophores and the environments they are exposed to. The properties of fluorophores are usually discriminated from one another based on the intensity, peak position and peak shape even though there is advancement on this technique involving measurement of fluorescence intensity at multiple excitations and emissions. The main drawback of this conventional method is that the fluorescence intensity largely depends on the fluorophore concentration and its uniformity of it within the sample. Often, the distribution of fluorescence probes in a complex, non-homogeneous system is non-uniform. Therefore, probing the physical and chemical properties in a complex system using the steady-state emission measurement can be problematic and sometimes leads to errors. However, the fluorescence lifetime of a fluorophore is known to be independent of the fluorophore concentration. Therefore, the fluorescence lifetime technique is considered a more robust technique for studying dynamic processes in complex systems. The resolution of the data obtained from fluorescence lifetime experiments is better than those obtained from steady-state measurement. The fluorescence phenomenon occurs in the nanoseconds time-scale, the information gathered from steady-state may represent only the averaged behaviour of the events that happened during the entire scan. In contrast, information is captured in the nanoseconds time-scale during the fluorescence lifetime measurements. This makes the lifetime technique more relevant and preferable for studying dynamics in many chemical and biochemical processes. Analysis of the fluorescence lifetime can provide information about molecular species, and their states and environments. The variations in fluorescence lifetime

are always correlated to the change in physical and chemical properties like viscosity, pH, temperature, polarity and solvation.[89]

Fluorescence lifetime measurement can be performed either by frequency-domain or time-domain techniques. The main difference between these two techniques is the signal acquisition. In the frequency-domain technique, the lifetime information is obtained by comparing a sinusoidal modulated excitation signal with the resulting sinusoidal modulated fluorescence signal. In time-domain measurements, the fluorescence signal is recorded as function of time delay following pulsed excitations. Historically, the frequency-domain technique was first introduced, and it uses simpler electronic instrumentations and excitations source requirements. The time domain was established later with the used of advanced microelectronic devices and ultrafast laser technology. Even though both techniques (frequency-domain and time-domain) are able to provide equivalent information, the selection of the most suitable technique is usually made based on the target application. The both techniques possess their own advantages and disadvantages in terms of cost and complexity, performance and acquisition time.

Even though the frequency-domain measurement is more straightforward and cheaper compared to the time-domain measurement, it possesses clear limitations in analysing a multi-component decays in the picosecond time scale. In the time domain measurement, a sample will be excited with a laser pulse with a duration much shorter than the lifetime of the fluorophore and the decay of fluorescence is recorded over a certain time frame. The typical laser pulse duration is in the picoseconds range while the fluorescence lifetime for most fluorophore usually ranges from picoseconds to nanoseconds. The lifetime data can be extracted either by time gating or via time-correlated single-photon counting (TCSPC). In the time gating technique, several fluorescence decays are captured at different time delays using

a time-gated detector and the lifetime of the fluorophore is calculated by fitting the data from experimental intensity with an exponential function. The TCSPC is based on the repetitive detection of single photons over several time periods as illustrated in **Figure 16**. The typical detection rate is about 1 photon per 100 excitation pulses. The time taken between the excitation pulse and the arrival of the photons is recorded using a single photon sensitive detector, such as a Photomultiplier Tube (PMT), a Microchannel Plate PMT (MCP), a Single Photon Avalanche Diode (SPAD) or a Hybrid PMT. The recorded data is tabulated as histogram that will form the decay profile of the fluorophore.

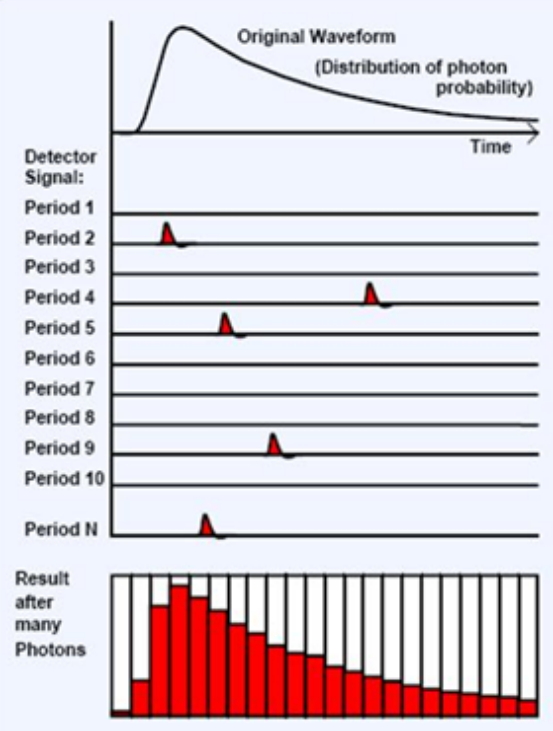

Figure 16: The principle of TCSPC. This figure is reproduced from other reference.[90]

The decay law postulates that if fluorophores are exposed to a pulse of light, a population of fluorophores will be excited to the excited state (n_o). The excited population will decay to the ground state with a rate constant of ($k_r + k_{nr}$) according to the equation **(3)**. The integrated form of equation **(3)** is presented as equation **(4)**. The decay process occurs randomly, and each of the excited fluorophores has the same probability to return to the ground state at any time.

$$\frac{dn}{dt} = -(k_r + k_{nr})n \tag{3}$$

$$n_t = n_\circ \times e^{-(k_r + k_{nr})t} = n_\circ \times e^{-(\frac{t}{\tau})} \tag{4}$$

The excited fluorophores decay exponentially to the ground state after *t* time. The lifetime (τ) is the reciprocal of the total decay rate of both rate constant i.e. $\tau = (k_r + k_{nr})^{-1}$. However, in the experiment the detector is not capable to directly count the exact number of excited molecules, but instead it measures intensity of light. The intensity of light is directly proportional to the number of excited molecules. Hence, the equation can also be expressed in terms of the time-dependent-intensity *I*.

$$I_t = I_\circ \times e^{-(\frac{t}{\tau})} \tag{5}$$

In the equation **(5)**, $I_\circ$ is the intensity at $t = 0$. The lifetime is then can be calculated from the slope of the decay plot of *ln I* versus *t*. In most cases, the lifetime is usually determined through a fitting the decay data using a mathematical model. As fluorescence lifetime is defined as the average time excited molecules spend in the excited state before they return to the ground state,

the average time <*t*> molecules spend in the excited state is obtained by averaging *t* over the intensity decay of the fluorophore according to the equation **(6)**.

$$\langle t \rangle = \frac{\int_{\circ}^{\infty} tI dt \quad \int_{\circ}^{\infty} te^{-(\frac{t}{\tau})} dt}{\int_{\circ}^{\infty} I dt \quad \int_{\circ}^{\infty} e^{-(\frac{t}{\tau})} dt} = \tau \qquad \textbf{(6)}$$

This is only applicable and true for a simple system with a mono-exponential decay. However, in most of real-life processes and complex systems, the excited molecules are usually exposed to a non-homogeneous environment and they are affected by various factors such as the presence of quenchers, energy-transfer processes between the members of population and different rates of molecular rotation. In a complex system where the photons decay is multi-exponential or non-exponential, a more rigorous method should be used to calculate the average lifetime. In the multi-exponential analysis, the photons are assumed to decay as the sum of individual single exponential decays and this statement can be translated into the mathematical equation as equation **(7)**.

$$I_t = \sum_{i=1}^{n} \alpha_i \, \mathrm{e}^{(\frac{-t}{\tau_i})} \qquad \textbf{(7)}$$

τ_i = decay time
α_i = amplitudes of the components at $t = 0$
n = number of decay times

This multi-exponential model can be used for both analyses, (i) analysis of samples that contain a mixture of fluorophores and (ii) analysis of samples that contain a single fluorophore that display a complex decay. The specific example of the latter case is the single-tryptophan protein which can exist in two states depending on the environment it is exposed to. If this

protein shows different conformations when it exposed and shielded from water, then each decay time can be assigned to each of the states. The meaning of the pre-exponential factor α_i is different for both cases. In the case of a single fluorophore that shows a complex decay, the fluorophore is assumed to have the same radiative decay rate in each environment. This means the α_i values represent the fraction of the molecules in each conformation at $t = 0$. In contrast, the meaning of α_i is more complex for samples that contain multiple fluorophores, when the relative value of α_i depends on many parameters including the concentration, absorption, quantum yields and intensities of each fluorophore. The value of α_i and τ_i can be used to determine the fractional contribution (f_1) of each decay time to the steady state intensity for both cases, however. The fractional contribution (f_i) is calculated using equation **(8)**.

$$f_i = \frac{\alpha_i \tau_i}{\sum_j \alpha_j \tau_j} \qquad \textbf{(8)}$$

For a sample containing more than one fluorophore, the f_i values represent the fractional intensity of each component(fluorophore) at the observation wavelength. However, these values may not have correlated to the expected intensities because of the complications of resolving a multi-exponential decay. The typical variable parameters in a multi-exponential analysis are n lifetimes and n or n-1 amplitudes. The total intensity is not measured in most multi-exponential analyses and both $\Sigma\alpha_i$ and Σf_i are normalized to unity. In the multi-exponential analyses, it is often useful to report the average lifetime. The average lifetime for a two-exponential decay can be calculated using equation **(9)**.

$$\bar{\tau} = \frac{\alpha_1 \tau_1^2 + \alpha_2 \tau_2^2}{\alpha_1 \tau_1 + \alpha_2 \tau_2} \qquad \textbf{(9)}$$

2.5 Fluorescent molecular rotors

One of the most classic example of fluorescent molecular rotors is *p*-*N*,*N*-dimethylamino benzonitrile (DMABN). The emission of DMABN in a polar solvent produces a dual emission spectrum which was first reported by Ernst Lippert in 1962.[91] **Figure 17** depicts the chemical structure of DMABN. He observed a dual fluorescence emission in solvents in which their polarity function (Δf) is in between 0.028 (1,4-dioxane) and 0.274 (*n*-butylnitrile). In the dual emission spectrum, the intensity of the red-shifted emission becomes stronger than the primary emission as the polarity of the solvent increases. The total emission intensity decreases as the polarity of solvents decreases, but the emission intensity increases as solvent viscosity increases. This was probably the starting point to the extensive and tremendous growth of research related to the syntheses and applications of molecular rotors. Today, many other molecular rotors have been synthesised, which are not limited to DMABN-related rotors. A model has been proposed by Grabowski and co-workers to explain the plausible mechanism of dual emission phenomenon of molecular rotors.[92] This model explains the dual emission phenomenon based on the formation of a twisted intramolecular charge transfer (TICT) complex.

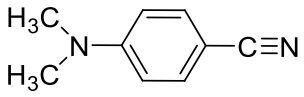

Figure 17: Chemical structure of DMABN.

The term 'molecular rotor' refers to a group of fluorescent molecules that can undergo an intramolecular charge transfer (ICT) process which induces formation of a complex called twisted intramolecular charge transfer (TICT) complex. The complex is formed via rotation of

one moiety in the fluorescence molecule. The rotation causes a change in the ground state and excited state energy levels. Upon light excitation, molecular rotors usually can return to the ground state from either the locally excited (LE) state or the TICT state. The relaxation from the twisted state usually has a lower energy compared to the one from the LE. The formation of the TICT is a solvent dependent process. The illustration of an intramolecular twisting process in DMABN is shown in **Figure 18**. The extent to which the molecule rotates depends on the viscosity and polarity of the solvent. This is the reason why molecular rotors have been extensively studied as a viscometer for probing and mapping the micro-viscosity in living cells,[12] polymers,[93] food products[94] and ionic liquids.[15]

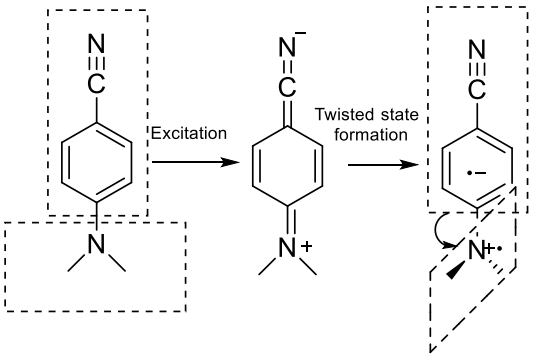

Figure 18: Illustration of intramolecular twisting process in DMABN.

The common features of molecular rotors are that they consist of three subunits, (i) an electron donor unit, (ii) an electron acceptor unit, and (iii) an electron-rich spacer unit that made up of alternating single and double bonds. The alternating single and double bonds link the donor and acceptor unit and thus enable the movement of electrons across the molecule. In the DMABN molecule, the electron donor group is dimethylamino, the electron acceptor group is

nitrile and the rest of molecule is the network for transferring electrons from the donor to the acceptor. In the ground state, the molecule is assumed to exist in a planar configuration and the excitation will induce delocalisation of electrons within the structure. The electrostatic forces will induce intramolecular charge transfer and the molecule will rotate to the non-planar (twisted) configuration. The energy profile diagram illustrating the excitation and relaxation process of the molecular rotor in planar and twisted configurations is shown in **Figure 19**.

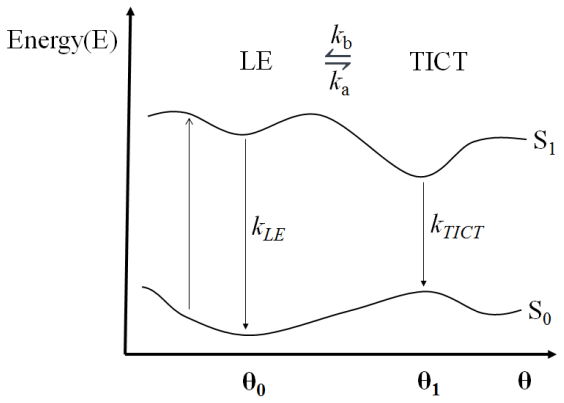

Figure 19: Energy profile diagram illustrates the relaxation processes of molecules in planar and twisted configurations.

Upon photon absorption, the rotor will be excited to the LE state in the planar configuration with the intramolecular rotation angle of zero or near zero(θ_0). Some of the excited LE molecules may undergo a 90°(θ_1) rotation induced by the intramolecular charge transfer process with a rate k_a and form the excited TICT molecule. The excited TICT molecule can return to the ground state with a rate k_{TICT} or else the molecule will return to the excited LE state with a rate k_b. However, the value of k_b is very small compared to the value of k_a. The LE

molecule will return to the ground state with a rate k_{LE}. Apart from temperature and pressure, the rate of change between the LE and TICT states depends on the polarity and viscosity of solvent.[95] Only one broad peak corresponding to the LE state is observed for the non-polar cyclohexane at excitation wavelengths ranging from 270–310 nm. In contrast, the emission of DMABN in the polar solvent acetonitrile shows a two-peak spectrum at excitation wavelengths ranging from 260–310 nm, which correspond the LE and TICT states. The intensities of the emission peak that correspond to the LE state increase with the increasing of excitation wavelength, but the peak corresponding to the TICT state shows a reverse trend to the LE state.

The viscosity dependence of the emission intensity of DMABN and other molecular rotors depends on many other factors such as twist angle, rotating volume of the twisting moiety, molecular shape, molecular size, etc. The size of the rotating moiety in DMABN is too small to cause a significant displacement of the solvent molecules in low viscosity molecular solvents such as cyclohexane and acetonitrile.[95] In addition, these low viscosity molecular solvents also exert very little friction to the twisting process. Thus, the TICT process of DMABN is found to be almost independent of viscosity in low viscosity media. However, the process shows the dependency on viscosity in moderate and high viscosity media.[96]

2.6 Correlation of fluorescence property of a molecular rotor to solvent viscosity

The fluorescence property of a molecular rotor (dye) can be utilised to estimate the viscosity of the solvent (*i.e.* solvating medium). The relationship between fluorescence quantum yield (ϕ) and solvent viscosity(η) is commonly expressed by a power-law, known as the Forster-Hoffmann equation **(10)**.[97,98]

$$\phi = C \cdot \left(\frac{\eta}{\sigma} \right)^{x} \qquad \textbf{(10)}$$

In the equation **(10)**, *C* is a dye-dependent constant, *x* is a dye and solvent dependent constant, and σ is a dye dependent constant related to the mechanical and electrostatic properties of the rotating moiety in the molecular rotor and has units of viscosity. The equation based on the assumption that the rotating moiety experiences micro-friction that can be linked to the bulk viscosity through the Debye-Stokes-Einstein model.[97]

For a molecular rotor, the fluorescence quantum yield (ϕ) and fluorescence lifetime (τ_f) are dependent on the angle of the internal torsional motion which affect the non-radiative rate constant (k_{nr}).[99] The relationship of these parameters is shown in equation **(11)**.

$$\phi = \frac{k_r}{k_r + k_{nr}} = k_r \tau_f \qquad \textbf{(11)}$$

In the literature, the constants *C* and σ^{-x} in equation **(10)** are often combined into a single constant, *z*, and thus the Forster-Hoffmann equation is reduced to:

$$\phi = z\eta^x \quad \textbf{(12)}$$

The combination of equation **(11)** and **(12)** yield the direct relationship between the fluorescence lifetime of a molecular rotor to viscosity.

$$z\eta^x = k_r\tau_f \quad \textbf{(13)}$$

$$\tau_f = \eta^x \times \frac{z}{k_r}$$

$$\log(\tau_f) = x\log\eta + \log(\frac{z}{k_r}) \quad \textbf{(14)}$$

Ideally, a plot of $\log\tau_f$ against $\log\eta$ will produce a straight line which can serve as a way to convert τ_f to η. Even though the fluorescence lifetime of molecular rotors generally increased with increasing viscosity of the solvent, it is quite rare to find an ideal system where the fluorescence lifetime changes linearly throughout the entire viscosity range studied as suggested by equation **(14)**. The log-log calibration plot of lifetime against viscosity of sulforhodamine B in glycerol/water mixtures and Cy3 in sucrose/water mixtures can only be fitted with a Hill Function instead of linear function.[100] In comparison, the log-log lifetime-viscosity calibration of BODIPY-C_{10} in methanol/glycerol mixtures seems to show a perfect linear relationship between 10 cP and 300 cP only and the deviation from linearity is obvious when the viscosity is less than 10 cP.[101] The fluorescence lifetime of 9-(2,2-dicyanovinyl)julolidine (DCVJ) increases linearly with increasing the viscosity of methanol/glycerol mixtures from 52 cP and 745 cP.[99] These observations suggest that this theoretical equation is not perfectly work for all system and may only be beneficial for very specific cases under certain conditions.

Chapter 3 Synthesis and Methodologies

3.1 Synthesis of low fluorescence background ionic liquids

The commercially available ionic liquids are usually not reliable, or at least they should be used with extra care, for any analytical research.[88] The production of low fluorescence background ionic liquids is essential for this project. This is because the ionic liquids produced are used in fluorescence lifetime experiments that utilised fluorescent molecular rotors to probe the viscosity of ionic liquids. Therefore, it is crucial to make sure that there is no external fluorescent species introduced to the ionic liquids during the synthesis stage. To achieve this objective, several specific aspects of the synthesis of the ionic liquids must be considered. These include the following:

a) The cleanliness of the glassware

   All glassware was washed thoroughly with 5 %(v/v) decon®90 solution in distilled water before rinsing with piranha solution (1:3, 30% hydrogen peroxide: 95-98% sulphuric acid). Piranha solution is a strong oxidising agent that will remove most organic residues from the surface of the glass. It will also hydroxylate the surface of the glassware making it highly hydrophilic. This will ease the cleaning of the glassware. After rinsing with piranha solution, the glassware was rinsed with distilled water to ensure total removal of all traces of contaminants and piranha solution remnants before performing a final rinse with ethanol. The glassware was then dried in a dedicated oven operating at 120°C. The use of grease on any joint of the glassware was avoided. Instead, thick-walled PTFE sleeves were used to eliminate the potential of contamination by grease.

b) Purity of the starting materials and solvents

The starting materials were extensively purified before use (see Section **3.1.1**), and dry solvents were used throughout the syntheses. The purchased solvents were of extra dry and extra pure grade (AcroSeal®) and were used as received. These solvents have moisture content less than 50 ppm and were stored over molecular sieves for prolonged shelf life. The synthesised ionic liquid precursors (halide intermediates) were recrystallized repeatedly until the colour of the solvent was colourless (see **Figure 20** for a visual picture of the recrystallisation process).

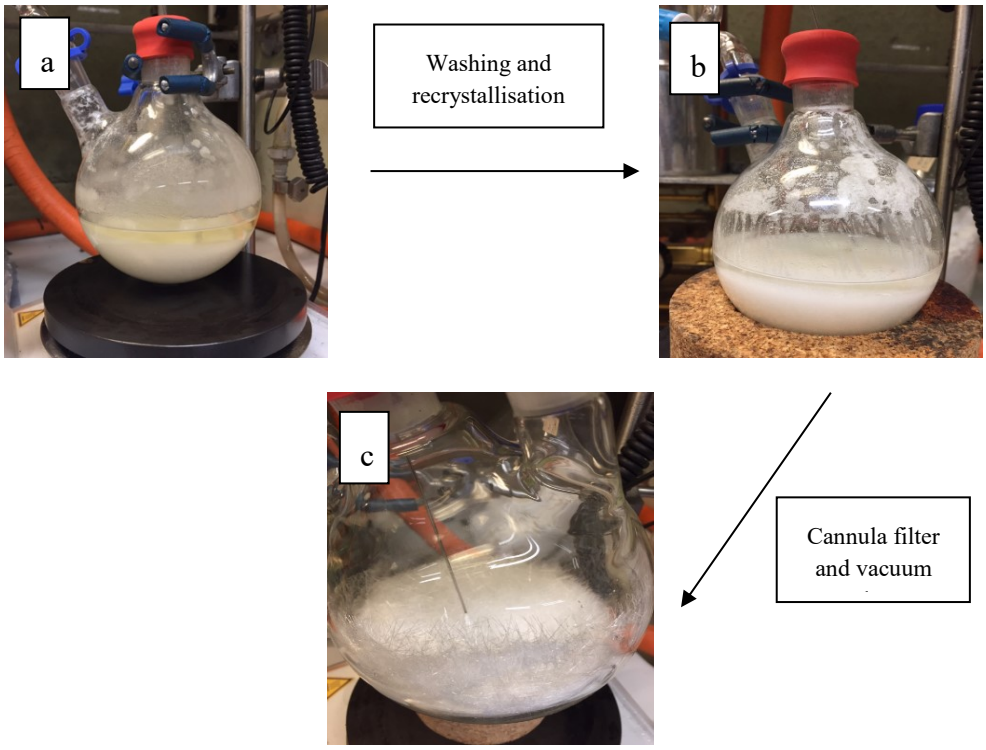

Figure 20: Purification of ionic liquid precursor. Picture (a) shows the yellowish solvent upon washing and first crystallisation process. Picture (b) shows the colourless solvent and white crystals after recrystallisation process. Picture (c) shows the final white crystals product of ionic liquid precursor.

c) Reaction conditions

Conventional methods for ionic liquid synthesis use a high temperature for the alkylation reaction to form the chloride intermediates (about 80°C) and the reaction can be completed in 2-3 days. The equivalent reactions were usually conducted at 50-60°C for making bromide intermediates and these reactions usually completed within 24 hours. Instead, in this work the reaction temperature for all the syntheses of halide intermediates (chloride or bromide salts) was kept mild *i.e.* about 65°C for forming the chloride intermediates and room temperature for bromide intermediates. The use of a lower temperature extends the time of reaction but based on our experience this is essential for minimising the formation of coloured contaminants in the halide intermediates. Removing the coloured contaminants from the chloride intermediates with a long alkyl chain ($6 \leq n < 12$) is a tedious process and sometimes total decolouration is not achievable. High temperatures (> 80 °C) can also lead to competitive side reactions such as the elimination reaction (see Section **3.2.1** and **Figure 24**) and cause charring, as well as alkyl chain scrambling of the cation.[24,84] **Figure 21** shows an example of scrambling of the 1-R_1-3-R_2-imidazolium cation. The low-temperature synthesis is suggested for making ionic liquids for spectroscopic works.[102] Additionally, all reactions should be performed in an inert environment of nitrogen or argon gas to prevent the absorption of moisture from the air.

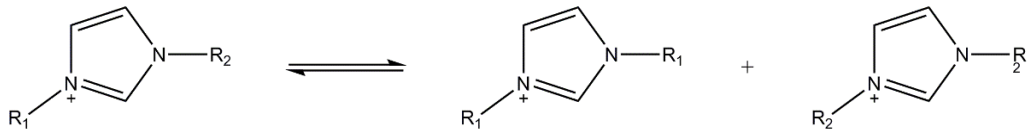

Figure 21:Scrambling of the 1-R_1-3-R_2-imidazolium cation.

d) Charcoal treatment

In order to produce a colourless and transparent ionic liquid. The final products were stirred with activated charcoal (Norit® SX ultra) for 24h followed by ordinary filtration using filter paper to remove the bulk of the charcoal. The liquids were then further filtered through a 0.2um PTFE filter to ensure complete removal of the particulates.

3.1.1 Purifications of starting materials

This section discusses the methodologies that were used to purify the starting materials in this study.

a) 1-methyllimidazole/N-methylpyrrolidine

1-methylimidazole and N-methylpyrrolidine were initially treated with potassium hydroxide (KOH) overnight. The mixture was distilled on the next day, and the distillate was collected. This process removes water from the starting materials. The distillate was then treated with freshly cut sodium metal (~1g sodium per 500 ml) and stirred overnight under nitrogen atmosphere. The mixture was distilled, and the distillate was collected for further use. The treatment of these chemicals with sodium metal is not only as part of the drying process but it also serves as the means for removing fluorescence contaminants from these chemicals.[75,103] Treatment of these chemicals with an alkali metal leads to the formation a black deposit onto the surface of the metal cubes. However, the fluorescence of the sample can only be reduced but not eliminated by this procedure.

b) Alkyl halides

The alkyl halides were shaken with concentrated sulphuric acid (H_2SO_4) repeatedly until the acid washing was colourless (see Figure 22 for visual picture). Then, the solutions were washed with distilled water followed by 5% aqueous solution of sodium bicarbonate ($NaHCO_3$) until the aqueous washing gave a pH equal to 5 or 6. This step was taken to remove the halogen acids and the alcohols originating from the preparation of the aliphatic haloalkanes.[104] The solutions were then washed again with distilled water before the organic layers were collected and treated with magnesium sulphate ($MgSO_4$) for 1 hour. The drying agent was then filtered off. This step is taken to remove the water originating from the washing process that might remain in the liquids. Finally, the liquids were dried over phosphorus pentoxide (P_2O_5) under nitrogen atmosphere overnight before being distilled to yield colourless liquids.

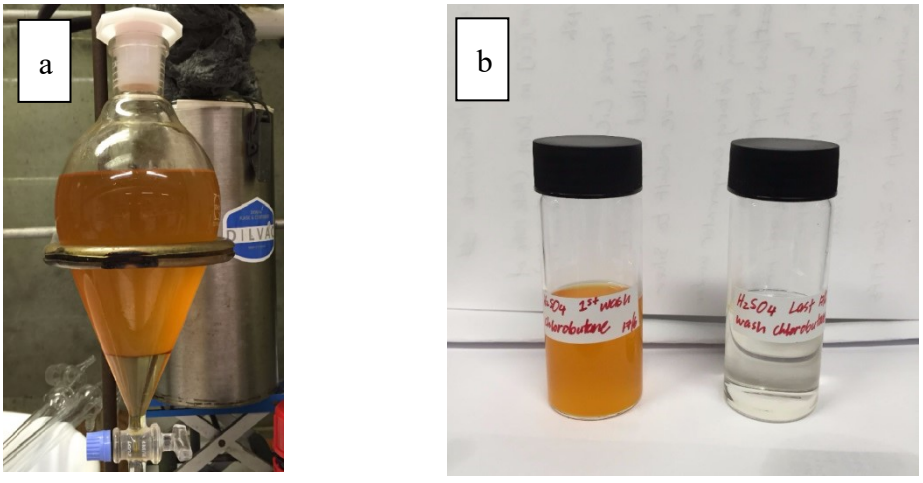

Figure 22: The purification of chlorobutane through washing with concentrated sulphuric acid (a) mixture of chlorobutane and sulphuric acid (b) the color of first acid washing (left) and last acid washing (right).

3.2 Synthesis of ionic liquids

3.2.1 General reaction

All ionic liquid precursors were synthesised via alkylation of 1-methylimidazole/N-methylpyrrolidine with the respective alkyl halide to produce the desired halide intermediate. The reaction occurred via a bimolecular nucleophilic substitution (S_N2) reaction. An example of the S_N2 reaction between 1-methylimidazole and 1-chlorobutane is shown in **Figure 23**. Typically, the nucleophilic substitution reaction is highly exothermic reaction and can lead to runaway reactions and the formation of side products.[88,105] Thus, as a precaution, the reaction was initially performed in an ice bath before the temperature was gradually increased if necessary, to a maximum temperature of 60°C. The reactivity of bromoalkanes in the alkylation reaction is high and thus the reaction is completed in hours or one day even it was performed at room temperature. In addition, the reactant was added slowly(dropwise) to prevent the formation of hot spots.[24]

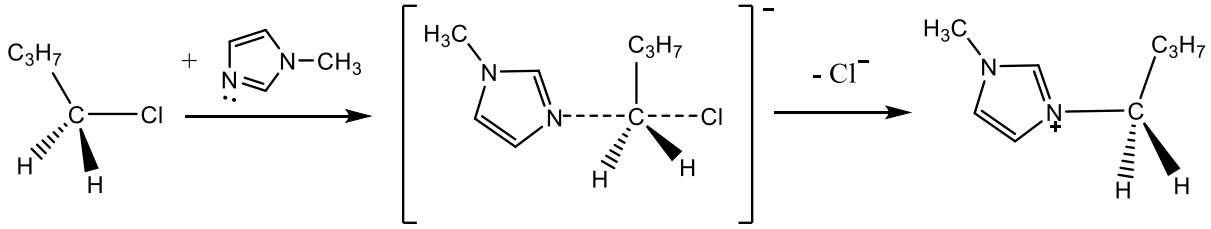

Figure 23: Formation of 1-butyl-3-methylimidazolium chloride via an S_N2 reaction.

It is also crucial to perform this reaction at a mild temperature to avoid competition from the bimolecular elimination reaction (E2) that could take place at elevated temperatures.[24] If the

E2 reaction occurs, the incoming 1-methylimidazole acts as a base rather than as a nucleophile. The base abstracts one of the protons from the haloalkane and leads to the formation of alkene. The E2 reaction is even more favourable if the incoming species is sterically hindered, which makes the proton abstraction easier. The possible E2 reaction mechanism between 1-methylimidazole and 1-chlorobutane is shown in **Figure 24**.

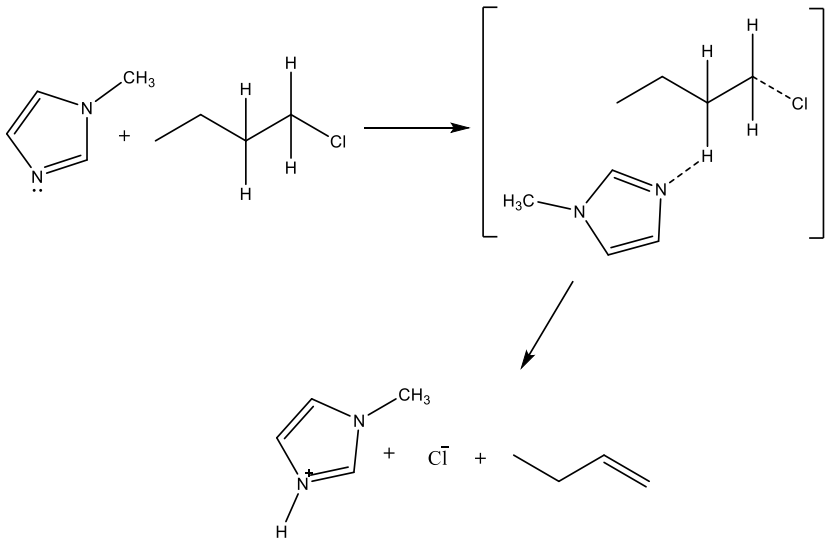

Figure 24: The possible E2 reaction mechanism between 1-methylimidazole and 1-chlorobutane.

The chloride or bromide intermediates produced from the alkylation were washed and recrystallised repeatedly (at least twice) before they were reacted with the respective lithium salt to produce the final product *i.e.* ionic liquid. The formation of the final product took place via a metathesis reaction. An example of the reaction scheme for formation of 1-butyl-3-methylimidazolium *bis*(trifluoromethylsulfonyl)imide, $[C_4C_1im][NTf_2]$, via the metathesis of

lithium *bis*(trifluoromethylsulfonyl)imide and 1-methyl-3-butylimidazolium chloride is shown in **Figure 25**.

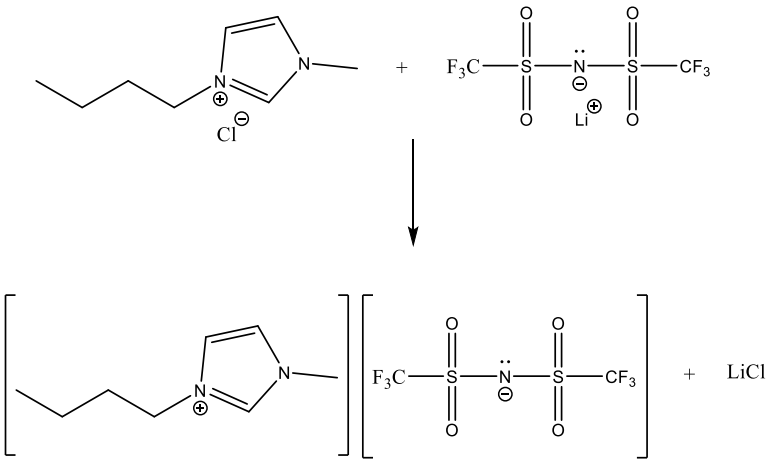

Figure 25: Metathesis reaction between halide intermediate and lithium salt.

The lithium chloride side product can be easily separated from the ionic liquid by filtration as they are insoluble with each other. Traces of the lithium salt that might have remained in the liquids was removed by careful washing of the ionic liquid with water. Silver nitrate was used as a confirmation test to test for the presence of chloride or bromide ions in the ionic liquid. Finally, the ionic liquid was washed with *n*-hexane in order to remove any organic impurities that might remained in the ionic liquids.[106] The solvent was then removed using rotary evaporator. The ionic liquid formed at this stage might not be colourless and optically transparent. Thus, treatment of the ionic liquid with activated charcoal becomes essential,[88,107] although this will result in loss of large amounts of the ionic liquid, typically >20%. The ionic liquid was stirred with activated charcoal overnight before being filtered with filter paper followed by filtration through a 0.2 μm PTFE filter to ensure complete removal of any

particulates. Finally, the liquid was dried in *vacuo* at 55-65°C for 2 days to remove any traces of water that remained in the ionic liquids. The low temperature was used here to avoid decomposition of the ionic liquid.[108] The details of syntheses and analytical results of each ionic liquid are presented in the following section (Section **3.2.2 – 3.2.19**).

3.2.2 Assessing fluorescence background of blank ionic liquids

The fluorescence background of the synthesized ionic liquids was evaluated by recording the absorption and emission spectra of blank ionic liquids and after addition of rotor dyes using a spectrofluorometer. It was also done by measuring the photon count number using a fluorescence microscope equipped with a time correlated single photon counting module. shows the excitation and emission spectra recorded for the as prepared $[C_4C_1im][NTf_2]$ ionic liquids. The $[C_4C_1im][NTf_2]$ ionic liquid prepared by unpurified starting materials showed a relatively higher excitation/emission background compared to the sample prepared using purified starting materials. Obviously, neither excitation nor emission peak can be observed from the spectra of purified sample indicating that the synthesized ionic is clean without any fluorophore. After addition of Cy3 into the purified ionic liquids, the excitation and emission maximum peaks are clearly observed at 561 nm and 573 nm, respectively. **Figure 27** shows the fluorescence excitation and emission spectra of ionic liquid in the before and after addition of Cy3.

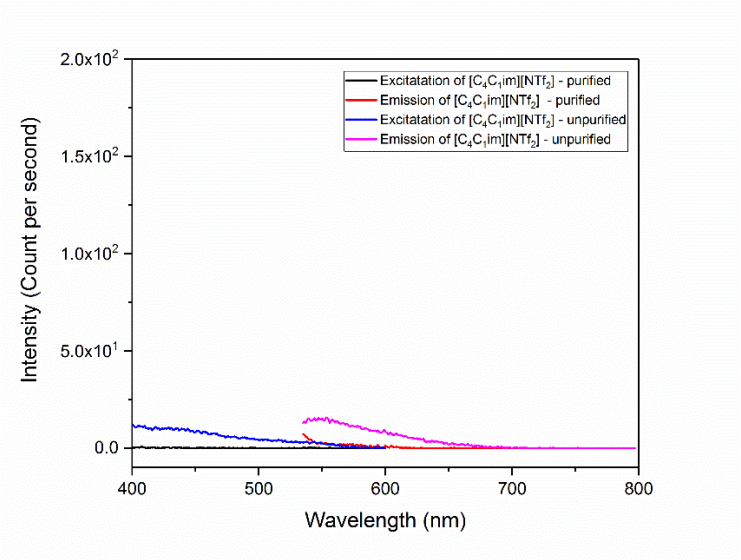

Figure 26: Fluorescence excitation and emission spectra of ionic liquids prepared using purified and unpurified starting materials.

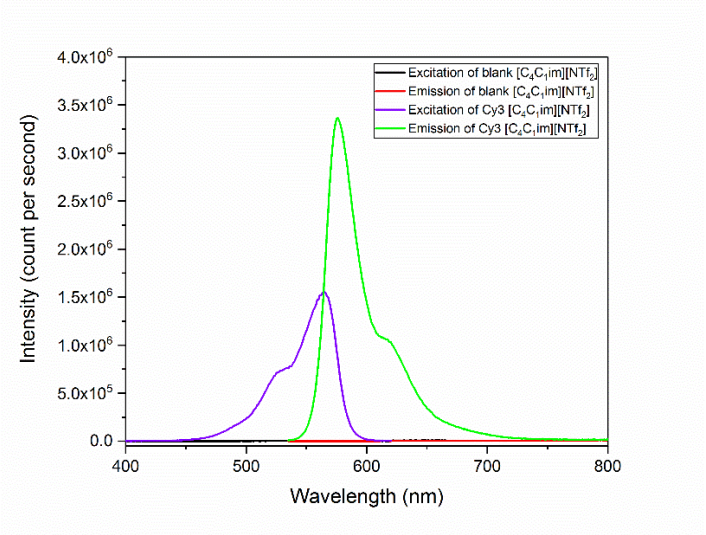

Figure 27: The excitation and emission spectra of purified ionic liquid in the absence and presence of Cy3. The excitation spectrum was acquired at 635nm and the emission spectrum is recorded at excitation wavelength of 520nm. Both excitation and emission slits were set at 2 nm.

The time-resolved fluorescence decay spectra were also recorded and used to monitor the fluorescence background of the ionic liquids in terms of photon count number. Because it is not possible to justify the absolute level of purity of sample in terms of photon count number, photon count number of ionic liquids were compared to the photon count generated by a non-fluorescence liquid *i.e.* deionized water. **Figure 28** shows the comparison of time-resolved fluorescence decays of two samples of $[C_4C_1im][NTf_2]$ prepared by two different procedures and compared to a deionized water sample.

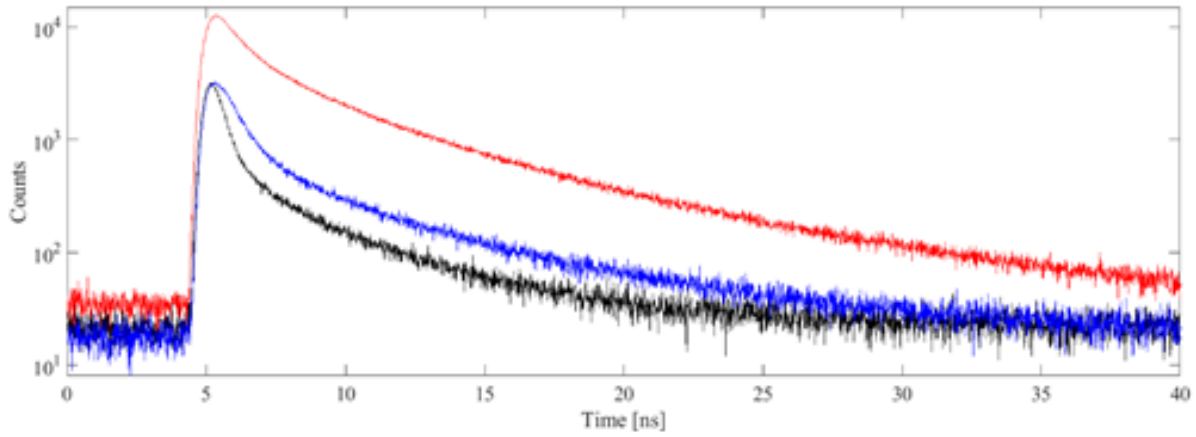

Figure 28: Time-resolved fluorescence decays of $[C_4C_1im][NTf_2]$ prepared by the standard synthetic procedures *i.e.* high reaction temperature >65˚C and un-purified starting materials (red), $[C_4C_1im][NTf_2]$ using the synthetic procedures stated in this work (blue) and deionized water (black).

It can be seen that the fluorescence background (maximum count number) of the $[C_4C_1im][NTf_2]$ sample, which was prepared via the synthetic procedures used in this study, is comparatively lower as compared the background of deionized water. In contrast, the photon count number for $[C_4C_1im][NTf_2]$ prepared by the normal synthetic procedure showed a higher

fluorescence background. It is about one order of magnitude higher than the other sample although physically both [C_4C_1im][NTf_2] samples appeared as colourless and clear liquids after being treated with activated charcoal prior to the fluorescence measurement. All the ionic liquids used for the fluorescence lifetime experiments in this work have the photon count number less than 10^4. The time-resolve fluorescence decays of other ionic liquids are presented the appendices in Section 7.4.

3.2.3 Synthesis of 1-ethyl-3-methylimidazolium bromide [C_2C_1im]Br

1-bromoethane (150 ml, 2.01 mol, 1.1 equivalent) was added dropwise to a cooled solution of 1-methylimidazole (146 ml, 1.82 mol, 1 equivalent) in 250 ml of dry ethyl acetate under constant stirring. The reaction mixture was stirred overnight at room temperature. White solid crystals were formed and the solvent was decanted from the flask via cannula filteration. The solid crystals were washed with extra dry ethyl acetate (3 × 100 ml) and dried under vacuum at room temperature. The white crystals were then dissolved in 200 ml of acetonitrile at 35°C and then left to recrystalise at -20°C overnight. The recrystallisation step was repeated twice. The solvent was then removed by cannula filtration and the white solid crystals were dried under vacuum for two days before further use (273 g, 78% yield).

^{1}H NMR (400MHz, DMSO-*d_6*) δ 9.37 (1H, s, N**C**HN), 7.88 (1H, s, NC**H**CHN), 7.78 (1H, s, NCHC**H**N), 4.22 (2H, t, $^3J_{HH}$ 7.3Hz, NC**H**$_2$CH$_3$), 3.88 (3H, s, NC**H**$_3$), 1.40 (3H, t, $^3J_{HH}$ 7.3Hz, NCH$_2$C**H**$_3$).

^{13}C NMR (100MHz, DMSO-*d_6*) δ 136.76 (s, N**C**HN), 123.97 (s, N**C**HCHN), 122.44 (s, NCH**C**HN), 44.57 (s, N**C**H$_2$CH$_3$), 36.23 (s, N**C**H$_3$), 15.66 (s, NCH$_2$**C**H$_3$).

m/z (ES$^+$) 111.09 ([C_2C_1im]$^+$, 100%); (ES$^-$) 79 ([^{79}Br]$^-$, 100%); (ES$^-$) 81([^{81}Br]$^-$, 97%)

Elemental analysis predicted C 37.69%, H 5.80%, N 14.66%

Elemental analysis measured C 37.80%, H 5.69%, N 14.49%

3.2.4 Synthesis of 1-ethyl-3-methylimidazolium *bis*(trifluoromethyl sulfonyl)imide [C_2C_1im][NTf_2]

In a 500 ml round bottom flask, lithium *bis*(trifluoromethylsulfonyl)imide (50.00 g, 0.17 mol, 1 equivalent) was added to a solution of 1-ethyl-3-methylimidazolium bromide (33.28 g, 0.17 mol, 1 equivalent) in 250 ml dichloromethane. The mixture was stirred overnight at room temperature. The white solid of lithium bromide was removed by filtration and the filtrate was then washed repeatedly with distilled water (6×50 ml) until the aqueous phase was confirmed free of bromide ion, via the silver nitrate test. The solvent was removed on the rotary evaporator and the resulting liquid was washed with 100 ml *n*-hexane before evaporating any remaining solvent. The resulted colourless oily liquid was stirred with activated charcoal overnight and then filtered through filter paper followed by a 0.2 μm PTFE membrane filter. The resulting liquid was dried *in vacuo* at 55 °C for 2 days to give a clear viscous liquid (58.67 g, 86 % yield).

^{1}H NMR (400MHz, DMSO-*d*$_6$) δ 7.97 (1H, s, N**C**HN), 6.91 (1H, s, NC**H**CHN), 6.84 (1H, s, NCHC**H**N), 3.66 (2H, q, $^3J_{HH}$ 7.3Hz, NC**H**$_2$CH$_3$), 3.34 (3H, s, NC**H**$_3$), 0.94 (3H, t, $^3J_{HH}$ 7.4Hz, NCH$_2$C**H**$_3$).

^{13}C NMR (101MHz, DMSO-*d*$_6$) δ 135.15 (s, N**C**HN), 124.05 (s, N**C**HCHN), 121.21 (s, NCH**C**HN), 119.28 (q, $^1J_{CF}$ 320.6Hz, **C**F$_3$), 44.20 (s, N**C**H$_2$CH$_3$), 34.92 (s, N**C**H$_3$), 13.54 (s, NCH$_2$**C**H$_3$).

m/z (ES$^+$) 111.1 ([C_2C_1im]$^+$, 100%); (ES$^-$) 279.8 ([NTf_2]$^-$, 100%)

Elemental analysis predicted C 24.54%, H 2.83%, N 10.74%
Elemental analysis measured C 24.96%, H 2.93%, N 10.44%

3.2.5 Synthesis of 1-propyl-3-methylimidazolium bromide [C_3C_1im]Br

1-bromopropane (150 ml, 1.65 mol, 1.1 equivalent) was added dropwise to a cooled and stirring solution of 1-methylimidazole (120 ml, 1.50 mol, 1 equivalent) in 200 ml of dry ethyl acetate. Once the addition was completed, the solution was left under continuous stirring overnight. Crystallisation of the product was observed the next day. The solvent and remaining reactants were removed by cannula filtration. The resulting crystals were washed with dry ethyl acetate (3 × 100 ml) and the product dissolved in acetonitrile and left to recrystallise from the solvent at -20°C. The recrystallisation process was repeated twice. The solvent was then removed by cannula filtration and the white solid crystals dried under vacuum for 2 days before further use. (72.8 g, 88 %yield).

^{1}H NMR (400MHz, DMSO-d_6) δ 9.30 (1H, s, N**C**HN), 7.84 (1H, s, NC**H**CHN), 7.77 (1H, s, NCHC**H**N), 4.16 (2H, t, $^3J_{HH}$ 7.3Hz, NC**H**$_2$ CH_2CH_3), 3.88 (3H, s, NC**H**$_3$), 1.80 (2H, t, NCH_2 C**H**$_2CH_3$), 0.85 (3H, t, $^3J_{HH}$ 7.4Hz, NCH_2CH_2C**H**$_3$).

^{13}C NMR (101MHz, DMSO-d_6) δ 137.02 (s, N**C**HN), 124.06 (s, N**C**HCHN), 122.74 (s, NCH**C**HN), 50.68 (s, N**C**$H_2CH_2CH_3$), 36.26 (s, N**C**H_3), 36.26 (s, NCH_2**C**H_2CH_3), 15.66 (s, NCH_2CH_2**C**H_3).

m/z (ES^+) 111.09 ($[C_2C_1im]^+$, 100%); (ES^-) 79 ($[^{79}Br]^-$, 100%); (ES^-) 81($[^{81}Br]^-$, 97%)

Elemental analysis (predicted) C 40.96%, H 6.39%, N 13.66%

Elemental analysis (measured) C 39.55%, H 6.74%, N 13.03%

3.2.6 Synthesis of 1-propyl-3-methylimidazolium *bis*(trifluoromethyl sulfonyl)imide [C_3C_1im][NTf_2]

Lithium bis(trifluoromethylsulfonyl)imide (45.00 g, 0.16 mol, 1 equivalent) and 1-propyl-3-methylimidazolium bromide (32.15 g, 0.16 mol, 1 equivalent) were mixed and stirred in 150 ml of dichloromethane and left under vigorous stirring overnight. The next day, the mixture

was filtered to remove the solid lithium bromide side product and the filtrate was then washed repeatedly with water (8 × 50 ml) until the aqueous phase gives a negative result to the silver nitrate test. The dichloromethane was removed under low heat on a rotary evaporator. The resulting liquid was washed with 100ml *n*-hexane before evaporating any remaining solvent. The resulting ionic liquid was then treated with activated charcoal at room temperature overnight. The bulk of the charcoal was removed with standard filtration using a filter paper followed by a 0.2 μm PTFE filter to ensure a complete removal of particulates. The filtrate was washed with 100ml n-hexane before the liquid was then dried overnight at 55 °C to yield a clear, colourless liquid (55.91 g, 88 % yield).

^{1}H NMR (400MHz, DMSO-*d*$_6$) δ 7.98 (1H, s, N**C**HN), 6.89 (1H, s, NC**H**CHN), 6.83 (1H, s, NCHC**H**N), 3.56 (2H, t, $^{3}J_{HH}$ 7.3Hz, NC**H**$_2$CH$_2$CH$_3$), 3.32 (3H, s, NC**H**$_3$), 1.30 (2H, h, $^{3}J_{HH}$ 7.3Hz, NCH$_2$C**H**$_2$CH$_3$), 0.32 (3H, t, $^{3}J_{HH}$ 7.4Hz, NCH$_2$CH$_2$C**H**$_3$).

^{13}C NMR (101MHz, DMSO-*d*$_6$) δ 135.39 (s, N**C**HN), 124.02 (s, N**C**HCHN), 122.88 (s, NCH**C**HN), 119.24 (q, $^{1}J_{CF}$ 320.6Hz, **C**F$_3$), 50.45 (s, N**C**H$_2$CH$_2$CH$_3$), 34.92 (s, N**C**H$_3$), 22.37 (s, NCH$_2$**C**H$_2$CH$_3$), 8.92 (s, NCH$_2$CH$_2$**C**H$_3$).

m/z (ES$^+$) 125.1 ([C$_2$C$_1$im]$^+$, 100%); (ES$^-$) 279.8 ([NTf$_2$]$^-$, 100%)

Elemental analysis (predicted) C 26.65%, H 3.23%, N 10.37%

Elemental analysis (actual) C 26.81%, H 3.04%, N 10.20%

3.2.7 Synthesis of 1-butyl-3-methylimidazolium chloride [C$_4$C$_1$im]Cl

1-chlorobutane (340 ml, 3.26 mol, 1.1 equivalent) was added dropwise to a cooled solution of 1-methylimidazole (235 ml, 2.96 mol, 1 equivalent) in 200 mL of extra dry ethyl acetate under constant stirring. The reaction mixture was stirred for 1 week at room temperature. The temperature was then increased gradually, in 10°C steps every 4 days, and finally held at 60°C for 3 weeks. Over this period, two layers were formed, and subsequently the reaction flask was

kept at -20°C for 2 days to induce the crystallisation process. After the crystallisation, the solvent was decanted, and the crystals washed with extra dry ethyl acetate (2 × 150 mL) before then recrystallising from acetonitrile twice to yield solid white crystals. The solid crystals were dried under vacuum before further use. (295.41 g, 57 % yield).

^{1}H NMR (400MHz, DMSO-*d*$_6$) δ 9.22 (1H, s, N**C**HN), 7.80 (1H, s, NC**H**CHN), 7.73 (1H, s, NCHC**H**N), 4.18 (2H, t, $^{3}J_{HH}$ 7.2Hz, NC**H**$_2$CH$_2$CH$_2$CH$_3$), 3.86 (3H, s, NC**H**$_3$),1.77 (2H, p, $^{3}J_{HH}$ 7.4Hz, NCH$_2$C**H**$_2$CH$_2$CH$_3$), 1.27 (2H,h, $^{3}J_{HH}$ 7.4Hz, N(CH$_2$)$_2$C**H**$_2$CH$_3$), 0.91 (3H, t, $^{3}J_{HH}$ 7.4Hz, N(CH$_2$)$_3$C**H**$_3$).

^{13}C NMR (101MHz, DMSO-*d*$_6$) δ 137.16 (s, N**C**HN), 124.09 (s, N**C**HCHN), 122.75 (s, NCH**C**HN), 48.94 (s, N**C**H$_2$(CH$_2$)$_2$CH$_3$), 36.21 (s, N**C**H$_3$), 31.83 (s, NCH$_2$**C**H$_2$CH$_2$CH$_3$), 19.24 (s, N(CH$_2$)$_2$**C**H$_2$CH$_3$), 13.75 (s, N(CH$_2$)$_3$**C**H$_3$).

m/z (LSIMS^{+}) 139([C$_4$C$_1$im]$^{+}$, 100%); (LSIMS^{-}) 35([^{35}Cl]$^{-}$, 100%), 37 ([^{37}Cl]$^{-}$, 33%)

Elemental analysis (predicted) C 55.96%, H 8.59%, N 16.03%
Elemental analysis (measured) C 56.08%, H 8.56%, N 15.69%

3.2.8 Synthesis of 1-butyl-3-methylimidazolium *bis*(trifluoromethyl sulfonyl)imide [C$_4$C$_1$im][NTf$_2$]

In a 500 ml round bottom flask, lithium *bis*(trifluoromethylsulfonyl)imide (71.15 g, 0.25 mol, 1 equivalent) was added to solution of 1-butyl-3-methylimidazolium chloride (43.29 g, 0.25 mol, 1 equivalent) in 300 ml of dichloromethane. The mixture was stirred for 24 hours at room temperature before filtering through filter paper. The filtrate was then washed copiously with distilled water (8 × 50 ml) until the aqueous phase became chloride free. Each of the aqueous washing was tested with silver nitrate. The solvent was removed on the rotary evaporator and the resulting liquid was washed with 150ml *n*-hexane before evaporating any remaining solvent. The obtained oily liquid was stirred with activated charcoal overnight and then filtered

through a standard filter paper followed by a 0.2 μm PTFE membrane filter. The resulting liquid was dried *in vacuo* at 55°C for 2 days to give clear viscous liquid (60.77 g, 58 % yield).

^{1}H NMR (400MHz, DMSO-d_6 capillary) δ 8.01 (1H, s, NC**H**N), 6.92 (1H, s, NC**H**CHN), 6.85 (1H, s, NCHC**H**N), 3.62 (2H, t, $^{3}J_{HH}$ 7.4Hz, NC**H**$_2$CH$_2$CH$_2$CH$_3$), 3.35 (3H, s, NC**H**$_3$),1.30 (2H, p, $^{3}J_{HH}$ 7.6Hz, NCH$_2$C**H**$_2$CH$_2$CH$_3$), 0.78 (2H, h, $^{3}J_{HH}$ 7.4Hz, N(CH$_2$)$_2$C**H**$_2$CH$_3$), 0.35 (3H, t, $^{3}J^{HH}$ 7.4Hz, N(CH$_2$)$_3$C**H**$_3$).

^{13}C NMR (101MHz, DMSO-d_6 capillary) δ 135.42 (s, N**C**HN), 122.89 (s, N**C**HCHN), 121.63 (s, NCH**C**HN), 119.30 (m, $^{1}J_{CF}$ 320.7Hz, **C**F$_3$), 48.85 (s, N**C**H$_2$ (CH$_2$)$_2$CH$_3$), 34.96 (s, NCH$_3$), 30.99 (s, NCH$_2$CH$_2$CH$_2$CH$_3$), 18.34 (s, N(CH$_2$)$_2$**C**H$_2$CH$_3$), 11.85 (N(CH$_2$)$_3$**C**H$_3$).

m/z (LSIMS$^+$) 139 ([C$_4$C$_1$im]$^+$, 100%); (LSIMS$^-$) 281 ([NTf$_2$]$^-$, 100%)

Elemental analysis (predicted) C 28.61%, H 3.57%, N 10.02%
Elemental analysis (measured) C 28.75%, H 3.66%, N 10.16%

3.2.9 Synthesis of 1-hexyl-3-methylimidazolium chloride [C$_6$C$_1$im]Cl

A solution of 1-methylimidazole (120 ml, 1.51 mol, 1 equivalent) in 200ml of dry acetonitrile was prepared in a 1000 ml round bottom flask. The mixture was cooled in an ice bath. 1-chlorohexane (227 ml, 1.66 mol, 1.1 equivalent) was then added dropwise to the solution. Once the addition was completed, the solution was stirred at room temperature for 1 week. The reaction temperature was heated to 60°C for 3 weeks. Two layers formed, and the lower ionic liquid layer was removed and washed with dry ethyl acetate and acetonitrile (5:1) (3 × 100 ml) before drying under vacuum. This resulted in a slightly pale yellow, viscous liquid (229.58 g, 75 % yield).

^{1}H NMR (400MHz, DMSO-d_6) δ 9.80 (1H, s, N**C**HN), 8.02 (1H, s, NC**H**CHN), 7.93 (1H, s, NCHC**H**N), 4.22 (2H, t, $^{3}J_{HH}$ 7.2Hz, NC**H**$_2$CH$_2$CH$_2$CH$_2$CH$_2$CH$_3$), 3.90 (3H, s, NC**H$_3$**),1.80 - 1.72(2H, m, NCH$_2$C**H**$_2$CH$_2$CH$_3$), 1.23 - 1.13 (6H, m, NCH$_2$CH$_2$C**H**$_2$C**H**$_2$C**H**$_2$CH$_3$), 0.84 - 0.76 (3H, m , N(CH$_2$)$_5$C**H**$_3$).

^{13}C NMR (101MHz, DMSO-*d*$_6$) δ 137.30 (s, N**C**HN), 123.99 (s, N**C**HCHN), 122.75 (s, NCH**C**HN), 49.02 (s, N**C**H$_2$(CH$_2$)$_3$CH$_3$), 36.11 (s, N**C**H$_3$), 31.02(s, NCH$_2$**C**H$_2$CH$_2$CH$_2$CH$_2$CH$_3$), 29.90 (s, NCH$_2$CH$_2$**C**H$_2$CH$_2$CH$_2$CH$_3$), 25.59(s, NCH$_2$CH$_2$CH$_2$**C**H$_2$CH$_2$CH$_3$), 22.34(s, NCH$_2$CH$_2$CH$_2$CH$_2$**C**H$_2$CH$_3$), 14.24(s, NCH$_2$CH$_2$CH$_2$CH$_2$CH$_2$**C**H$_3$).

m/z (ES$^+$) 167.15 ([C$_6$C$_1$im]$^+$, 100%); (ES$^-$) 34.9([^{35}Cl]$^-$, 100%), 36.9 ([^{37}Cl]$^-$, 33%)

Elemental analysis (predicted) C 59.20%, H 9.45%, N 13.82%
Elemental analysis (measured) C 58.93%, H 9.15%, N 12.51%

3.2.10 Synthesis of 1-hexyl-3-methylimidazolium *bis*(trifluoromethyl sulfonyl)imide [C$_6$C$_1$im][NTf$_2$]

In a 500 ml round bottom flask, 1-hexyl-3-methylimidazolium chloride (35.30 g, 0.17mol, 1 equivalent) was dissolved in 200 ml of dichloromethane. Lithium *bis*(trifluoromethylsulfonyl)imide (50.00 g, 0.17 mol, 1 equivalent) was added to the solution and the mixture was stirred overnight at room temperature. The reaction mixture was then filtered and the filtrate washed copiously with distilled water (7 × 50 mL) until the aqueous phase became chloride free, which was confirmed by the silver nitrate test. The solvent was removed on a rotary evaporator and the resulting liquid was washed with 150ml *n*-hexane before evaporating any remaining solvent. The obtained oily liquid was stirred with activated charcoal overnight and then filtered through filter paper followed by filtration through a 0.2 µm PTFE membrane filter. The resulting liquid was dried *in vacuo* at 55 °C for 2 days to give a clear viscous liquid (48.31 g, 62% yield).

^{1}H NMR (400MHz, DMSO-*d*$_6$ capillary) δ 8.06 (1H, s, NC**H**N), 6.94 (1H, s, NC**H**CHN), 6.86 (1H, s, NCHC**H**N), 3.64 (2H, t, $^3J_{HH}$ 7.4Hz, NC**H**$_2$CH$_2$CH$_2$CH$_2$CH$_2$CH$_3$), 3.36 (3H, s, NC**H**$_3$), 1.47-1.22 (2H, m, NCH$_2$C**H**$_2$CH$_2$CH$_2$CH$_2$CH$_3$), 0.98-0.61 (6H, m, NCH$_2$CH$_2$C**H**$_2$C**H**$_2$C**H**$_2$CH$_3$), 0.31 (3H, t, NCH$_2$CH$_2$CH$_2$CH$_2$CH$_2$C**H**$_3$).

^{13}C NMR (101MHz, DMSO-*d*$_6$ capillary) δ 135.43 (s, N**C**HN), 122.92 (s, N**C**HCHN), 121.66 (s, NCH**C**HN), 116.13 (m, $^1J_{CF}$ 320.7Hz, **C**F$_3$), 49.13 (s, N**C**H$_2$ (CH$_2$)$_4$CH$_3$), 35.00(s, N**C**H$_3$),

30.19 (s, $NCH_2\mathbf{C}H_2CH_2CH_2CH_2CH_3$), 29.14 (s, $NCH_2CH_2\mathbf{C}H_2CH_2CH_2CH_3$), 24.84 (s, $NCH_2CH_2CH_2\mathbf{C}H_2CH_2CH_3$), 21.41 (s, $NCH_2CH_2CH_2CH_2\mathbf{C}H_2CH_3$), 12.55 (s, $NCH_2CH_2CH_2CH_2CH_2\mathbf{C}H_3$).

m/z (ES^+) 167.1 ($[C_6C_1im]^+$, 100%); (ES^-) 279.8 ($[NTf_2]^-$, 100%)

Elemental analysis (predicted) C 32.19%, H 4.28%, N 9.39%
Elemental analysis (measured) C 32.07%, H 4.17%, N 9.31%

3.2.11 Synthesis of 1-octyl-3-methylimidazolium *bis*(trifluoromethyl sulfonyl)imide $[C_8C_1im][NTf_2]$

This ionic liquid was synthesised by Ryan Clark, member of Welton Research Group. Upon receiving the sample, it was treated with activated charcoal overnight and the bulk charcoal was removed following standard procedures i.e. using a standard filter paper followed by filtration through a 0.2 μm PTFE membrane filter. The resulting liquid was dried *in vacuo* at 55 °C for 2 days to give colourless and transparent viscous liquid.

^{1}H NMR (400MHz, DMSO-*d*$_6$ capillary) δ 8.10 (1H, s, NC**H**N), 6.97 (1H, s, NC**H**CHN), 6.89 (1H, s, NCHC**H**N), 3.67 (2H, t, $^3J_{HH}$ 7.3Hz, $NC\mathbf{H}_2CH_2(CH_2)_5CH_3$), 3.39 (3H, s, $NC\mathbf{H}_3$), 1.38 (2H, q, $NCH_2C\mathbf{H}_2(CH_2)_5CH_3$), 0.97-0.57 (10H, m, $NCH_2CH_2(C\mathbf{H}_2)_5CH_3$), 0.35 (3H, t, $^3J_{HH}$ 7.3Hz, $NCH_2CH_2(CH_2)_5C\mathbf{H}_3$).

^{13}C NMR (101MHz, DMSO-*d*$_6$ capillary) δ 135.47 (s, N**C**HN), 122.97 (s, N**C**HCHN), 121.70 (s, NCH**C**HN), 116.16 (m, $^1J_{CF}$ 320.8Hz, $\mathbf{C}F_3$), 49.19 (s, $N\mathbf{C}H_2$ $(CH_2)_6CH_3$), 35.05(s, $N\mathbf{C}H_3$), 30.97 (s, $NCH_2\mathbf{C}H_2CH_2CH_2CH_2CH_2CH_2CH_3$), 29.29 (s, N $NCH_2CH_2\mathbf{C}H_2CH_2CH_2CH_2CH_2CH_3$), 28.23 (s, $NCH_2CH_2CH_2\mathbf{C}H_2CH_2CH_2CH_2CH_3$), 28.13 (s, $NCH_2CH_2CH_2CH_2\mathbf{C}H_2CH_2CH_2CH_3$), 25.30 (s, $NCH_2CH_2CH_2CH_2CH_2\mathbf{C}H_2CH_2CH_3$), 21.79 (s, $NCH_2CH_2CH_2CH_2CH_2CH_2\mathbf{C}H_2CH_3$), 12.85 (s, $NCH_2CH_2CH_2CH_2CH_2CH_2CH_2\mathbf{C}H_3$).

m/z (ES^+) 195.2 ($[C_8C_1im]^+$, 100%); (ES^-) 279.9 ($[NTf_2]^-$, 100%)

Elemental analysis (predicted) C 35.34%, H 4.88%, N 8.84%

Elemental analysis (actual) C 35.55%, H 4.82%, N 8.99%

3.2.12 Synthesis of 1-dedocyl-3-methylimidazolium chloride [$C_{12}C_1$im]Cl

In a 1000 ml round bottom flask, 1-methylimidazole (61 ml, 0.77 mol, 1 equivalent) was mixed with 150 ml of dry ethyl acetate. The mixture was cooled in ice bath, and 1-chlorododecane (200 ml, 0.85 mol, 1.1 equivalent) was added dropwise to the mixture. The mixture was stirred under a nitrogen environment at room temperature for three days before the reaction temperature was increased gradually, in steps of 10°C every three-day until maximum temperature of 55°C. After three weeks the reaction mixture was cooled to room temperature, and the solvent removed under vacuum using a rotary evaporator to yield a yellowish greasy solid. The solid was washed three times with 100mL of dry ethyl acetate and acetonitrile (5:1). The greasy solid dissolved in acetonitrile at 35°C and a white solid precipitated out from the solvent upon cooling in a dry ice bath. The solvent was removed by cannula filter, and the final product was dried at 35°C under vacuum (160 g, 72% yield).

^{1}H NMR (400MHz, DMSO-*d_6*) δ 9.44 (1H, s, N**C**HN), 7.86 (1H, s, NC**H**CHN), 7.79 (1H, s, NCHC**H**N), 4.21 (2H, t, $^3J_{HH}$ 8Hz, NC**H**$_2$CH$_2$(CH$_2$)$_9$CH$_3$), 3.88 (3H, s, NC**H**$_3$), 1.76(2H, q, NCH$_2$C**H**$_2$(CH$_2$)$_9$CH$_3$), 1.24(18H, s, NCH$_2$CH$_2$(C**H**$_2$)$_9$CH$_3$), 0.85 (3H, t, $^3J_{HH}$ 6.6Hz NCH$_2$CH$_2$(CH$_2$)$_9$C**H**$_3$).

^{13}C NMR (101MHz, DMSO-*d_6*) δ 137.15 (s, N**C**HN), 124.04 (s, N**C**HCHN), 122.73 (s, NCH**C**HN), 49.16 (s, N**C**H$_2$C$_{11}$H$_{23}$), 40.43 (s, N**C**H$_3$), 36.18(s, N-CH$_2$-**C**H$_2$-C$_{10}$H$_{23}$), 31.77(s, NC$_2$H$_4$-**C**H$_2$-C$_9$H$_{19}$), 29.91(s, N-C$_3$H$_6$-**C**H$_2$-C$_8$H$_{17}$), 29.50(s, N-C$_4$H$_8$-**C**H$_2$-C$_7$H$_{15}$), 29.43(s, N-C$_5$H$_{10}$-**C**H$_2$-C$_6$H$_{13}$), 29.32(s, N-C$_6$H$_{12}$-**C**H$_2$-C$_5$H$_{11}$), 29.19(s, N-C$_7$H$_{14}$-**C**H$_2$-C$_4$H$_9$), 28.88(s, N-C$_8$H$_{16}$-**C**H$_2$-C$_3$H$_7$), 25.98(s, N-C$_9$H$_{18}$-**C**H$_2$-C$_2$H$_5$), 22.57(s, N-C$_{10}$H$_{20}$-**C**H$_2$-C$_2$H$_5$), 14.41(s, N-C$_{11}$H$_{22}$-**C**H$_3$).

m/z (ES$^+$) 251.2 ([$C_{12}C_1$im]$^+$, 100%); (ES$^-$) 34.9 ([^{35}Cl]$^-$, 71%); (ES$^-$) 36.9([^{37}Cl]$^-$, 29%)

Elemental analysis (predicted) C 67.00%, H 10.89%, N 9.77%
Elemental analysis (measured) C 66.89%, H 10.77%, N 9.89%

3.2.13 Synthesis of 1-dodecyl-3-methylimidazolium *bis*(trifluoromethyl sulfonyl)imide [$C_{12}C_1$im][NTf_2]

Lithium bis(trifluoromethylsulfonyl)imide (50 g, 0.174 mol, 1 equivalent) was added to a solution of 1-dedocyl-3-methylimidazolium chloride (49.97 g, 0.174 mol, 1 equivalent) in 200 ml dichloromethane. The resulting mixture was stirred for 24 hours before it being filtered to remove the lithium chloride precipitate. The dichloromethane phase was then washed with distilled water (6 × 50 ml) until the washings gave a negative result to the silver nitrate test. The dichloromethane was removed under vacuum on a rotary evaporator, and the resulting liquid was further washed with 50 ml *n*-hexane. The liquid was then treated with activated charcoal at room temperature overnight. The bulk of the charcoal was removed with standard filtration through filter paper and then through a 0.2 μm PTFE filter to ensure completed removal of the charcoal particulates. The liquid was then dried overnight at 55°C to yield a clear, colourless liquid (79.75 g, 86 % yield).

^{1}H NMR (400MHz, DMSO-d_6) δ 8.14 (1H, s, N**C**HN), 6.99 (1H, s, NC**H**CHN), 6.91 (1H, s, NCHC**H**N), 3.88-3.56(2H, m, NC**H**$_2$CH$_2$(CH$_2$)$_9$CH$_3$), 3.41 (3H, s, NC**H**$_3$), 1.40(2H, s, NCH$_2$C**H**$_2$(CH$_2$)$_9$CH$_3$), 1.08-0.59(18H, m, NCH$_2$CH$_2$(C**H**$_2$)$_9$CH$_3$), 0.41 (3H, t, $^3J_{HH}$ 6.2Hz NCH$_2$CH$_2$(CH$_2$)$_9$C**H**$_3$).

^{13}C NMR (101MHz, DMSO-d_6 capillary) δ 135.31 (s, N**C**HN), 123.00 (s, N**C**HCHN), 121.69 (s, NCH**C**HN), 116.18 (m, $^1J_{CF}$ 320.9Hz, **C**F$_3$), 49.20 (s, N**C**H$_2$C$_{11}$H$_{23}$), 35.09 (s, N**C**H$_3$), 31.40 (s, NCH$_2$**C**H$_2$C$_{10}$H$_{21}$), 29.40 (s, NC$_2$H$_4$**C**H$_2$C$_9$H$_{19}$), 29.12 (s, N NC$_3$H$_6$**C**H$_2$C$_8$H$_{17}$), 29.02 (s, NC$_4$H$_8$**C**H$_2$C$_7$H$_{15}$), 29.00 (s, NC$_5$H$_{10}$**C**H$_2$C$_6$H$_{13}$), 28.85 (s, NC$_6$H$_{12}$**C**H$_2$C$_5$H$_{11}$), 28.81 (s, NC$_7$H$_{14}$**C**H$_2$C$_4$H$_9$), 28.37 (s, NC$_8$H$_{16}$**C**H$_2$C$_3$H$_7$), 25.47 (s, NC$_9$H$_{18}$**C**H$_2$C$_2$H$_5$), 22.08(s, NC$_{10}$H$_{20}$**C**H$_2$CH$_3$), 13.14 (s, NC$_{11}$H$_{22}$**C**H$_3$).

m/z (ES$^+$) 251.2 ([$C_{12}C_1$im]$^+$, 100%); (ES$^-$) 279.9([NTf_2]$^-$, 100%)

Elemental analysis (predicted) C 40.67%, H 5.88%, N 7.90%

Elemental analysis (actual) C 40.84%, H 5.97%, N 7.84%

3.2.14 Synthesis of tributyl-hexylphosphonium bis(trifluoromethylsulfonyl) imide [P_{4446}][NTf_2]

This ionic liquid was synthesised by Dr. Liu Qing Shan, a postdoctoral researcher in the Welton Research Group. Upon receiving the sample, the sample was treated with activated charcoal overnight and the bulk charcoal was removed by using a filter paper. The sample was then filtered through a 0.2 μm PTFE membrane filter to remove any remaining particulates. The resulting liquid was dried *in vacuo* at 55 °C for two days to give a colourless and transparent highly viscous liquid.

^{1}H NMR (400 MHz, DMSO-d_6) δ 2.18 (8H, m, P[C*H*$_2$(CH$_2$)$_2$CH$_3$]$_3$[C*H*$_2$(CH$_2$)$_4$CH$_3$]), 1.44 (16H, m, P[CH$_2$(C*H*$_2$)$_2$CH$_3$]$_3$[CH$_2$(C*H*$_2$)$_2$(CH$_2$)$_2$CH$_3$]), 1.30 (4H, m, P[(CH$_2$)$_3$(C*H*$_2$)$_2$CH$_3$]), 0.93 (12H, m, P[(CH$_2$)$_3$C*H*$_3$]$_3$[(CH$_2$)$_5$C*H*$_3$])

^{13}C NMR (101 MHz, DMSO-d_6) δ 119.65 (q, $^1J_{CF}$ = 320.6 Hz, *C*F$_3$), 30.37 (s, P[*C*H$_2$(CH$_2$)$_4$CH$_3$]), 29.76 (d, P[*C*H$_2$(CH$_2$)$_2$CH$_3$]$_3$), 23.34 (d, P[CH$_2$*C*H$_2$(CH$_2$)$_3$CH$_3$]), 22.62 (d, P[CH$_2$*C*H$_2$CH$_2$CH$_3$]$_3$), 21.81 (s, P[(CH$_2$)$_2$*C*H$_2$(CH$_2$)$_2$CH$_3$]), 20.51 (d, P[(CH$_2$)$_2$*C*H$_2$CH$_3$]$_3$), 17.48 (d, P[(CH$_2$)$_3$*C*H$_2$CH$_2$CH$_3$]), 17.29 (d, P[(CH$_2$)$_3$*C*H$_3$]$_3$), 13.78 (d, P[(CH$_2$)$_4$*C*H$_2$CH$_3$]), 13.16 (d, P[(CH$_2$)$_4$*C*H$_3$]).

Elemental analysis (predicted) C 42.30%, H 7.11%, N 2.47%

Elemental analysis (measured) C 42.04%, H 6.93%, N 2.21%

3.2.15 Synthesis of 1-butyl-1-methylpyrrolidinium chloride [C_4C_1pyrr]Cl

1-chlorobutane (230 ml, 2.20 mol, 1.1 equivalent) was added dropwise to a cooled and stirring solution of *N*-methylpyrrolidine (208 ml, 2.00 mol, 1 equivalent) in 200 ml of ethyl acetate. The mixture was stirred at room temperature for one week under a nitrogen atmosphere. The reaction temperature was then increased to 60°C for three weeks. The reaction was then cooled to -20°C for 2 days to induce the crystallisation process**.** The remaining solvent was removed by cannula filteration, and the solid crystals were washed with dry ethyl acetate (2 × 100 ml)

before being recrystallised twice from acetonitrile (2 × 150 ml). Resulting crystals were dried *in vacuo* for two days to yield white crystals (152.84 g, 43%).

^{1}H NMR (400MHz, DMSO-d_6) δ 3.61-3.44 (4H, m, 2×C$_\alpha$**H**$_2$), 3.34-3.32 (2H, m, NC**H**$_2$CH$_2$CH$_2$CH$_3$), 3.03 (3H, s, NC**H**$_3$), 2.19-1.97 (4H, m, 2×C$_\beta$**H**$_2$), 1.74-1.61 (2H, m, NCH$_2$C**H**$_2$CH$_2$CH$_3$), 1.31 (2H, h, $^{3}J_{HH}$ 7.4Hz, N(CH$_2$)$_2$C**H**$_2$CH$_3$),0.93 (3H, t, $^{3}J_{HH}$ 7.4Hz, N(CH$_2$)$_3$C**H**$_3$)

^{13}C NMR (101MHz, DMSO-d_6) δ 63.81 (s, 2×**C**$_\beta$H$_2$), 63.08 (s, 2×**C**$_\alpha$H$_2$), 47.94 (s, N**C**H$_3$), 25.42 (s, N**C**H$_2$(CH$_2$)2CH$_3$), 21.53(s, NCH$_2$**C**H$_2$CH$_2$CH$_3$), 19.79 (s, N(CH$_2$)$_2$**C**H$_2$CH$_3$), 14.00 (s, N(CH$_2$)$_3$**C**H$_3$)

m/z (LSIMS$^+$) 142 ([C$_4$C$_1$pyrr]$^+$, 100%); (LSIMS$^-$) 35 ([^{35}Cl]$^-$, 100%); (LSIMS$^-$) 37([^{37}Cl]$^-$, 28%)

Elemental analysis (predicted) C 60.77%, H 11.34%, N 7.88%

Elemental analysis (measured) C 59.53%, H 11.44%, N 7.76%

3.2.16 Synthesis of 1-butyl-1-methypyrrolidinium *bis*(trifluoromethyl sulfonyl)imide [C$_4$C$_1$pyrr][NTf$_2$]

In a 500 mL round bottom flask, 1-butyl-1-methylpyrrolidinium chloride (35 g, 0.20 mol, 1 equivalent) was dissolved in 150 ml of dichloromethane. Lithium *bis*(trifluoromethylsulfonyl)imide (57 g, 0.20 mol, 1 equivalent) was added to the flask and the mixture stirred for 24 hours under a nitrogen atmosphere. The mixture was then filtered and the filtrate washed copiously with distilled water (8 × 100 ml) until the aqueous phase gave a negative result to the silver nitrate test. The solvent was then removed using a rotary evaporator and the residue was washed twice with *n*-hexane (2 × 50 ml). The remaining solvent was removed by rotary evaporator and the liquid was treated with activated charcoal overnight. Finally, the mixture was filtered through a 0.2 µm PTFE filter before drying in *vacou* at 55 °C for 2 days to yield a colourless, oily ionic liquid (67g, 80% yield).

^{1}H NMR (400MHz, DMSO-*d*$_6$ capillary) δ 3.46 (4H, m, 2×C$_\alpha$**H**$_2$), 3.35 (2H, m, NC**H**$_2$CH$_2$CH$_2$CH$_3$), 2.98 (3H, s, NC**H**$_3$), 2.09 (4H, broad s, 2xC$_\beta$**H**$_2$), 1.68 (2H, m, NCH$_2$C**H**$_2$CH$_2$CH$_3$), 1.32 (2H, sextet, $^{3}J_{HH}$ 7.4Hz, N(CH$_2$)$_2$C**H**$_2$CH$_3$),0.94 (3H, t, $^{3}J_{HH}$ 7.4Hz, N(CH$_2$)$_3$C**H**$_3$).

^{13}C NMR (101MHz, DMSO-*d*$_6$) δ 124.90-115.26 (m, $^{1}J_{CF}$ 300.98Hz, CF$_3$), δ 63.88 (s,2×**C**$_\beta$H$_2$), 63.38 (s, 2×**C**$_\alpha$H$_2$), 47.92 (s, N**C**H$_3$), 25.38 (s, N**C**H$_2$(CH$_2$)2CH$_3$), 21.52(s, NCH$_2$**C**H$_2$CH$_2$CH$_3$), 19.76 (s, N(CH$_2$)$_2$**C**H$_2$CH$_3$), 13.89(s, N(CH$_2$)$_3$**C**H$_3$).

m/z (LSIMS$^+$) 142 ([C$_4$C$_1$pyrr]$^+$, 100%); (LSIMS$^-$) 280 ([NTf$_2$]$^-$, 100%).

Elemental analysis (predicted) C 31.20%, H 4.73%, N 6.62%

Elemental analysis (measured) C 31.30%, H 4.77%, N 6.72%

3.2.17 Synthesis of 1-butyl-3-methylimidazolium tetrafluoroborate [C$_4$C$_1$im][BF$_4$]

In a 500 ml round bottom flask, sodium tetrafluoroborate (47.73 g, 0.27 mol, 1 equivalent) was added to a solution of 1-butyl-3-methylimidazolium chloride (29.99 g, 0.27 mol, 1 equivalent) in 200 ml of dichloromethane. The mixture was stirred for 24 hours at room temperature before the filtration through a filter paper. The filtrate was then washed with distilled water (9 × 10 ml) until the aqueous phase became chloride free which was confirmed by the silver nitrate test. The solvent was removed on a rotary evaporator and the resulting liquid was washed with *n*-hexane (50 ml) before evaporating any remaining solvent. The recovered oily liquid was stirred with activated charcoal overnight and then filtered through filter paper followed by a 0.2 μm PTFE membrane filter. The resulting liquid was dried *in vacuo* at 55 °C for 2 days to give clear viscous liquid (38.97 g, 63% yield).

^{1}H NMR (400MHz, DMSO-*d*$_6$ capillary) δ 8.00 (1H, s, NC**H**N), 6.92 (1H, s, NC**H**CHN), 6.87 (1H, s, NCHC**H**N), 3.54 (2H, t, $^{3}J_{HH}$ 7.1Hz, NC**H**$_2$CH$_2$CH$_2$CH$_3$), 3.27 (3H, s, NC**H**$_3$), 1.15

(2H, p, $^{3}J_{HH}$ 7.6Hz, $NCH_2C\mathbf{H}_2CH_2CH_3$), 0.60 (2H, h, $^{3}J_{HH}$ 7.4Hz, $N(CH_2)_2C\mathbf{H}_2CH_3$), 0.16 (3H, t, $^{3}J^{HH}$ 7.4Hz, $N(CH_2)_3C\mathbf{H}_3$).

^{13}C NMR (101MHz, DMSO-*d*$_6$ capillary) δ 135.96 (s, N**C**HN), 122.80 (s, N**C**HCHN), 121.48 (s, NCH**C**HN), 48.43 (s, N**C**H_2 $(CH_2)_2CH_3$), 34.84 (s, NCH_3), 30.95 (s, $NCH_2CH_2CH_2CH_3$), 18.30 (s, $N(CH_2)_2\mathbf{C}H_2CH_2CH_3$), 12.08 ($N(CH_2)_3\mathbf{C}H_3$).

m/z (ES^+) 139.31 ($[C_4C_1im]^+$, 100%); (ES^-) 87 ($[BF_4]^-$, 100%)

Elemental analysis (predicted) C 42.48%, H 6.69%, N 12.39%

Elemental analysis (measured) C 42.08%, H 6.42%, N 12.84%

3.2.18 Synthesis of 1-butyl-3-methylimidazolium hexafluorophosphate [C_4C_1im][PF_6]

In a 500 ml round bottom flask, potassium hexafluorophosphate (47.45 g, 0.27 mol, 1 equivalent) was added to a solution of 1-butyl-3-methylimidazolium chloride (49.98 g, 0.27 mol, 1 equivalent) in 150 ml dichloromethane. The mixture was stirred for 24 hours at room temperature before filtration through a filter paper. The filtrate was then washed with distilled water (5 × 50 ml) until the aqueous phase became chloride free which was confirmed by the silver nitrate test. The solvent was removed on a rotary evaporator and the resulting liquid was washed with *n*-hexane (50 ml) before evaporating any remaining solvent. The obtained oily liquid was stirred with activated charcoal overnight and then filtered through filter paper followed by a 0.2 µm PTFE membrane filter. The resulting liquid was dried *in vacuo* at 55 °C for 2 days to give clear and colourless of highly viscous liquid (58.12 g, 75% yield).

^{1}H NMR (400MHz, DMSO-*d*$_6$ capillary) δ 8.00 (1H, s, NC**H**N), 6.92 (1H, s, NC**H**CHN), 6.87 (1H, s, NCHC**H**N), 3.54 (2H, t, $^{3}J_{HH}$ 7.1Hz, $NC\mathbf{H}_2CH_2CH_2CH_3$), 3.27 (3H, s, $NC\mathbf{H}_3$), 1.15 (2H, p, $^{3}J_{HH}$ 7.6Hz, $NCH_2C\mathbf{H}_2CH_2CH_3$), 0.60 (2H, h, $^{3}J_{HH}$ 7.4Hz, $N(CH_2)_2C\mathbf{H}_2CH_3$), 0.16 (3H, t, $^{3}J^{HH}$ 7.4Hz, $N(CH_2)_3C\mathbf{H}_3$).

^{13}C NMR (101MHz, DMSO-*d*$_6$ capillary) δ 135.96 (s, N**C**HN), 122.80 (s, N**C**HCHN), 121.48 (s, NCH**C**HN), 48.43 (s, N**C**H$_2$ (CH$_2$)$_2$CH$_3$), 34.84 (s, NCH$_3$), 30.95 (s, NCH$_2$CH$_2$CH$_2$CH$_3$), 18.30 (s, N(CH$_2$)$_2$**C**H$_2$CH$_2$CH$_3$), 12.08 (N(CH$_2$)$_3$**C**H$_3$).

m/z (ES$^+$) 139.31 ([C$_4$C$_1$im]$^+$, 100%); (ES$^-$) 144.9 ([PF$_6$]$^-$, 100%)

Elemental analysis (predicted) C 33.78%, H 5.32%, N 9.86%

Elemental analysis (measured) C 33.65%, H 5.54%, N 10.05%

3.2.19 Synthesis of 1-butyl-3-methylimidazolium trifluoromethanesulfonate [C$_4$C$_1$im][CF$_3$SO$_3$]

In a 500 ml round bottom flask, lithium trifluoromethanesulfonate (36.49 g, 0.21 mol, 1 equivalent) was added to a solution of 1-butyl-3-methylimidazolium chloride (24.99 g, 0.21 mol, 1 equivalent) in 150 ml of dichloromethane. The mixture was stirred overnight at room temperature before the filtration through a filter paper. The filtrate was then washed with distilled water (10 × 5 ml) until the aqueous phase became chloride free, which was confirmed by the silver nitrate test. The solvent was removed on a rotary evaporator and the resulting liquid was washed with *n*-hexane (100 ml) before evaporating any remaining solvent. The obtained oily liquid was stirred with activated charcoal overnight and then filtered through filter paper followed by a 0.2 µm PTFE membrane filter. The resulting liquid was dried *in vacuo* at 55 °C for 2 days to give clear and colourless of highly viscous liquid (31.67 g, 52 % yield).

^{1}H NMR (400MHz, DMSO-*d*$_6$ capillary) δ 8.39 (1H, s, NC**H**N), 7.16 (1H, s, NC**H**CHN), 7.09 (1H, s, NCHC**H**N), 3.69 (2H, t, $^3J_{HH}$ 7.2Hz, NC**H**$_2$CH$_2$CH$_2$CH$_3$), 3.42 (3H, s, NC**H**$_3$), 1.31 (2H, p, $^3J_{HH}$ 7.3Hz, NCH$_2$C**H**$_2$CH$_2$CH$_3$), 0.75 (2H, h, $^3J_{HH}$ 7.3Hz, N(CH$_2$)$_2$C**H**$_2$CH$_3$), 0.32 (3H, t, $^3J^{HH}$ 7.4Hz, N(CH$_2$)$_3$C**H**$_3$).

^{13}C NMR (101MHz, DMSO-*d*$_6$ capillary) δ 136.29 (s, N**C**HN), 122.96 (s, N**C**HCHN), 121.74 (s, NCH**C**HN), 120.34 (m, $^{1}J_{CF}$ 320.4Hz, **C**F_3), 48.62 (s, N**C**H_2 $(CH_2)_2CH_3$), 35.06 (s, NCH_3), 31.09 (s, $NCH_2CH_2CH_2CH_3$), 18.42 (s, $N(CH_2)_2$**C**H_2CH_3), 12.11 ($N(CH_2)_3$**C**H_3).

m/z (ES^+) 139.11 ($[C_4C_1im]^+$, 100%); (ES^-) 148.90 ($[CF_3SO_3]^-$, 100%)

Elemental analysis (predicted) C 37.47%, H 5.24%, N 9.72%

Elemental analysis (measured) C 37.41%, H 5.69%, N 9.26%

3.3 Viscosity measurements

The viscosity of the synthesised ionic liquids was measured using a TA Instruments' AR2000EX rheometer fitted with a Peltier plate as a temperature regulator. The measurements were performed using a 40 mm diameter and 2° steel truncated cone geometry. For each measurement, the angular velocities were set to between 0.1 and 10 radians per second and the viscosities were measured as function of shear rates. The error of the instrument was about 5%. A blanket of nitrogen was used to cover the sample to make sure an inert atmosphere was maintained during the measurements. This precaution was taken to prevent the sample from absorbing the water from its surrounding, which may affect the measured viscosity value. A schematic illustration representing the cone and plate rheometer assembly is shown in **Figure 29**. Analysis of data was carried out using TA Instruments' Universal Analysis 2000 (Version 4.5A).

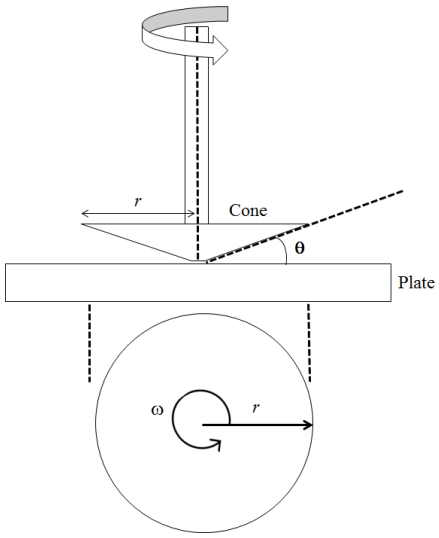

Figure 29 : Schematic illustration of cone and plate rheometer.

The rotational viscometer consisted of two elements which are, a rotating cone with radius *r* and fixed element *i.e.* the Peltier plate. Liquid sample is placed between the cone and plate. The cone is rotated at different fixed speeds (ω) therefore shearing the liquid at a defined shear rate. At the same time, the viscometer measure the torque resistance experienced by the cone at each of the speed of rotation. This torque measurement is referred as shear rate. Dynamic viscosity of the liquid is calculated from the ratio of the shear stress to the shear rate according to the equations **(15) - (17)** .

$$\text{Shear stress (dynes/cm}^2\text{)} = \frac{\tau}{\frac{2}{3}\pi r^3} \tag{15}$$

$$\text{Shear rate (sec}^{-1}\text{)} = \frac{\omega}{\sin\theta} \tag{16}$$

$$\text{Viscosity (centipoise / mPa}\cdot\text{S)} = \frac{\text{Shear stress} \times 100}{\text{Shear rate}} \tag{17}$$

τ = percent full scale torque (dyne-cm)
r = cone radius (cm)
ω = Cone speed (rad sec^{-1})
θ = Cone angle (degree)

3.4 Density measurements

The density of the synthesised ionic liquids was measured using Anton Paar DMA38 oscillating U-tube density meter. The density is measured from an electronic measurement of the frequency of oscillation based on the mass-spring model. A counter mass is mounted on the U-tube container which is filled with the sample. The frequency of oscillation of the container changes after a sample is introduced to the tube and the magnitude of the change is a function of sample mass. The density of a sample can therefore be determined from the measured mass and volume of the sample.

The density measurements were performed at 25°C. The reported error of the instrument was about ±0.001 gcm^{-3}. About 0.7-1.0 ml of sample was injected into U-tube using a plastic syringe. The liquid was left to equilibrate with the cell for at least four minutes before the measurement was recorded. For each liquid, the reported value is the average of three measurements.

3.5 Water content

The water content of the ionic liquids was measured via Karl-Fischer titration on a Mettler Toledo C20 Compact Karl-Fischer Coulometer titrator. The working principle in coulometric titration involve the use of current to quantify the concentration of the unknown species. A constant current is applied to a system until one of the species in the system is oxidized or reduced to a new state, which will cause a significant change to the potential of the working electrode. The amount of the current (ampere) and time (seconds) is quantified and used to determine the amount of the unknown species.

The Karl-Fischer reaction is a reaction that has been used to determine the amount of water in a sample. This reaction is based on two chemical reactions. First, an alcohol (usually methanol or ethanol), SO_2 and a base (R-N) react to produce an allylsulfide intermediate.

$$CH_3OH + SO_2 + R\text{-}N \rightleftharpoons [R\text{-}NH]SO_3CH_3$$

Then, this intermediate reacts with I_2 and H_2O in equimolar ratios. The amount of iodide complex formed can be correlated to the amount of water present in the sample.

$$[R\text{-}NH]SO_3CH_3 + I_2 + H_2O + 2RN \rightarrow [R\text{-}NH]SO_4CH_3 + 2[R\text{-}NH]I^-$$

Sampling was repeated three times and an averaged result reported. The amount of water is reported in ppm.

3.6 Electrochemical experiments

3.6.1 Preparation of polydimethylsiloxane (PDMS) cell

The PDMS cell was made using the Sylgard® 184 Silicone Elastomer Kit produced by Dow Corning. In the preparation, the curing agent was added to the PDMS with a ratio of 1:10. The mixture was stirred until well mixed and then allowed to rest for 5 minutes. The mixture was then put into a vacuum desiccator and evacuated periodically until the air bubbles added during the stirring process were removed. The liquid was then return to normal atmospheric pressure before pouring into a plastic petri dish. The mixture was then heated in an oven operated at 80°C for 45 minutes until fully cured. The fully cured PDMS was pulled off from petri dish and cut into a square shape with dimension of approximately 15mm (l) × 15mm (w) × 7mm (h). A cylindrical void with a diameter of 3 mm was made in the middle of cube using a biopsy punch (KAI Medical BP-30F).

3.6.2 Indium-Tin Oxide (ITO)-PDMS cell

The ITO-PDMS cell was designed so that an electrochemical cell can be fitted into a confocal microscope stage and ITO electrode plays the role of the electrode and therefore replace the need for ordinary microscope glass coverslips or additional electrodes. The ITO coated coverslips (22 x 40 mm) were purchased from SPI Supplies with a thickness of #1.5 (0.16 – 0.19 mm), resistivity of 8 -12 Ohms/square, and a silver busbar at either end of the conductive face. Silver conductive adhesive paint (Electrolube) and non-conductive copper tape (Advance Tapes AT525) purchased from RS Online were used to form the connection to the conductive ITO side of the coverslips. **Figure 30** illustrates the schematic of electrochemical cell set-up

used for the fluorescence lifetime measurements and he ITO-PDMS cell in use on the optical setup.

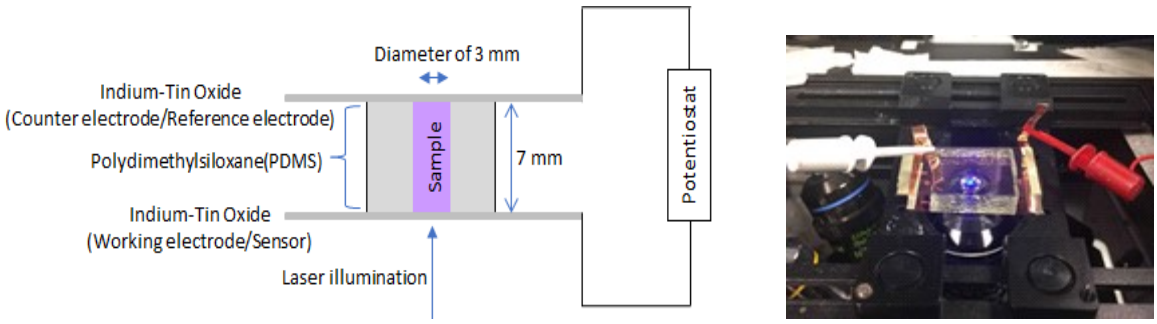

Figure 30: Schematic of ITO-PDMS cell used for electrochemical and fluorescence lifetime measurements (left), and the ITO-PDMS cell in use on the optical setup (right).

3.6.3 Conductivity measurements

Ionic conductivity can be measured by a wide variety method which employs either direct current (DC) or alternating current (AC). In this project, the ionic conductivity of liquid electrolytes is measured using the AC complex impedance technique. In this technique, a two-electrode cell is used to measure the complex impedance of electrolytes (Z). The complex impedance arises from some contribution of resistive (R) and capacitive(C) of the electrolyte system, which can be described using the following equation (**18**)

$$Z = \sqrt{\left(\frac{1}{\omega C}\right)^2 + R^2} \qquad \textbf{(18)}$$

ω = the frequency of the AC modulation

According to this equation, as the frequency AC increases, the capacitive contribution to the impedance becoming much less significant than the contribution from the resistive. Therefore, at high frequency the equation (**18**) can be reduced to equation (**19**).

$$Z = R \tag{19}$$

Under this circumstance, the ionic conductivity(κ) can be calculated from the resistivity of the electrolyte using the equation **(20)**.

$$\kappa = \frac{L}{A} \times \frac{1}{R} = C \times \frac{1}{R} = C \times G \tag{20}$$

L = distance between the two electrodes (cm)
A = Area of electrode (cm^2)
C = cell constant
R = resistance
G = conductance

The term L/A also known as cell constant (C). Theoretically, the value of the cell constant can be calculated from the ratio of distance between the two electrodes(cm) to the effective area of the electrodes (cm^2). However, it is not practical to accurately measure these two parameters. Instead, the cell constant is usually determined by measuring the resistance of the cell containing solutions of known conductivity *i.e.* standard solutions. The impedance measurements are normally carried out at high frequency, up to a few kHz so that the capacitive contribution to the cell impedance is minimized. The impedance data collected from standard electrochemical impedance hardware such as potentiometer or impedance analyser consist of real and imaginary components. The data is plotted in the form of the Nyquist plot and the resistance is taken as the point at which the data crosses the real axis (*i.e.* the x-axis) at high frequency.

In this study, the electrochemical measurements were made using the custom made PDMS cell. The design of the cell is discussed in the previous section. An Autolab PGSTAT 204 potentiometer was used to perform the conductivity measurements. Three National Institute of Standard and Technology (NIST) traceable standard solutions by Reagecons were used to determine the cell constant. The conductivity of the three standard solutions were 84, 1413 and 12280 µS cm^{-1}, respectively. The slope of plot conductance against the conductivity of the standard solutions gave the value of the cell constant. The cell constant was determined to be 0.09155 cm (see **Figure 31**).

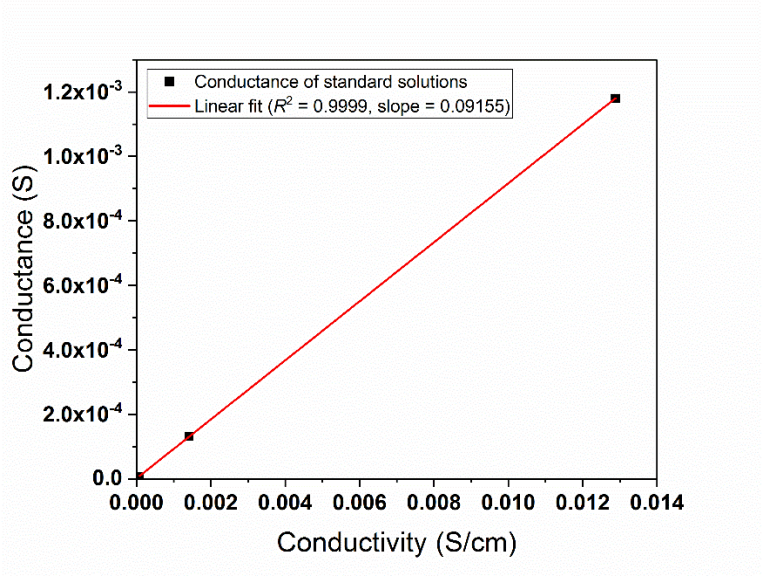

Figure 31: The plot of conductance against conductivity of standard solutions in the ITO cell. The linear fitting with goodness of fit, $R^2 = 0.9999$.

In this study, the conductivity measurements were made with an amplitude of 1 mV and frequencies in the range of 0.1 Hz to 1 × 10^5 Hz. The Nyquist plot obtained from the conductivity measurement of an ionic liquid is presented in **Figure 32**. The conductance of the

ionic liquid was extracted from the *x*-axis intersection of the semicircle fitting at higher conductance. The data was analysed using the NOVA (version 1.11) Metrohm Autolab software. The conductivity value was then calculated using Equation **(20)**.

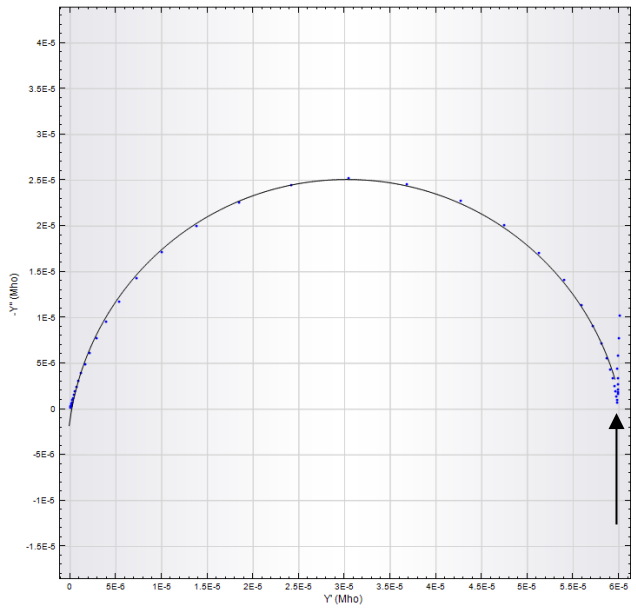

Figure 32: The example of Nyquist plot of an ionic liquid. The arrow shows the x-intersection value used for conductivity calculation.

3.7 Nuclear magnetic resonance (NMR) methods

3.7.1 Standard NMR method

The NMR spectra of the synthesised samples were recorded using 400 MHz Bruker BioSpin GmbH spectrometer. The chemical shifts relative to tetramethylsilane (TMS) were reported as ppm and the *J*-coupling constants are reported in Hz.

3.7.2 Pulsed gradient stimulated echo (PGSTE) NMR

The pulsed gradient spin echo-NMR (PGSE-NMR) is a well-established technique for measuring the self-diffusion coefficient of ions and molecules in ionic liquids. This technique was developed by Stejskal and Tanner in 1965 following the discovery of spin echoes by Hahn in 1950.[109] Determination of diffusion coefficients by PGSE-NMR method involves the use of spin echo experiment with the application of two subsequent gradient radio rf-pulses at 90°–180°. The application of these gradient pulses caused the magnetic field to become inhomogeneous over two periods of time. The gradient pulses produce a linear gradient magnetic field, which varies the precessions of the nuclei in the field. The NMR signal is sensitive to the differences in the locations of the nuclei between the two pulse periods. If a change in location by self-diffusion occurs, it will result in signal attenuation (increased intensity of echo). The magnitude of the change is directly proportional to the intensity of the gradient pulses (g) applied.

As ionic liquids are normally more viscous liquids compared to other molecular solvent, it is advantageous to use pulse gradient stimulated echo-NMR(PGSTE-NMR), which use a three-rf pulse experiment instead of two-rf pulse for normal echo.[110] The use of three pulses can produce up to five spin echoes and it was observed by Hahn that the echo produced an interval after the third rf pulse is identical to the one between the first two pulses. This echo has been called “stimulated echo”. Viscous systems usually have a combination of low transverse relaxation times and diffusivities (*D*), which make it difficult to get a measurable echo signal attenuation even after the largest practicable field gradient is used. It also needs substantially longer times delays in order to reduce the noise level by relaxation. A schematic illustration of

the pulse gradient spin-echo NMR sequence for measuring self-diffusion is presented in **Figure 33**.

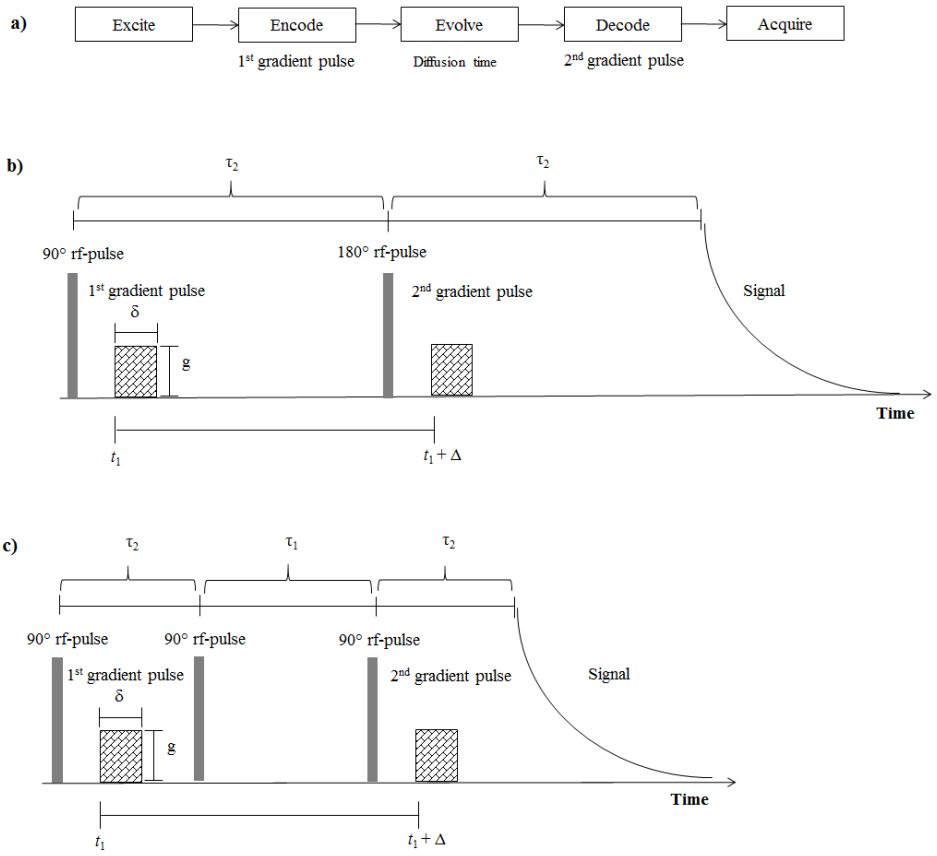

Figure 33: a) The essential components of a PGSE NMR diffusion experiment. b) The schematic illustration of PGSE-NMR sequence. C) The schematic illustration of PGSTE-NMR sequence.

Following the standard 90° pulse, a magnetic field gradient with length δ and field strength g is inserted into each of the time delay(τ) after a short delay. Briefly, the standard 90° rf-pulse rotates the macroscopic magnetization from the z-axis into the x-y plane. The insertion of the gradient pulse will cause the spin of the nuclei within the sample to experience a different local magnetic field and therefore losing coherency. The application of the second gradient pulse of equal duration δ and magnitude g will completely diminish the effect caused by the first

gradient, and all spins will refocus, provided the spins remained exactly at the same position. However, if the self-diffusion has caused the nuclei to change their spatial position, the second gradient pulse does not completely reverse the process, and this attenuates the echo amplitude. The change in amplitude with the applied gradient can be correlated to the movement of nuclei using the equation **(21)**.

$$\ln(E) = \ln(\frac{S}{S_{g=0}}) = -\gamma^2 g^2 dD\partial^2(\Delta - \frac{\partial}{3}) \quad \textbf{(21)}$$

S = spin echo signal intensity

γ= gyromagnetic ratio

As the diffusion experiment is normally conducted with various magnetic field gradients, the value of D can be determined from the slope of the straight-line plot of $\ln(S/S_{g=0})$ against the series of the magnetic field strengths, g^2. An example of a PGSTE NMR report is presented in **Figure 34** -

Figure 35.

The PGSTE-NMR measurements were carried out using a Bruker 500 MHz AVANCE III HD spectrometer running TopSpin 3.2. The instrument is equipped with a z-gradient bbo/5 mm tuneable SmartProbe and a GRASP II gradient spectroscopy accessory having a maximum gradient output of 53.5 G cm^{-1} (5.35 G $cm^{-1}A^{-1}$). The diffusivity of the cations of ionic liquids and the probe molecules were obtained from the ^{1}H PGSTE-NMR and the diffusivity of the anions of liquids was obtained from ^{19}F PGSTE-NMR. The ^{1}H PGSTE-NMR measurements were carried out using the ledbpgp2 Bruker pulse program at a frequency of 500.13 MHz with a spectral width of 5500 Hz. A relaxation time delay of 12 s was applied along the diffusion time of 150 ms and longitudinal eddy current delay of 5 ms. Bipolar gradients pulses (δ/2) of

5 ms and homospoil gradient pulses of 1.1ms were used for all measurements. The same pulse program was used for the ^{19}F DOSY NMR and the spectra were recorded at a frequency of 470.59 MHz with a spectral width of 18800 Hz. The bipolar gradient pulses, homospoil gradient pulses and diffusion time for ^{19}F DOSY NMR were set at 3 ms, 1.1 ms, and 200 ms respectively. The ^{1}H and ^{19}F data were analysed using the Bruker Dynamics Centre Software (version 2.1.7) and the error of measurements were estimated using Monte Carlo simulation with confidence level of 95%.

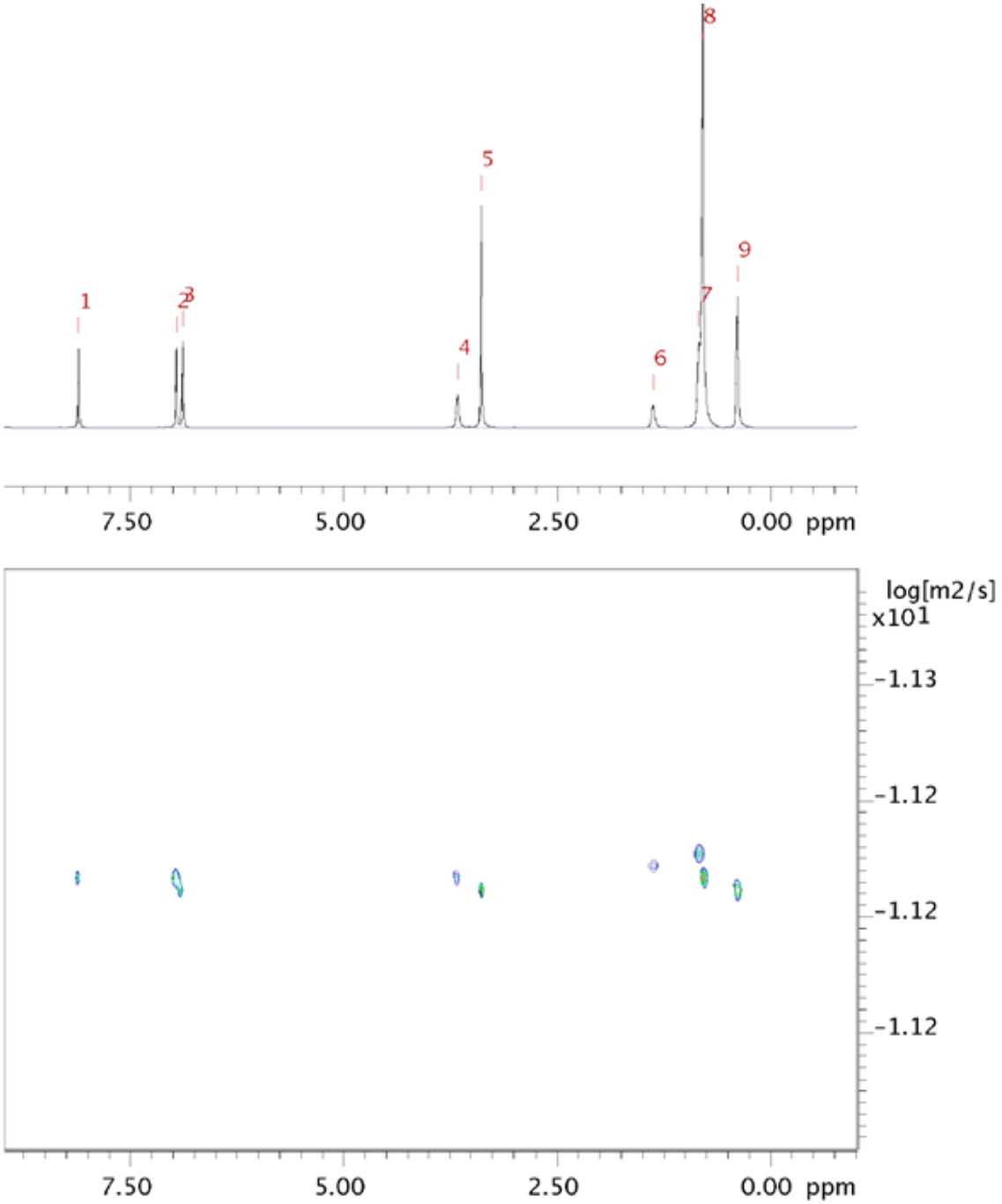

Figure 34: Part of the report produced by the Bruker Diffusion Analysis Software showing the ^{1}H NMR spectrum for $[C_{12}C_{1}im][NTf_2]$ and the diffusivities corresponds to each of detected NMR peak.

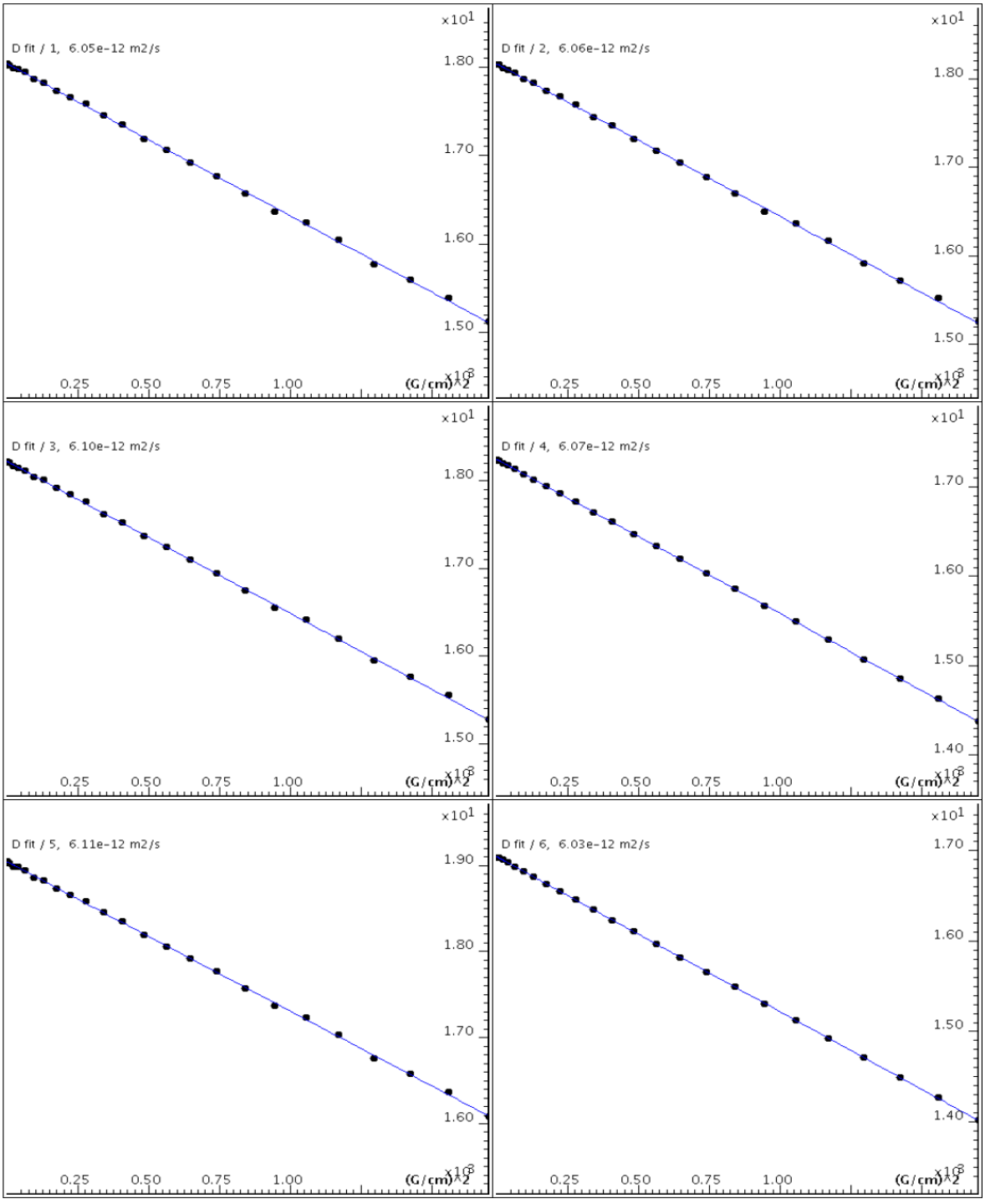
D fit / 1, 6.05e-12 m2/s
D fit / 2, 6.06e-12 m2/s
D fit / 3, 6.10e-12 m2/s
D fit / 4, 6.07e-12 m2/s
D fit / 5, 6.11e-12 m2/s
D fit / 6, 6.03e-12 m2/s
x10^1
x10^8
(G/cm)^2
0.25
0.50
0.75
1.00
1.80
1.70
1.60
1.50
1.40
1.90

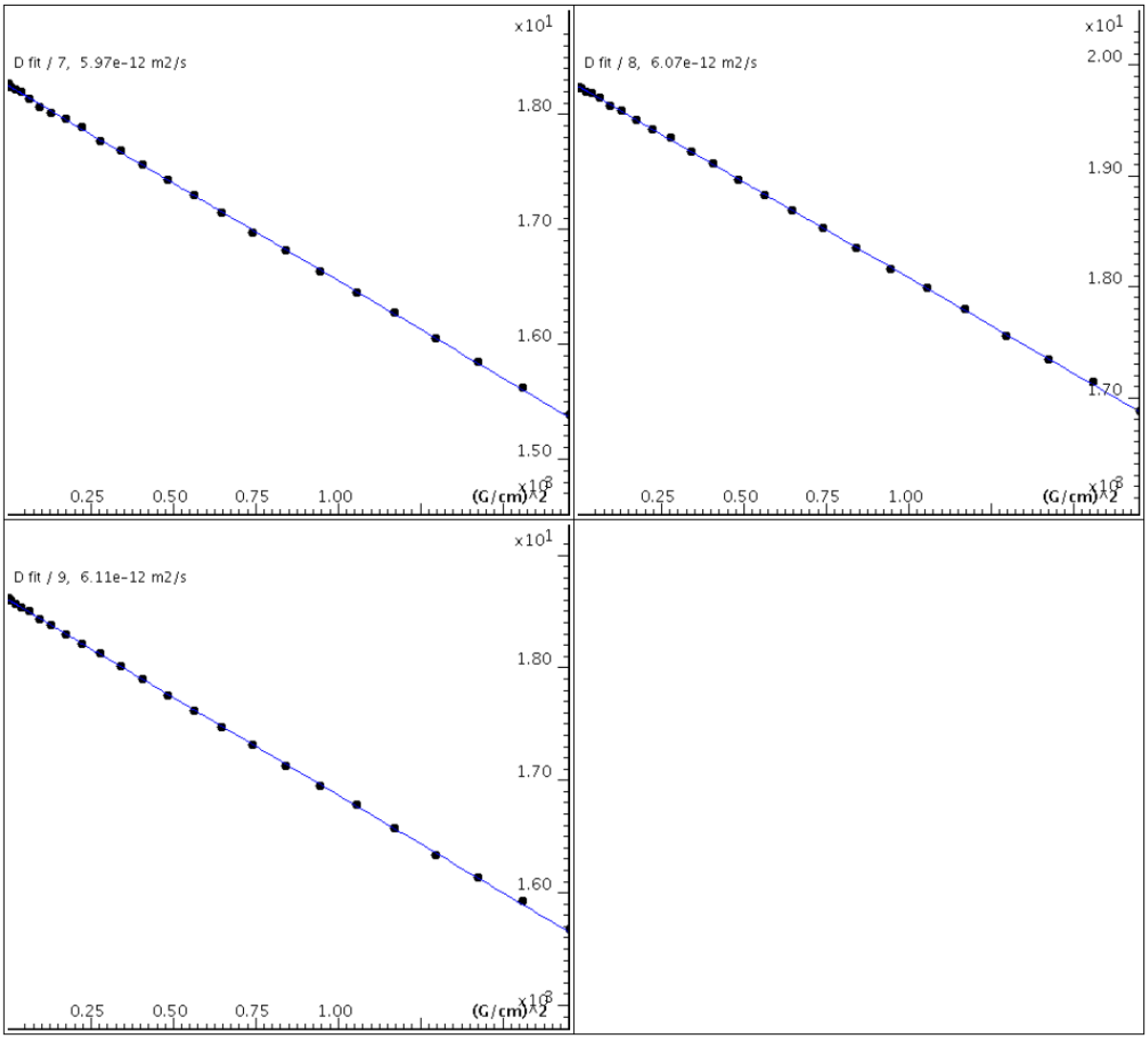

Figure 35: The plots of $\ln(S/S_{g=0})$ versus g^2 for all NMR peaks (1- 9) of $[C_{12}C_1im][NTf_2]$.

3.8 Fluorescence lifetime experiments

3.8.1 Materials

a) Cy3 was purchased from Alfa Aesar (96% purity) and used without purification. The solutions for all measurements was prepared by appropriate dilution of a 6.09 mM stock solution of Cy3 in methanol.

b) DCVJ was purchased from Sigma Aldrich (≥97.0% purity) and used without any further purification. The solutions for all measurements was prepared by appropriate dilution of 6.016 mM stock solution of DCVJ in methanol.

c) BODIPY-C_{10} was synthesised according to the procedure reported elsewhere.[111,112] The solutions for all measurements was prepared by appropriate dilution of 7.009 mM stock solution of BODIPY-C_{10} in methanol.

3.8.2 Steady state fluorescence measurement

The excitation and emission fluorescence spectra were recorded using a Fluoromax-4 spectroflurometer (Jobin-Yvon;Horiba). All the measurements were carried out at 25°C. The temperature of the sample was controlled using a Peltier thermostat cuvette holder (F3004, Jobin-Yvon; Horiba) with temperature control accuracy to 0.5°C. The absorption spectra of the dyes were recorded using a Perkin Elmer Lambda 25 spectrophotometer. The samples were contained in a 10 mm path length quartz cuvette for all measurements.

3.8.3 Time-resolved fluorescence lifetime

The time-resolved fluorescence lifetime experiments were conducted using an inverted confocal laser scanning microscope (IX71, Olympus) integrated to a custom-built detection

path. The schematic representation of the setup of fluorescence lifetime experiment is illustrated in **Figure 36**. The sample was excited with a laser light using pulsed diode laser LDH-P-C-470 (PicoQuant GmbH) operating at 466nm. The laser head was connected to PDL800-B (PicoQuant GmbH) laser driver, which was used to control the laser power and to enable user to select the repetition frequencies. The driver has a base frequency of 40MHz with a maximum power of 1.35mW. The repetition frequency can be further reduced by division of 1, 2, 4, 8 or 16.

Briefly, a pulsed laser light was directed through a long-pass dichroic mirror and focus on the sample using a high numerical aperture objective. The resulting fluorescence light emission was collected via the same objective and pass through the long pass dichroic mirror. The transmitted fluorescence light emission was then focused by a lens onto a confocal pinhole. Only signal originating from focal plane will pass through the pinhole and all the lights transmitted from other than focal plane was reflected by the pinhole. The fluorescence light was captured by avalanche photodiode detector (APD) operating in single photon counting mode. The time of photon arrival was recorded by the TCSPC module SPC-130-EM (Becker & Hickl GmbH) and the time delay between the laser pulse and the arrival of the photon was recorded in data files. The output data from the detector was also fed to a multifunctional card (PCI 6601, National Instruments) for data monitoring and acquisition purposes. The card was set to operate in counter mode using LabVIEW software written by Edel Research Group. Using this configuration, the real-time data can be monitored, and the data is presented in term of photon count rate and autocorrelation function. This setup also served the platform for detector and pinhole alignment.

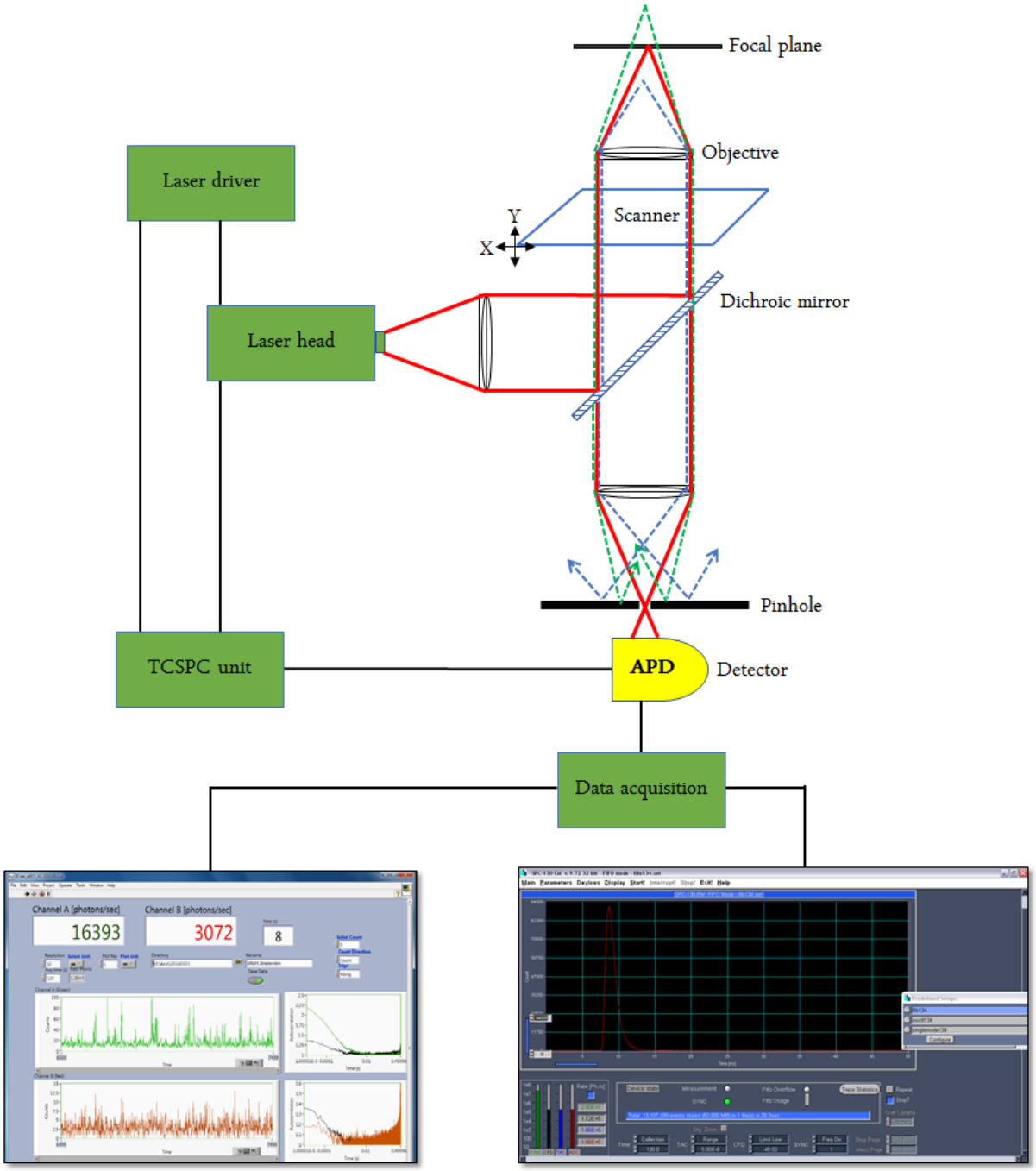

Figure 36: Schematic representation of confocal microscope and the integrated system used for fluorescence lifetime data acquisition.

The fluorescence lifetime decay histogram produced by the SPC-130-EM was analysed using a modified version of the *JLife* program written at Imperial College, with amplitudes and lifetimes loosely constrained to give positive, non-zero values. The interface of the *JLife* program is shown in **Figure 37**. The lifetime data in a *.spc* file format was loaded to the program together with the instrument response function (IRF) file. This is the convolution of the overall measurement system including the laser source, detectors as well as the TCSPC electronics. The IRF is typically measured using a dye with a very short lifetime, in the range of picoseconds. In this study, the IRF was recorded using 15 µM solution of auramine O in distilled water. The IRF was fitted to the measured data using the sqp algorithm with an error tolerance of 10^{-6}. Fluorescence decay was treated as an n component exponential decay of the form shown in equation **(22)**.

$$I(t) = bkg + IRF \otimes \sum_{i=1}^{n} \alpha_i \exp(\frac{-t}{\tau_i}) \qquad \textbf{(22)}$$

where I is fluorescence intensity at time t, bkg is the background counts, t is the time vector of the experiment, α_i is amplitude of component i, IRF is the measured instrument response function, and τ is lifetime of component i. The goodness of fit was judged based on the reduced chi-square (χ^2) values. Theoretically, the best fit has χ^2 value of 1 but this value is difficult to achieve in many cases the acceptable value of χ^2 may vary from case to case. All presented data was from fittings with χ^2 values of less than 1.5. The residual values were plotted at the bottom of each fitting for visual inspection. The residual plot showed how the residuals vary and distributed along a line cantered at zero.

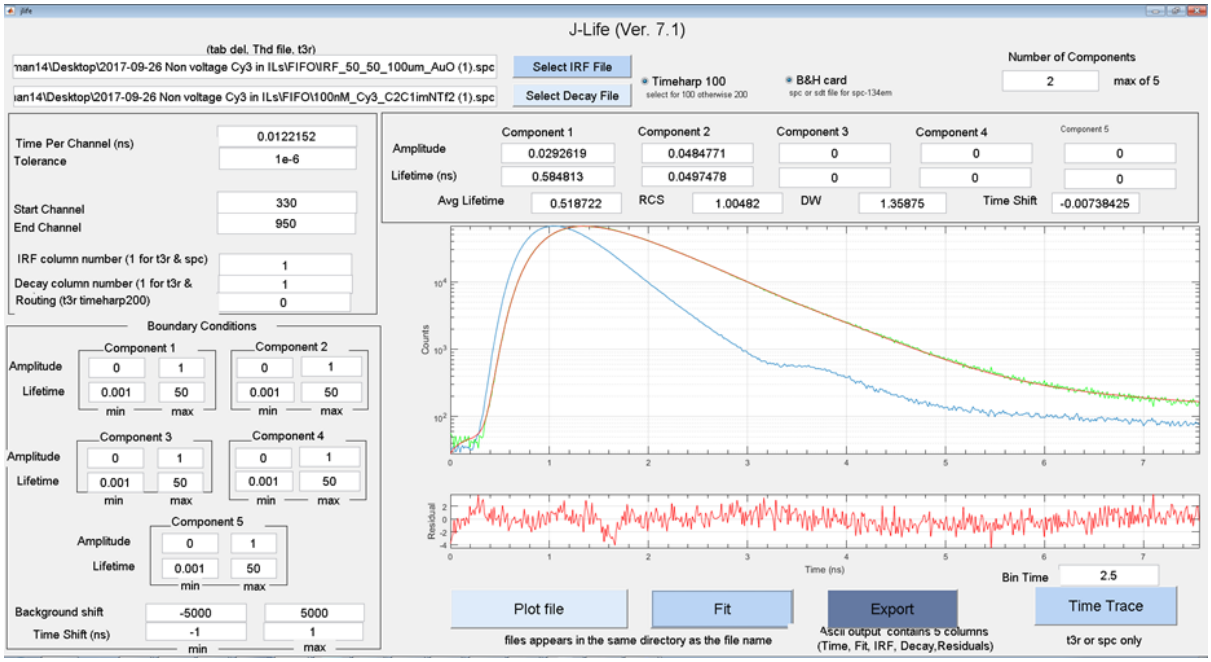

Figure 37: The interface of *J-Life* program used to extract fluorescence lifetime from fluorescence decay curve. The green line is represented the fluorescence decay of Cy3 in $[C_2C_1im][NTf_2]$ and the blue line is showed the IRF decay curve of auramine O. The fluorescence decay was fitted (red line) with two lifetime components resulting in reduced chi-squared (χ_R^2) of ~1.00. The residuals of the fitting are plotted at the bottom of the graph.

Chapter 4 Characterisation of the Physical Properties of Ionic Liquids

4.1 Introduction

The early research on ionic liquids has centred on providing basic data on their physical and/or chemical properties so that they can be used as reference as such available in National Institute of Standards and Technology (NIST). The acquisition of this data has provided a platform for better understanding of the correlation between the nature and structure of the cation and anion of ionic liquids and their resulting physical properties. Purity of the ionic liquid is one of the main concerns when it comes to measuring their physical properties. The presence of contaminants can affect the physical and chemical properties of the ionic liquids.[25] Examples of possible contaminants include water and halide ions, which mainly originate from the starting materials and solvents used during the synthesis of the liquids. The properties of some ionic liquids that are intrinsically hydrophilic make them tend to absorb water from their surroundings and therefore their physical and chemical properties are susceptible to the humidity of the environment. A number of studies exist which have quantified these contaminants and investigated how they affect the overall physical and chemical properties of the ionic liquids.[25,78,83] With the large volume of data available, physical property values can be used as indicators of the purity of ionic liquids. However, developing a systematic understanding of the physical and chemical properties of ionic liquids is significantly more complex compared with molecular solvents or other liquid electrolytes, due to the high number of possible combinations of anions and cations and their functionalities. The following sections

(**Section 4.5** to **section 4.5**) represent the results and discussion of the physical properties (*i.e.* density, viscosity, conductivity and diffusivity) of the synthesised ionic liquids and the correlation of these properties.

4.2 Viscosity

Viscosity (η) can be defined as the resistance of a liquid to flow. The viscosity of a fluid arises from a continual brushing together of the molecules which are in contact to each other. A relatively high viscosity compared to molecular solvents has been a long-time known property that limits the application of ionic liquids as solvents and electrolytes, particularly for applications that demand higher mass transport properties. The model that developed from the hole theory can be used to explain the viscosity of both ionic and molecular fluids. The hole theory was originally described by Furth.[113,114] According this theory, a liquid structure is composed of a continuous phase permeated by a large number of holes. The number of holes in the liquid are comparable to the number of particles of the liquids. This theory was developed to explain the thermal and viscous properties of liquids based of the motion of the holes within the continuous phase. Studies have suggested that conductivity and viscosity of a liquid can be related to the average lifetime of the holes.[114] It is measured by the time for which the holes last before they been occupied by the molecules or ions of the liquid.[113] Essentially, a molecule or ion that sits next to the hole tends to move and occupy the free volume that is available and this is governed by the free energy of the molecule or ion. Thus, the random movement of molecule or ion from one hole to another between different layers of a liquid will create momentum transfer and viscous drag in a moving liquid.[115]

According to hole theory, the holes in ionic liquids are formed due the thermally generated fluctuation in local density when an ionic material undergoes a melting process. The size of the holes is varying, and locality of the holes is also randomly distributed across the liquid. Over a time, these holes undergo constant flux. The viscosity of a fluid is modelled based on the assumption that the molecules or ions in the fluid behave like an ideal gas,[116] but their movement is restricted by the availability of suitably sized of holes for the molecules or ions to move into. Thus, equation **(23**) can be used to calculate viscosity of a fluid.

$$\eta = \frac{m\bar{c} / 2.12\sigma}{P(R > r)} \qquad \textbf{(23)}$$

In the equation **(23**), m is the molecular mass, $\bar{c}$ is the average speed of molecule (=$(8kT/\pi m)^{1/2}$), σ is the collision diameter of the molecules (=$4\pi r^2$) and $P(R>r)$ is the probability of finding a hole with radius (R) greater than the radius of solvent molecules (r). It is given by integration of the following equation (equation **(24**)).[115,117]

$$PdR = \frac{16}{15\pi^{1/2}} a^{7/2} R^2 e^{-aR} dR \qquad \textbf{(24)}$$

where a = $4\pi\gamma/kT$, γ is the surface tension, k is Boltzmann constant and T is absolute temperature.

The previous study has suggested that the average diameter of the holes in a molten salt is in the range of 1.5 – 2.5Å and this is similar to dimension of the ions of 1.0 – 2.6Å.[115,118] Thus, it is possible for the ions to occupy the holes without facing a huge physical constraint.[115] The

radius of the average size hole, ‹*R*› is related to the surface tension of the liquid (γ) as expressed by equation **(25)**

$$4\pi \left\langle R^2 \right\rangle = \frac{3.5kT}{\gamma} \quad \textbf{(25)}$$

Abbott has used the hole theory to quantitively explain the viscosity of room temperature ionic liquids, molten salts and molecular liquids.[118] Among these three types of liquids, room temperature ionic liquids have the highest viscosity in the range of $10^1 – 10^3$ mPa s while most of the molten salts and molecular liquids only have viscosities in the range of about 1 – 5 mPa s. To explain the huge differences in viscosity between these liquids, it is necessary to quantitively account for the differences between the size of the ions and holes in each type of the liquid. Abbott has found that the probability of finding an ion-sized hole in a room temperature ionic liquid is very low, in the order of $10^{-4} – 10^{-5}$ compared to the molten salt system which have the probability close to unity. However, there is a weak correlation between the probability of finding ion-sized hole and viscosity for molecular solvents. He further used the probability values to estimate of viscosity of the liquids using equation **(23)** and found that the calculated viscosities have a relatively good correlation to the measured viscosities.

In this study, the viscosity of ionic liquids was measured using a cone and plate viscometer as discussed in **Section 3.3**. The viscosities of selected molecular solvents and ionic liquids at 25°C are presented in **Table 2**. The viscosities of ionic liquids are slightly higher compared to most molecular solvents such as water (H_2O) and ethanol (CH_3CH_2OH). This is due to the nature of ionic liquids which comprise of bulky cations and anions. The ability of anions to form weak hydrogen bonds with the cations also affects the viscosities of ionic liquids.[30]

Significant research has been focused on producing ionic liquids with lower viscosities that would improve ion transport in ionic liquids. Although mixing of ionic liquids with molecular solvent is considered an effective method to reduce the viscosity, it is not a preferable way as the mixing can cause an increase in the vapour pressure and flammability, and a lower the electrochemical stability.

Table 2: Viscosity of selected molecular solvents and ionic liquids at 25°C.

Liquid	Viscosity, η (cP)	
	Experimental	**Literature**
H_2O	-	0.89[119]
CH_3CH_2OH	-	1.07[119]
CH_2OHCH_2OH	-	16.10[119]
PEG200	47.30 ± 0.38	49.724,[120] 48.157[121]
PEG400	94.67 ± 2.12	90.701,[120] 92.797[121]
$[C_2C_1im][NTf_2]$	27.44 ± 0.84	25,[122] 33.36,[123] 28[124]
$[C_3C_1im][NTf_2]$	42.93 ± 1.46	43.7,[125]45.748[126]
$[C_4C_1im][NTf_2]$	49.27 ± 0.13	44,[122] 50.05,[127] 49.9[128]
$[C_6C_1im][NTf_2]$	65.30 ± 0.85	59,[122] 70.614,[126] 68,[129] 69.43[130]
$[C_8C_1im][NTf_2]$	90.04 ± 2.85	93.053,[126] 92.51,[131] 90.0[128]
$[C_{12}C_1im][NTf_2]$	147.97 ± 1.01	130.5,[132] 125,[133] 154.33[126]
$[C_4C_1pyrr][NTf_2]$	76.14 ± 0.84	76.73,[127] 76.54,[134] 77.650[135]
$[P_{4446}][NTf_2]$	234.37± 7.13	257,[136] 207.71,[137] 261[138]
$[C_4C_1im][BF_4]$	83.48 ± 4.89	120, [139] 71.7,[140] 110.308,[141]107.5,[142] 99.6[128]
$[C_4C_1im][PF_6]$	259.17 ± 8.20	264.5,[143] 282.2,[144] 273[145]
$[C_4C_1im][CF_3SO_3]$	66.40 ± 0.53	76.96[146] 84.4,[128] 83.2[147]

The viscosities of the ionic liquids are similar to the viscosities of viscous molecular solvent ethylene glycol (CH_2OHCH_2OH) and similar liquid polymeric materials. For example, the viscosities of $[C_4C_1im][NTf_2]$ and $[C_4C_1pyrr][NTf_2]$ are found to be very similar to the viscosity of poly(ethylene glycol) with an average molecular weight of 200 g mol^{-1} (PEG200) and poly(ethylene glycol) with average molecular weight of 400 g mol^{-1} (PEG400), respectively. It is worth mentioning that the measured viscosities are consistent with those reported in the literature except for the hydrophilic ionic liquids *i.e.* $[C_4C_1im][BF_4]$ and $[C_4C_1im][CF_3SO_3]$. The deviation of the measured values compared with literature values is more than 5%, which exceeded the error associated with the instrument. However, the viscosity values reported in literature are also scattered from each other by more than 5%. This suggests that the big difference between the reported values is not only associated with the instrument but might be due the differences in the quality of the measured ionic liquids. These two ionic liquids, $[C_4C_1im][BF_4]$ and $[C_4C_1im][CF_3SO_3]$, are moderately hydrophilic in nature and they interact easily with water. Water is often used to wash out the remaining halide impurities from these ionic liquids during their preparation. Excessive washing causes the ionic liquids to absorb a large volume of water and hence reduces the viscosity of the ionic liquids.[25,126] In contrast, incomplete washing causes the ionic liquids to be contaminated with chloride ions which increase the viscosity of the liquids.[25] Even though the viscosity measurement was performed under a nitrogen atmosphere, exposing the ionic liquids to the atmosphere is sometimes unavoidable especially during the process of transferring and optimising the volume of sample at the instrument. This will also allow the ionic liquids to absorb moisture from the atmosphere.

The viscosity of an ionic liquid is strongly dependent on its anion and cation constituents. Varying the alkyl chain length (n) of the imidazolium cation $[C_nC_1im]^+$ in $[NTf_2]^-$-based ionic liquids resulted in increased viscosity of ionic liquids. This can be seen clearly in **Figure 38**, as the alkyl chain length of the imidazolium cation is increased from n = 2 to n = 12, the viscosity of $[C_nC_1im][NTf_2]$ steadily increased.

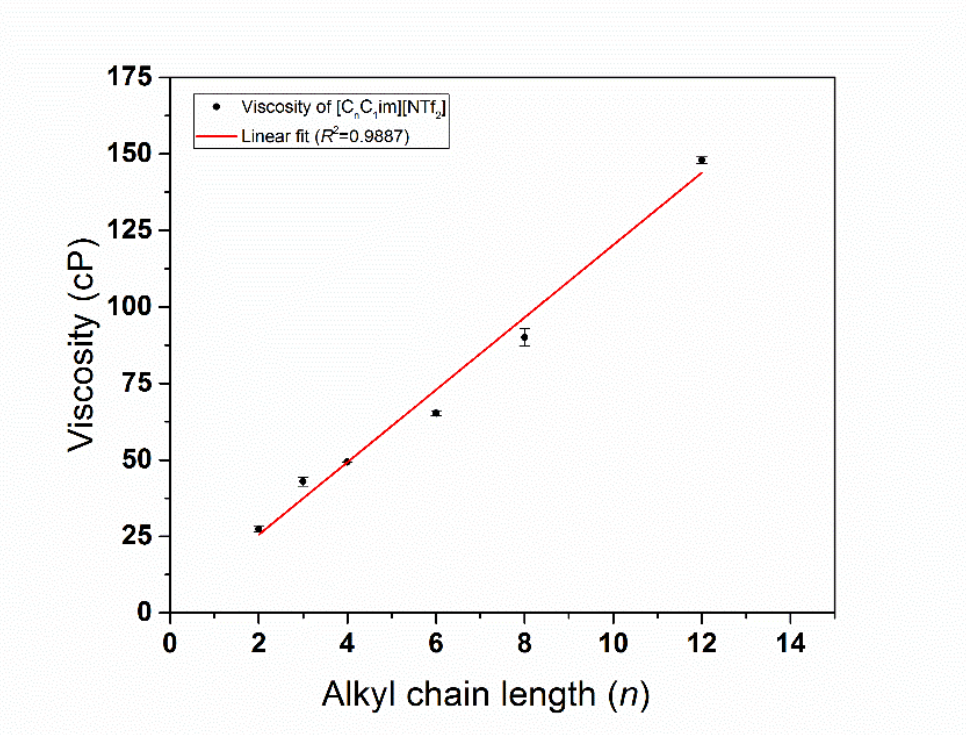

Figure 38: Viscosity of $[C_nC_1im][NTf_2]$ as a function alkyl chain length (n).

The main reason for this observation is that, with a longer alkyl chain attached to the imidazolium ring, the cation become bulkier and heavier making the liquid to flow slower due its mass. Additionally, the longer alkyl chain also contributes to increased Van der Waals forces between the alkyl chains which restrict the movement of the ionic component.[148] The

increasing viscosity with longer alkyl substituents has been reported in literature for many ionic liquids including $[C_nC_1im][X]$, where [X] = $[BF_4]$,$[PF_6]$,$[CF_3SO_3]$ and $[NO_3]$.[148] Replacing the imidazolium cation in $[C_4C_1im][NTf_2]$ with other cations such as pyrrolidinium $[C_4C_1pyrr]^+$ and phosphonium$[P_{4446}]^+$ greatly affected the viscosity of ionic liquids. The viscosity is increased from 49.27 cP to 76.14 cP when the imidazolium cation was replaced with a pyrrolidinium and further increased to 207.71 cP when the cation was replaced by the $[P_{4446}]^+$ cation. The main contributors to these differences might be the size and molar mass of the cation. For comparison, $[P_{4446}]^+$ has a molar mass of 287.32 g mol^{-1} while $[C_4C_1pyrr]^+$ has molar mass of 142.22 g mol^{-1}. Furthermore, the structural geometry these three cations are different. The structural geometry of the $[C_4C_1im]^+$ is planar compared to $[P_{4446}]^+$ which has tetrahedral geometry. The $[C_4C_1pyrr]^+$ sits in between these two cations in terms of the planarity of its structural geometry. The planar structure is believed to facilitate movement of the ions and hence leads to a lower viscosity.

The effect of varying the anion constituent in 1-butyl-3-methylimidazolium based ionic liquids $[C_4C_1im][X]$ (X= $[NTf_2]^-$, $[CF_3SO_3]^-$, $[BF_4]^-$, $[PF_6]^-$) can be observed from the data presented here. The order of viscosity of $[C_4C_1im][X]$ is as follows: $[NTf_2]^- < [CF_3SO_3]^- < [BF_4]^- < [PF_6]^-$. There is no clear correlation between the viscosity and mass/size of anion ($[NTf_2]^-$ = 280.14 g mol^{-1}, $[CF_3SO_3]^-$ = 149.07 g mol^{-1}, $[BF_4]^-$ = 86.80 g mol^{-1}, $[PF_6]^-$ = 144.96 g mol^{-1}). Although the size and mass of the anions could affect the viscosity to a certain extent, there are other factors that contribute to the viscosity differences. One such factor is the surface tension (γ) of the ionic liquids as suggested by equations **(23)** - **(25)**. The surface tension is inversely proportional to the radius of holes in the liquids. Thus, ionic liquids with a higher surface tension will have smaller holes which thus lead to a higher viscosity. The reported surface

tension for $[C_4C_1im][NTf_2]$, $[C_4C_1im][BF_4]$ and $[C_4C_1im][PF_6]$ are 37.5, 46.6 and 48.8 $mN^{-1}m^{-1}$, respectively.[149] It can be observed that the changing trend of surface tension of these ionic liquids are parallel to the variations of their viscosity.

Another possible factor is the ability of the anions to form hydrogen bonds with the cations.[23,150] The $[PF_6]^-$ anion forms a more viscous ionic liquid compared to $[NTf_2]^-$ anion due to different ability to form hydrogen bonds with the anion. The $[NTf_2]^-$ anion is a relatively weak base compared to $[PF_6]^-$ due to the delocalization of negative charges over the two sulfoxide groups. Other studies suggest that the structure of the anions (symmetry vs. asymmetry) and charge distributions within the ions affect the viscosity of ionic liquids.[151] Ionic liquids with a more symmetric anion will have a higher viscosity. This can be seen clearly if the viscosity of $[C_4C_1im][NTf_2]$ is compared to the viscosity of $[C_4C_1im][BF_4]$ or $[C_4C_1im][PF_6]$. However, it is difficult to quantitively determine the contributions of each factor to the viscosity variations found in the different ionic liquids.

The viscosities of the ionic liquids were measured over a wide range of temperatures in order to study the effect of temperature on viscosity. Clearly, the viscosity of all ionic liquids decreased with the increasing in temperature (see **Figure 39**). This observation is similar to the trend that is normally observed in most other liquids including the molecular solvents. At higher temperature the molecules in the liquids possess higher kinetic energy and they move at a faster rate. Therefore, they can overcome the cohesive forces more easily than at lower temperatures and the resistance of the liquid to flow reduces. The quantitative relationship of the viscosity of a liquid with temperature was been proposed by Reynolds in 1886 and can be mathematically expressed as equation **(26)**.

$$\eta \propto \exp(\frac{const.}{T}) \quad \textbf{(26)}$$

According to this equation, the viscosity of a liquid changes exponentially with the temperature. As can be seen from the plots in **Figure 39**, the viscosity of all ionic liquids decreases exponentially with increasing temperature.

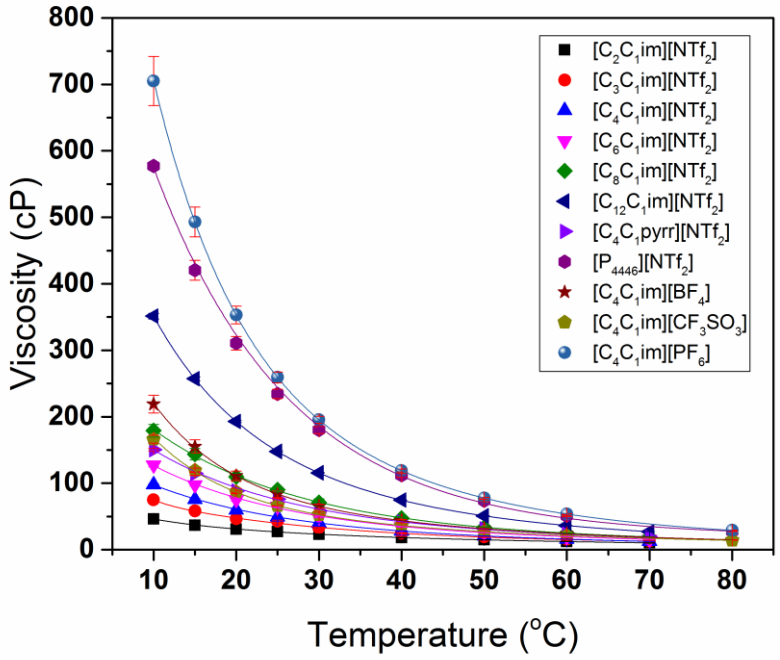

Figure 39: Viscosity of ionic liquids as a function of temperature.

The Arrhenius model has been developed to describe the dependency of shear viscosity on the temperature. The mathematical equation that express the relationship is shown below (equation **(27)**).

$$\eta = \eta_{\infty} \times e^{\frac{E_{\eta}}{RT}} \quad \textbf{(27)}$$

The activation energy for viscous flow (E_η) and the viscosity at infinite temperature(η_∞) were determined from the slope and y-axis intercept of the linear plot of ln η against $1/T$. The value of E_η quantified the minimum energy barrier required for the ions to move past each other and its value can be correlated to the structural information of the ionic liquids. A higher value of E_η means it is harder for ions to move past each other. This usually corresponds to ionic liquids that comprise of larger sized ions and/or have stronger intermolecular force. However, the impact of intermolecular forces on viscosity is diminished at infinite temperature and this leaves the geometric structure as the only factor that affects the viscosity. The plot of ln η against $1/T$ for a series of 1-alkyl-3-methylimidazolium imide [$C_nC_1$im][NTf_2] with different alkyl chain length(n) is shown in **Figure 40**. All the ionic liquids in this series are well fitted to the Arrhenius model with $R^2 > 0.99038$. The E_η value increases with increasing the alkyl chain lengths (see **Table 3**). This is mainly due to the increasing molar mass of the cation as the alkyl chain length increases which means more energy is required for the ions to move. The intermolecular forces present in these ionic liquids are similar although the magnitude of the intermolecular forces might vary slightly with the lengthening of the alkyl chain. Thus, the contribution of intermolecular forces to the variations of E_η for this series of ionic liquids is believed to be minimal. On the other hand, the value of η_∞ is slightly decreased with the increasing alkyl chain length, which indicates the molar mass and intermolecular forces effects are not significant at infinite temperature.

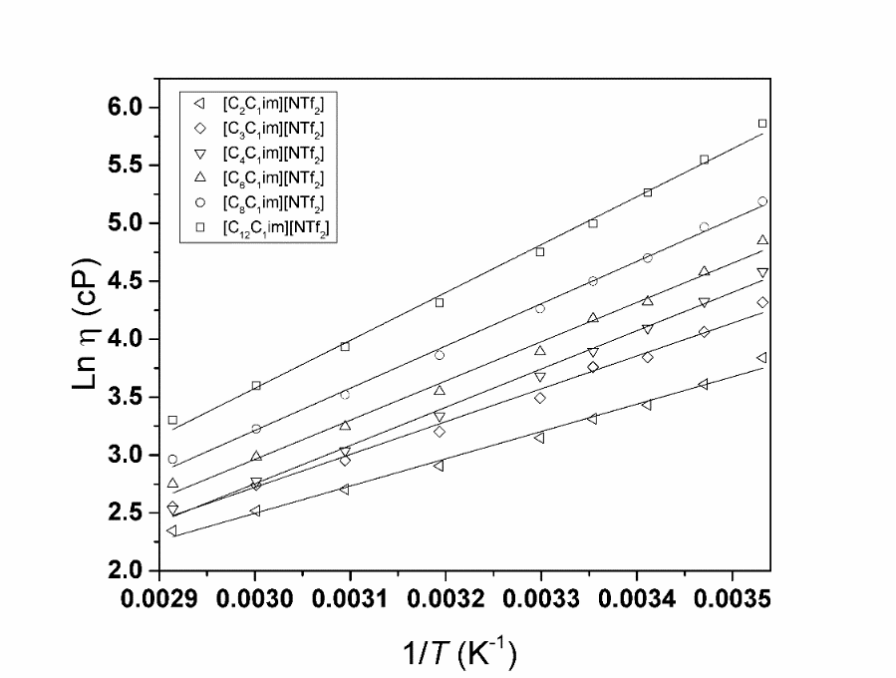

Figure 40: Arrhenius plot for 1-alkyl-3-methylimidazolium imide ([$C_nC_1$im][NTf_2], n = 2,3,4,6,8 and 12) ionic liquids.

Table 3: The quantities of E_η and η_∞ and R^2 extracted from Arrhenius's plot for 1-alkyl-3-methylimidazolium bis(trifluoromethylsulfonyl)imide ([$C_nC_1$im][NTf_2], n = 2,3,4,6,8 and 12) ionic liquids.

Ionic liquid	E_η **(J mol^{-1})**	η_∞ **× 10^{-3} (cP)**	R^2
[C_2C_1im][NTf_2]	2355.92	10.34	0.99141
[C_3C_1im][NTf_2]	2834.75	3.08	0.99038
[C_4C_1im][NTf_2]	3302.94	0.78	0.99562
[C_6C_1im][NTf_2]	3387.18	0.75	0.99321
[C_8C_1im][NTf_2]	3648.09	0.44	0.99726
[$C_{12}C_1$im][NTf_2]	4134.17	0.15	0.99589

The Arrhenius plot of ionic liquids with the common cation of 1-butyl-3-methylimidazolium $[C_4C_1im]^+$ is shown in **Figure 41**. Different anions were paired to 1-butyl-3-methylimidazolium cation *i.e.* $[NTf_2]^-$, $[CF_3SO_3]^-$, $[BF_4]^-$ and $[PF_6]^-$. The coefficient of determination (R^2) of the fit for the hydrophilic ionic liquids $[C_4C_1im][BF_4]$ and $[C_4C_1im][CF_3SO_3]$ were relatively lower compared to the hydrophobic ionic liquids. This is might be due to the intrinsic nature of the hydrophobic ionic liquids to absorb moisture from the environment. The variation of the E_η values presented in **Table 4** is inconsistent with the variation of the molar mass of cations. The molar mass of the anion in increasing order is: $[BF_4]^- < [PF_6]^- < [CF_3SO_3]^- < [NTf_2]^-$. The variation of E_η is observed to be largely governed by the structural properties of the anion. Ionic liquids with a more symmetric anion possess a higher E_η value and those with a less symmetric anion possess a lower E_η value. The interaction of symmetric ions is usually more effective and leads to a stronger intermolecular force. This observation suggests that the structural property and thus the intermolecular forces factor is a more dominant factor than the molar mass in determining the value of E_η.

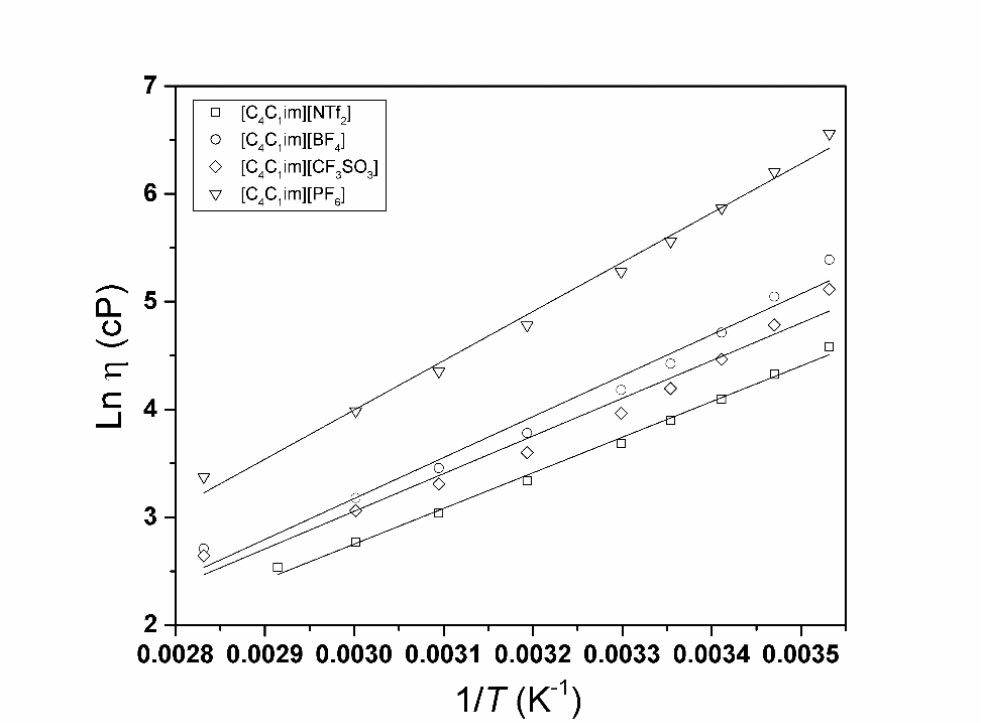

Figure 41 : The Arrhenius plot of 1-butyl-3-methylimidazolium based ionic liquids with different anions.

Table 4: The quantities of E_η and η_∞ and R^2 extracted from Arrhenius's plot of 1-butyl-3-methylimidazolium based ionic liquids with different anions.

Ionic liquid	E_η **(J mol^{-1})**	η_∞ **× 10^{-3} (cP)**	R^2
$[C_4C_1im][NTf_2]$	3302.94	0.78	0.99562
$[C_4C_1im][CF_3SO_3]$	3492.50	0.60	0.98044
$[C_4C_1im][BF_4]$	3798.16	0.27	0.97585
$[C_4C_1im][PF_6]$	4566.80	0.06	0.99247

The Arrhenius plot of ionic liquids with a common anion *i.e.* $[NTf_2]^-$ is presented in **Figure 41** and the parameters extracted from the graph are summarised in **Table 4**. The magnitude of E_η varies consistently with the molar mass of the cations as well as the geometric structure of the ions. The molar mass of the cations in increasing order is as follows: $[C_4C_1im]^+$< $[C_4C_1pyrr]^+$< $[P_{4446}]^+$. The structural geometry of the $[C_4C_1im]^+$ cation is more planar compared to the structure of the $[C_4C_1pyrr]^+$ cation. The planar structure of the $[C_4C_1im]^+$ ions can facilitate the flow while the non-planar structure of the $[C_4C_1pyrr]^+$ cations can cause entanglement and this becomes a resistance against the movement of the ions. The presence of four, bulky and relatively long alkyl groups attached to the central core in the $[P_{4446}]^+$ cation has contributed to the structure having a high molar mass. The difference in length of the alkyl groups leads to the asymmetric structure in $[P_{4446}][NTf_2]$. Both factors contribute to the high E_η value observed $[P_{4446}][NTf_2]$.

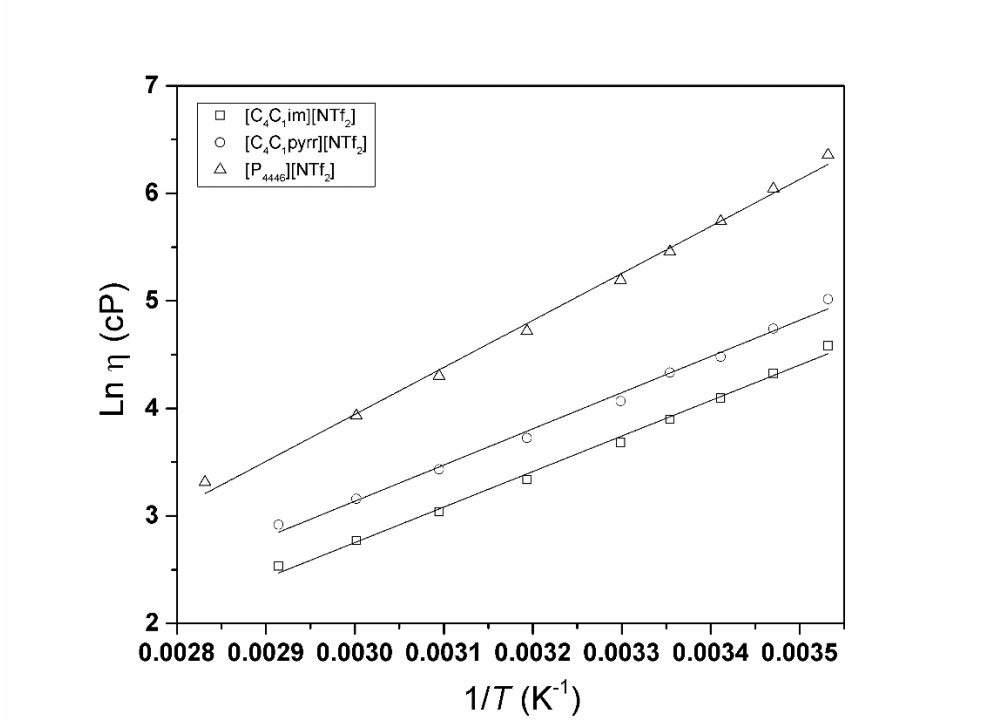

Figure 42: The Arrhenius plot of $[NTf_2]^-$ based ionic liquids with different cations.

Table 5: The quantities of E_η and η_∞ and R^2 extracted from Arrhenius plot of $[NTf_2]^-$ ionic liquids with different cations.

Ionic liquid	E_η **(J mol^{-1})**	η_∞ **× 10^{-3} (cP)**	R^2
$[C_4C_1im][NTf_2]$	3302.94	0.78	0.99562
$[C_4C_1pyrr][NTf_2]$	3365.76	0.95	0.99408
$[P_{4446}][NTf_2]$	4371.96	0.10	0.99562

4.3 Ionic conductivity

Ionic conductivity (κ) is one of the most important criteria when selecting electrolytes for electrochemical applications. Ionic conductivity is a measure of the available charge carriers and their mobility.[23] Room temperature ionic liquids possess reasonably high ionic conductivities (up to 20 mS cm^{-1}) compared to some non-aqueous solvents/electrolytes.[152] However, their conductivities are significantly lower than concentrated aqueous electrolytes and molten salts. The relatively high viscosity of ionic liquids has a negative impact on their ionic conductivity. Even though ionic liquids consist entirely of ions, their conductivities are usually lower than the expected due to possible ion pairing and aggregation of ions.[128] The mobility of the ions in ionic liquids also restricted due to the large size and complex structure of the ions in many ionic liquids.

As discussed in the previous section (see section 4.2), the high viscosity of ionic liquids arises from the low probability of finding holes with suitable dimensions (r > R).Then it makes sense to relate ion motion to the migration of holes in the opposite direction. Since the probability of finding holes with a suitable size is very low (10^{-6}),[117] then it can be assumed that the holes exist at infinite dilution. At infinite dilution, the movement of the holes are independent of each other and can be described by the following Stokes-Einstein equation (equation **(28)**)

$$\lambda_{+} = \frac{z^2 Fe}{6\pi\eta r_{+}} \qquad \textbf{(28)}$$

where z is the charge of the ion, F is Faraday constant, η is viscosity, e is the electronic charge and r_+ is ionic radius. Then, the total molar conductivity of the system can be calculated from the summation of the molar conductivity of the anion and cation (equation **(29)**)

$$\Lambda = \lambda_+ + \lambda_- \quad \textbf{(29)}$$

and an expression for ionic conductivity can be written as equation **(30)**

$$\kappa = \frac{z^2 Fe\rho}{6\pi\eta M_w}(r_+^{-1} + r_-^{-1}) \quad \textbf{(30)}$$

An equation derived from the modified Stokes-Einstein equation to express the conductivity of charge in room temperature ionic liquids has been introduced by Bonhote *et al.*. The conductivity can be expressed as equation **(31**).

$$\kappa = yF^2\rho / (6\pi N_A M_w \eta)[(\xi_+ r_+)^{-1} + (\xi_- r_-)^{-1}] \quad \textbf{(31)}$$

where y is the degree of dissociation, F is Faraday constant, ρ is the density, M_w is the molar mass of the ionic liquid and N_A is the Avogadro constant. The terms ξ_+ and ξ_- are the microviscosity factors referred to as "correction" factors which express the specific interaction between the mobile ions in the melt and r_+ and r_- are the radii of the cation and anion, respectively. From this equation, the qualitative relationship between conductivity and the physical parameters expressed by equation **(31**) can be verified. This equation also highlights the importance of considering ionic radii as a factor in searching for highly conducting ionic liquids rather than focusing on the viscosity factors only.

Based on previous studies, ionic conductivity has a weak correlation with the size and type of the cation of the ionic liquids.[23] However, it has no clear correlation to the type or size of the ionic liquid anion. For example, ionic liquids with a smaller anion, $[CH_3COO]^-$ have a lower ionic conductivity than those with the bigger anion, $[(CF_3SO_2)_2N]^-$.[23] Another important factor that affects the conductivity is temperature. The conductivity of ionic liquids at elevated temperature usually demonstrates Arrhenius behaviour. However, the conductivity deviates from linearity as the temperature approaches the glass transition temperature (T_g) of the ionic liquid due to the transition of the state of the materials. The presence of contaminants also affects the ionic conductivity of ionic liquids. Contamination of chloride ions increases the viscosity of ionic liquids and this might supress ionic conductivity of ionic liquids.[25] In contrast, contamination by water leads to high ionic conductivity as the viscosity of the ionic is decreased with the addition of water.[25] Slight differences between the conductivities recorded here and those by other research groups could be due to the presence of contaminations and also due to the different way the measurements were conducted.

The ionic conductivities of the ionic liquids were measured using a custom-built ITO-PDMS electrochemical cell (See section **3.6.2**). The ionic conductivities of the ionic liquids at 25°C are presented in **Table 6**. The measured conductivity values are in good agreement with the literature values except for the hydrophilic ionic liquids *i.e.* $[C_4C_1im][BF_4]$ and $[C_4C_1im][CF_3SO_3]$. The same trend that was observed in the viscosity results and the reason for this observation has been discussed in **Section 4.2**. The most significant variability of the measured and literature values was recorded for $[C_4C_1im][BF_4]$. It has been reported that this ionic liquid undergoes hydrolysis easily at moderate temperature and the degree of hydrolysis is markedly dependent on the temperature.[86] The heating procedure applied to this ionic liquid

as drying procedure might induce hydrolysis of the anion into hydrofluoric acid and other ions which in turn might contribute to the higher ionic conductivity.

Table 6: Ionic conductivities of ionic liquids at 25°C.

Liquid	**Conductivity (mS/cm)**	
	Experimental	**Literature**
H_2O	6.46 ± 0.18 (μs/cm)	5.5 (μs/cm)[153]
$[C_2C_1im][NTf_2]$	9.36 ± 0.24	9.1,[128] 9.12[154]
$[C_3C_1im][NTf_2]$	5.68 ± 0.15	
$[C_4C_1im][NTf_2]$	3.76 ± 0.06	3.8,[128] 4.034,[155] 4.06[154]
$[C_6C_1im][NTf_2]$	2.13 ± 0.04	2.17,[129] 2.174,[130] 2.2,[128] 2.18[154]
$[C_8C_1im][NTf_2]$	1.33 ± 0.02	1.3[128]
$[C_{12}C_1im][NTf_2]$	0.67 ± 0.01	
$[C_4C_1pyrr][NTf_2]$	2.79 ± 0.06	2.770,[127] 2.755,[134] 2.8[128]
$[P_{4446}][NTf_2]$	0.43 ± 0.03	0.419,[137] 0.43[138]
$[C_4C_1im][BF_4]$	4.18 ± 0.21	1.73,[156] 3.6,[128] 1.98[157]
$[C_4C_1im][PF_6]$	1.81 ± 0.08	1.46, [156] 1.5,[128]1.46[154]
$[C_4C_1im][CF_3SO_3]$	3.37 ± 0.16	2.9,[128] 2.90[158]

The conductivity of 1-alkyl-3-methylimidazolium bis(trifluoromethylsulfonyl)imide $[C_nC_1im][NTf_2]$ decreased with increasing alkyl chain length (*n*). The variation of the conductivity of the 1-butyl-3-methylimidazolium $[C_4C_1im]^+$ based ionic liquids with different anions follows the following order: $[C_4C_1im][PF_6] < [C_4C_1im][CF_3SO_3] < [C_4C_1im][NTf_2] < [C_4C_1im][BF_4]$. There is no clear correlation of the measured conductivity value with the size and/or molar mass of the anions. However, the variation of conductivities of the ionic liquids with different cations show some consistent variation in terms of molar mass. This can be seen by comparing the conductivity of these ionic liquids: $[P_{4446}][NTf_2]$ (287.29 $gmol^{-1}$) < $[C_{12}C_1im][NTf_2]$ (251.32 $gmol^{-1}$) < $[C_8C_1im][NTf_2]$ (195.32 $gmol^{-1}$) < $[C_4C_1pyrr][NTf_2]$ (142.15 $gmol^{-1}$) < $[C_4C_1im][NTf_2]$ (139.21 $gmol^{-1}$). The structural geometry of the cations has also been reported to play a role in determining the conductivity of ionic liquids. The conductivity will decrease with decreasing planarity of the cationic core.[159,160] This can be seen by comparing the conductivity of these three ionic liquids: $[C_4C_1im][NTf_2]$, $[C_4C_1pyrr][NTf_2]$ and $[P_{4446}][NTf_2]$. The conductivities of these ionic liquids are 3.76, 2.79 and 0.43 mS cm^{-1}, respectively. The geometric structure of the imidazolium ring is rather flat compared to the tetraalkylphosphonium which adopts a tetrahedral arrangement. In comparison, the pyrrolidinium cation adopts an intermediate geometry which is between these two ionic liquids shows an intermediate conductivity as well.

4.4 Diffusivity

Diffusion is the process of transportation of ions or molecules in a volume of space. This process is usually influenced by several external forces such as temperature, pressure and concentration. Diffusion phenomena are commonly observed in many natural processes in living organisms such as the human body and plants. The intrinsic property of ions or molecules that are constantly moving in random direction *i.e.* Brownian motion serves as the basic mechanism of the diffusion process.[161] The Brownian motion of ions or molecules by a translational process will cause a concentration gradient across the space volume of a liquid. The rate at which the concentration gradient occurs is equivalent to translational diffusion. The random movement also causes the orientation of ions or molecules to change, and the rate of change in orientation over time is equivalent to rotational diffusion. The driving forces of the diffusion process is usually expressed in terms of diffusion fluxes and diffusion potentials. Fick's first law correlates the diffusion flux density to the concentration gradient of diffused particles. The constant that relate the proportionality of these two parameters is called diffusion coefficient. For a system with two components undergoing one-dimensional diffusion in the *z*-direction, the mathematical expression of the Fick's first law can be presented in equation **(32)**.

$$\bar{j} = -D_i \frac{\partial c_i}{\partial z} \quad (i = 1, 2) \tag{32}$$

$\bar{j}$ = particle flux

$\frac{\partial c_i}{\partial z}$ = concentration gradient at *z*-direction

D_i = diffusion coefficient

In a liquid system like room temperature ionic liquids, translational diffusion plays an important role for mass transport and it also helps promote chemical reactions via collisions. At the equilibrium state, all ions or molecules are assumed to have the same probability to occupy the space volume of the liquids. The process that occurs by virtue of random motion of the ions or molecules of the liquid is called self-diffusion.

The commonly used techniques to study the diffusivities of ions and molecules in ionic liquids include impedance spectroscopy, NMR spectroscopy and fluorescence spectroscopy. The variations in temporal time scale of diffusion processes perceived by these different measurement techniques lead to slight variation in the value of diffusion coefficient reported here as well as in the literature. The impedance spectroscopy measurement involves the indirect measurement of diffusivities. The diffusion coefficient (D_{imp}) is calculated from the impedance data using the Nernst-Einstein equation (see **equation (34) , Section 4.5).** The magnitude of the diffusion coefficient obtained from the impedance spectroscopy is different from the diffusion coefficient (D_{NMR}) obtained from the NMR measurement due to the different way the diffusion phenomena are perceived by these experimental techniques. The ratio of D_{NMR} to D_{imp} is called the Haven ratio which denotes the ionicity of the ionic liquids.[162]

Table 7 summarizes the translational diffusion coefficients of anions and cations in ionic liquids measured by PGSTE-NMR. The diffusivities of the cations in the neat ionic liquids are generally faster than the anions. This observation is consistent with those reported in the literature.[128,163] For $[C_4C_1im][X]$, the order of diffusion of the anions is $[NTf_2]^- > [BF_4]^- > [PF_6]^- > [CF_3SO_3]^-$. The diffusivity of both the anion and cation of 1-alkyl-3-methylinidazolium

bis(trifluoromethylsulfonyl)imide ([$C_nC_1$im][NTf_2]) is decreased with the increasing of the alkyl chain length (*n*). This is mainly due to the increased in viscosity with the increasing of the alkyl chain length. Thus, the ions diffuse slower in a more viscous medium. In general, the dependency of diffusivity on viscosity is observed in all measured ionic liquids. The correlations between diffusivity and other transport properties *i.e.* viscosity and conductivity are discussed in **Section 4.6**.

Table 7: The translational diffusion coefficients of ions in ionic liquids at 25°C.

Ionic liquid	Cation diffusivity, D^+ (m^2 s^{-1})		Anion diffusivity, D^- (m^2 s^{-1})	
	Experiment	Literature	Experiment	Literature
$[C_2C_1im][NTf_2]$	$5.08\times10^{-11} \pm 1.05\times10^{-14}$	4.4×10^{-11} at 20°C[128]	$2.76\times10^{-11} \pm 5.87\times10^{-16}$	2.5×10^{-11} at 20°C[128]
$[C_3C_1im][NTf_2]$	$3.36\times10^{-11} \pm 1.37\times10^{-14}$		$2.06\times10^{-11} \pm 2.57\times10^{-16}$	
$[C_4C_1im][NTf_2]$	$2.77\times10^{-11} \pm 1.77\times10^{-14}$	2.2×10^{-11} at 20°C[128]	$1.84\times10^{-11} \pm 1.94\times10^{-16}$	1.6×10^{-11} at 20°C[128]
$[C_6C_1im][NTf_2]$	$1.68\times10^{-11} \pm 8.34\times10^{-15}$	1.3×10^{-11} at 20°C[128]	$1.51\times10^{-11} \pm 1.61\times10^{-16}$	1.2×10^{-11} at 20°C[128]
$[C_8C_1im][NTf_2]$	$1.17\times10^{-11} \pm 2.19\times10^{-14}$	9.1×10^{-12} at 20°C[128]	$1.01\times10^{-11} \pm 4.01\times10^{-16}$	8.8×10^{-12} at 20°C[128]
$[C_{12}C_1im][NTf_2]$	$6.06\times10^{-12} \pm 5.53\times10^{-15}$		$3.16\times10^{-12} \pm 8.52\times10^{-16}$	
$[C_4C_1pyrr][NTf_2]$	$1.68\times10^{-11} \pm 1.43\times10^{-14}$	1.3×10^{-11} at 20°C[128]	$1.37\times10^{-11} \pm 1.43\times10^{-14}$	1.1×10^{-11} at 20°C[128]
$[P_{4446}][NTf_2]$	$3.17\times10^{-12} \pm 3.55\times10^{-15}$	3.30×10^{-12}[136]	$4.38\times10^{-12} \pm 3.36\times10^{-16}$	4.64×10^{-12}[136]
$[C_4C_1im][BF_4]$	$1.39\times10^{-11} \pm 7.24\times10^{-15}$	1.1×10^{-11} at 20°C[128]	$1.33\times10^{-11} \pm 2.66\times10^{-16}$	1.0×10^{-11} at 20°C[128]
$[C_4C_1im][PF_6]$	$6.43\times10^{-12} \pm 3.45\times10^{-15}$	5.0×10^{-11} at 20°C[128]	$4.93\times10^{-12} \pm 4.81\times10^{-16}$	3.8×10^{-11} at 20°C[128]
$[C_4C_1im][CF_3SO_3]$	$1.66\times10^{-11} \pm 1.18\times10^{-14}$	1.3×10^{-11} at 20°C[128]	$1.25\times10^{-11} \pm 1.04\times10^{-16}$	1.0×10^{-11} at 20°C[128]

With the advancement of the technology, it is becoming possible to probe or tag ions or molecules without appreciably changing their physical and chemical properties. The trajectory of the labelled ions or molecules across a medium can then be monitored over a certain time scale and this is usually reported as a self-diffusion coefficient. This is usually done in fluorescence correlation spectroscopy (FCS) experiments. In this study, the diffusion of two probe molecules, Rh123 and BODIPY-C_{10} in ionic liquids were measured using the PGSTE NMR. **Table 8** summarizes the translational diffusion coefficients of ions and the probe molecules in ionic liquids. The results show that the addition of Rh123 and BODIPY-C_{10} to the ionic liquids did not affect the diffusivity of the cations of either ionic liquid. The diffusivity of the cations *i.e.* $[C_4C_1im]^+$ and $[C_4C_1pyrr]^+$ remains approximately the same as they were in the pure ionic liquids. Similarly, the addition of Rh123 to both ionic liquids does not affect the diffusivity of the anions. However, the addition of BODIPY-C_{10} to these ionic liquids did lower the diffusivity of the anions by one order of magnitude. This indicates BODIPY-C_{10} might have specific interactions with the anions. Interestingly, the diffusivity of the both probe molecules shows a consistence dependency on the viscosity of the ionic liquids. The viscosity ratio of $[C_4C_1pyrr][NTf_2]$ to $[C_4C_1im][NTf_2]$ is about 1.545 (76.15cP/49.27cP) . The diffusivity of Rh123 is reduced by about the same factor *i.e.* 1.597 ($9.97\times10^{-12}/6.24\times10^{-12}$) as the medium is changed to the more viscous medium. Similarly, the diffusivity of BODIPY-C_{10} is decreased by a factor of 1.487 ($7.53\times10^{-12}/1.12\times10^{-11}$) when the medium is changed from $[C_4C_1im][NTf_2]$ to $[C_4C_1pyrr][NTf_2]$. The results indicate that these fluorescence probes have the potential to be used as probe molecules to estimate the micro-viscosity of ionic liquids.

Table 8: The translational diffusion coefficients of ions and probe molecules in ionic liquids at 25°C.

Ionic liquid	Cation diffusivity, D^+ ($m^2\ s^{-1}$)	Anion diffusivity, D^- ($m^2\ s^{-1}$)	Probe diffusivity, P ($m^2\ s^{-1}$)
$[C_4C_1im][NTf_2]$ + Rh123	$2.78\times10^{-11} \pm 1.17\times10^{-14}$	$2.07\times10^{-11} \pm 1.39\times10^{-16}$	$9.97\times10^{-12} \pm 4.03\times10^{-12}$
$[C_4C_1pyrr][NTf_2]$ + Rh123	$1.76\times10^{-11} \pm 7.49\times10^{-15}$	$1.36\times10^{-11} \pm 1.48\times10^{-16}$	$6.24\times10^{-12} \pm 5.20\times10^{-12}$
$[C_4C_1im][NTf_2]$ + BODIPY-C_{10}	$2.05\times10^{-11} \pm 1.71\times10^{-14}$	$6.70\times10^{-12} \pm 2.11\times10^{-16}$	$1.12\times10^{-11} \pm 3.61\times10^{-12}$
$[C_4C_1pyrr][NTf_2]$ + BODIPY-C_{10}	$1.75\times10^{-11} \pm 1.47\times10^{-14}$	$6.03\times10^{-12} \pm 2.52\times10^{-16}$	$7.53\times10^{-12} \pm 3.14\times10^{-12}$

4.5 Density

The densities (ρ) of the ionic liquids were measured at 25°C, and their values, along with selected molecular solvents are presented in **Table 9**. In general, most ionic liquids are denser than water and most molecular solvents. Based on the literature, the density of known ionic liquids ranges from 1.0 – 1.6 gcm^3.[164] All measured density values are in a good agreement with those in the literature.

The density of $[C_nC_1im][NTf_2]$ ionic liquids gradually decreased with increasing alkyl length from 1.5184 gcm^{-3} to 1.2437 gcm^{-3} for $n = 2$ to $n = 12$. A similar trend was observed by Kolbeck *et al.*, and the trend is reported to be independent of the nature of the anion and the cation head groups.[165] In general, the addition of $-CH_2-$ units causes an increase in the overall size of the cations and thus leads to an expansion of free volume within the liquid. Molecular dynamics simulation studies have suggested that dispersive interactions between the alkyl tails of ionic liquid cations are expected to increase with increasing alkyl chain lengths and this causes nanostructure separation of the cations into polar and non-polar regions.[166,167] This means with the increasing chain length, the non-polar regions occupy more space (volume) and thus lower the density. The trend of the data presented here agrees with that reported in the literature.[148,159,168]

Table 9: Density of selected molecular solvents and ionic liquids at 25°C.

Liquid	Density, ρ (g/cm^3)	
	Experimental	**Literature**
H_2O	0.9970 ± 0.0001	0.9970[169]
CH_3OH	0.7864	0.7866[125]
PEG200	1.1205	1.1211,[121] 1.1209[120]
PEG400	1.1219 ± 0.0001	1.1224,[121] 1.1219[125]
$[C_2C_1im][NTf_2]$	1.5184 ± 0.0001	1.519,[122] 1.518,[170] 1.5192,[171] 1.5168[172]
$[C_3C_1im][NTf_2]$	1.4745 ± 0.0001	1.4744,[125] 1.4740,[173] 1.4757[174]
$[C_4C_1im][NTf_2]$	1.4358 ± 0.0002	1.436,[122]1.434,[127] 1.434,[175] 1.438[171]
$[C_6C_1im][NTf_2]$	1.3714 ± 0.0001	1.372,[122] 1.371,[129] 1.372[130]
$[C_8C_1im][NTf_2]$	1.3201 ± 0.0001	1.320,[122] 1.321,[131]1.320[128]
$[C_{12}C_1im][NTf_2]$	1.2437 ± 0.0002	1.2480,[132]1.2429[133]
$[C_4C_1pyrr][NTf_2]$	1.3940 ± 0.0001	1.3946,[127]1.3945,[134] 1.3949,[135] 1.3953[176]
$[P_{4446}][NTf_2]$	1.1842	1.183,[136]1.1903,[137]1.18[138]
$[C_4C_1im][BF_4]$	1.2010 ± 0.0002	1.2111,[141]1.2111,[177] 1.2968,[178]1.2010[179]
$[C_4C_1im][PF_6]$	1.3674 ± 0.0001	1.3661,[175]1.3698,[143]1.3675,[144] 1.3675[145]
$[C_4C_1im][CF_3SO_3]$	1.2974 ± 0.0001	1.2968,[178]1.3056,[146]1.2976,[180] 1.3038[179]

A lower density ionic liquid can be produced by changing the head group of the cation. For example, changing the head group from an imidazolium to a pyrrolidinium causes the density to decrease from 1.4358 gcm^{-3} to 1.3940 gcm^{-3}. This may be due the structural geometry of the imidazolium ring which has a planar structure which allows for denser packing of ions compared to the pyrrolidinium cation. The density is lowest when the head group is changed to a phosphonium. The measured density for the $[P_{4446}][NTf_2]$ ionic liquid is 1.1842 gcm^{-3} . This is believed to be due to the simpler structure of the phosphonium core ion compared to the delocalised aromatic ring of the imidazolium and the charged ring of the pyrrolidinium ions.

The effects of the anions on the density of the ionic liquids can be observed by substituting the anion of the $[C_4C_1im][NTf_2]$ with other anions such as $[BF_4]^-$, $[PF_6]^-$ and $[CF_3SO_3]^-$. The density of the ionic liquid is progressively reduced in the following order: $[C_4C_1im][NTf_2]$ > $[C_4C_1im][PF_6]$ > $[C_4C_1im][CF_3SO_3]$ > $[C_4C_1im][BF_4]$. However, no systematic variation of density is observed in term of the size of the anions.

4.6 Correlation of transport properties of ionic liquids

The data from the diffusion process will always have a significant relationship to other transport related properties such as viscosity, conductivity and density. An example of equations that can be used to express the relationship between these transport properties are the Nernst-Einstein and Stokes-Einstein equations. Viscosity and diffusivity are two properties that are closely related to each other and both have a huge impact on the dynamics of a fluid. The viscosity and diffusivity are related to each other according to the Stokes-Einstein equation **(33)**.

$$D = \frac{k_B T}{c\pi\eta r_i} \qquad \textbf{(33)}$$

In equation **(33)**, η is the viscosity of the liquid, D is the diffusion coefficient, r_i is the hydrodynamic radius, T is the absolute temperature, k_B is the Boltzmann constant (1.38×10^{-23} JK^{-1}) and c is constant. From equation **(33)**, the magnitude of diffusivity is inversely proportional to the magnitude viscosity measured by the rheometer. As can be seen from the graph in **Figure 43**, the total diffusivity of ions in ionic liquids is related linearly to their fluidity ($1/\eta$) with a goodness of fit of 0.9822. This indicates that the microscopic ions diffusion coefficients are in good agreement with the viscosity measured by the rheometer.

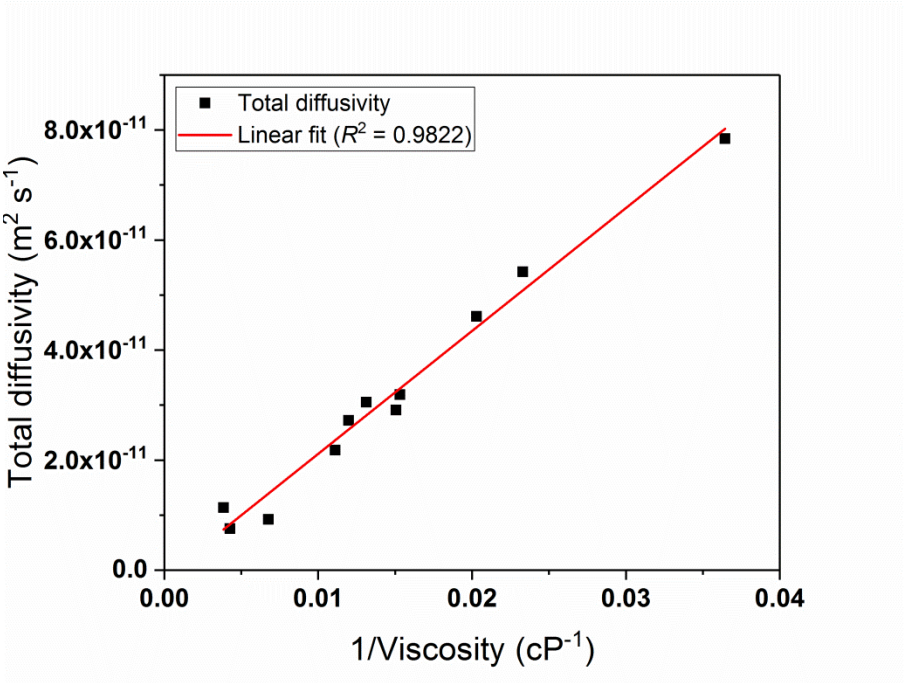

Figure 43: The relationship between the total diffusivity of ions and viscosity of ionic liquids.

The Nernst-Einstein equation was used to calculate the molar conductivity from the diffusivity values that obtained from PGSTE-NMR.

$$\Lambda_{NMR} = \frac{N_A \cdot e^2}{kT} \cdot (D^+ + D^-) \qquad \textbf{(34)}$$

In the equation **(34)** , N_A is Avogadro's number, *e* is the electronic charge, k is Boltzmann's constant and D^+ and D^- are the diffusion coefficients of the cation and anion, respectively.

The molar conductivity value calculated from the Nernst-Einstein equation can represents the maximum conductivity a liquid could possess by assuming all the diffusing ionic species detected by PGSTE NMR contribute to the conduction process. The assumption is made based on the fact that the equilibrium time for the ion-pairing process is much faster than the NMR

time scale (10^{-9}-10^{-10} s).[128] However, only the charged species that contribute to the conductivity are detected by impedance measurement and ion-pairs do not contribute to the conduction process. Therefore, the molar conductivity measured by impedance could be lower than the molar conductivity estimated from NMR. The molar conductivity of the ionic liquids is calculated from the measured ionic conductivity value using the following equation **(35)**:

$$\Lambda = \frac{\kappa \times M_W}{\rho} \qquad \textbf{(35)}$$

The calculated molar conductivities from both methods are shown in **Table 10**. The ratio of the molar conductivity value obtained from impedance measurement to the value of molar conductivity obtained from PGSTE-NMR measurement (Haven ratio, $\Lambda_{imp} / \Lambda_{NMR}$) can serve as a quantitative measurement of the degree of 'ionicity' of an ionic liquid. It can be seen that the $\Lambda_{imp} / \Lambda_{NMR}$ values are less than unity for all the liquids, which indicates that not all diffusive ions in ionic liquids were contributing to the ionic conduction. The reason for this observation might be due to the formation of ions aggregates or clusters within the ionic liquids' structures.

The ionicity of the $[C_nC_1im][NTf_2]$ ionic liquids decrease from 0.82 to 0.59 as the alkyl chain length is increased from $n = 2$ to $n = 8$, which is consistent with the trend that was observed by Tokuda and co-workers.[128] The decrease of the ionicity is associated with the stronger alkyl chain-ion inductive forces and hydrocarbon-hydrocarbon dispersive forces with the addition of $-CH_2$ units. However, the ionicity suddenly increases to the highest value of 0.83 for $n = 12$. The observation can be probably related to the tendency of ionic liquids with a long side chain to form microscopic segregation of ionic and hydrophobic regions.[47] It is also worth to note

that long chain 1-aklyl-3-methylimidazolium ionic liquids such as 1-decyl-3-methylimidazolium bromide and 1-dedocyl-3- methylimidazolium bromide possess surfactant property.[181,182] These properties maybe serve the way for the charged moieties to retain its charge and thus can lead to a higher ionicity.

The ionicity of $[C_4C_1im]^+$ paired with different anions follows the following order: $[C_4C_1im][PF_6]$ (0.93) > $[C_4C_1im][BF_4]$ (0.77) > $[C_4C_1im][CF_3SO_3]$ (0.65) > $[C_4C_1im][NTf_2]$ (0.63). The anionic structure has been reported to affect the ionicity of ionic liquids. Tsuzuki and co-workers have calculated the atomic charges of these anions based on ab initio molecular orbital calculation.[183] A larger negative atomic charge was found at the oxygen atoms of $[CF_3SO_3]^-$ and $[NTf_2]^-$ cations and this provides a stronger coordination site for interaction with the $[C_4C_1im]^+$ cation. However, a less negative charge on the fluorine atoms was found in $[PF_6]^-$ and $[BF_4]^-$ anions thus these anions are expected to have a weaker interaction the $[C_4C_1im]^+$ cation than $[CF_3SO_3]^-$ and $[NTf_2]^-$ anions. The weaker interaction means the anions are more likely to remain dissociated ions rather than form neutral pairs or aggregates. The small and spherical anions combined with a well distributed negative charge across the $[PF_6]^-$ and $[BF_4]^-$ structures also contributes to the loss of specific interacting sites with the positively charged cation. The effect of the cations can be seen by comparing the ionicity of these three ionic liquids: $[C_4C_1im][NTf_2]$, $[C_4C_1pyrr][NTf_2]$ and $[P_{4446}][NTf_2]$. The order of the ionicity is $[C_4C_1pyrr][NTf_2] \approx [P_{4446}][NTf_2] > [C_4C_1im][NTf_2]$. The positive charge of $[C_4C_1im]^+$ is concentrated on the C_2-H side of the imidazolium ring, making it easier for an anion to approach the cation. However, for the aliphatic $[C_4C_1pyrr]$ and $[P_{4446}]$ cations, the charge is well distributed over the whole structure making the cations have no specific sites to interact with the anion.

However, it is worth to mentioned that the Nernst-Einstein equation that has been used here to calculate the ionicity of ionic liquids was originally developed to relate the molar conductivity and self-diffusion of electrolyte systems where the ions move independently as in electrolyte solutions at infinite dilution. However, previous studies have shown that the relation also can be applied to ionic crystals with the addition of a 'correction factor' as suggested by Bardeen and Herring(1952).[184] A study on applicability of the Nernst-Einstein equation to calculate molar conductivity from self-diffusion coefficients of sodium and chloride ions in molten sodium chloride has been conducted by Borucka *et al*. [184] The calculated molar conductivity of the molten salt deviates about 40% compared to the measured value, and they conclude that the Nernst-Einstein equation is might not valid for the high temperature molten salt sodium chloride (>800ºC). Thus, the applicability of the Nernst-Eisntein equation to ionic liquid system also can be questionable, although it has been widely used in many ionic liquid literatures.

Table 10: The molar conductivity values of the ionic liquids calculated from the impedance measurement (Λ_{imp}) and NMR measurements(Λ_{NMR}). The ratio of the $\Lambda_{imp} / \Lambda_{NMR}$ represents the ionicity of the respective ionic liquid.

Ionic Liquid	Molecular weight, M_w (g mol^{-1})	Molar conductivity, Λ_{imp} (S cm^2 mol^{-1})	Molar conductivity, Λ_{NMR} (S cm^2 mol^{-1})	Ionicity, $\Lambda_{imp}/\Lambda_{NMR}$
$[C_2C_1im][NTf_2]$	391.31	2.412	2.945	0.82
$[C_3C_1im][NTf_2]$	405.34	1.561	2.036	0.77
$[C_4C_1im][NTf_2]$	416.36	1.098	1.732	0.63
$[C_6C_1im][NTf_2]$	447.42	0.695	1.198	0.58
$[C_8C_1im][NTf_2]$	475.47	0.479	0.819	0.59
$[C_{12}C_1im][NTf_2]$	531.57	0.286	0.346	0.83
$[C_4C_1pyrr][NTf_2]$	422.30	0.845	1.146	0.74
$[P_{4446}][NTf_2]$	567.44	0.206	0.284	0.73
$[C_4C_1im][BF_4]$	226.02	0.787	1.021	0.77
$[C_4C_1im][CF_3SO_3]$	288.29	0.710	1.093	0.65
$[C_4C_1im][PF_6]$	284.18	0.396	0.427	0.93

Another approach that can be used to qualitatively access the ionicity of ionic liquids is by calculating the product of molar conductivity (Λ_{imp}) and viscosity (η). This is known as Walden rule and it can be mathematically expressed as the following equation **(36)**:

$$\Lambda_{imp} \times \eta = k \qquad \textbf{(36)}$$

In the equation **(36)** k is a temperature dependent constant. The Walden plot of log molar conductivity against reciprocal log of viscosity of the ionic liquids studied is shown in **Figure 44**. It relates the mobility of the ions to the fluidity of the medium.

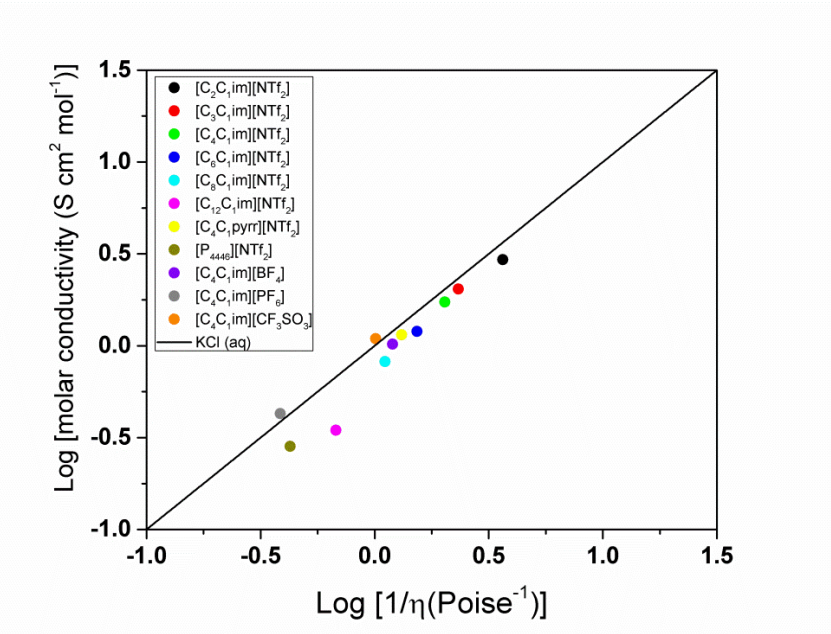

Figure 44: The Walden plot of ionic liquids studied.

The Walden rule was originally developed to describe the properties of dilute aqueous solution of electrolytes, but its application has now been expanded to other types of electrolytes including non-aqueous solutions, molten salts, as well as ionic liquids. Data obtain from

measurements of an aqueous solution of 0.01M KCl are often used to construct the calibration line in the Walden plot. The calibration line is regarded as 'ideal' because in such highly diluted solution there are no ion-ion interactions and all ions should exist as free ions. Deviation from the ideal line could be used as a sign of decreased ionicity. Angell *et al*. have introduced a following diagram (see **Figure 45**) that allows for classification of electrolyte systems into various classes.

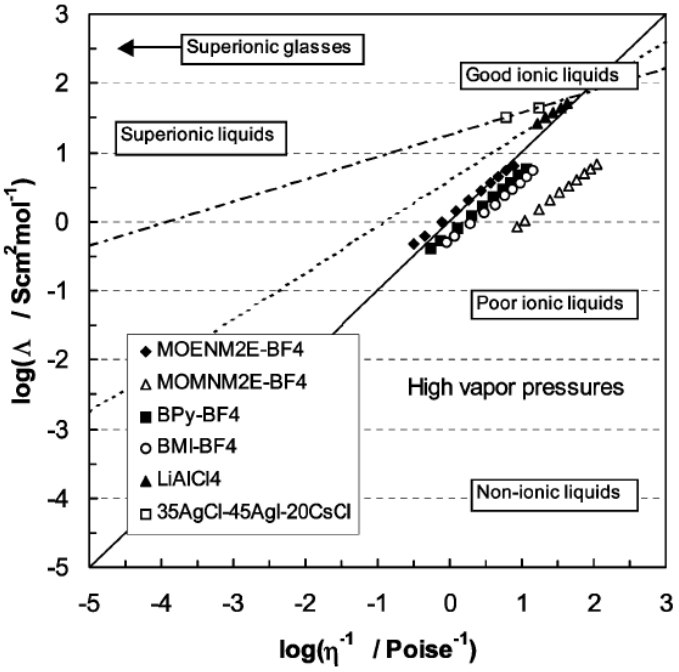

Figure 45: The classification of ionic liquids based on Walden plot proposed by Angell an co-workers.[185]

As can be seen from the plot, all ionic liquids used in this study fall within the area of good ionic liquids. However, all the points are shown to deviate from the ideal line suggesting that the degree of ion dissociation is less than 100%, in a good agreement with the ionicity values calculated from the ratio ($\Lambda_{imp}/\Lambda_{NMR}$). Two ionic liquids, $[C_{12}C_1][NTf_2]$ and $[P_{4446}][NTf_2]$ show

the largest deviation from the ideal line. This might correlate with the relatively high viscosity of these two ionic compared to the others. Upon thorough observation, the deviation is found to be strongly dependent on the viscosity of the ionic liquids. This can be clearly seen by comparing the distribution of Walden product of $[C_nC_1im][NTf_2]$ with n = 2, 3, 4, 6, 8 and 12. The deviation is generally larger as the alkyl chain length (n) is decrease, which indicates the molar conductivity is not proportionally changing with viscosity as diffusivity does (see **Figure 43**).

An adjusted Walden plot has been introduced by MacFarlane *et al.* in 2009 which includes the contribution of ion sizes in the evaluation of ionicity of ionic liquids.[8] They have calculate the effective radii of ions from molecular volumes using equation **(37)** with the assumption that the ions studied have a spherical shape. This assumption can also be argued because most of the ions which are used to make ionic liquids have complex structures and they are not spherical, unlike the simple ions like K^+ and Cl^-.

$$V^{theory} = \frac{4}{3}\pi r_{ion}^3 \qquad \textbf{(37)}$$

The importance of considering the role of ionic radii is deduced from the Stokes-Einstein equation (refer to equation **(33)**) and therefore, for 1:1 electrolyte, the adjusted Walden rule (equation **(36)**)can be rewritten as

$$\Lambda_{imp} = k \times \eta^{-1}\left(\frac{1}{r^+} + \frac{1}{r^-}\right) \qquad \textbf{(38)}$$

Thus, the adjusted Walden plot is $\log \Lambda_{imp}$ against $\log\left[\eta^{-1}\left(\frac{1}{r^+} + \frac{1}{r^-}\right)\right]$ as suggested by the

equation **(38)**. The incorporation of the radii terms in the Walden plot seems essential as the radius is one of the non-constant variables in the Stokes-Einstein equation from which Walden rule is derived. From their results, incorporating the radii terms into the Walden plot have caused a significant change to the deviation from the ideal 0.01M KCl line and the deviation gives a better correlation to the physical properties (*i.e.* viscosity and conductivity) and reflects the state ions in ionic liquids. From the data presented in that paper, the deviation from the ideal line is surprisingly high for ionic liquids, as high as 0.91 when the typical Walden plot is used. However, the values derived from the adjusted Walden plot however show a lower deviation <0.31 which represents a more logical correlation that might be expected for ionic liquids.

4.7 Concluding remarks

Some of the physical properties' values reported here were found to vary considerably compared to those reported in the literature. The main reason behind this observation is that some ionic liquids, such as $[C_4C_1im][BF_4]$ and $[C_4C_1im][CF_3SO_3]$, are naturally hydrophilic. Additionally some of the ionic liquid anions (e.g. $[PF_6]^-$ and $[BF_4]^-$) can react with water. Hence the synthesis, purification and handling of these ionic liquids was difficult and thus their level of purity remained questionable. For these reasons, only $[NTf_2]^-$ based ionic liquids were used for fluorescence lifetime experiments in Chapter 5. The advantages of using $[NTf_2]^-$ based ionic liquids include:

i. They are relatively air and water stable. Some $[NTf_2]^-$ based ionic liquids show some useful properties such as good ionic conductivity.
ii. The synthesis of the $[NTf_2]^-$ based ionic liquids is relatively fast and easier control compared to other anions.
iii. The $[NTf_2]^-$ based ionic liquids are some of the most studied ionic liquids, and the results obtained here can be easily compared and verified with the those in the literature.

Chapter 5 Fluorescence Lifetime in Ionic Liquids

5.1 Photo-physical of molecular rotors in ionic liquids

The goal of this experiment was to gain an insight into the behaviour and potential of molecular rotors as micro-viscometers for ionic liquids. This was achieved by comparing the photophysical properties of molecular rotors *i.e.* the fluorescence intensity in a series of ionic liquids of known viscosity. It is worth mentioning that the fluorescence intensity not only depends on viscosity but also the polarity of the medium.[96] The main drawback of intensity-based measurements is that they suffer from uncertainties due to variations in the fluorophore concentration and inhomogeneities in the optical properties of the solvent (medium).[111] In this study, a series of 1-alkyl-3-methyl-imidazalium *bis*(trifluoromethyl sulfonyl)imide [$C_nC_1$im][NTf_2] with n = 2, 3, 4, 6, 8 and 12 liquids which consist of same type of anions and cations but having different viscosities were used. The types of intermolecular forces that exist in these ionic liquids are the same while the magnitude of forces should only vary very slightly with the lengthening of the alkyl chain length. In this way, the possibility of having complications due to different types of intermolecular forces or polarity in the ionic liquids could be minimised.

The ground-state absorption and steady-state fluorescence emission spectra of three molecular rotors; 3,3'-Diethylthiacarbocyanine iodide (Cy3), *meso*-alkoxyphenyl-4,4’-difuoro-4-bora-3a,4adiaza-s-indacene (BODIPY-C_{10}) and 9-(2,2-dicyanovinyl)julolidine (DCVJ) were recorded in a series of ionic liquids, 1-alkyl-3-methyl-imidazalium *bis*(trifluoromethyl sulfonyl)imide [$C_nC_1$im][NTf_2] (n = 2, 3, 4, 6, 8 and 12) that have different viscosities. The

properties and behaviour of these molecular rotors in molecular solvents have been extensively reported but limited or no information is available for systems consisting of ionic liquids as solvents.

The chemical structure of Cy3 is presented in the **Figure 46**. Cy3 is a cationic dye with a single positive charge. **Figure 47** shows the ground-state absorption and steady-state emission spectra of Cy3 in the [$C_nC_1$im][NTf_2] ionic liquids. The absorption maximum (λ_{max} absorption) of Cy3 in these ionic liquids are observed between 560nm and 564 nm. The λ_{max} emission of Cy3 is progressively changed from 572 nm to 576 nm as the alkyl chain length (n) is increased from n = 2 to n = 12 as summarized in **Table 11**. These changes are probably due to the slightly different environments experienced by the rotor.

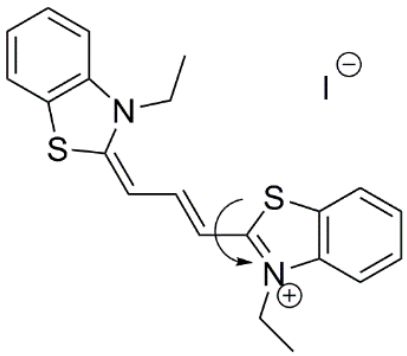

Figure 46: The chemical structure of Cy3.The arrow shows the internal torsional motion position for the dye to rotate.

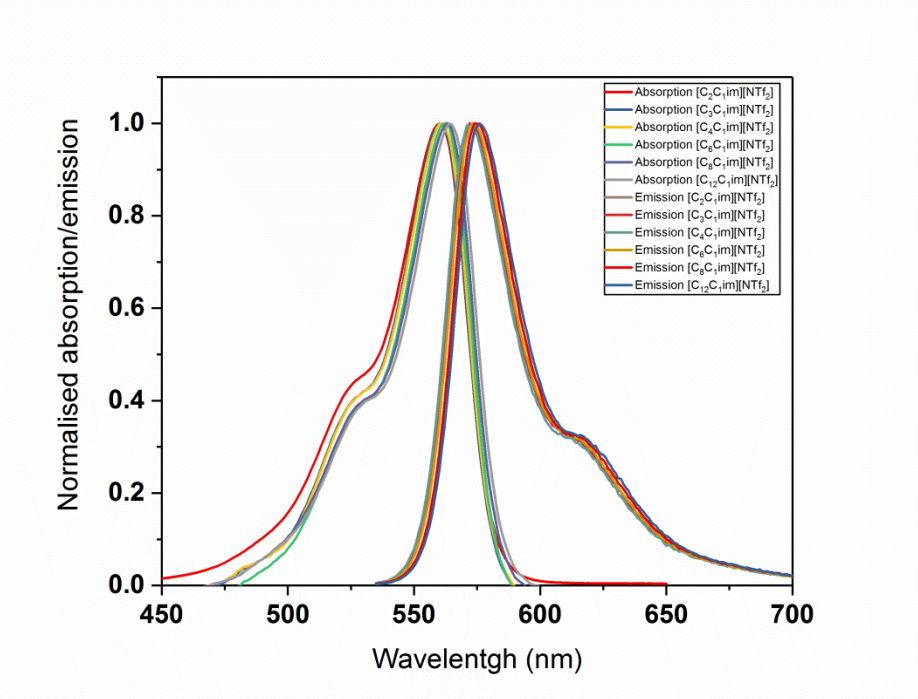

Figure 47: Ground-state absorption and steady-state emission spectra of Cy3 in $[C_nC_1im][NTf_2]$ ionic liquids, n = 2, 3, 4, 6, 8, 12.

Table 11: The maximum absorption (λ_{max} absorption) and maximum emission (λ_{max} absorption) of Cy3 in $[C_nC_1im][NTf_2]$ ionic liquids, n = 2, 3, 4, 6, 8, 12.

Ionic Liquid	λ_{max} absorption (nm)	λ_{max} emission (nm)
$[C_2C_1im][NTf_2]$	560	572
$[C_3C_1im][NTf_2]$	560	572
$[C_4C_1im][NTf_2]$	561	573
$[C_6C_1im][NTf_2]$	562	573
$[C_8C_1im][NTf_2]$	563	574
$[C_{12}C_1im][NTf_2]$	564	576

This dye has been reported to be able to act as a molecular rotor, and it has been utilised to probe micro-viscosity in various systems including cellular membranes and aerosols.[12,100] The viscosity dependence of the emission intensity of Cy3 in these ionic liquids is shown in **Figure 48**. The emission intensity of Cy3 increased with increasing the viscosity of ionic liquids. The λ_{max} emission of Cy3 changes linearly with the viscosity of ionic liquids. The plot of λ_{max} emission against viscosity of ionic liquids is presented in **Figure 49**. This is an indication that Cy3 can be used as molecular rotor for estimating micro-viscosity in ionic liquids within the measured viscosity range. The intensity of λ_{max} emission does not solely depend on the viscosity of the ionic liquids, it could also be depending on the polarity of ionic liquids. However, the use of the same type of ionic liquids perhaps could minimise the contribution of polarity effect.

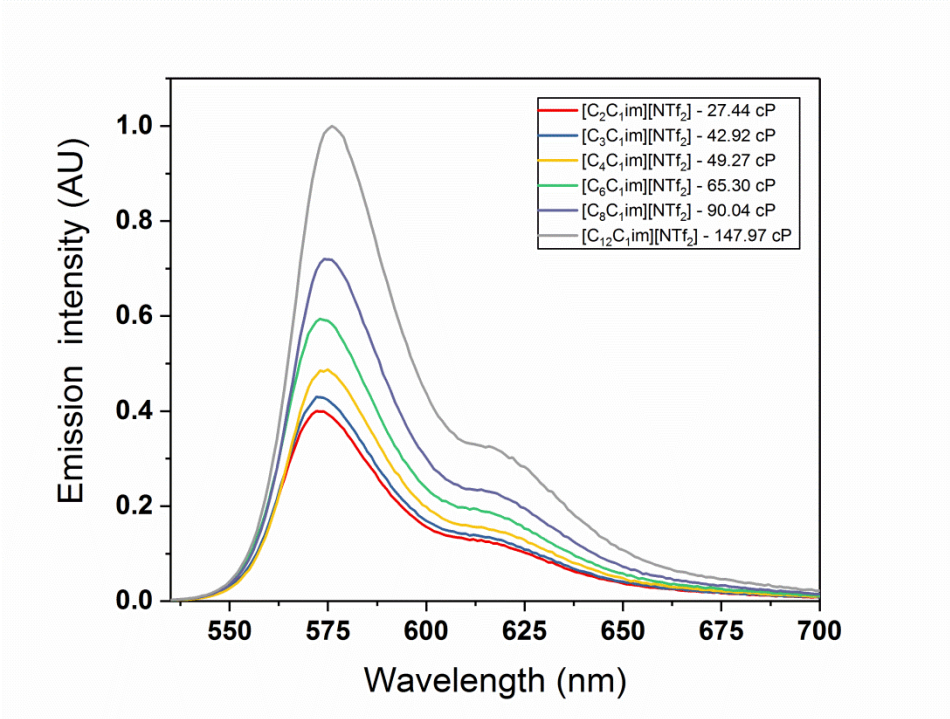

Figure 48: Steady-state fluorescence emission spectra of Cy3 in $[C_nC_1im][NTf_2]$ ionic liquids of different viscosity.

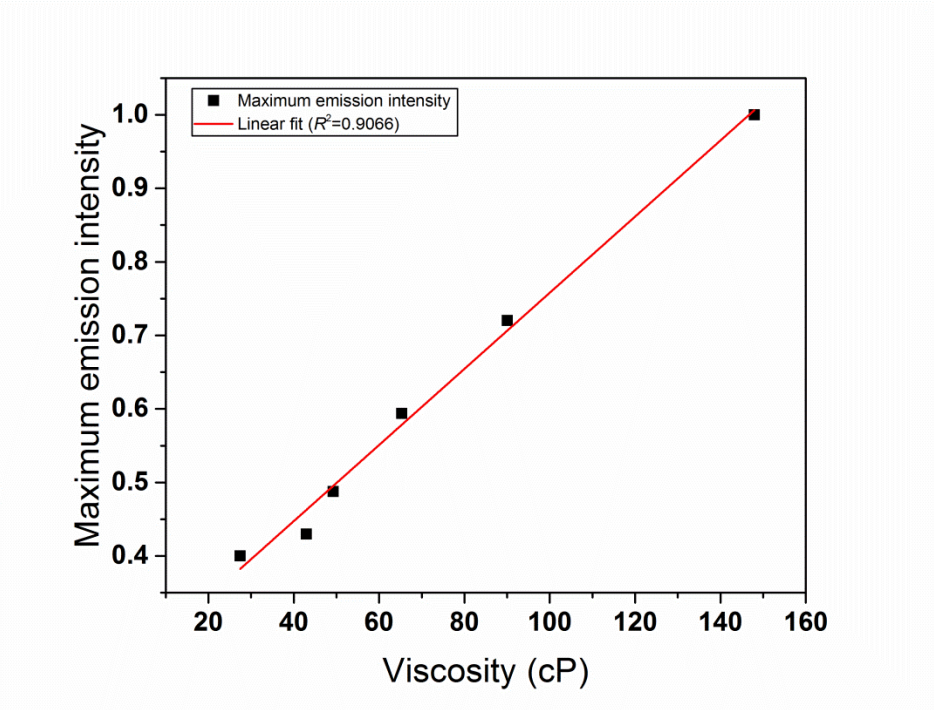

Figure 49: Steady-state fluorescence emission maximum of Cy3 trend in $[C_nC_1im][NTf_2]$ ionic liquids of different viscosity.

The chemical structure of BODIPY-C_{10} is shown in **Figure 50**. It is considered as neutral dye as it has no intrinsic charge. BODIPY-C_{10} is highly hydrophobic and it has been previously studied to probe the viscosity of atmospheric aerosol and microbubble.[101,186] The ground-state absorption and steady-emission spectra of BODIPY-C_{10} in $[C_nC_1im][NTf_2]$ are presented in **Figure 51**. The λ_{max} absorption is observed between 496-497 nm and a blue shifted λ_{max} emission is observed between 511-512 nm. **Table 12** summarizes the maximum absorption (λ_{max} absorption) and maximum emission (λ_{max} emission) of BODIPY-C_{10} in $[C_nC_1im][NTf_2]$ ionic liquids, n = 2, 3, 4, 6, 8, 12.

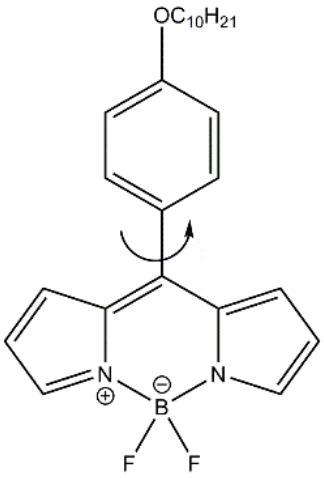

Figure 50: The chemical structure of BODIPY-C_{10}. The arrow shows the internal torsional motion position for the dye to rotate.

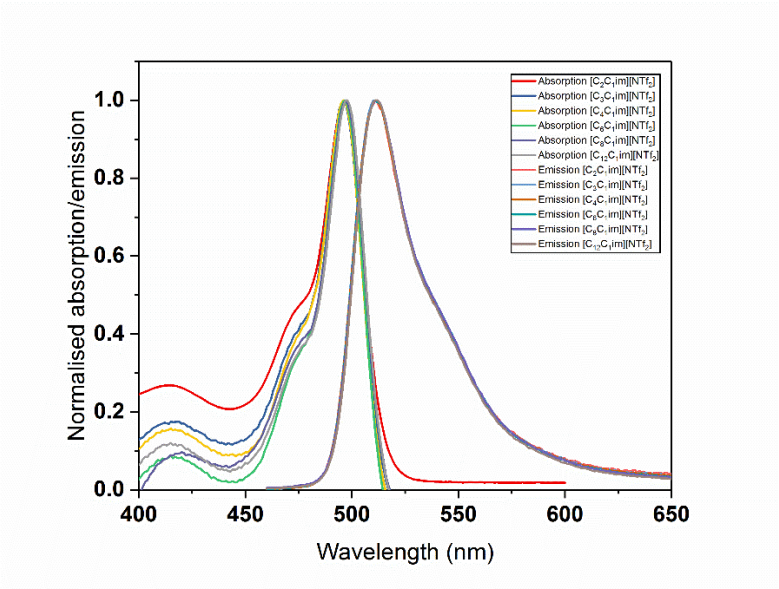

Figure 51: Ground-state absorption and steady-state emission spectra of BODIPY-C_{10} in $[C_nC_1im][NTf_2]$ ionic liquids, n = 2, 3, 4, 6, 8, 12.

Table 12: The maximum absorption (λ_{max} absorption) and maximum emission (λ_{max} absorption) of BODIPY-C_{10} in [$C_nC_1$im][NTf_2] ionic liquids, n = 2, 3, 4, 6, 8, 12.

Ionic Liquid	λ_{max} absorption (nm)	λ_{max} emission (nm)
[C_2C_1im][NTf_2]	496	511
[C_3C_1im][NTf_2]	496	511
[C_4C_1im][NTf_2]	496	511
[C_6C_1im][NTf_2]	497	511
[C_8C_1im][NTf_2]	497	511
[$C_{12}C_1$im][NTf_2]	497	512

Referring to **Figure 52**, it can be observed that the emission intensity of BODIPY-C_{10} increases with the increasing of viscosity of [$C_nC_1$im][NTf_2] ionic liquids. The observed increase in fluorescence intensity is due to the restricted rotation of the phenyl group in higher viscosity media which reduces relaxation via the populating of the dark excited state.[111] The emission intensity changes exponentially (R^2=0.9514) with the viscosity of [$C_nC_1$im][NTf_2] ionic liquids as shown in **Figure 51**. The λ_{max} emission of BODIPY-C_{10} remains relatively constant at ~511nm as the viscosity of ionic liquids change from 27.44 cP to 147.97 cP. The slight different in the shifting trend of λ_{max} absorption and λ_{max} emission of Cy3 and BODIPY- C_{10} in the ionic liquids might be due the different polarizability of the two dyes.

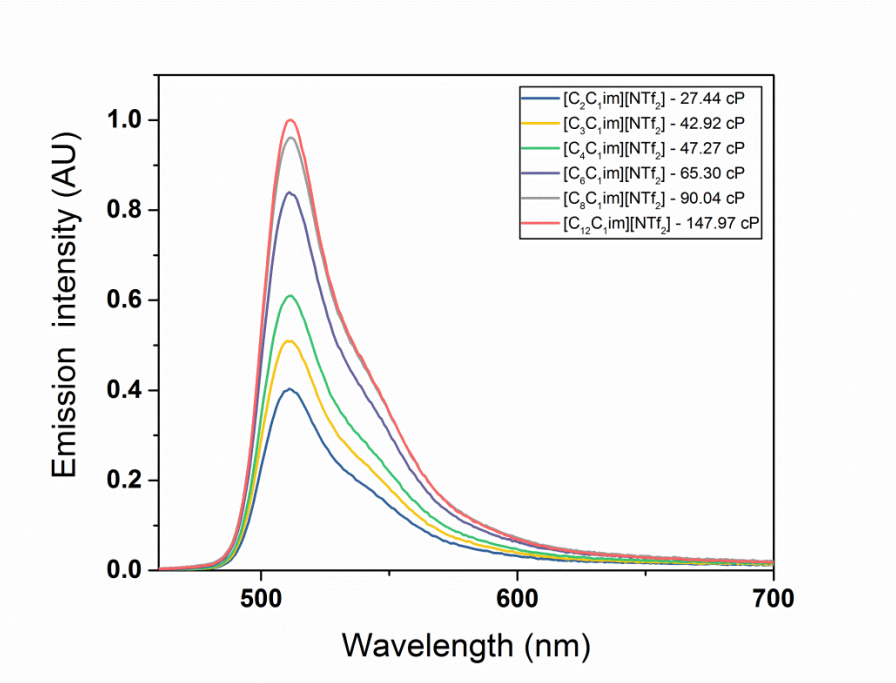

Figure 52: Steady-state fluorescence emission spectra of BODIPY-C_{10} in [$C_nC_1$im][NTf_2] ionic liquids of different viscosity.

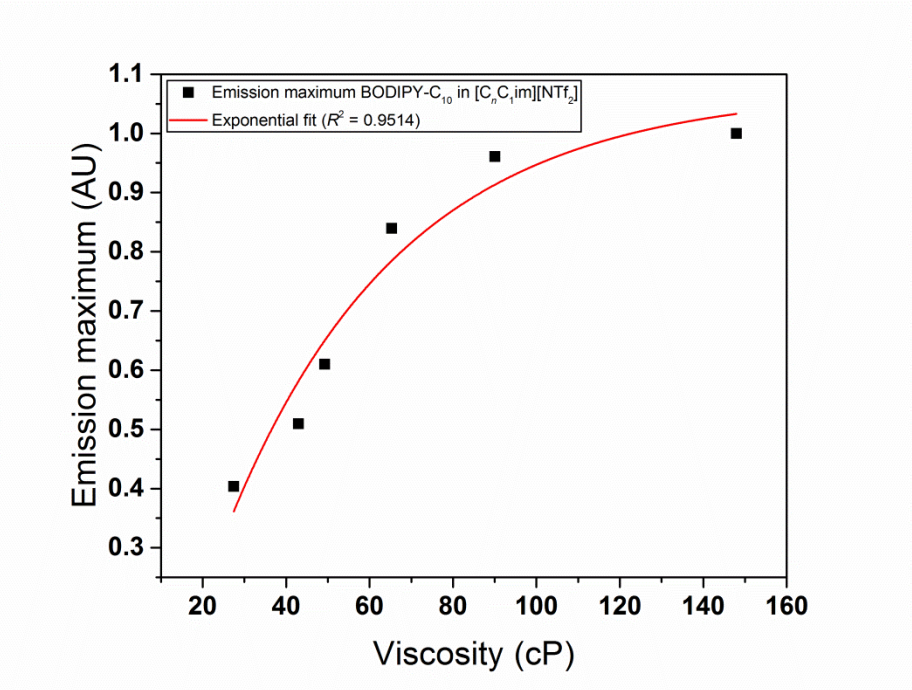

Figure 53: Steady-state fluorescence emission maximum of BODIPY-C_{10} trend in [$C_nC_1$im][NTf_2] ionic liquids of different viscosity.

Figure 54 shows the chemical structure of DCVJ. DCVJ is a well-studied molecular rotor in which its fluorescence efficiency can be correlated to the viscosity of its containing medium.[187,188] The absorption and emission of this molecular rotor in $[C_nC_1im][NTf_2]$(n = 2, 3, 4, 6 and 8) ionic liquids and the λ_{max} absorption and λ_{max} emission appear at about ~462nm and ~495nm, respectively (see **Figure 55**). **Table 13** summarizes the maximum absorption (λ_{max} absorption) and maximum emission (λ_{max} absorption) of Cy3 in $[C_nC_1im][NTf_2]$ ionic liquids, n = 2, 3, 4, 6, 8.

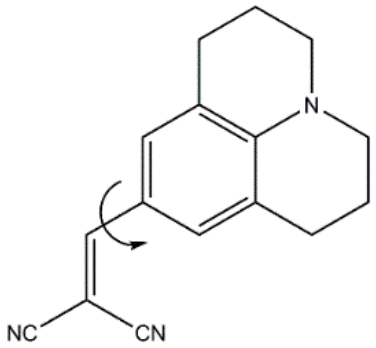

Figure 54: The chemical structure of DCVJ. The arrow shows the internal torsional motion position for the dye to rotate.

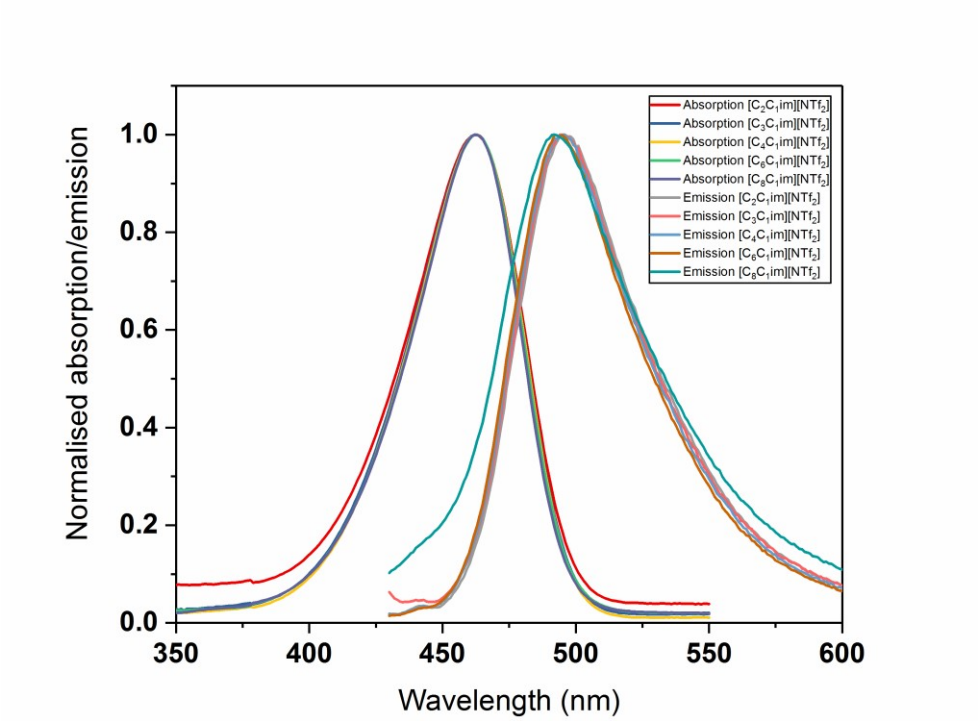

Figure 55: Ground-state absorption and steady-state emission spectra of DCVJ in $[C_nC_1im][NTf_2]$(n = 2, 3, 4, 6 and 8).

Table 13: The maximum absorption (λ_{max} absorption) and maximum emission (λ_{max} absorption) of DCVJ in $[C_nC_1im][NTf_2]$ ionic liquids, n = 2, 3, 4, 6, 8.

Ionic Liquid	λ_{max} absorption (nm)	λ_{max} emission (nm)
$[C_2C_1im][NTf_2]$	462	495
$[C_3C_1im][NTf_2]$	462	496
$[C_4C_1im][NTf_2]$	463	495
$[C_6C_1im][NTf_2]$	463	492
$[C_8C_1im][NTf_2]$	463	492

The emission intensity of DCVJ is found to increase with the increasing viscosity of the ionic liquids as illustrated in **Figure 56**. The λ_{max} emission of DCVJ responses linearly (R^2=0.9977) to the change in the viscosity. DCVJ is a neutral and hydrophobic dye so it expected to have a good solubility in the hydrophobic ionic liquids.[96] The λ_{max} emission of DCVJ was found to progressively decreases from ~496nm to ~493 as the viscosity of ionic liquids is increased.

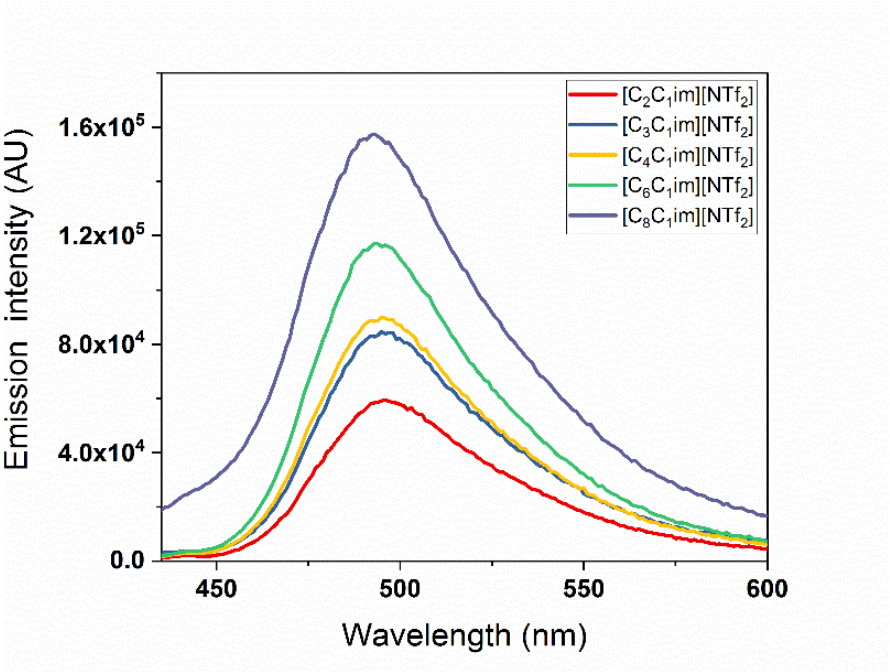

Figure 56: Steady-state fluorescence emission spectra of DCVJ in ionic liquids of different viscosity.

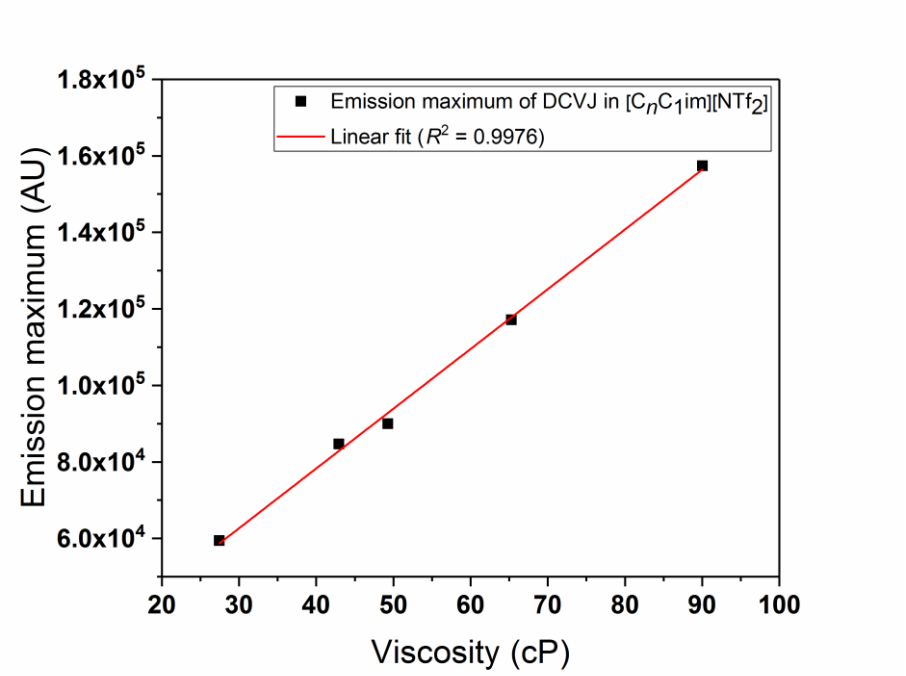

Figure 57: Steady-state fluorescence emission maximum of DCVJ trend in ionic liquids of different viscosity.

The general observation of the photophysical properties of these three molecular rotors in the $[C_nC_1im][NTf_2]$ ionic liquids are that the absorption and emission varies slightly with the change in the structure of these ionic liquids. This variation can be attributed to the slightly different polarities of the solvent *i.e.* ionic liquids. A study conducted by Paul and Samanta showed that the variation of λ_{max} absorption and λ_{max} emission of DCVJ does not vary consistently with the viscosity of ionic liquids as was observed in this study. Instead, the values are much more affected by the structure of the anions and cations.[13] This implies that polarity plays a major role in determining the λ_{max} absorption and λ_{max} emission of some fluorescence molecular rotors. Polarity scale measurements based on coupling constant of Isotropic A, an electron paramagnetic resonance (EPR) probe show that the polarity scale of $[C_nC_1im][BF_4]$ (n = 2, 4, 6, 8 and 10) decreases with increasing alkyl chain length. The values of the coupling

constant (*i.e.* polarity scale) are 15.96, 15.91, 15.80, 15.78 and 15.79 for n = 2, 4, 6, 8 and 10, respectively.[189] This indicates that lengthening the alkyl chain affects the polarity of ionic liquids and this might account for the variation in λ_{max} absorption and λ_{max} emission observed in this study. Apart from this, the different in polarizability of the dyes in ionic liquids might also responsible for the changes and their trends.

As has been mentioned before, fluorescence properties can be affected by both the polarity and viscosity of the medium. Attempts to discriminate the effects of solvent polarity and solvent viscosity in the fluorescence properties of molecular rotors in selected molecular solvents has been undertaken by Haidekker *et al*.[96] The results shows that the emission wavelength of Coumarins was affected by solvent polarity, but neither viscosity nor polarity had a major impact on the observed emission intensity. The measurements based on 4,4-dimethylaminobenzonitrile (DMABN), however show a very complex dependency of emission intensity on both viscosity and polarity. In contrast, the emission of DCVJ is highly dependent on viscosity with a low sensitivity towards solvent polarity. This implies that the effects of polarity and viscosity generally cannot be unambiguously decoupled from each other and the effects also vary specifically depending on the type of molecular rotors involved and perhaps the medium. While the polarity of ionic liquids is not well understood,[189] it is even more challenging to understand the effect of both solvent polarity and viscosity to photophysical of molecular rotors. It would be interesting if a similar and systematic study on ionic liquid and molten salt systems could be performed. In these systems, the environment experienced by the molecular rotor will be totally different to the environment of a molecular solvent system, which usually consist of small and neutral molecules. However, this is beyond the scope of this study, but it is included as recommendation for the future work.

5.2 Fluorescence lifetime of ionic liquids

The time resolved decays of [$C_nC_1$im] [NTf_2] (*n* = 2, 3, 4, 6, 8 and 12) and [P_{4446}][NTf_2] were first recorded in order to analyse any inherent fluorescence background of the ionic liquids. The observed decays can be fitted with a tri-exponential fit in which the three components are assigned the labels τ_1, τ_2 and τ_3. The calculated lifetimes of each component and their contribution to the overall decay are presented in **Table 14**. The number of components observed in this study is consistent with the reported fluorescence decays of [C_4C_1im] [BF_4], [C_4C_1im][PF_6] and [$C_nC_1$im] [NTf_2] (*n* = 2 and 4) which also consist of three decay components.[106,190,191] Two of these components were assigned to associated structures which are believed to be due to the cation-cation and anion-cation interactions in the ionic liquid, and the remaining decay component was assigned to the internal fluorescence of imidazolium ring.[106,190,191] However, the assignment of the fastest decay component τ_3 in this study is not appropriate in these experiments as the calculated lifetime is too close to the limit of detection of the spectrometer, which is 0.1 ns. Thus, the source of the signal cannot be clearly identified, either it is originating from the ionic liquids or it results from scattering. The existence of intrinsic fluorescence property in ionic liquids is not an unusual observation. The existence of two fluorescence components in [C_4C_1im][BF_4] has been demonstrated by Seoncheol *et al.* using 2D-scan fluorescence spectroscopy.[192] Further investigation by fluorescence correlation spectroscopy (FCS) experiments convinced them that the source of the unique fluorescence of observed in the ionic liquid arises from aggregation of the ionic liquid's ions. It also worth to highlight that ionic liquids have demonstrated a unique fluorescence property. The fluorescence spectra of ionic liquids do not obey Kasha's rule like most of organic molecules do.[192] According to

Kasha's rule, the emission of phosphorescence or fluorescence is appreciably yield from the lowest excited state, *i.e.* the emission is independent of excitation wavelength. However, the dependency of fluorescence emission on the excitation wavelength in neat $[C_2C_1im][BF_4]$ and $[C_4C_1im][BF_4]$ ionic liquids has been reported in the literature.[190,192] These observations have stimulate continuous interest in exploring the fluorescence properties of ionic liquids.

Table 14 : The fluorescence lifetimes of ionic liquids and their percent contributions to the overall decay.

Ionic liquid	τ_1 (ns)	Contribution (%)	τ_2 (ns)	Contribution (%)	τ_3 (ns)	Contribution (%)
$[C_2C_1im][NTf_2]$	6.17 ± 0.53	33.1	1.52 ± 0.22	21.0	0.107 ± 0.012	45.9
$[C_3C_1im][NTf_2]$	6.12 ± 0.21	36.9	1.40 ± 0.09	22.9	0.115 ± 0.004	40.2
$[C_4C_1im][NTf_2]$	6.27 ± 0.25	38.3	1.42 ± 0.15	23.9	0.123 ± 0.019	37.8
$[C_6C_1im][NTf_2]$	6.34 ± 0.31	38.9	1.32 ± 0.09	25.7	0.137 ± 0.010	35.4
$[C_8C_1im][NTf_2]$	6.24 ± 0.29	41.2	1.57 ± 0.16	26.5	0.125 ± 0.010	32.3
$[C_{12}C_1im][NTf_2]$	6.98 ± 0.20	42.4	1.61 ± 0.09	31.0	0.158 ± 0.013	26.5
$[P_{4446}][NTf_2]$	6.85 ± 0.18	43.7	1.52 ± 0.07	20.7	0.096 ± 0.006	35.6

5.3 Fluorescence lifetime of Cy3 in $[NTf_2]^-$ based ionic liquids

The fluorescence lifetime of Cy3 was measured in the ionic liquids $[C_nC_1im][NTf_2]$ (n = 2, 3, 4, 6, 8 and 12 and $[P_{4446}][NTf_2]$. Cy3 is a cationic fluorescence molecular rotor with a single positive charge distributed across its large symmetrical structure. As all the ionic liquids used in this work were $[NTf_2]^-$ based ionic liquids, the rotor was expected to be solvated by the negatively charge anions in all cases, thus minimise the effects of polarity that could arise from variation of the chemical structure of the components in the system. The fluorescence lifetime of Cy3 was plotted against the viscosity of the ionic liquids measured by a rheometer (see **Figure 58**). This provides a lifetime-viscosity calibration for the measurements of the effect of electric fields on the viscosity of $[C_4C_1im][NTf_2]$. The calibration was also compared to the commonly used calibration of Cy3 in a molecular solvent system consisting of sucrose/water mixtures.[101]

The analysis of the time resolved decays of Cy3 in the ionic liquids $[C_nC_1im][NTf_2]$ (n = 2, 3, 4, 6) showed that these system could be fitted using a biexponential fit. One of the components is assigned to the fluorescence lifetime arise from ionic liquid (τ_A) and another component is assigned to the fluorescence lifetime of Cy3 (τ_{Cy3}). The time resolved decays for other ionic liquids, however, can only be fitted with a triexponential fit resulting in an additional component associated with the ionic liquids (τ_B). The best fitting was chosen based on the minimum reduced chi squared (RCS) values that could be achieved by the regression fitting. This is achieved when no significant improvement of RCS is observed with addition of further

components to the fitting. The lifetime of the all components from the Cy3 in the ionic liquids are summarised in **Table 15**.

The lifetime associated with the ionic liquid (τ_A) is found to fall below and close to the detection limit of the spectrometer, as mentioned before. Thus, these lifetimes cannot be assigned to any physical process and they are not discussed in detail. Similar to the observations of blank ionic liquid systems, the second component (τ_B) is only observed in the ionic liquids with a higher viscosity *i.e.* [C_8C_1im][NTf_2], [$C_{12}C_1$im][NTf_2] and [P_{4446}][NTf_2]. In general, the fluorescence lifetime of Cy3 increased with the increasing viscosity of the ionic liquids. It can be seen from **Figure 58**, that the viscosities of ionic liquids with a relatively short alkyl chain length (n = 2, 3 and 4), calculated from the lifetime-viscosity calibration of Cy3 in water/sucrose ($\eta_{water/suc}$) solution (red line), are higher than those viscosities measured by the rheometer (η_{rheo}) (black crosses). However, as the alkyl chain length increases (n = 6, 8, 12), the $\eta_{water/suc}$ is closer to the η_{rheo}. The $\eta_{water/suc}$ for the most viscous ionic liquid [P_{4446}][NTf_2] is deviates largely from the η_{rheo}.

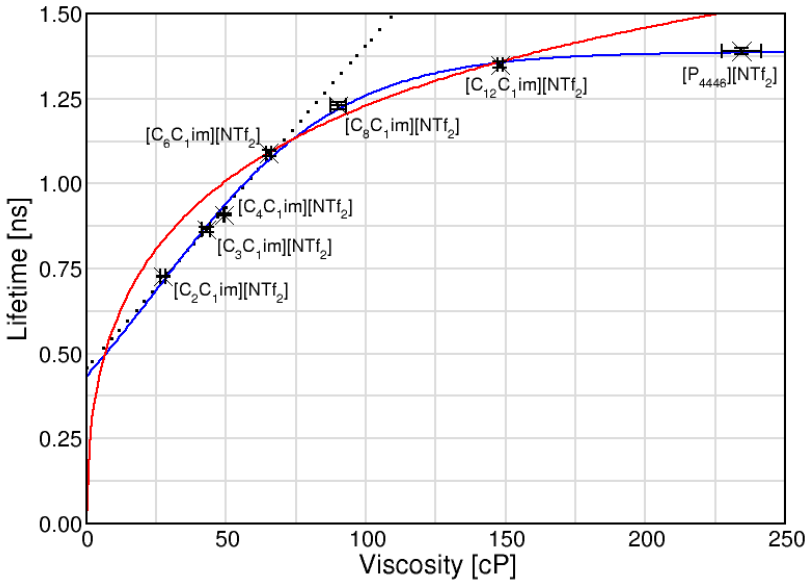

Figure 58: Fluorescence lifetime of Cy3 in the ionic liquids [C$_n$C$_1$im][NTf$_2$] (n = 2, 3, 4, 6, 8 and 12) and [P$_{4446}$][NTf$_2$], plotted against the ionic liquid viscosities. The red curve is the literature sucrose calibration and the blue curve is the logistic unction fitted to the ionic liquid data. The dotted line is the linear fitting of [C$_n$C$_1$im][NTf$_2$] (n = 2, 3, 4, 6).

Table 15: The fluorescence lifetime and percent contribution of all the components extracted from time resolved decay of Cy3 in $[NTf_2]^-$ based ionic liquids.

Ionic liquid	τ_{Cy3} (ns)	Contribution (%)	τ_A (ns)	Contribution (%)	τ_B (ns)	Contribution (%)
$[C_2C_1im][NTf_2]$	0.727 ± 0.003	85.18	0.023 ± 0.003	14.82	-	-
$[C_3C_1im][NTf_2]$	0.865 ± 0.009	85.63	0.027 ± 0.004	14.37	-	-
$[C_4C_1im][NTf_2]$	0.908 ± 0.003	85.78	0.020 ± 0.005	14.22	-	-
$[C_6C_1im][NTf_2]$	1.090 ± 0.005	86.94	0.017 ± 0.006	13.06	-	-
$[C_8C_1im][NTf_2]$	1.227 ± 0.004	83.64	0.058 ± 0.005	10.53	3.75 ± 0.10	5.83
$[C_{12}C_1im][NTf_2]$	1.352 ± 0.005	83.13	0.045 ± 0.004	11.23	4.01 + 0.22	2.64
$[P_{4446}][NTf_2]$	1.385 ± 0.005	85.73	0.039 ± 0.004	12.04	3.79 ± 0.23	2.23

The deviations between the viscosity predicted by the molecular rotor (η_{FL}) from η_{rheo} is common in many fluorescence spectroscopy-based experiments. For example, the viscosity predicted based on measurement of photoluminescence quantum yields of a molecular rotor, 1,1-dimethyl-2,3,4,5-tetraphenylsilole in $[C_4C_1im][BF_4]$, $[C_4C_1im][PF_6]$ or $[C_8C_1im][BF_4]$ is lower than those measured by viscometer. In contrast, the viscosities derived by fluorescence measurements are higher than measured viscosity for Thioflavin-T in $[C_2C_1im][FAP]$ and $[(HO)_2C_2C_1im][FAP]$ (FAP = tris(penta fluoroethyl)trifluorophosphate)[193] and for 9-(dicyanovinyl) julolidine in $[C_2C_1im][NTf_2]$, $[C_4C_1im][NTf_2]$, $[(HO)_2C_2C_1im][NTf_2]$, $[C_2C_1im][EtSO_4]$, $[C_4C_1im][BF_4]$ or $[(HO)_2C_2C_1im][BF_4]$.[13] These observations might be related to the effects of microheterogeneity that has been reported to occur in certain ionic liquids and might also due the variation in the free volume available around the rotor. The solvent-solute interactions between the ionic species and rotor also might contribute to the differences between the η_{FL} and η_{rheo}.

It may be better to conduct the lifetime-viscosity calibration based on ionic liquid system itself due to the expectation that the environment experience by the rotor in molecular solvents is largely different than that in ionic liquids. In a molecular system, the rotor is generally surrounded by, and moving through, relatively small and neutral molecules. In contrast, the anion and/or cation of ionic liquids usually have a comparable size to the rotor and all of them are charged species. This might be the explanation for the two different calibration curves produced in the system comprised of molecular solvents and of ionic liquids (See **Figure 58**). The lifetime-viscosity calibration of Cy3 in water/sucrose system can be fitted using a Hill

function[100] while the calibration ionic liquids data can be fitted to a logistic function according to the equation **(39)**.

$$\tau = A / (1 + \exp(B(\eta - C))) \quad \textbf{(39)}$$

where A, B and C are constants for which the values were determined to be 1.383, -0.0307 and 25.804, respectively.

Another interesting observation was that the lifetime-viscosity calibration in $[C_nC_1im][NTf_2]$ (n = 2, 3, 4, 6) ionic liquids can be fitted with a straight line of the equation $\tau = 0.0095\eta + 0.4595$ with a goodness of fit of 0.9925. Structural microheterogeneity in ionic liquids has been studied both theoretically and experimentally.[47] It has been reported that the non-polar alkyl chains of the imidazolium ionic liquids with n < 6 tend to aggregate to form a discrete non-polar microphase and their structure is dominated by the polar domains which consist of the positively charged head of the imidazolium cation and the negatively charge anion form a continuous ionic phase. The formation of the continuous ionic phase in ionic liquids with n < 6 is consistent with the linear increase of the measured Cy3 lifetime in these ionic liquids. The levelling of the change in the lifetime of Cy3 in $[C_8C_1im][NTf_2]$ and $[C_{12}C_1im][NTf_2]$ can probably be ascribed to the constant feature of the structure observed in ionic liquids with n ≥7 in which the structure is dominated by the continuous non-polar phase.[167,194,195] This shows that a chain length of n = 6 is probably the turning point where the continuous non-polar phase start to dominate the structure. Under these conditions, the local viscosity environment surrounding the Cy3 no longer increases in the same way as the bulk viscosity measured by rheometer. The lifetime of the Cy3 in $[P_{4446}][NTf_2]$ also fall below the value that straight line would predict. The phosphonium ionic liquids are less well studied and

no structural investigations of $[P_{4446}][NTf_2]$ itself have been reported in the literature. The closest structures that are available are for $[P_{4444}]Cl$ and $[P_{4448}]Cl$.[196] Both are described as having interpenetrating polar and non-polar networks, with $[P_{4448}]Cl$ having a greater separation of ionic domains. The fluorescence lifetime of Cy3 in $[P_{4446}][NTf_2]$ suggests that it behaves in a similar manner as the longer chain imidazolium ionic liquids *i.e.* $[C_nC_1im][NTf_2]$ (n = 8 or 12).

5.4 Fluorescence lifetime of BODIPY-C_{10} in $[NTf_2]^-$ based ionic liquids

The fluorescence lifetime of BODIPY-C_{10} was also measured in $[C_nC_1im][NTf_2]$ (n = 2, 3, 4, 6, 8 and 12) and $[P_{4446}][NTf_2]$, with a similar trend of variation in the lifetime of BODIPY-C_{10} observed. The plot of lifetime of BODIPY-C_{10} against viscosity of ionic liquids can be fitted with an exponential function with goodness of fit, R^2 = 0.9958 as shown in **Figure 59**. Again, the plot of lifetime of BODIPY-C_{10} against viscosity of the $[C_nC_1im][NTf_2]$ (n = 2, 3, 4, 6) ionic liquids is well fitted with a straight-line equation with a goodness of fit R^2 = 0.9928. The lifetime-viscosity calibration of BODIPY-C_{10} is usually performed using methanol/glycerol mixtures.[100] In this molecular solvent system, the time resolved fluorescence signal of BODIPY-C_{10} decayed monoexponentially in the mixtures and the lifetime of the dye was found to change linearly with the viscosity of the mixture.[100,197] However, the time resolved fluorescence signals of BODIPY-C_{10} in ionic liquids shows bi-exponential decays. The fluorescence lifetimes of both components and their contributions extracted from the time resolved decays of BODIPY-C_{10} in the ionic liquids are listed in **Table 16**. The first component was assigned to the fluorescence lifetime arising from BODIPY-C_{10} (τ_{BDP}) and the second component(τ_a) is believed to arise due the inherent fluorescence of the ionic liquids. As can be seen in **Table 16**, the fluorescence lifetime of BODIPY-C_{10} increased with the increasing of viscosity of the ionic liquids, and the contributions of the BODIPY-C_{10} fluorescence signal is relatively high, i.e. >84% in all cases.

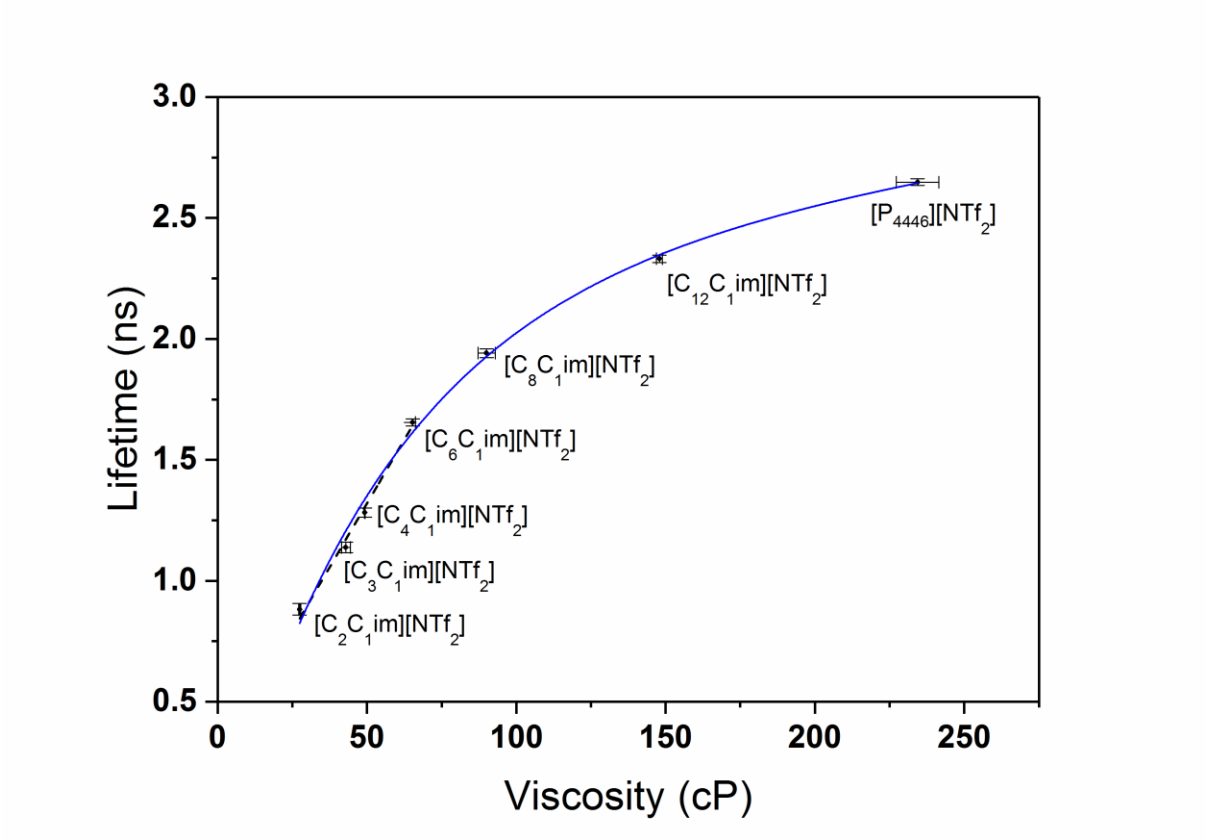

Figure 59: Fluorescence lifetime of BODIPY-C_{10} in the ionic liquids [$C_nC_1$im][NTf_2] (n = 2, 3, 4, 6, 8 and 12) and [P_{4446}][NTf_2], plotted against the ionic liquid viscosities.

Table 16: The fluorescence lifetime and percent contribution of all the components extracted from time resolved decay of BODIPY-C_{10} in $[NTf_2]^-$ based ionic liquids.

Ionic liquid	τ_{BDP} (ns)	Contribution (%)	τ_a (ns)	Contribution (%)
$[C_2C_1im][NTf_2]$	0.882 ± 0.024	84.94	0.181 ± 0.019	15.06
$[C_3C_1im][NTf_2]$	1.138 ± 0.022	90.04	0.203 ± 0.019	9.96
$[C_4C_1im][NTf_2]$	1.282 ± 0.019	91.78	0.221 ± 0.015	8.22
$[C_6C_1im][NTf_2]$	1.655 ± 0.014	93.38	0.282 ± 0.015	6.62
$[C_8C_1im][NTf_2]$	1.941 ± 0.018	91.77	0.422 ± 0.039	8.23
$[C_{12}C_1im][NTf_2]$	2.331 ± 0.015	92.03	0.674 ± 0.063	7.97
$[P_{4446}][NTf_2]$	2.648 ± 0.014	92.88	0.532 ± 0.031	7.12

5.5 Fluorescence lifetime under influence of electric field

The fluorescence lifetime of Cy3 was observed before, during and after a +2V potential was applied to the ionic liquid *i.e.* [C_4C_1im][NTf_2]. The fluorescence lifetime was first recorded at 0V vs. the open circuit potential (OCP) for 120s. After that, a +2V potential (*vs.* OCP) was applied and maintained for 120s before the potential was brought back to the initial condition of 0V vs. OCP. The fluorescence lifetime was then recorded for another 600s. The graph illustration of potential-time program used for this experiment is shown in **Figure 60** (A). The fluorescence lifetime of Cy3 (τ_{Cy3}) was measured at four different distances *i.e.* 1, 10, 25 and 50 μm relative to the working electrode.

The application of +2V potential has shown some effect to the viscosity of the liquid. **Table 17** summarises the τ_{Cy3} after application of the +2V potential and the predicted viscosity by the various calibration curves. The application of the potential, in general, caused the τ_{Cy3} to increase and with a magnitude of their changes follow the order: τ_{Cy3} (25 μm) > τ_{Cy3} (10 μm) > τ_{Cy3} (1 μm) with τ_{Cy3} (50 μm) ≈ τ_{Cy3} (pre-potential). The distances at which these observations were made are much larger than the usual distance used under conventional electrolyte theories, as well as other various type of measurements for studying the behaviour of ionic liquids at various interfaces.

Table 17: The fluorescence lifetime of Cy3 in $[C_4C_1im][NTf_2]$ at different distances from the working electrode and the corresponding viscosity derived from the lifetime-viscosity calibrations curve after application of +2V potential. Data is averaged over the entire plateau range (marked with the red horizontal line) in the time series profiles.

Position	τ_{Cy3} **(ns)**	$\eta_{\text{FL-logistic}}$	$\eta_{\text{FL-linear}}$	$\eta_{FL-sucwater}$
Pre-potential	0.854 ± 0.010	41.1	41.5	29.7
1 µm	1.08 ± 0.04	66.6	65.3	63.0
10 µm	1.21 ± 0.04	88.2	79.0	94.4
25 µm	1.41 ± 0.04	undefined	100.1	172.7
50 µm	0.903 ± 0.012	46.0	46.7	35.2

In order to get the overall view of the effect of using different calibration approach, the apparent viscosity of $[C_4C_1im][NTf_2]$ after application of the potential were estimated using all the three calibration curves (see **Figure 58**). It is apparent that only measurement at 25 µm show a large difference in the viscosities obtained by these different methods. Despite this quantitative difference, the qualitative result remains the same in that $\eta(25\ \mu m) > \eta(10\ \mu m) > \eta(1\ \mu m)$.

At 1 µm from the working electrode the calculated viscosities of $[C_4C_1im][NTf_2]$ during and after the application of potential are similar to each other, and to that of $[C_6C_1im][NTf_2]$ with no applied potential. At 10 µm, the calculated viscosity of $[C_4C_1im][NTf_2]$ after application of potential is similar to that of $[C_8C_1im][NTf_2]$ with no applied potential. At 25 µm from the electrode, the calculated viscosity of $[C_4C_1im][NTf_2]$ after application of potential is greater than that of $[C_{12}C_1im][NTf_2]$ with no applied potential for the sucrose calibration and between that of $[C_8C_1im][NTf_2]$ and $[C_{12}C_1im][NTf_2]$ with no applied potential using the linear

calibration. For the ionic liquid logistic function-based calibration, τ_{Cy3} is above the limit of the function so the viscosity is undefined. Regardless of the calibration used, this clearly indicates an increase in the apparent viscosity surrounding the molecular rotor. This increase is greater as the distance from the electrode increases. This is opposite to what would be expected, as screening from the ionic liquid ions should reduce the effect of the electrode as the distance from the electrode increases.

Similar to the differences between the value of τ_{Cy3} at different depths, there are very clear temporal differences with the decay. There are delays between the potential being applied and τ_{Cy3} reaching the maximum value (Δt_{onset}) and a delay between the potential being removed and τ_{Cy3} decreasing to a steady value ($\Delta t_{persist}$). **Figure 60** shows how the values vary over the time of measurement. At 1 µm from the electrode surface τ_{Cy3} increases immediately upon the application of potential and returns to the pre-potential value 20 seconds after removal of the potential. At 10 µm it takes 20 seconds for the full effect of the applied potential to be seen, and 60 seconds after removal of the potential τ_{Cy3} has decreased to a plateau. It appears that τ_{Cy3} measured at 25 µm plateaus 120 seconds after application of potential. After removal of the potential the system had not relaxed to a plateau value after 600 seconds. These timescales are extremely long compared to what could be expected. Even the processes on a molecular level are in the order of seconds, whereas here we observe effects that last for over 10 minutes. The speed of the dynamics is that the change is fastest at 1 µm, followed by 10 µm, followed by 25 µm with regards to both the increase and decrease in τ_{Cy3}. This highlights that both the

increase and decrease of the rotor lifetime in the ionic liquid propagates from the electrode into the bulk.

However, the timescales of these changes in viscosity are not directly related to the changes in current flow, with the build-up of charge being complete approximately 60 seconds after application of potential, and complete discharge is achieved in less than 30 seconds after removal of the potential . The τ_{Cy3} at 10 μm does not return to the pre-potential value. The post-potential value of τ_{Cy3} at 0.94 ns is greater than the pre-potential value of τ_{Cy3} at 0.84 ns and persists to the last of our measurements (600 seconds post-potential). As the applied potential is inside the electrochemical window of the ionic liquid, this indicates that the observed change in the ionic liquid system caused by the electric field at this distance is not reversible upon return to open circuit potential (OCP).

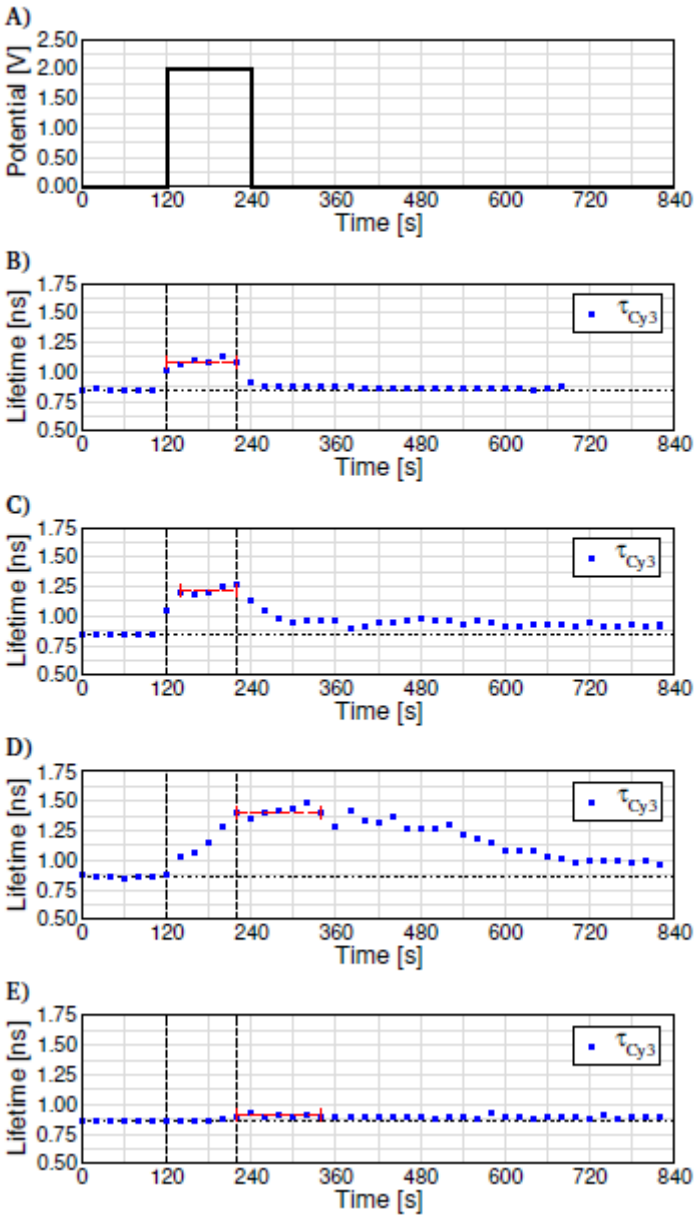

Figure 60: **A)** Potential-time program used for fluorescence lifetime experiments. Time trace graph of lifetime of Cy3 at distances of **(B)** 1 µm, **(C)** 10 µm, **(D)** 25 µm, and **(E)** 50 µm from the electrode. Dotted vertical lines show the first and last data point during the field application. Red horizontal lines show the data used to calculate τ_{Cy3} under potential.

The applied potential also affects the measured photons per second from the sample (see **Figure 61**). Again, the observed order of the effect is 25 μm > 10 μm > 1 μm > 50 μm; however, this measurement now shows an effect of the potential at 50 μm from the electrode, whereas the rotor lifetime does not change. As with the change in τ_{Cy3}, the onset of this effect is much quicker closer to the electrode, and also recovers much quicker closer to the electrode, again suggesting the formation of meta-stable structures. The reduction in the number of photons can be hypothesised to come from an electrophoretic effect, where the electric field causes movement of charged particles. As Cy3 is positively charged, it would be expected to be repelled from the electrode when the positive potential is applied. Unlike in a molecular solvent, there is also a very high concentration of other positively charged species in the $[C_4C_1im]^+$ cation and local electrical neutrality is expected to be maintained. Additionally, from **Figure 61** it seems that the Cy3 is repelled from the electrode, perhaps preferentially over $[C_4C_1im]^+$. This could be due to its larger size, movement of one Cy3 cation from the electrode leaves a larger void for packing more anions closer to the electrode than movement of one $[C_4C_1im]^+$ cation. Since the background photons per second from the neat ionic liquid is 6,000 photons per second, it is possible to estimate the change in concentration of Cy3 at the various distances from the electrode as the potential is applied. Assuming the background from the ionic liquids does not change in the field, and with the initial concentration of Cy3 in ionic liquids being 100 nM, the concentration drops to 10.5, 8.4, 6.3 and 46.3 nM at 1, 10, 25 and 50 μm, respectively.

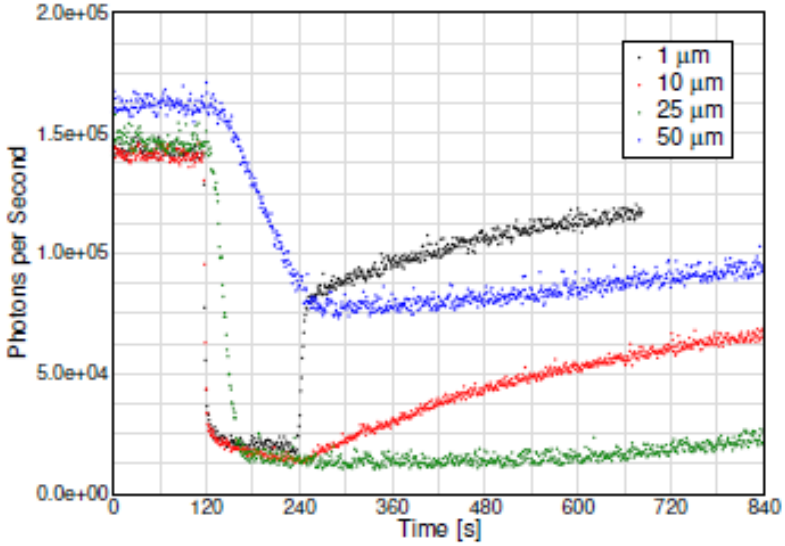

Figure 61: Number of photons per second for each experiment at 1 µm, 10 µm, 25 µm, and 50 µm.

These results observed here are not entirely without precedent. Long-range (ca. 100 µm from a charged interface) effects were seen in a study of fluorescence anisotropy decay of resorufin, creysl violet and nile red in $[C_4C_1im][BF_4]$ in contact with a charged silica surface.[198] The charged probes were much more affected than the neutral probe. However, while these results were used to support charge induced long-range order, they were not directly related to an increase in viscosity. As well as being long range effects, there are long timescales associated with these processes. It takes in the order of tens of seconds for the effect to propagate from the electrode, and again this increased at greater distances from the electrode. It is also the case that the relaxation back to pre-potential conditions was always slower than the build-up of the effect.

Recently, another unusually long timescale process has been observed. Anaredy and Shaw generated ordered thin films of $[C_2C_1im][NTf_2]$ of *ca.* 2 mm thickness by rotating a metal (Ag or Au) disk through a droplet of the ionic liquid.[199] After rotation of the disk was halted they found the orientation of the anion relaxed back to its initial state over the period of 50 minutes; this effect was observed for a number of different ionic liquids. Hysteresis effects have also been seen in several IL based electrochemical systems and have been attributed to slow rearrangements processes of the ions close to the electrode surface.[200–206] It should be noted that when the potential is applied there is a driving force to give the structural change, but on return to OCP there is not; there is just an absence of the original driving force. Hence, it is not necessarily surprising that the relaxation process is longer than the initial structure-forming process. A number of molecular dynamics simulations have shown that electric fields can cause a change in the structure of ionic liquid ions, with a strong preference for stretched configurations of the alkyl chains of the cations, leading to nematic structures being formed in the most extreme cases.[207–209] Although such dramatic changes are unlikely at the electric field strengths used here, changes in the structures of the ions is an intriguing concept to consider. The results that are presented in this study occur at distances and timescales that are longer than expected but do appear to be related to other reported observations and suggests the formation of metastable structures in ionic liquids.

Another result that needs to be considered is the current flow profile which was recorded throughout the experiments and an example of the current flow is shown in **Figure 62**. A similar trend of current flow profile is observed for all measurements. Upon a closer observation, there has been sign of faradaic current generated during the application of +2V versus OCP (see figure **Figure 62** (b)). In addition, the exposure of the ionic liquid to 10 cycles

of voltage between -4.5V to 4.2V also show sign of generation of the faradaic current (see **Figure 63**).

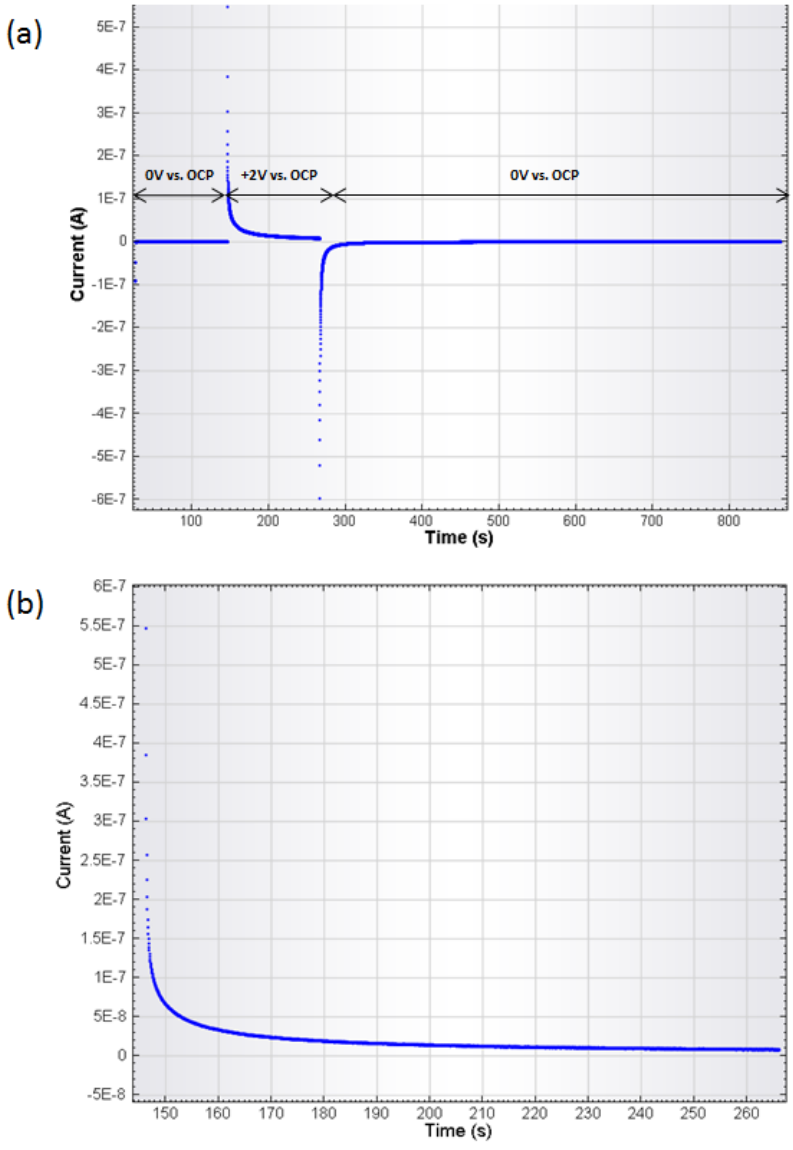

Figure 62: The profile of current flow across the electrochemical cell at 1µm, (a) for the whole-time experiment (b) during application of +2V vs. OCP.

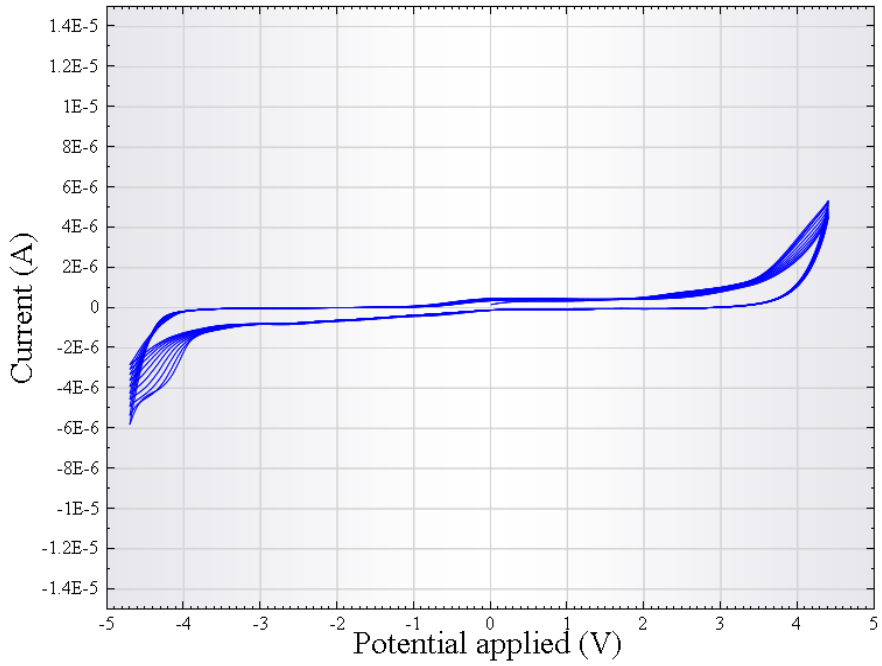

Figure 63: Current produce by 1-butyl-3-methylimidazolium bis(trifluoromethylsulfonyl)imide $[C_4C_1im][NTf_2]$ as exposed to 10 cycles of voltage between -4.5 V to 4.2 V in ITO-PDMS cell.

The faradaic current is generally produced from a reversible reduction-oxidation processes which involves an electron transfer reaction. The integration of the chronoamperometry curve gives the area under graph (see **Table 18**) which represents the amount of charge (Q) involved in the oxidation or reduction reactions. Using the coulometry technique, the amount of analyte involved in reaction (W) can be calculated based on Faraday's law:

$$W = \frac{QM}{nF} \tag{40}$$

In the equation **(40)** *M* is the formula weight of the analyte, *n* is the number of electrons and F is the Faraday's constant.

Table 18: Area under graph for chronoamperometry curve during the application of +2V vs. OCP

Position	Area under the curve = Charge, Q (Coulombs)
1 µm	2.42×10^{-6}
10 µm	5.15×10^{-6}
25 µm	3.08×10^{-5}
50 µm	1.04×10^{-5}

From the chronoamperometry data, it can be hypothesised that there might be an electrochemical reaction that takes place due to the application of +2V. The chemical species involved in the electrochemical reaction could come from the ionic liquid solution or the electrode itself. As the ionic liquid used in this experiment *i.e.* $[C_4C_1im][NTf_2]$ is relatively stable and has a wide electrochemical window, the observed faradaic current might come from the oxidation/reduction reaction that leads to dissolution ITO electrode. The chemical instability of ITO surface against aggressive acidic and basic solutions has been reported by Stotter *et al*.[210] They found out that morphology of ITO surface has changed significantly after it being exposed to 20 potential cycles between -1.1 to 0.3 V in 1M nitric acid and 1M sodium hydroxide. The morphology of the surface was degraded from a smooth and continuous surface to rough surface with formation of grains of 100nm in diameter as shown by the atomic force micrographs. A study conducted by Senthilkumar *et al.* showed that the light transmittance of the ITO showed a significant reduction from 80% to 40% upon exposure to

potential cycling in phosphate buffer in the range of 0.2-1.0 V and physically ITO films become more opaque as number of potential cycles is increased.[211] Further investigation by X-ray fluorescence spectroscopy (XRF) showed a change in composition of indium and tin after the ITO being exposed to the potential cycling.

Based on these previous studies, it can be hypothesised that similar events might happen when ionic liquid and ITO system is used in the chronoamperometry experiments. If dissolution of ITO is assumed to occur in this study, the possible oxidation process can only be related to oxidation of the oxygen in the ITO lattice (O^{2-}) as oxidation of In^{3+} and Sn^{4+} is impossible.[212] The In-O and Sn-O bonding at the surface of ITO can be broken and molecular oxygen will be produced following the production intermediate atomic oxygen. The plausible for the oxidation reactions are as the following:

$$O^{2-}_{lattice} \rightarrow O + 2e^- \quad \textbf{(41)}$$

$$2O \rightarrow O_2(g) \quad \textbf{(42)}$$

Thus, the overall chemical reactions that might represents the dissolution of In_2O_3 and SnO_2 are as the following:

$$2In_2O_3 \rightarrow 4In^{3+} + 3O_2(g) + 12e^- \quad \textbf{(43)}$$

$$SnO_2 \rightarrow Sn^{4+} + O_2(g) + 4e^- \quad \textbf{(44)}$$

In this study, if the dissolution of In_2O_3 and SnO_2 has happened during the application of the +2V potential, it will affect the physical viscosity of the ionic liquid. This can be correlated to change in viscosity that we observed by the fluorescence lifetime studies. However, upon observation throughout the experiment, no visible gas bubble is formed after each experiment

and the resistance of ITO surface is maintained before and after use. Moreover, the dissolution of In^{3+} and Sn^{4+} into solution of Cy3 ionic liquid may also affect the fluorescence of Cy3. Metal binding has been reported able to change the fluorescence properties of a fluorophore as chelating or binding of the metal by changing its electronic and molecular structure the flourophore.[212] This will lead to change to a change in fluorescence intensity and/or wavelength of light emission or absorption. The presence of metal ions has been reported to cause fluorescence quenching of both singlet and triplet states of organic fluorophores.[213,214] Then, it also possible to relate dissolution of ITO to the reduction in fluorescence signal (photon count) as +2V voltage is applied (see **Figure 61**).Thus, it is recommended that the other analytical testing is used order to confirm whether the observed viscosity change upon application of +2V is due to the molecular dynamics change (discussed earlier) or due the dissolution of ITO into ionic liquid. The recommendations to improve this study will be discussed in Chapter 6.

Chapter 6 Conclusions and Recommendations

6.1 Conclusions and Recommendations

Low fluorescence background ionic liquids were successfully synthesised and characterised. This was achieved through the careful use of clean glassware and highly pure starting materials. Recrystallisation of halide intermediates and treatment of the final products using activated charcoal seems essential for producing good quality ionic liquids for fluorescence studies. The characterisations and comparisons of the physical and chemical properties of the ionic liquids served as one crucial method to preliminarily evaluate the purity of the ionic liquids. Measurement of the ionic liquids' electrochemical properties were successfully conducted in a custom-made ITO-PDMS cell and the conductive ITO coverslip replaced the need for a glass coverslip that is usually used in confocal microscope for fluorescence lifetime measurements.

Measurements of photo-physical properties of Cy3, BODIPY-C_{10} and DCVJ in ionic liquids revealed that these rotors have a great potential to be used as probes to determine local viscosities within ionic liquids. The fluorescence emission intensity of these molecular rotors showed a dependency on the viscosity of the ionic liquids. Comparison of the fluorescence lifetime of Cy3 and BODIPY-C_{10} in ionic liquids compared to molecular solvent systems suggest that it is essential to specifically develop a lifetime-viscosity calibration curve based on the ionic liquid system of interest. Using a lifetime-viscosity calibration based on molecular solvents is not appropriate for ionic liquid systems due to the different environment the molecular rotor is exposed to in ionic liquids (ionic) compared to molecular solvents (non-

ionic). Moreover, the nanostructure of ionic liquids may have an influence on the fluorescence lifetime of the molecular rotors in ionic liquids.

The molecular rotor Cy3 was successfully used to probe the viscosity of the ionic liquid $[C_4C_1im][NTf_2]$ at various distances from an electrode when a potential of +2V was applied. The application of the electric potential to a solution of Cy3 in $[C_4C_1im][NTf_2]$ seems to increase the viscosity as showed by the increased in fluorescence lifetime of Cy3. If only the fluorescence data is considered, the observed increase in viscosity can be attributed to the change in molecular dynamics of the system. In addition, the chronoamperometry data gathered along with the fluorescence lifetime experiments give additional information which lead to another hypothesis that there are electrochemical reactions occurred in the system upon the application of +2V potential. The most possible electrochemical reactions could come from the oxidation and reduction of the ITO electrode. A concrete conclusion is hard to be made and further experiment and deeper analysis is required in order to find the right conclusion for this study.

As for the recommendations, the following works are suggested for the improvement and expansion of this study.

I. To further study the stability of ITO over ionic liquids when potential is applied to the system. These probably can be done by further analyses of chemical composition of ionic liquids after each experiment and also by examining the physical properties of the ITO using various microscopy techniques.

II. The design of the cell also can be improved by changing the currently used 2-electrode system with a 3-electrode system, in which a proper potential window can be measured so that the stability of the system against the applied potential can be studied. Replacing the ITO with a more stable electrode could also be useful as the stability of ITO over ionic liquids and voltage can be questioned.

III. A systematic study of the fluorescence lifetimes of molecular rotors in other species of ionic liquids. Apart from varying the alkyl chain length, the viscosity of ionic liquids can also be changed by varying the identity of the cations and anions, changing the temperature and by addition of a lithium salt with a common anion.

IV. Measurement of surface tensions of the ionic liquids also could be useful to be done as surface tension is one of the measurable physical properties that can be related to the viscosity of ionic liquids. This will enable a deeper understanding of transport properties of the liquids.

V. As the components of ionic liquids comprise of both negatively and positively charged species, it is beneficial to comprehensively study the role and effect of the charge of the molecular rotors and their interaction with both negatively and positively charge surfaces.

VI. Other fluorescence spectroscopy techniques such as fluorescence correlation spectroscopy (FCS) should be used to corroborate the current results.

Chapter 7 References and Appendices

7.1 List of references

1. Galiński, M., Lewandowski, A. & Stepniak, I. Ionic liquids as electrolytes. *Electrochim. Acta* **51**, 5567–5580 (2006).

2. Wishart, J. F. Energy applications of ionic liquids. *Energy Environ. Sci.* **2**, 956–961 (2009).

3. Watanabe, M. *et al.* Application of ionic liquids to energy storage and conversion materials and devices. *Chem. Rev.* **117**, 7190–7239 (2017).

4. Abbott, A. P. & McKenzie, K. J. Application of ionic liquids to the electrodeposition of metals. *Phys. Chem. Chem. Phys.* **8**, 4265–4279 (2006).

5. Zhang, Q., Wang, Q., Zhang, S., Lu, X. & Zhang, X. Electrodeposition in ionic liquids. *ChemPhysChem* **17**, 335–351 (2016).

6. Wei, D. & Ivaska, A. Applications of ionic liquids in electrochemical sensors. *Anal. Chim. Acta* **607**, 126–135 (2008).

7. Noda, A., Hayamizu, K. & Watanabe, M. Pulsed-Gradient Spin−Echo 1H and 19F NMR Ionic Diffusion Coefficient, Viscosity, and Ionic Conductivity of Non-Chloroaluminate Room-Temperature Ionic Liquids. *J. Phys. Chem. B* **105**, 4603–4610 (2001).

8. MacFarlane, D. R. *et al.* On the concept of ionicity in ionic liquids. *Phys. Chem. Chem. Phys.* **11**, 4962–4967 (2009).

9. Fedorov, M. V. & Kornyshev, A. A. Ionic liquids at electrified interfaces. *Chem. Rev.* **114**, 2978–3036 (2014).

10. Gebbie, M. A. *et al.* Long range electrostatic forces in ionic liquids. *Chem. Commun.*

53, 1214–1224 (2017).

11. Haidekker, M. A. & Theodorakis, E. A. Molecular rotors—fluorescent biosensors for viscosity and flow. *Org. Biomol. Chem.* **5**, 1669–1678 (2007).

12. Kuimova, M. K. Mapping viscosity in cells using molecular rotors. *Phys. Chem. Chem. Phys.* **14**, 12671 (2012).

13. Paul, A. & Samanta, A. Free volume dependence of the internal rotation of a molecular rotor probe in room temperature ionic liquids. *J. Phys. Chem. B* **112**, 16626–16632 (2008).

14. Jameson, L. P., Kimball, J. D., Gryczynski, Z., Balaz, M. & Dzyuba. Effect of ionic liquids on the conformation of a porphyrin-based viscometer. *RSC Adv.* **3**, 18300–18304 (2013).

15. Scalise, R. E., Caradonna, P. A., Tracy, H. J., Mullin, J. L. & Keirstead, A. E. 1,1-Dimethyl-2,3,4,5-tetraphenylsilole as a molecular rotor probe to investigate the microviscosity of imidazolium ionic liquids. *J. Inorg. Organomet. Polym. Mater.* **24**, 431–441 (2014).

16. Kimball, J. D. *et al.* BODIPY–BODIPY dyad: assessing the potential as a viscometer for molecular and ionic liquids. *RSC Adv.* **5**, 19508–19511 (2015).

17. Walden, P. About the molecular and electrical conductivity of some molten salts. *Bull. Imp'eriale Acad'emie St. P'etersbg. Sci.* **8**, 405–422 (1914).

18. Graenacher, C. Cellulose solution. (1934).

19. Plechkova, N. V. & Seddon, K. R. Applications of ionic liquids in the chemical industry. *Chem. Soc. Rev.* **37**, 123–150 (2008).

20. Newington, I., Perez-Arlandis, J. M. & Welton, T. Ionic Liquids as designer solvents for nucleophilic aromatic substitutions. *Org. Lett.* **9**, 5247–5250 (2007).

21. Plechkova, N. & Seddon, K. R. Ionic Liquids: "Designer" Solvents for Green Chemistry. in *Methods and Reagents for Green Chemistry* 103–130 (Wiley-Blackwell,

2007). doi:10.1002/9780470124086.ch5

22. Marsh, K. N., Deev, A., Wu, A. C.-T., Tran, E. & Klamt, A. Room temperature ionic liquids as replacements for conventional solvents – A review. *Korean J. Chem. Eng.* **19**, 357–362 (2002).

23. Wasserscheid, P. & Welton, T. *Ionic liquids in Synthesis*. **7**, (Wiley-VCH Verlag GmbH & Co. KGaA, 2002).

24. Hallett, J. P. & Welton, T. Room-temperature ionic liquids: Solvents for synthesis and catalysis. 2. *Chem. Rev.* **111**, 3508–3576 (2011).

25. Seddon, K. R., Stark, A. & Torres, M.-J. Influence of chloride, water, and organic solvents on the physical properties of ionic liquids. *Pure Appl. Chem* **72**, 2275–2287 (2000).

26. Weingärtner, H. *Understanding ionic liquids at the molecular level: Facts, problems, and controversies*. *Angewandte Chemie - International Edition* **47**, (Wiley-VCH Verlag GmbH & Co. KGaA, 2008).

27. Welton, T. Room-temperature ionic liquids. Solvents for synthesis and catalysis. *Chem. Rev.* **99**, 2071–2083 (1999).

28. Sheldon, R. Catalytic reactions in ionic liquids. *Chem. Commun.* 2399–2407 (2001). doi:10.1039/b107270f

29. Cole, A. C. *et al.* Novel Brønsted acidic ionic Liquids and their use as dual solvent - catalysts. *J. Am. Chem. Soc.* **124**, 5962–5963 (2002).

30. Steinruck, H.-P. & Wasserscheid, P. Ionic liquids in catalysis. *Catal. Letters* **145**, 380–397 (2015).

31. Huddleston, J. G., Willauer, H. D., Swatloski, R. P., Visser, A. E. & Rogers, R. D. Room temperature ionic liquids as novel media for ' clean ' liquid – liquid extraction. *Chem. Commun.* **0**, 1765–1766 (1998).

32. Swatloski, R. P., Spear, S. K., Holbrey, J. D. & Rogers, R. D. Dissolution of cellose

with ionic liquids. *J. Am. Chem. Soc.* **124**, 4974–4975 (2002).

33. MacFarlane, D. R., Kar, M. & Pringle, J. M. Electrochemistry of and in Ionic Liquids. in *Fundamentals of Ionic Liquids: From Chemistry to Applications* 177–207 (Wiley-Blackwell, 2017). doi:10.1002/9783527340033.ch7

34. Mahony, A. M. O., Silvester, D. S., Aldous, L., Hardacre, C. & Compton, R. G. Effect of water on the electrochemical window and potential limits of room-temperature ionic liquids. *J. Chem. Eng. Data* **53**, 2884–2891 (2008).

35. Wadhawan, J. D. *et al.* Water-induced accelerated ion diffusion : voltammetric studies in 1-methyl-3- [2,6-(S)-dimethylocten-2-yl]imidazolium tetrafluoroborate, 1-butyl-3-methylimidazolium tetrafluoroborate and hexafluorophosphate ionic liquids. *New J. Chem.* **24**, 1009–1015 (2000).

36. Stafford, G. R. & Haarberg, G. M. The electrodeposition of Al-Nb alloys from chloroaluminate electrolytes. *Plasmas Ions* **1**, 35–44 (1999).

37. Frischknecht, A. L., Halligan, D. O. & Parks, M. L. Electrical double layers and differential capacitance in molten salts from density functional theory. *J. Chem. Phys.* **141**, (2014).

38. Bard, A. J. & Faulkner, L. R. *Electrochemical Methods: Fundamentals and Applications, 2nd Edition*. (Wiley Textbooks, 2000).

39. Stojek, Z. The electrical double layer and its structure. *Electroanal. Methods Guid. to Exp. Appl.* 3–9 (2010). doi:10.1007/978-3-642-02915-8_1

40. Kornyshev, A. A. Double-Layer in Ionic Liquids: Paradigm Change? *J. Phys. Chem. B* **111**, 5545–5557 (2007).

41. Kłos, J. & Lamperski, S. Analysis of electrical double layer structure in molten salts. *J. Chem. Phys.* **150**, 64704 (2019).

42. Kisza, A. The capacitance of the electric double layer of electrodes in molten salts. *J. Electroanal. Chem.* **534**, 99–106 (2002).

43. Fedorov, M. V & Kornyshev, A. A. Ionic liquid near a charged wall: structure and capacitance of electrical double layer. *J. Phys. Chem. B* **112**, 11868–11872 (2008).

44. Gebbie, M. A., Dobbs, H. A., Valtiner, M. & Israelachvili, J. N. Long-range electrostatic screening in ionic liquids. *Proc. Natl. Acad. Sci.* **112**, 7432–7437 (2015).

45. Smith, A. M., Lee, A. A. & Perkin, S. The Electrostatic Screening Length in Concentrated Electrolytes Increases with Concentration. *J. Phys. Chem. Lett.* **7**, 2157–2163 (2016).

46. Hayes, R. *et al.* Double layer structure of ionic liquids at the Au(111) electrode interface : An atomic force microscopy investigation. *J. Phys. Chem. C* **115**, 6855–6863 (2011).

47. Hayes, R., Warr, G. G. & Atkin, R. Structure and Nanostructure in Ionic Liquids. *Chem. Rev.* **115**, 6357–6426 (2015).

48. Ohno, H. *Electrochemical Aspects of Ionic Solids*. *Key Engineering Materials* **125**–**126**, (John Wiley & Sons, 1997).

49. Girard, G. M. A. *et al.* Electrochemical and physicochemical properties of small phosphonium cation ionic liquid electrolytes with high lithium salt content. *Phys. Chem. Chem. Phys.* **17**, 8706–8713 (2015).

50. Yoshida, K. *et al.* Oxidative-stability enhancement and charge transport mechanism in glyme–lithium salt equimolar complexes. *J. Am. Chem. Soc.* **133**, 13121–13129 (2011).

51. Seki, S. *et al.* Effects of non-equimolar lithium salt glyme solvate ionic liquid on the control of interfacial degradation in lithium secondary batteries. *RSC Adv.* **6**, 33043–33047 (2016).

52. Largeot, C. *et al.* Relation between the ion size and pore size for an electric double-layer capacitor. *J. Am. Chem. Soc.* **130**, 2730–2731 (2008).

53. Béguin, F., Presser, V., Balducci, A. & Frackowiak, E. Carbons and electrolytes for

advanced supercapacitors. *Adv. Mater.* **26**, 2219–2251 (2014).

54. Macfarlane, D. R. *et al.* Energy applications of ionic liquids. *Energy Environ. Sci.* **7**, 232–250 (2014).

55. Zhong, C. *et al.* A review of electrolyte materials and compositions for electrochemical supercapacitors. *Chem. Soc. Rev.* **44**, 7484–7539 (2015).

56. Watanabe, M. Design and materialization of ionic liquids based on an understanding of their fundamental properties. *Electrochemistry* **84**, 642–653 (2016).

57. Michot, T., Nishimoto, A. & Watanabe, M. Electrochemical properties of polymer gel electrolytes based on poly(vinylidene fluoride) copolymer and homopolymer. *Electrochim. Acta* **45**, 1347–1360 (2000).

58. Susan, M. A. B. H., Kaneko, T., Noda, A. & Watanabe, M. Ion gels prepared by in situ radical polymerization of vinyl monomers in an ionic liquid and their characterization as polymer electrolytes. *J. Am. Chem. Soc.* **127**, 4976–4983 (2005).

59. Ueno, K., Hata, K., Katakabe, T., Kondoh, M. & Watanabe, M. Nanocomposite ion gels based on silica nanoparticles and an ionic liquid: Ionic transport, viscoelastic properties, and microstructure. *J. Phys. Chem. B* **112**, 9013–9019 (2008).

60. Khanmirzaei, M. H., Ramesh, S. & Ramesh, K. Hydroxypropyl cellulose based non-volatile gel polymer electrolytes for dye-sensitized solar cell applications using 1-methyl-3-propylimidazolium iodide ionic liquid. *Sci. Rep.* **5**, 1–7 (2015).

61. Kubo, W. *et al.* Photocurrent-determining processes in quasi-solid-state dye-sensitized solar cells using ionic gel electrolytes. *J. Phys. Chem. B* **107**, 4374–4381 (2003).

62. Kambe, S., Nakade, S., Kitamura, T., Wada, Y. & Yanagida, S. Influence of the electrolytes on electron transport in mesoporous TiO2-electrolyte systems. *J. Phys. Chem. B* **106**, 2967–2972 (2002).

63. Kawano, R. & Watanabe, M. Anomaly of charge transport of an iodide/tri-iodide redox couple in an ionic liquid and its importance in dye-sensitized solar cells. *Chem.*

Commun. 2107–2109 (2005). doi:10.1039/b418031c

64. Maase, M., Massonne, K. & Vagt, U. BASIL™—BASF's Processes Based on Ionic Liquids. *Chemfiles Volume 5 Article 6* Available at: https://www.sigmaaldrich.com/technical-documents/articles/chemfiles/basil-basf-s-processes.html. (Accessed: 9th July 2018)

65. Maase, M. & Massonne, K. Biphasic acid scavenging utilizing ionic liquids: The first commercial process with ionic liquids. in *Ionic Liquids IIIB: Fundamentals, Progress, Challenges, and Opportunities* **902**, 126–132 (2005).

66. Kerton, F. & Marriott, R. *Alternative solvents for green chemistry*. (The Royal Society of Chemistry, 2013). doi:10.1039/9781849736824

67. Weyershausen, B., Hell, K. & Goldschmidtstrasse, D. A. G. Ionic liquids at Degussa : Catalyst heterogenization in an industrial process. in *Ionic Liquids IIIB: Fundamentals, Progress, Challenges, and Opportunities* 133–143 (2005).

68. Siriwardana, A. I. Industrial Applications of Ionic Liquids. in *Electrochemistry in Ionic Liquids: Volume 2: Applications* (ed. Torriero, A. A. J.) 563–603 (Springer International Publishing, 2015). doi:10.1007/978-3-319-15132-8_20

69. Weyershausen, B. & Lehmann, K. Industrial application of ionic liquids as performance additives. *Green Chem.* **7**, 15–19 (2005).

70. Honeywell UOP. Honeywell UOP Introduces Ionic Liquids Alkylation Technology. 1 (2016). Available at: https://www.uop.com/?press_release=honeywell-uop-introduces-ionic-liquids. (Accessed: 9th July 2018)

71. Timken, H. K. *Isoalky ™ Technology : Next generation alkylate gasoline manufacturing process technology*. (2017).

72. Holbrey, J. D. *et al.* Efficient, halide free synthesis of new, low cost ionic liquids: 1,3-dialkylimidazolium salts containing methyl- and ethyl-sulfate anions. *Green Chem.* **4**, 407–413 (2002).

73. Ue, M., Takeda, M., Takahashi, T. & Takehara, M. Ionic liquids with low melting points and their application to double-layer capacitor electrolytes. *Electrochem. Solid-State Lett.* **5**, A119–A121 (2002).

74. de Zeeuw, R. A., Jonkman, J. H. G. & van Mansvelt, F. J. W. Plasticizers as contaminants in high-purity solvents: A potential source of interference in biological analysis. *Anal. Biochem.* **67**, 339–341 (1975).

75. Armarego, W. L. F. & Chai, C. L. L. Chapter 1 - Common Physical Techniques Used in Purification. in *Purification of Laboratory Chemicals (Sixth Edition)* (eds. Armarego, W. L. F. & Chai, C. L. L.) 1–60 (Butterworth-Heinemann, 2009). doi:https://doi.org/10.1016/B978-1-85617-567-8.50009-3

76. Deyhimi, F. & Coles, J. A. Rapid silylation of a glass surface: Choice of reagent and effect of experimental parameters on hydrophobicity. *Helv. Chim. Acta* **65**, 1752–1759

77. Pape, P. G. *Silylating Agents*. *Kirk-Othmer Encyclopedia of Chemical Technology* (2017). doi:10.1002/0471238961.1909122516011605.a01.pub3

78. Andanson, J. M., Meng, X., Traïkia, M. & Husson, P. Quantification of the impact of water as an impurity on standard physico-chemical properties of ionic liquids. *J. Chem. Thermodyn.* **94**, 169–176 (2016).

79. Villagrán, C., Deetlefs, M., Pitner, W. R. & Hardacre, C. Quantification of halide in ionic liquids using ion chromatography. *Anal. Chem.* **76**, 2118–2123 (2004).

80. Vander Hoogerstraete, T., Jamar, S., Wellens, S. & Binnemans, K. Determination of halide impurities in ionic liquids by total reflection X-ray fluorescence spectrometry. *Anal. Chem.* **86**, 3931–3938 (2014).

81. Cammarata, L., Kazarian, S. G., Salter, P. A. & Welton, T. Molecular states of water in room temperature ionic liquids. *Phys. Chem. Chem. Phys.* **3**, 5192–5200 (2001).

82. Holbrey, J. D., Seddon, K. R. & Wareing, R. A simple colorimetric method for the quality control of 1-alkyl-3-methylimidazolium ionic liquid precursors. *Green Chem.* **3**, 33–36 (2001).

83. Bonta, M. *et al.* Determination of residual chloride content in ionic liquids using LA-ICP-MS. *RSC Adv.* **6**, 90273–90279 (2016).

84. Earle, M. J., Gordon, C. M., Plechkova, N. V, Seddon, K. R. & Welton, T. Decolorization of ionic liquids for spectroscopy. *Anal. Chem.* **79**, 758–764 (2007).

85. Swatloski, R. P., Holbrey, J. D. & Rogers, R. D. Ionic liquids are not always green: Hydrolysis of 1-butyl-3- methylimidazolium hexafluorophosphate. *Green Chem.* **5**, 361–363 (2003).

86. Freire, M. G., Neves, C. M. S. S., Marrucho, I. M., Coutinho, J. A. P. & Fernandes, A. M. Hydrolysis of tetrafluoroborate and hexafluorophosphate counter ions in imidazolium-based ionic liquids. *J. Phys. Chem. A* **114**, 3744–3749 (2010).

87. Wang, B., Qin, L., Mu, T., Xue, Z. & Gao, G. Are ionic liquids chemically stable? *Chem. Rev.* **117**, 7113–7131 (2017).

88. Burrell, A. K., Del Sesto, R. E., Baker, S. N., McCleskey, T. M. & Baker, G. A. The large scale synthesis of pure imidazolium and pyrrolidinium ionic liquids. *Green Chem.* **9**, 449–454 (2007).

89. Lakowicz, J. *Principles of Fluorescence Spectroscopy*. *Principles of Fluorescent Spectroscopy* (Springer, 2010).

90. Becker, W. *The Bh TCSPC Handbook*. (Becker & Hickl, 2014).

91. Lippert, E., Luder, W. & Boos, H. Fluorescence spectrum and Franck Condon principle in solutions of aromatic compounds. in *Advances in Molecular Spectroscopy* 443–457 (1962). doi:10.1016/B978-1-4832-1332-3.50070-6

92. Grabowski, Z. R., Rotkiewicz, K. & Siemiarczuk, A. Dual fluorescence of donor-acceptor molecules and the twisted intramolecular charge transfer (TICT) states. *J. Lumin.* **18**–**19**, 420–424 (1979).

93. A. Haidekker, M., Lichlyter, D., Ben-Johny, M. & A. Grimes, C. Probing polymerization dynamics with fluorescent molecular rotors and magnetoelastic

sensors. *Sens. Lett.* **4**, 257–261 (2006).

94. Alhassawi, F. M., Corradini, M. G., Rogers, M. A. & Richard, D. Potential applications of luminescent molecular rotors in food science and engineering. *Crit. Rev. Food Sci. Nutr.* 1–15 (2017). doi:10.1080/10408398.2017.1278583

95. Atsbeha, T., Mohammed, A. M. & Redi-abshiro, M. Excitation wavelength dependence of dual fluorescence of DMABN in polar solvents. *J. Fluoresc.* **20**, 1241–1248 (2010).

96. Haidekker, M. A., Brady, T. P., Lichlyter, D. & Theodorakis, E. A. Effects of solvent polarity and solvent viscosity on the fluorescent properties of molecular rotors and related probes. *Bioorg. Chem.* **33**, 415–425 (2005).

97. Howell, S., Dakanali, M., Theodorakis, E. A. & Haidekker, M. A. Intrinsic and extrinsic temperature-dependency of viscosity-sensitive fluorescent molecular rotors. *J. Fluoresc.* **22**, 457–465 (2012).

98. Förster, T. & Hoffmann, G. Die Viskositätsabhängigkeit der Fluoreszenzquantenausbeuten einiger Farbstoffsysteme (effect of viscosity on the fluorescence quantum yield of some dye systems). *Zeitschrift für Physikalische Chemie* **75**, 63 (1971).

99. Levitt, J. a. *et al.* Fluorescence anisotropy of molecular rotors. *ChemPhysChem* **12**, 662–672 (2011).

100. Hosny, N. a *et al.* Fluorescent lifetime imaging of atmospheric aerosols: a direct probe of aerosol viscosity. *Faraday Discuss.* **165**, 343–356 (2013).

101. Hosny, N. a. *et al.* Mapping microbubble viscosity using fluorescence lifetime imaging of molecular rotors. *Proc. Natl. Acad. Sci.* **110**, 9225–9230 (2013).

102. Nockemann, P., Binnemans, K. & Driesen, K. Purification of imidazolium ionic liquids for spectroscopic applications. *Chem. Phys. Lett.* **415**, 131–136 (2005).

103. Earle, M. J. *et al.* The distillation and volatility of ionic liquids. *Nature* **439**, 831–834

(2006).

104. Armarego, W. L. F. & Chai, C. L. L. Chapter 2 - Chemical methods used in purification. in *Purification of Laboratory Chemicals (Sixth Edition)* (eds. Armarego, W. L. F. & Chai, C. L. L.) 61–79 (Butterworth-Heinemann, 2009). doi:https://doi.org/10.1016/B978-1-85617-567-8.50010-X

105. Waterkamp, D. A. *et al.* Synthesis of ionic liquids in micro-reactors - A process intensification study. *Green Chem.* **9**, 1084–1090 (2007).

106. Paul, A. & Samanta, A. Optical absorption and fluorescence studies on imidazolium ionic liquids comprising the bis(trifluoromethanesulphonyl)imide anion. *J. Chem. Sci* **118**, 335–340 (2006).

107. Stark, A. *et al.* Purity specification methods for ionic liquids. *Green Chem.* **10**, 1152–1161 (2008).

108. Fox, D. M. *et al.* Flammability, thermal stability, and phase change characteristics of several trialkylimidazolium salts. *Green Chem.* **5**, 724–727 (2003).

109. Hahn, E. L. Spin echoes. *Phys. Rev.* **80**, 580–594 (1950).

110. Tanner, J. E. Use of the stimulated echo in NMR diffusion studies. *J. Chem. Phys.* **52**, 2523–2526 (1970).

111. Kuimova, M. K., Yahioglu, G., Levitt, J. a. & Suhling, K. Molecular rotor measures viscosity of live cells via fluorescence lifetime imaging. *J. Am. Chem. Soc.* **130**, 6672–6673 (2008).

112. Wagner, R. W. & Lindsey, J. S. Boron-dipyrromethene dyes for incorporation in synthetic multi-pigment light-harvesting arrays. *Pure Appl. Chem.* **68**, 1373–1380 (1996).

113. Fürth, R. On the theory of the liquid state: III. The hole theory of the viscous flow of liquids. *Math. Proc. Cambridge Philos. Soc.* **37**, 281–290 (1941).

114. Auluck, F. C. & Kothari, D. S. The hole theory of liquids. *Nature* **153**, 777 (1944).

115. Bockris, J. O. & Reddy, A. K. N. *Modern Electrochemistry*. *Springer US* **1**, (Springer US, 1998).

116. Atkins, P., Atkins, P. W. & de Paula, J. *Atkins' Physical Chemistry*. (OUP Oxford, 2014).

117. Abbott, A. P. Model for the conductivity of ionic liquids based on an infinite dilution of holes. *ChemPhysChem* **6**, 2502–2505 (2005).

118. Abbott, A. P. Application of hole theory to the viscosity of ionic and molecular liquids. *ChemPhysChem* **5**, 1242–1246 (2004).

119. Lide, D. R. *CRC Handbook of Chemistry and Physics*. (CRC Press, 2005). doi:978-1466571143

120. Bajić, D. M. *et al.* Densities, viscosities, and refractive indices of the binary systems (PEG200 + 1,2-propanediol, +1,3-propanediol) and (PEG400 + 1,2-propanediol, +1,3-propanediol) at (288.15 to 333.15) K and atmospheric pressure: Measurements and modeling. *J. Chem. Thermodyn.* **57**, 510–529 (2013).

121. Ottani, S., Vitalini, D., Comelli, F. & Castellari, C. Densities, viscosities, and refractive indices of poly(ethylene glycol) 200 and 400 + cyclic ethers at 303.15 K. *J. Chem. Eng. Data* **47**, 1197–1204 (2002).

122. Hyun, B.-R., Dzyuba, S. V., Bartsch, R. A. & Quitevis, E. L. Intermolecular dynamics of room-temperature ionic liquids: femtosecond optical Kerr effect measurements on 1-Alkyl-3-methylimidazolium bis((trifluoromethyl)sulfonyl)imides. *J. Phys. Chem. A* **106**, 7579–7585 (2002).

123. Yao, H. *et al.* Densities and viscosities of the binary mixtures of 1-ethyl-3-methylimidazolium bis(trifluoromethylsulfonyl)imide with N -methyl-2-pyrrolidone or ethanol at T = (293.15 to 323.15) K. *J. Chem. Eng. Data* **57**, 875–881 (2012).

124. McEwen, A. B. Electrochemical properties of imidazolium salt electrolytes for electrochemical capacitor applications. *J. Electrochem. Soc.* **146**, 1687–1695 (1999).

125. Gómez, E., Calvar, N., Macedo, E. A. & Domínguez, Á. Effect of the temperature on the physical properties of pure 1-propyl 3-methylimidazolium bis (trifluoromethylsulfonyl) imide and characterization of its binary mixtures with alcohols. *J. Chem. Thermodyn.* **45**, 9–15 (2012).

126. Tariq, M. *et al.* Viscosity of (C2-C14) 1-alkyl-3-methylimidazolium bis(trifluoromethylsulfonyl)amide ionic liquids in an extended temperature range. *Fluid Phase Equilib.* **301**, 22–32 (2011).

127. Vranes, M., Dozic, S., Djeric, V. & Gadzuric, S. Physicochemical characterization of 1-butyl-3-methylimidazolium and 1-butyl-1-methylpyrrolidinium bis(trifluoromethylsulfonyl)imide. *J. Chem. Eng. Data* **57**, 1072–1077 (2012).

128. Tokuda, H., Tsuzuki, S., Susan, M. A. B. H., Hayamizu, K. & Watanabe, M. How ionic are room-temperature ionic liquids? An indicator of the physicochemical properties. *J. Phys. Chem. B* **110**, 19593–19600 (2006).

129. Kandil, M. E., Marsh, K. N. & Goodwin, A. R. H. Measurement of the viscosity, density, and electrical conductivity of 1-hexyl-3-methylimidazolium bis(trifluorosulfonyl)imide at temperatures between (288 and 433) K and pressures below 50 MPa. *J. Chem. Eng. Data* **52**, 2382–2387 (2007).

130. Santos, F. J. V., De Castro, C. A. N., Mota, P. J. F. & Ribeiro, A. P. C. Electrical conductivity and viscosity of 1-hexyl-3-methylimidazolium bis(trifluorosulfonyl)imide, [C6mim] [(CF3SO2)2N]. *Int. J. Thermophys.* **31**, 1869–1879 (2010).

131. Andreatta, A. E., Arce, A., Rodil, E. & Soto, A. Physical and excess properties of (methyl acetate + methanol + 1-octyl-3-methyl-imidazolium bis(trifluoromethylsulfonyl)imide) and its binary mixtures at T = 298.15 K and atmospheric pressure. *J. Chem. Thermodyn.* **41**, 1317–1323 (2009).

132. Hazrati, N., Abdouss, M., Miran Beigi, A. A., Pasban, A. A. & Rezaei, M. Physicochemical properties of long chain alkylated imidazolium based chloride and bis(trifluoromethanesulfonyl)imide ionic liquids. *J. Chem. Eng. Data* **62**, 3084–3094

(2017).

133. Domańska, U. & Wlazło, M. Thermodynamics and limiting activity coefficients measurements for organic solutes and water in the ionic liquid 1-dodecyl-3-methylimidzolium bis(trifluoromethylsulfonyl) imide. *J. Chem. Thermodyn.* **103**, 76–85 (2016).

134. Harris, K. R., Woolf, L. A., Kanakubo, M. & Ruther, T. Transport properties of N-butyl-N -methylpyrrolidinium bis(trifluoromethylsulfonyl)amide. *J. Chem. Eng. Data* **56**, 4672–4685 (2011).

135. Gaciño, F. M., Regueira, T., Lugo, L., Comuñas, M. J. P. & Fernández, J. Influence of molecular structure on densities and viscosities of several ionic liquids. *J. Chem. Eng. Data* **56**, 4984–4999 (2011).

136. Philippi, F., Rauber, D., Zapp, J. & Hempelmann, R. Transport properties and ionicity of phosphonium ionic liquids. *Phys. Chem. Chem. Phys.* **19**, 23015–23023 (2017).

137. Zheng, Q.-G., Liu, H., Xia, Q., Liu, Q.-S. & Mou, L. Density , dynamic viscosity and electrical conductivity of two hydrophobic phosphonium ionic liquids. *Acta Phys.-Chim.Sin.* **33**, 736–743 (2017).

138. Vega, J. A., Zhou, J. & Kohl, P. A. Electrochemical comparison and deposition of lithium and potassium from phosphonium- and ammonium-TFSI ionic liquids. *J. Electrochem. Soc.* **156**, A253A-259 (2009).

139. Shim, T., Lee, M. H., Kim, D. & Ouchi, Y. Comparison of photophysical properties of the hemicyanine dyes in ionic and nonionic solvents. *J. Phys. Chem. B* **112**, 1906–1912 (2008).

140. Qi, M., Wu, G., Li, Q. & Luo, Y. γ-Radiation effect on ionic liquid [bmim][BF4]. *Radiat. Phys. Chem.* **77**, 877–883 (2008).

141. Wang, J., Tian, Y., Zhao, Y. & Zhuo, K. A volumetric and viscosity study for the mixtures of 1-n-butyl-3- methylimidazolium tetrafluoroborate ionic liquid with acetonitrile, dichloromethane, 2-butanone and N, N-dimethylformamide. *Green Chem.*

5, 618–622 (2003).

142. Song, D. & Chen, J. Densities and viscosities for ionic liquids mixtures containing [eOHmim][BF4], [bmim][BF4] and [bpy][BF4]. *J. Chem. Thermodyn.* **77**, 137–143 (2014).

143. Moosavi, M., Daneshvar, A. & Sedghamiz, E. Rheological properties of {[bmim]PF6 + methanol} mixtures at different temperatures, shear rates and compositions. *J. Mol. Liq.* **209**, 693–705 (2015).

144. Fan, W., Zhou, Q., Sun, J. & Zhang, S. Density, excess molar volume, and viscosity for the methyl methacrylate + 1-butyl-3-methylimidazolium hexafluorophosphate ionic liquid binary system at atmospheric pressure. *Engineering* **54**, 2307–2311 (2009).

145. Harris, K. R., Kanakubo, M. & Woolf, L. A. Temperature and pressure dependence of the viscosity of the ionic liquids 1-hexyl-3-methylimidazolium hexafluorophosphate and 1-butyl-3-methylimidazolium bis(trifluoromethylsulfonyl)imide. *J. Chem. Eng. Data* **52**, 1080–1085 (2007).

146. Shamsipur, M., Beigi, A. A. M., Teymouri, M., Pourmortazavi, S. M. & Irandoust, M. Physical and electrochemical properties of ionic liquids 1-ethyl-3-methylimidazolium tetrafluoroborate, 1-butyl-3-methylimidazolium trifluoromethanesulfonate and 1-butyl-1-methylpyrrolidinium bis(trifluoromethylsulfonyl)imide. *J. Mol. Liq.* **157**, 43–50 (2010).

147. McHale, G. *et al.* Density-viscosity product of small-volume ionic liquid samples using quartz crystal impedance analysis. *Anal. Chem.* **80**, 5806–5811 (2008).

148. Seddon, K. R., Stark, A. & Torres, M.-J. Viscosity and density of 1-alkyl-3-methylimidazolium ionic liquids. in *ACS Symposium Series* **819**, 34–49 (2002).

149. Abbott, A. P. Application of hole theory to the viscosity of ionic and molecular liquids. *ChemPhysChem* **5**, 1242–1246 (2004).

150. Hunt, P. A., Ashworth, C. R. & Matthews, R. P. Hydrogen bonding in ionic liquids. *Chem. Soc. Rev.* **44**, 1257–1288 (2015).

151. Huddleston, J. G. *et al.* Characterization and comparison of hydrophilic and hydrophobic room temperature ionic liquids incorporating the imidazolium cation. *Green Chem.* **3**, 156–164 (2001).

152. Hapiot, P. & Lagrost, C. Electrochemical reactivity in room-temperature ionic liquids electrochemical reactivity in room-temperature Ionic liquids. *Chem. Rev.* **108**, 2238–2264 (2008).

153. Water conductivity. *Lenntech* Available at: https://www.lenntech.com/applications/ultrapure/conductivity/water-conductivity.htm. (Accessed: 7th July 2018)

154. Widegren, J. A., Saurer, E. M., Marsh, K. N. & Magee, J. W. Electrolytic conductivity of four imidazolium-based room-temperature ionic liquids and the effect of a water impurity. *J. Chem. Thermodyn.* **37**, 569–575 (2005).

155. Pan, Y. *et al.* Physical and transport properties of bis(trifluoromethylsulfonyl)imide-based room-temperature ionic liquids: Application to the diffusion of tris(2,2′-bipyridyl)ruthenium(II). *J. Electrochem. Soc.* **158**, F1–F9 (2011).

156. Olivier-Bourbigou, H. & Magna, L. Ionic liquids: Perspectives for organic and catalytic reactions. *J. Mol. Catal. A Chem.* **182**–**183**, 419–437 (2002).

157. Li, W. J., Han, B. X., Tao, R. T., Zhang, Z. F. & Zhang, J. L. Measurement and correlation of the ionic conductivity of ionic liquid-molecular solvent solutions. *Chinese J. Chem.* **25**, 1349–1356 (2007).

158. Stoppa, A., Zech, O., Kunz, W. & Buchner, R. The conductivity of imidazolium-based ionic liquids from (-35 to 195) °C. A. variation of cations alkyl chain. *J. Chem. Eng. Data* **55**, 1768–1773 (2010).

159. Bonhôte, P., Dias, A.-P., Papageorgiou, N., Kalyanasundaram, K. & Grätzel, M. Hydrophobic, highly conductive ambient-temperature molten salts. *Inorg. Chem.* **35**, 1168–1178 (1996).

160. Buzzeo, M. C., Evans, R. G. & Compton, R. G. Non-haloaluminate room-temperature

ionic liquids in electrochemistry - A review. *ChemPhysChem* **5**, 1106–1120 (2004).

161. Freedman, D. *Brownian Motion and Diffusion*. (Springer New York, 2012). doi:https://doi.org/10.1007/978-1-4615-6574-1

162. Murch, G. E. The haven ratio in fast ionic conductors. *Solid State Ionics* **7**, 177–198 (1982).

163. Monteiro, M. J., Camilo, F. F., Ribeiro, M. C. C. & Torresi, R. M. Ether-bond-containing ionic liquids and the relevance of the ether bond position to transport properties. *J. Phys. Chem. B* **114**, 12488–12494 (2010).

164. Marsh, K. N., Boxall, J. A. & Lichtenthaler, R. Room temperature ionic liquids and their mixtures - a review. *Fluid Phase Equilib.* **219**, 93–98 (2004).

165. Kolbeck, C. *et al.* Density and surface tension of ionic liquids. *J. Phys. Chem. B* **114**, 17025–17036 (2010).

166. Wang, Y. & Voth, G. A. Unique spatial heterogeneity in ionic liquids. *J. Am. Chem. Soc.* **127**, 12192–12193 (2005).

167. Canongia Lopes, J. N. A. & Pádua, A. A. H. Nanostructural organization in ionic liquids. *J. Phys. Chem. B* **110**, 3330–3335 (2006).

168. Dzyuba, S. V. & Bartsch, R. A. Influence of structural variations in 1-alkyl(aralkyl)-3-methylimidazolium hexafluorophosphates and bis(trifluoromethyl-sulfonyl)imides on physical properties of the ionic liquids. *ChemPhysChem* **3**, 161–166 (2002).

169. Tanaka, M., Girard, G., Davis, R., Peuto, A. & Bignell, N. Recommended table for the density of water between 0 and 40 degree Celcius based on recent experimental reports. *Metrologia* **38**, 301–309 (2001).

170. Fröba, A. P., Kremer, H. & Leipertz, A. Density, refractive index, interfacial tension, and viscosity of ionic liquids [EMIM][EtS4], [EMIM][NTf2], [EMIM][N(CN)2], and [OMA][NTf2] in dependence on temperature at atmospheric pressure. *J. Phys. Chem. B* **112**, 12420–12430 (2008).

171. Krummen, M., Wasserscheid, P. & Gmehling, J. Measurement of activity coefficients at infinite dilution in ionic liquids using the dilutor technique. *J. Chem. Eng. Data* **47**, 1411–1417 (2002).

172. Miran Beigi, A. A., Abdouss, M., Yousefi, M., Pourmortazavi, S. M. & Vahid, A. Investigation on physical and electrochemical properties of three imidazolium based ionic liquids (1-hexyl-3-methylimidazolium tetrafluoroborate, 1-ethyl-3-methylimidazolium bis(trifluoromethylsulfonyl) imide and 1-butyl-3-methylimidazolium methylsulfate). *J. Mol. Liq.* **177**, 361–368 (2013).

173. Seoane, R. G., González, E. J. & González, B. 1-Alkyl-3-methylimidazolium bis(trifluoromethylsulfonyl)imide ionic liquids as solvents in the separation of azeotropic mixtures. *J. Chem. Thermodyn.* **53**, 152–157 (2012).

174. Esperança, J. M. S. S. *et al.* Density, speed of sound, and derived thermodynamic properties of ionic liquids over an extended pressure range. 4. [C3mim][NTf2] and [C5mim][NTf2]. *J. Chem. Eng. Data* **51**, 2009–2015 (2006).

175. Troncoso, J., Cerdeiriña, C. A., Sanmamed, Y. A., Romaní, L. & Rebelo, L. P. N. Thermodynamic properties of imidazolium-based ionic liquids: densities, heat capacities, and enthalpies of fusion of [bmim][PF6] and [bmim][NTf2]. *J. Chem. Eng. Data* **51**, 1856–1859 (2006).

176. Fadeeva, T. A. *et al.* Interactions between water and 1-butyl-1-methylpyrrolidinium ionic liquids. *J. Chem. Phys.* **143**, 1–11 (2015).

177. Tian, Y., Wang, X. & Wang, J. Densities and viscosities of 1-butyl-3-methylimidazolium tetrafluoroborate + molecular solvent binary mixtures. *J. Chem. Eng. Data* **53**, 2056–2059 (2008).

178. Deetlefs, M., Seddon, K. R. & Shara, M. Predicting physical properties of ionic liquids. *Phys. Chem. Chem. Phys.* **8**, 642–649 (2006).

179. Soriano, A. N., Doma, B. T. & Li, M. H. Measurements of the density and refractive index for 1-n-butyl-3-methylimidazolium-based ionic liquids. *J. Chem. Thermodyn.*

41, 301–307 (2009).

180. García-Miaja, G., Troncoso, J. & Romaní, L. Excess properties for binary systems ionic liquid + ethanol: Experimental results and theoretical description using the ERAS model. *Fluid Phase Equilib.* **274**, 59–67 (2008).

181. Firestone, M. A. *et al.* Lyotropic liquid-crystalline gel formation in a room-temperature ionic liquid. *Langmuir* **18**, 7258–7260 (2002).

182. Inoue, T., Ebina, H., Dong, B. & Zheng, L. Electrical conductivity study on micelle formation of long-chain imidazolium ionic liquids in aqueous solution. *J. Colloid Interface Sci.* **314**, 236–241 (2007).

183. Tsuzuki, S., Tokuda, H., Hayamizu, K. & Watanabe, M. Magnitude and directionality of interaction in ion pairs of ionic liquids: Relationship with ionic conductivity. *J. Phys. Chem. B* **109**, 16474–16481 (2005).

184. Borucka, A. Z., Bockris, J. O. M. & Kitchener, J. A. Self-diffusion in molten sodium chloride: a test of the applicability of the Nernst—Einstein equation. *Proc. R. Soc. London. Ser. A. Math. Phys. Sci.* **241**, 554–567 (2006).

185. Xu, W., Cooper, E. I. & Angell, C. A. Ionic liquids: Ion mobilities, glass temperatures, and fragilities. *J. Phys. Chem. B* **107**, 6170–6178 (2003).

186. Hosny, N. a. *et al.* Direct imaging of changes in aerosol particle viscosity upon hydration and chemical aging. *Chem. Sci.* **7**, 1357–1367 (2016).

187. Law, K. Y. Fluorescence probe for microenvironments: anomalous viscosity dependence of the fluorescence quantum yield of p-N,N-dialkylaminobenzylidenemalononitrile in 1-alkanols. *Chem. Phys. Lett.* **75**, 545–549 (1980).

188. Loutfy, R. O. & Law, K. Y. Electrochemistry and spectroscopy of intramolecular charge-transfer complexes. p-N,N-Dialkylaminobenzylidenemalononitriles. *J. Phys. Chem.* **84**, 2803–2808 (1980).

189. Wang, X., Chen, K., Yao, J. & Li, H. Recent progress in studies on polarity of ionic liquids. *Sci. China Chem.* **59**, 517–525 (2016).

190. Paul, A., Mandal, P. K. & Samanta, A. On the optical properties of the imidazolium ionic liquids. *J. Phys. Chem. B* **109**, 9148–9153 (2005).

191. Paul, A., Mandal, P. K. & Samanta, A. How transparent are the imidazolium ionic liquids ? A case study with 1-methyl-3-butylimidazolium hexafluorophosphate , [bmim][PF6]. *Chem. Phys. Lett.* **402**, 375–379 (2005).

192. Cha, S., Shim, T., Ouchi, Y. & Kim, D. Characteristics of visible fluorescence from ionic liquids. *J. Phys. Chem. B* **117**, 10818–10825 (2013).

193. Singh, P. K., Mora, A. K. & Nath, S. Free volume dependence of an ionic molecular rotor in fluoroalkylphosphate (FAP) based ionic liquids. *Chem. Phys. Lett.* **644**, 296–301 (2016).

194. Shimizu, K., Bernardes, C. E. S. & Canongia Lopes, J. N. Structure and aggregation in the 1-alkyl-3-methylimidazolium Bis(trifluoromethylsulfonyl)imide ionic liquid homologous series. *J. Phys. Chem. B* **118**, 567–576 (2014).

195. Pontoni, D., Haddad, J., Di Michiel, M. & Deutsch, M. Self-segregated nanostructure in room temperature ionic liquids. *Soft Matter* **13**, 6947–6955 (2017).

196. Wang, Y. L., Li, B., Sarman, S. & Laaksonen, A. Microstructures and dynamics of tetraalkylphosphonium chloride ionic liquids. *J. Chem. Phys.* **147**, (2017).

197. Vyšniauskas, A. *et al.* SI Unravelling the effect of temperature on viscosity-sensitive fluorescent molecular rotors. *Chem. Sci.* **6**, 5773–5778 (2015).

198. Ma, K., Jarosova, R., Swain, G. M. & Blanchard, G. J. Charge-induced long-range order in a room-temperature ionic liquid. *Langmuir* **32**, 9507–9512 (2016).

199. Anaredy, R. S. & Shaw, S. K. Long-range ordering of ionic liquid fluid films. *Langmuir* **32**, 5147–5154 (2016).

200. Motobayashi, K., Minami, K., Nishi, N., Sakka, T. & Osawa, M. Hysteresis of

potential-dependent changes in ion density and structure of an ionic liquid on a gold electrode: In situ observation by surface-enhanced infrared absorption spectroscopy. *J. Phys. Chem. Lett.* **4**, 3110–3114 (2013).

201. Uysal, A. *et al.* Structural origins of potential dependent hysteresis at the electrified graphene/ionic liquid interface. *J. Phys. Chem. C* **118**, 569–574 (2014).

202. Lucio, A. J. & Shaw, S. K. Capacitive hysteresis at the 1-ethyl-3-methylimidazolium tris(pentafluoroethyl)-trifluorophosphate-polycrystalline gold interface. *Anal. Bioanal. Chem.* **410**, 4575–4586 (2018).

203. Makino, S., Kitazumi, Y., Nishi, N. & Kakiuchi, T. Charging current probing of the slow relaxation of the ionic liquid double layer at the Pt electrode. *Electrochem. commun.* **13**, 1365–1368 (2011).

204. Motobayashi, K. *et al.* Potential-induced restructuring dynamics of ionic liquids on a gold electrode: Steric effect of constituent ions studied by surface-enhanced infrared absorption spectroscopy. *J. Electroanal. Chem.* **800**, 126–133 (2017).

205. Zhou, W., Xu, Y. & Ouchi, Y. Hysteresis effects in the in-situ SFG and differential capacitance measurements on metal electrode/ionic liquids interface. *ECS Trans.* **50**, 339–348 (2012).

206. Drüschler, M. *et al.* New insights into the interface between a single-crystalline metal electrode and an extremely pure ionic liquid: slow interfacial processes and the influence of temperature on interfacial dynamics. *Phys. Chem. Chem. Phys.* **14**, 5090–5099 (2012).

207. Zhao, Y. *et al.* Structure of ionic liquids under external electric field: a molecular dynamics simulation. *Mol. Simul.* **38**, 172–178 (2012).

208. Daily, J. W. & Micci, M. M. Ionic velocities in an ionic liquid under high electric fields using all-atom and coarse-grained force field molecular dynamics. *J. Chem. Phys.* **131**, 94501 (2009).

209. Wang, Y. Disordering and reordering of ionic liquids under an external electric field.

J. Phys. Chem. B **113**, 11058–11060 (2009).

210. Stotter, J., Show, Y., Wang, S. & Swain, G. Comparison of the electrical, optical, and electrochemical properties of diamond and indium tin oxide thin-film electrodes. *Chem. Mater.* **17**, 4880–4888 (2005).

211. Senthilkumar, M., Mathiyarasu, J., Joseph, J., Phani, K. L. N. & Yegnaraman, V. Electrochemical instability of indium tin oxide (ITO) glass in acidic pH range during cathodic polarization. *Mater. Chem. Phys.* **108**, 403–407 (2008).

212. Kraft, A., Hennig, H., Herbst, A. & Heckner, K. H. Changes in electrochemical and photoelectrochemical properties of tin-doped indium oxide layers after strong anodic polarization. *J. Electroanal. Chem.* **365**, 191–196 (1994).

213. Varnes, A. W., Dodson, R. B. & Wehry, E. L. Interactions of transition-metal ions with photoexcited states of flavins. Fluorescence quenching studies. *J. Am. Chem. Soc.* **94**, 946–950 (1972).

214. Exclted, Q. O. F. The quenching of organic singlet. *Chem. Phys. Lett.* **47**, (1977).

7.2 NMR spectra

^{1}H NMR [C_2C_1im][NTf_2]

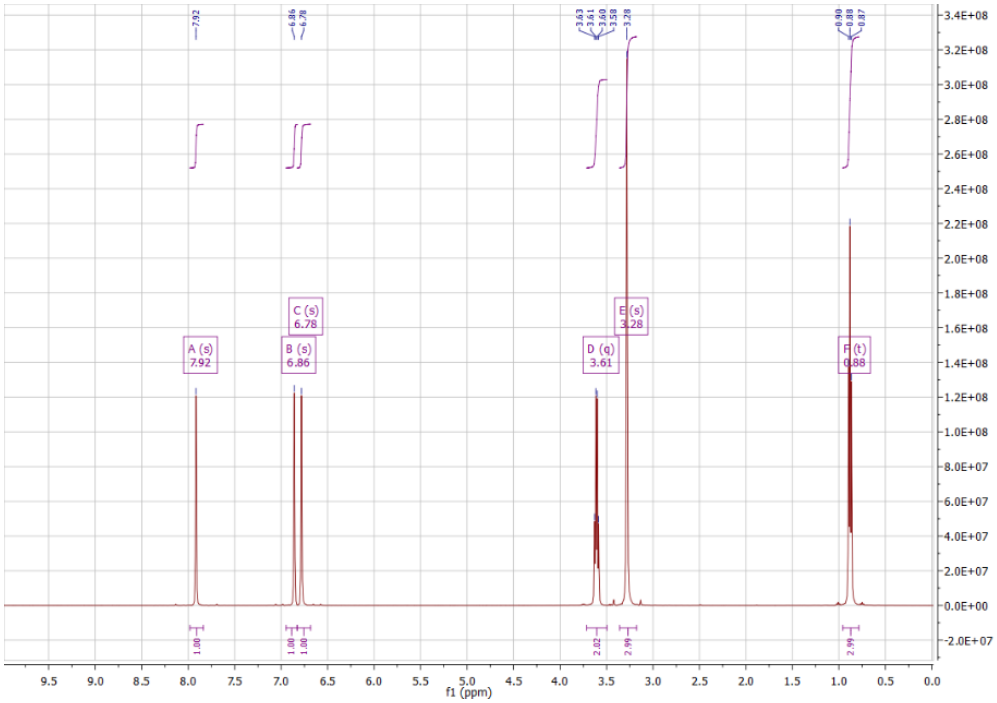

^{13}C [C_2C_1im][NTf_2]

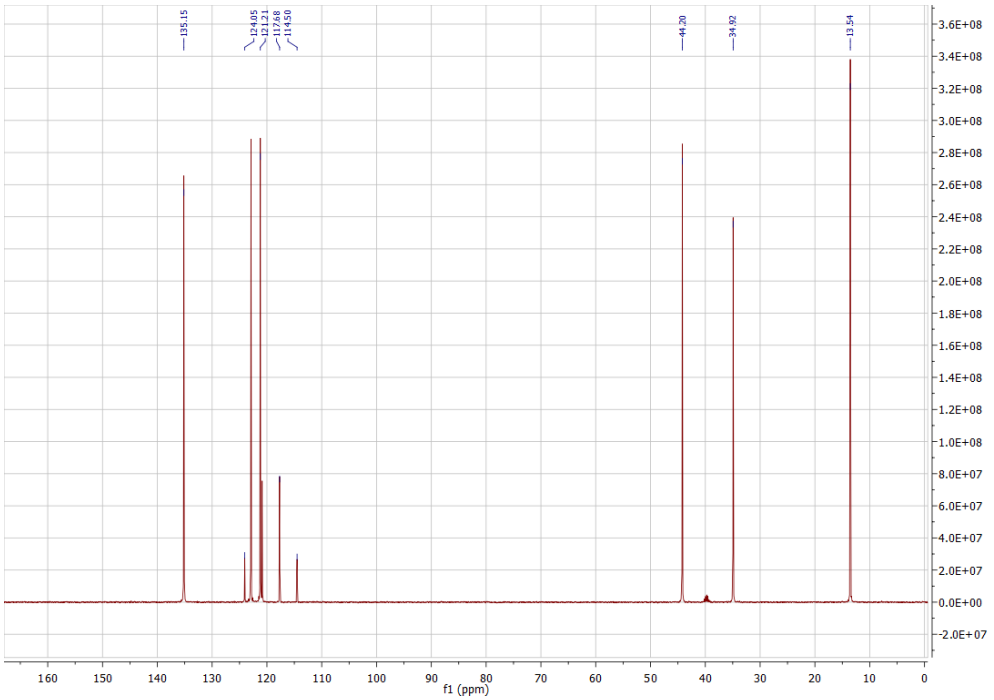

^{1}H NMR [C_3C_1im][NTf_2]

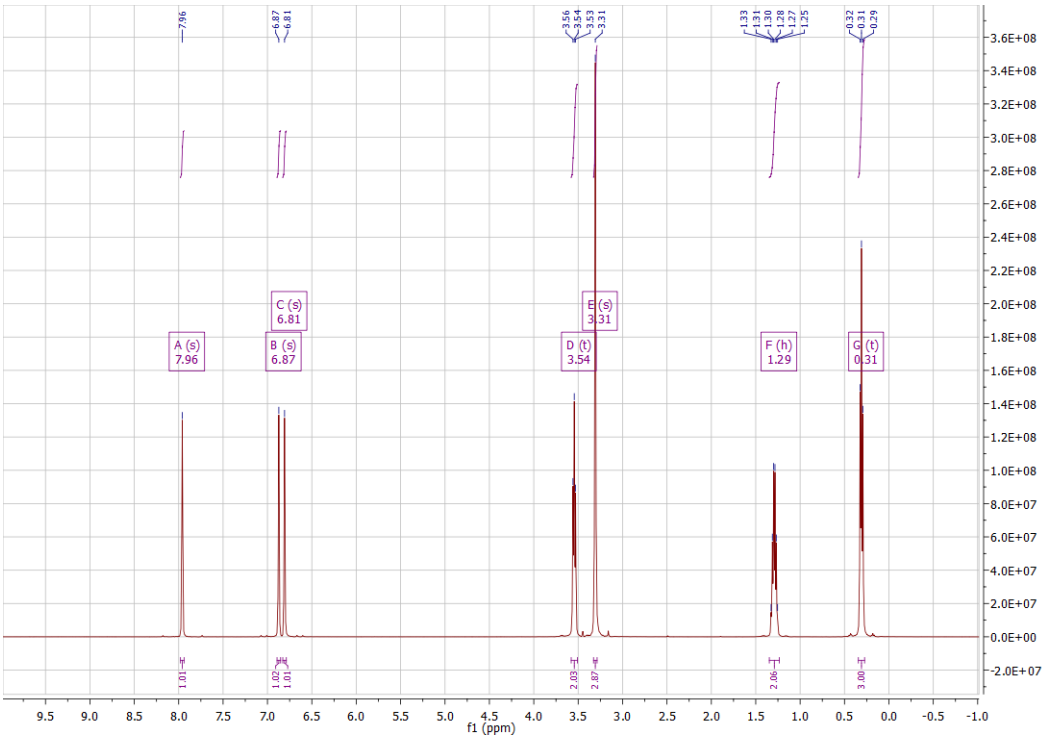

^{13}C [C_3C_1im][NTf_2]

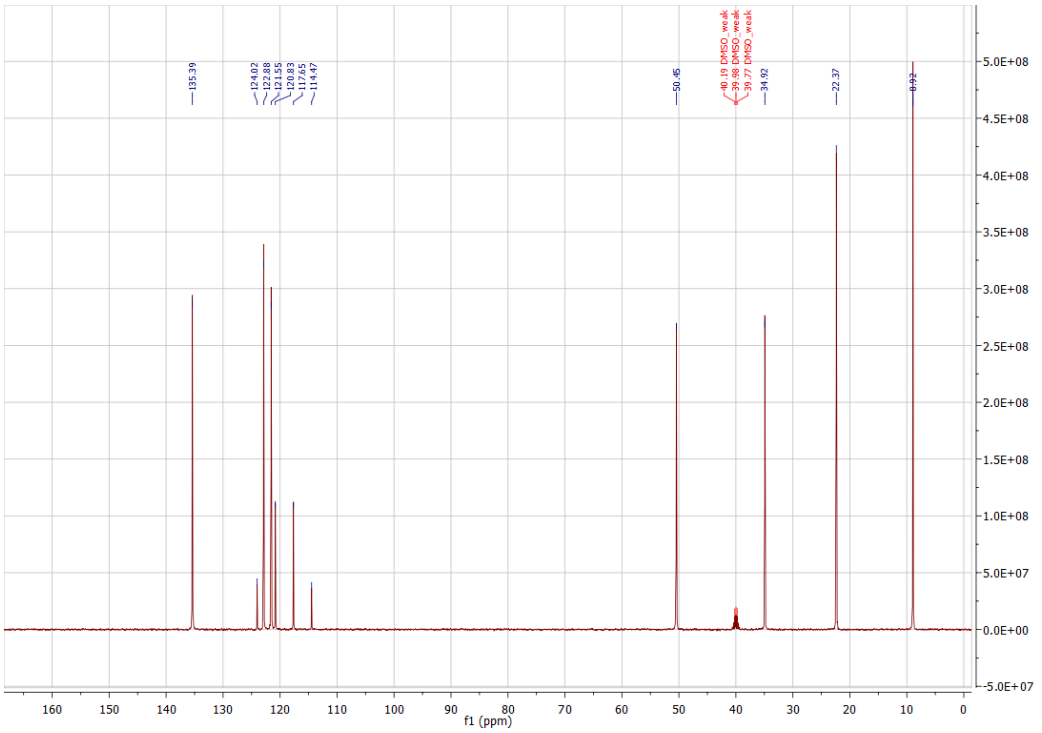

^{1}H NMR [C$_4$C$_1$im][NTf$_2$]

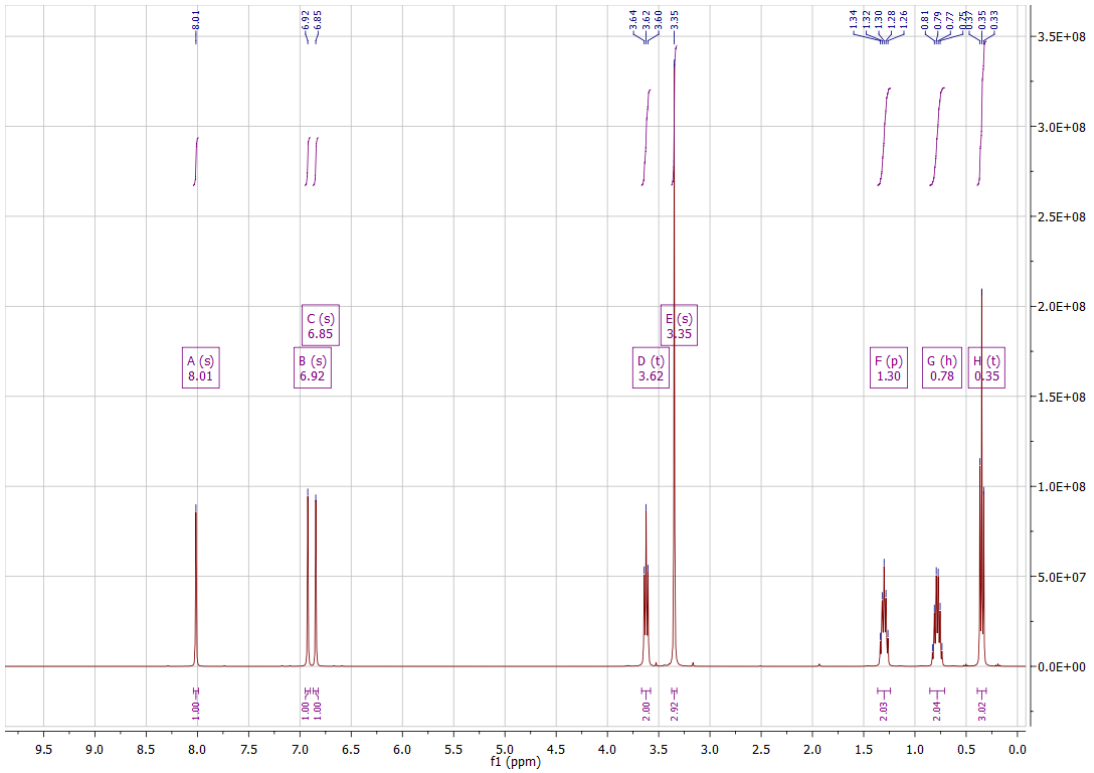

^{13}C [C$_4$C$_1$im][NTf$_2$]

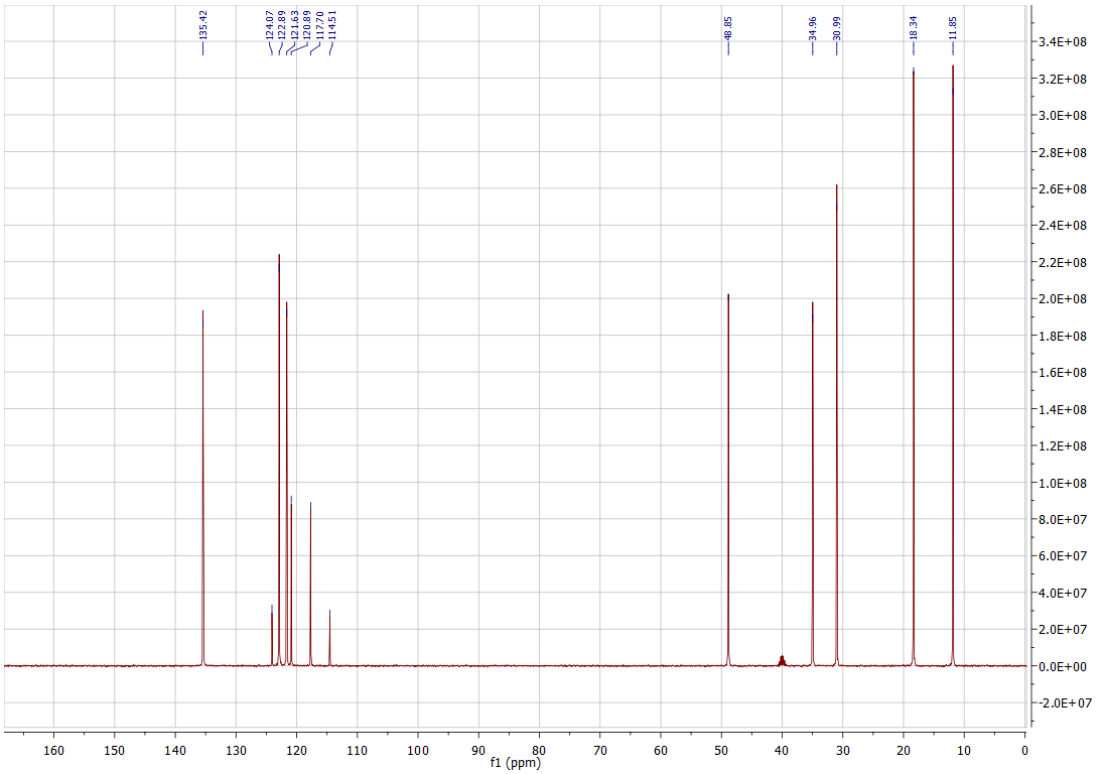

^{1}H NMR [C_6C_1im][NTf_2]

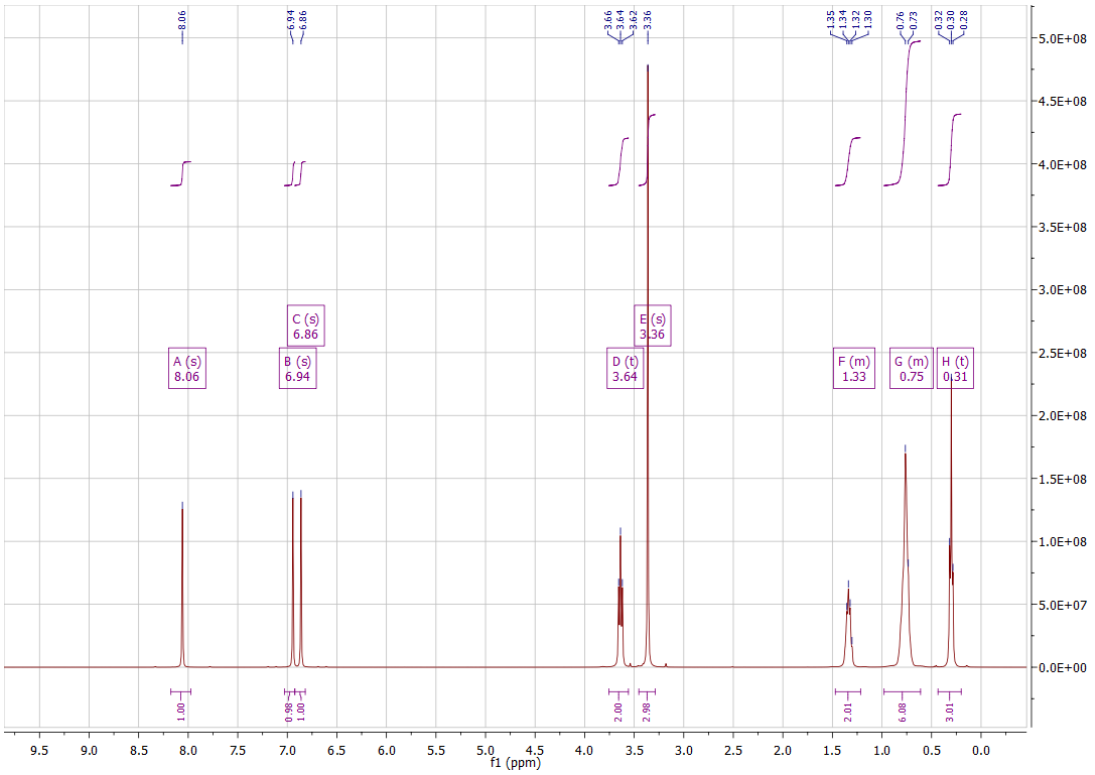

^{13}C [C_6C_1im][NTf_2]

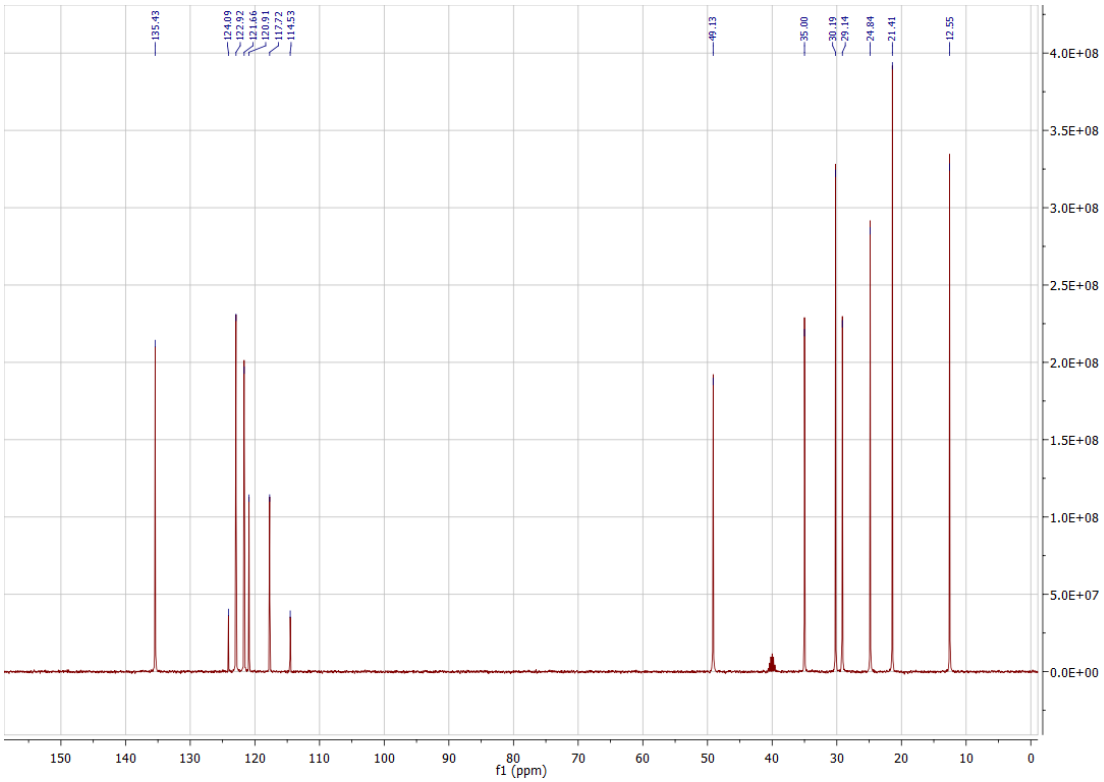

^{1}H NMR [C$_8$C$_1$im][NTf$_2$]

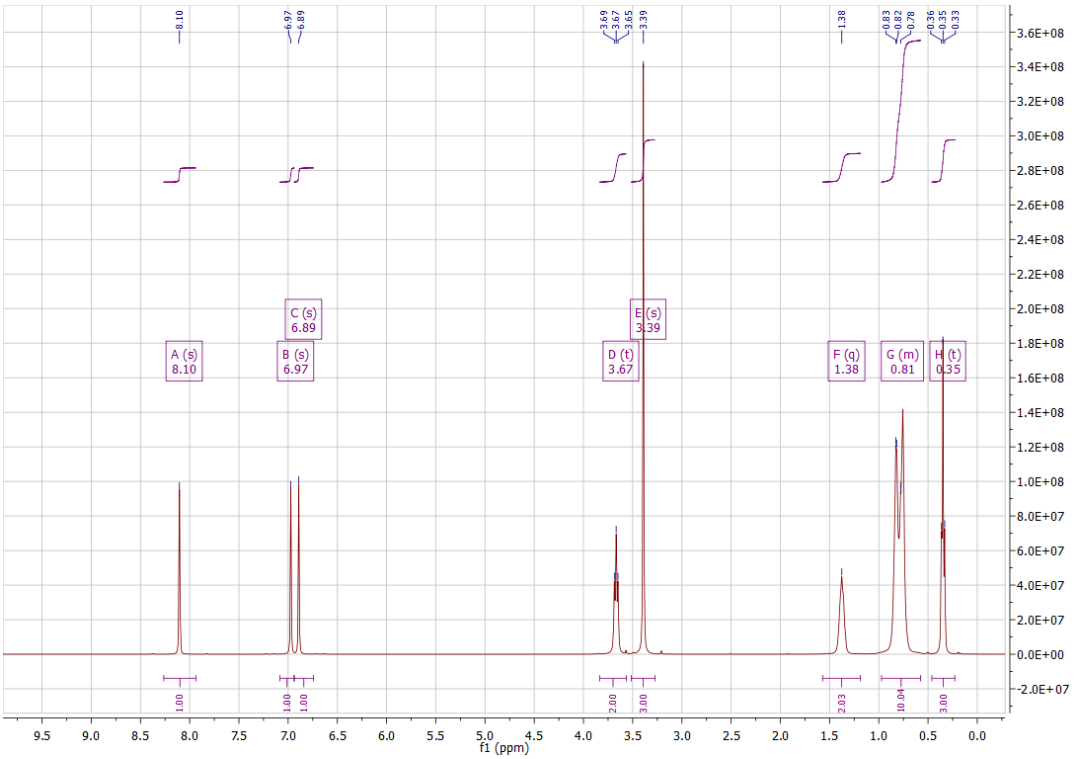

^{13}C [C$_8$C$_1$im][NTf$_2$]

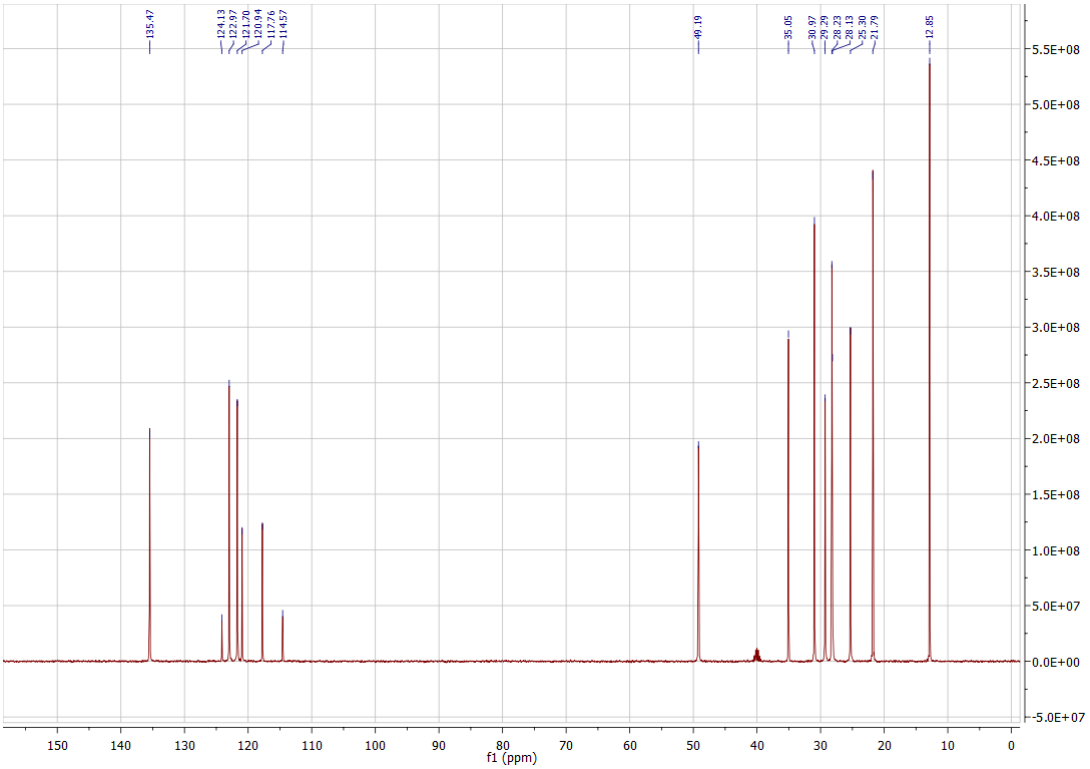

^{1}H NMR [$C_{12}C_{1}$im][NTf_2]

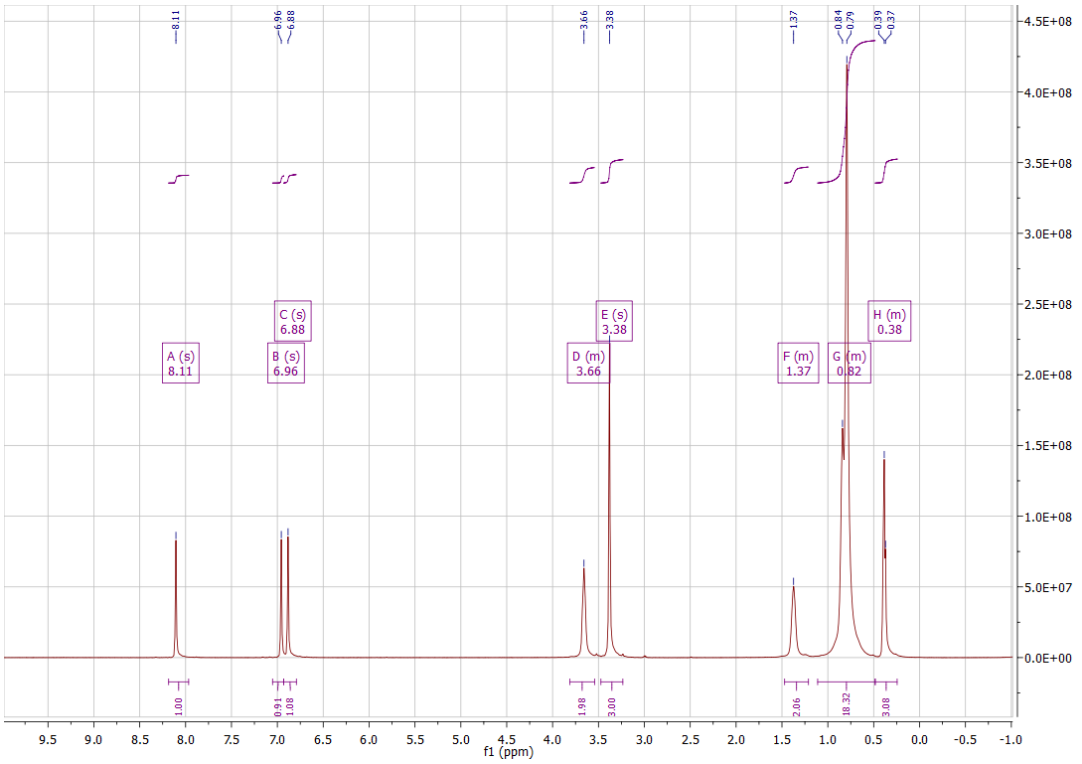

^{13}C [$C_{12}C_{1}$im][NTf_2]

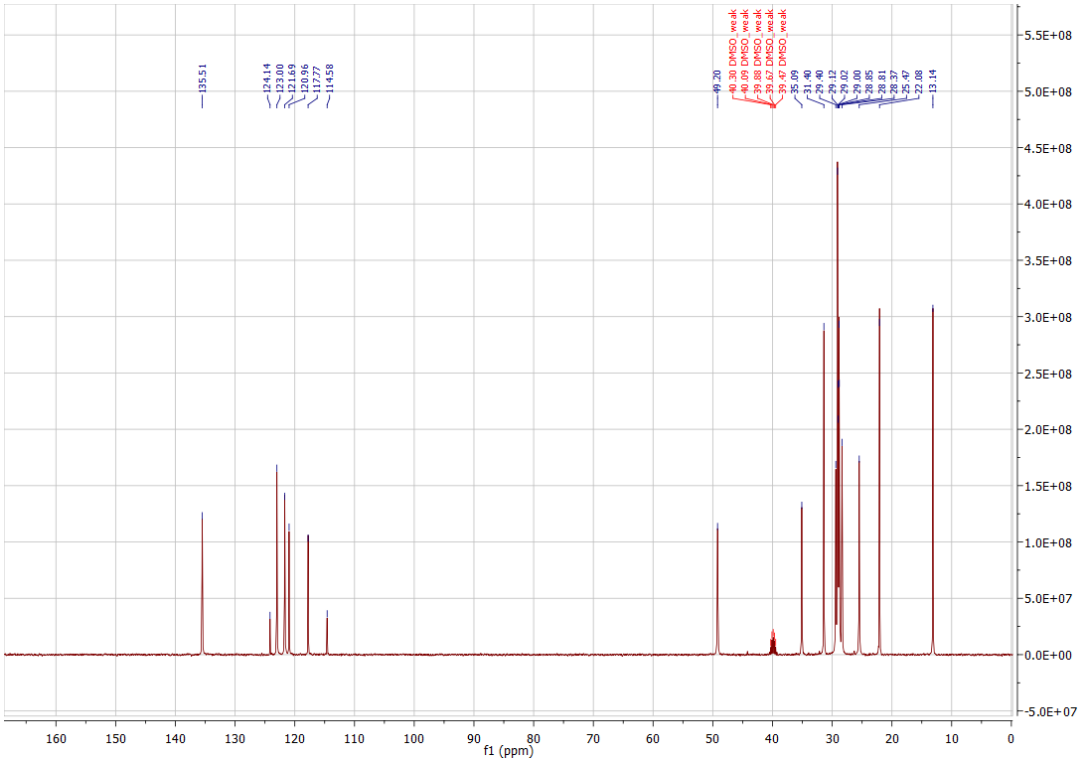

^{1}H NMR [C$_4$C$_1$pyrr][NTf$_2$]

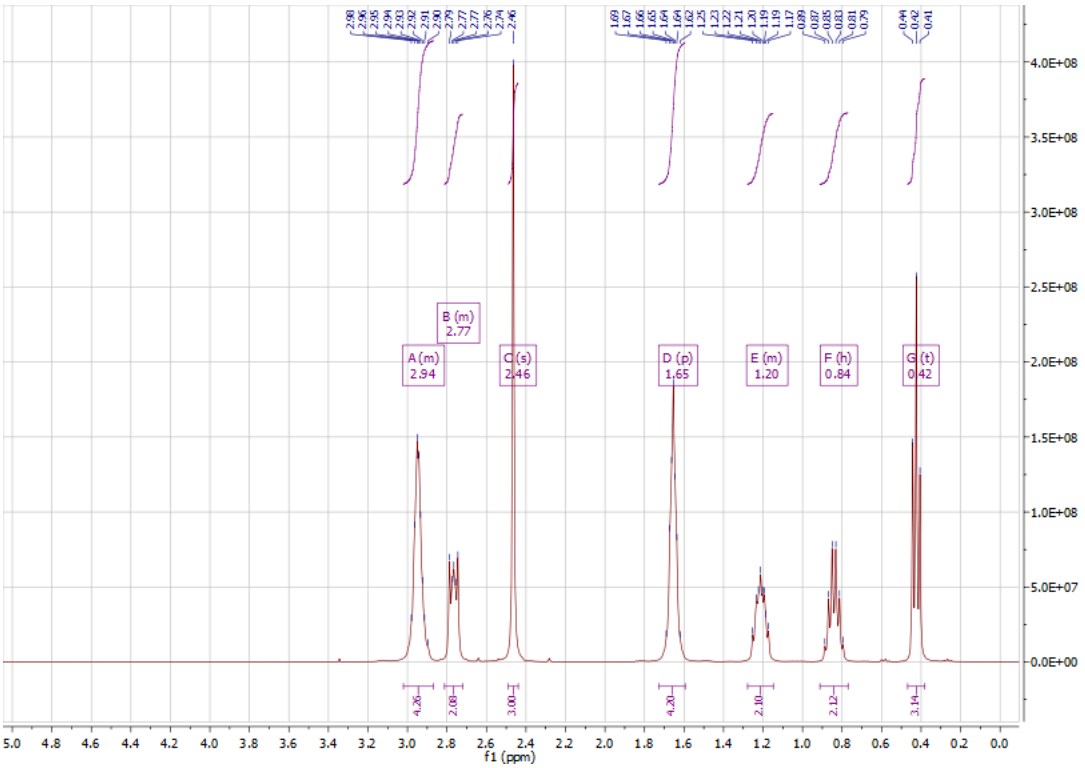

^{13}C NMR [C$_4$C$_1$pyrr][NTf$_2$]

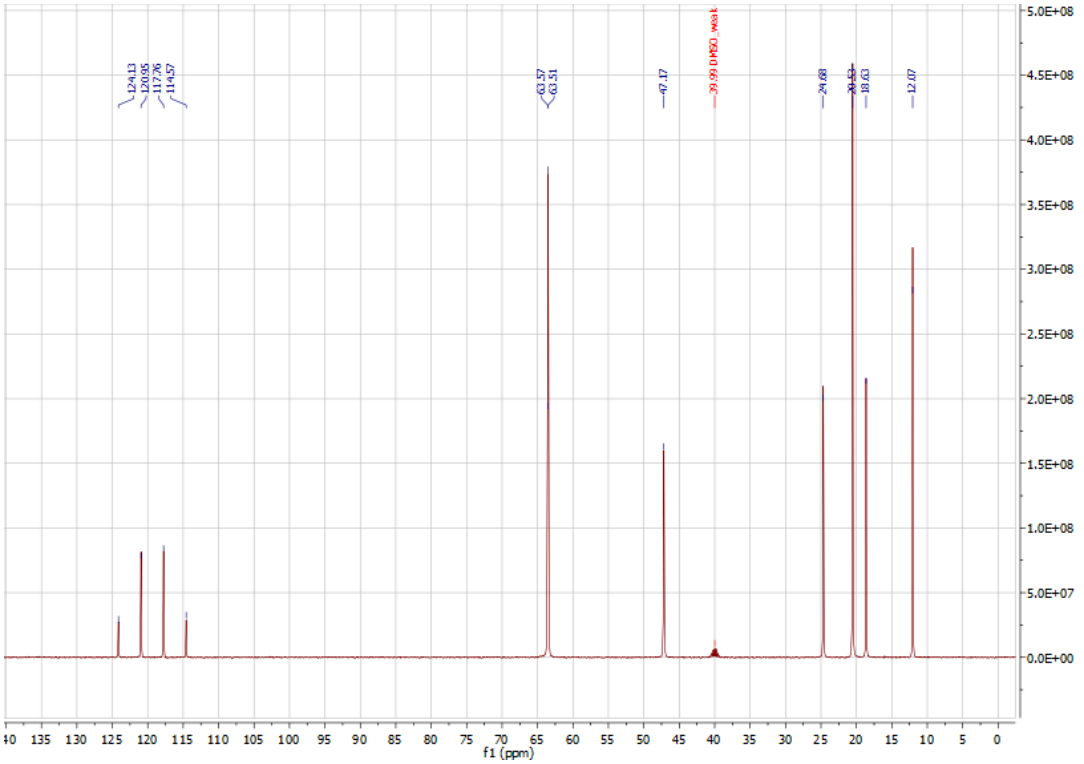

^{1}H NMR [P_{4446}][NTf_2]

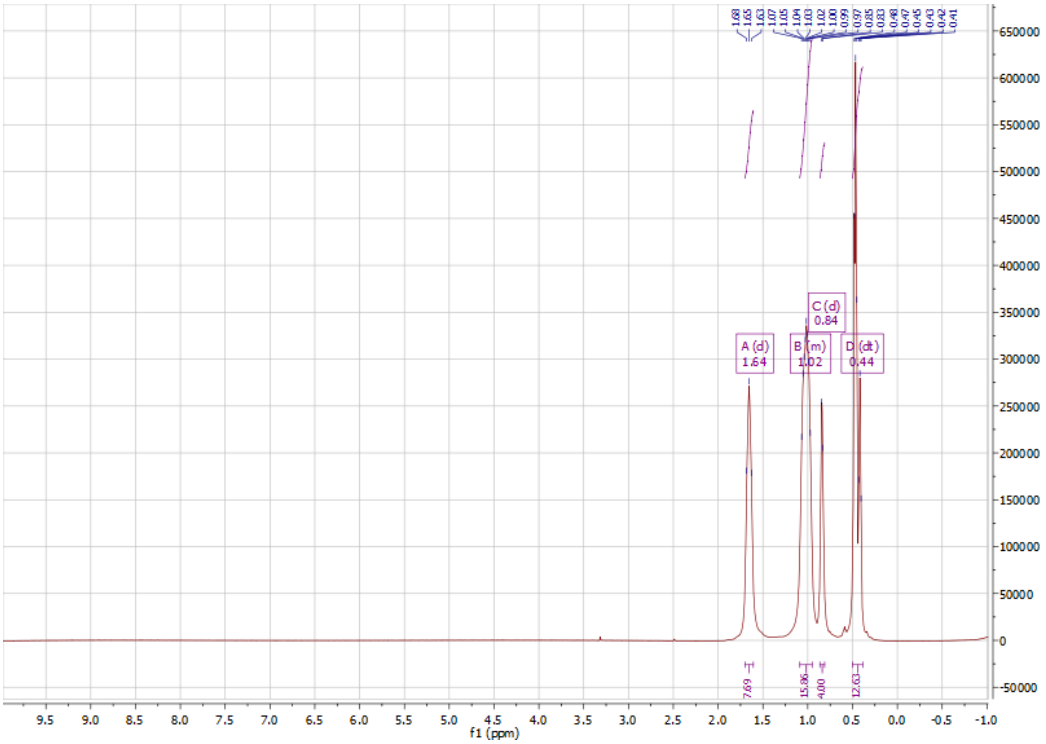

^{13}C NMR [P_{4446}][NTf_2]

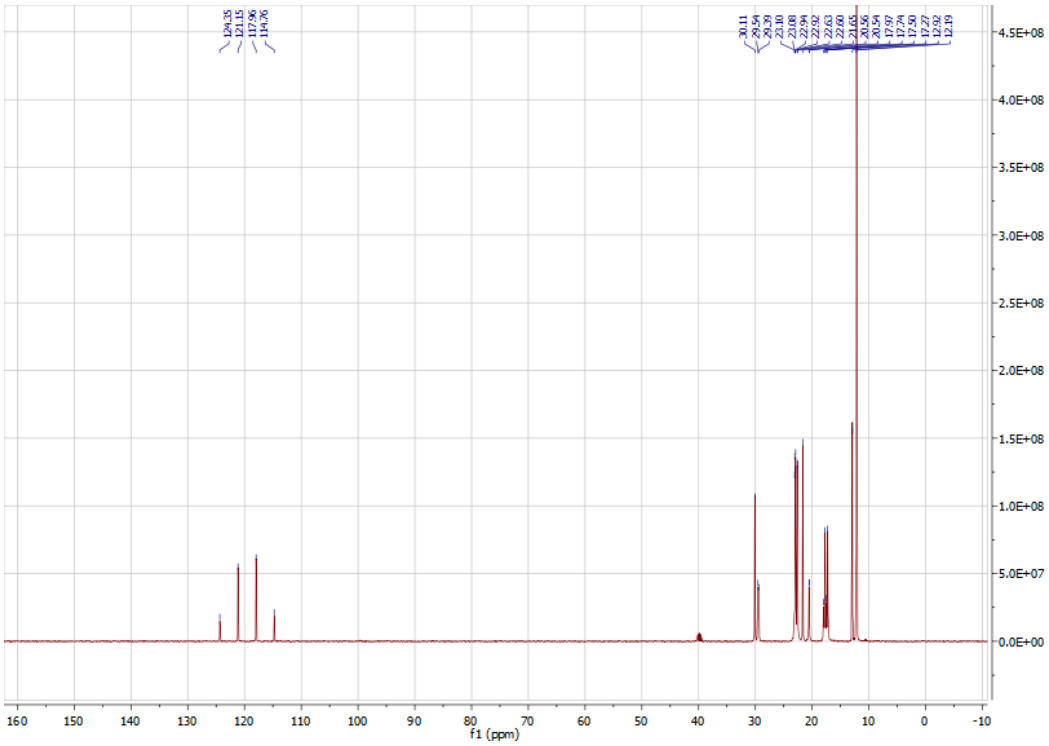

^{1}H NMR [C$_4$C$_1$im][BF$_4$]

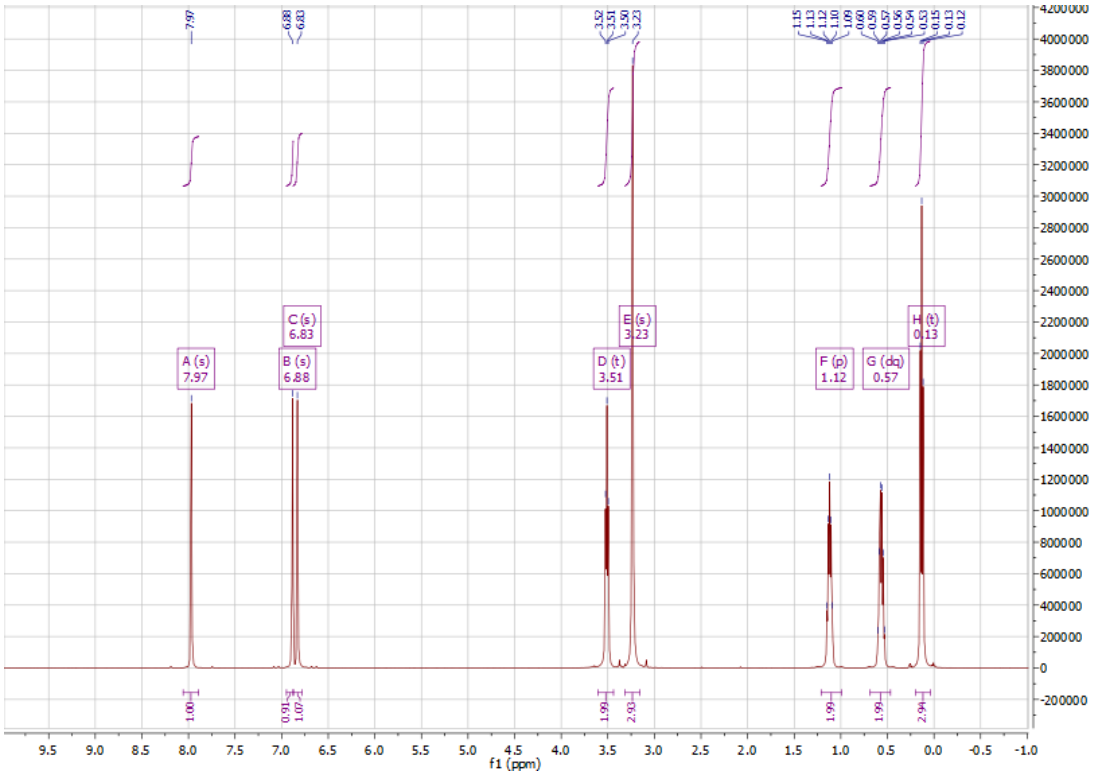

^{13}C NMR [C$_4$C$_1$im][BF$_4$]

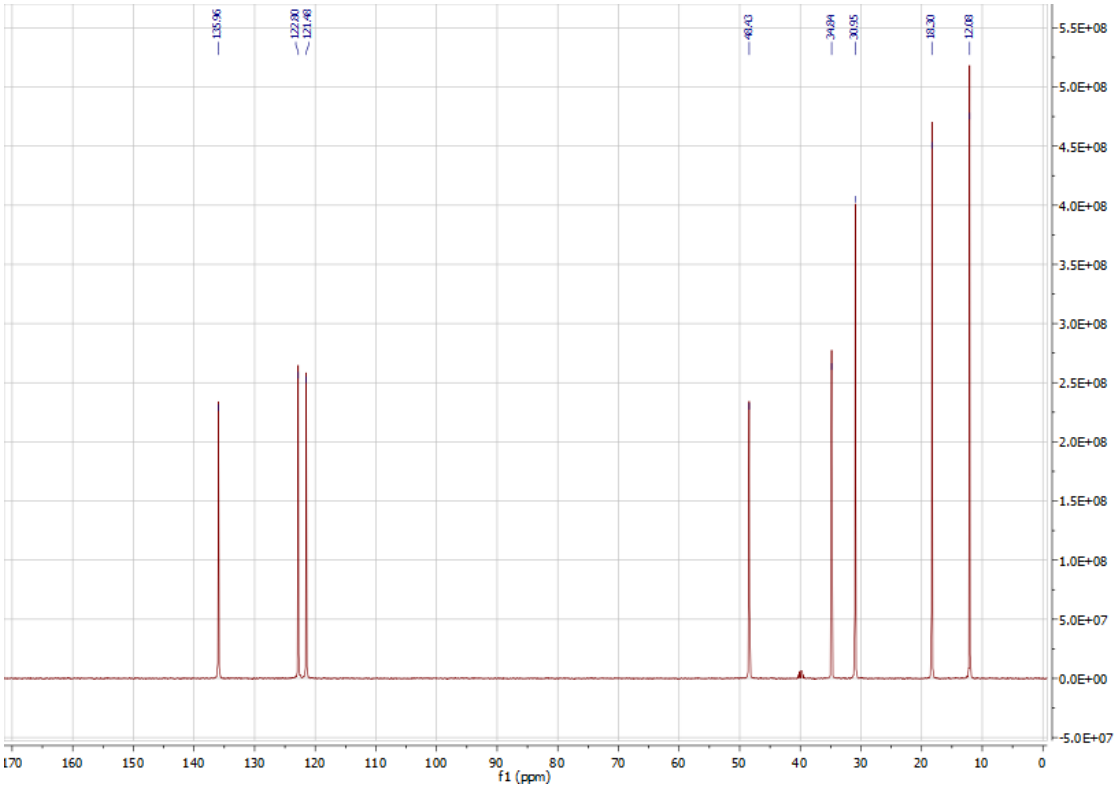

^{1}H NMR [C$_4$C$_1$im][PF$_6$]

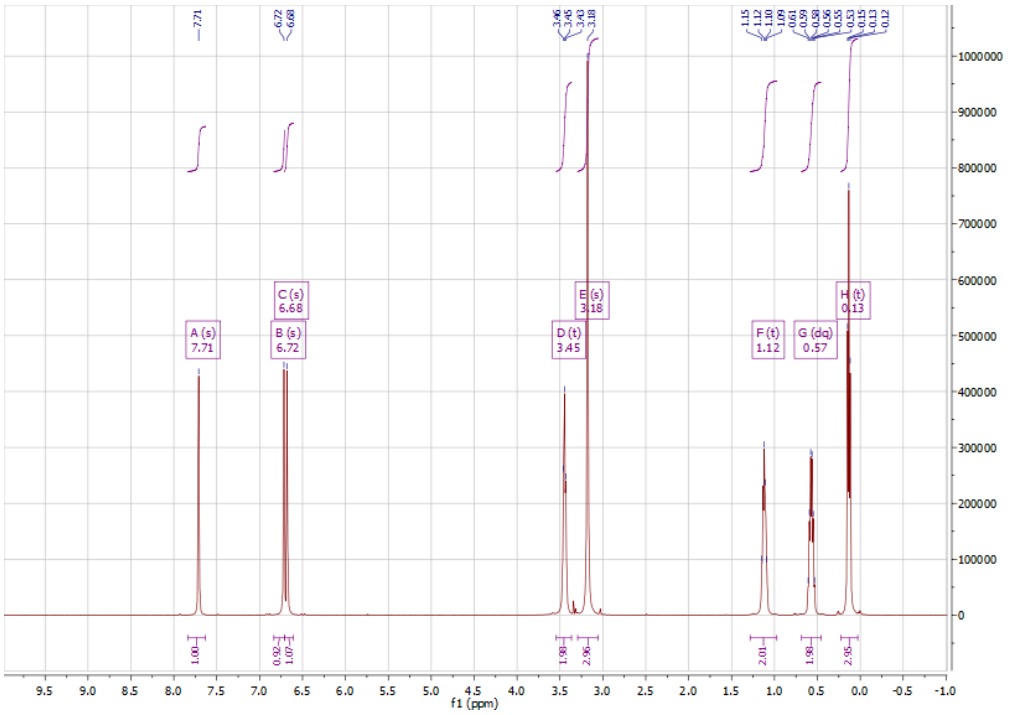

^{13}C NMR [C$_4$C$_1$im][PF$_6$]

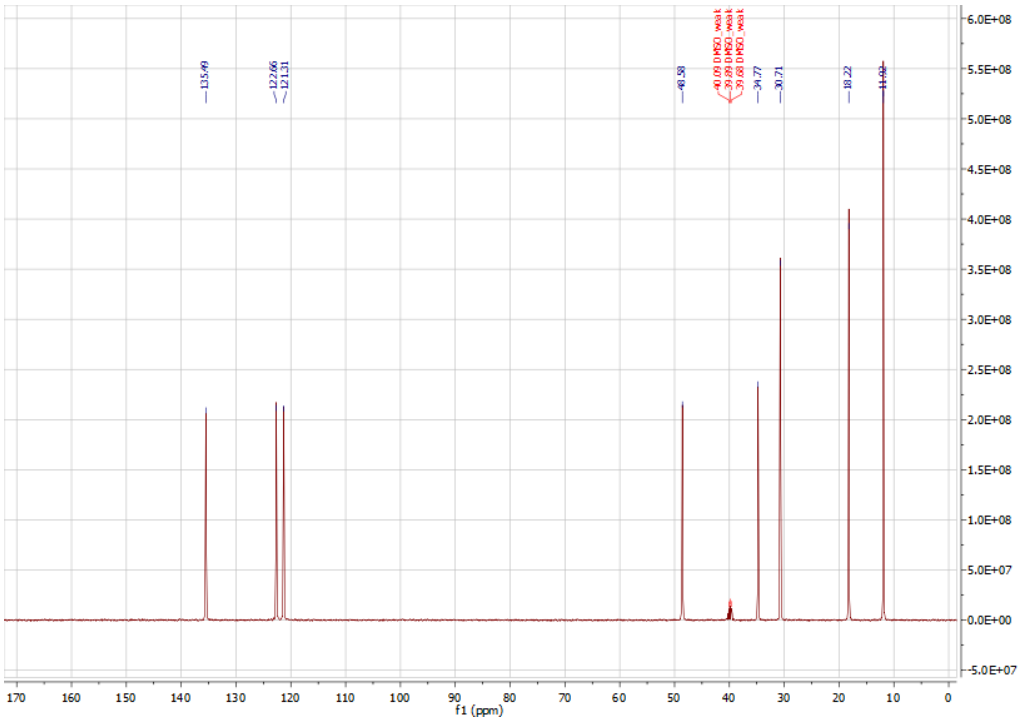

^{1}H NMR [C$_4$C$_1$im][CF$_3$SO$_3$]

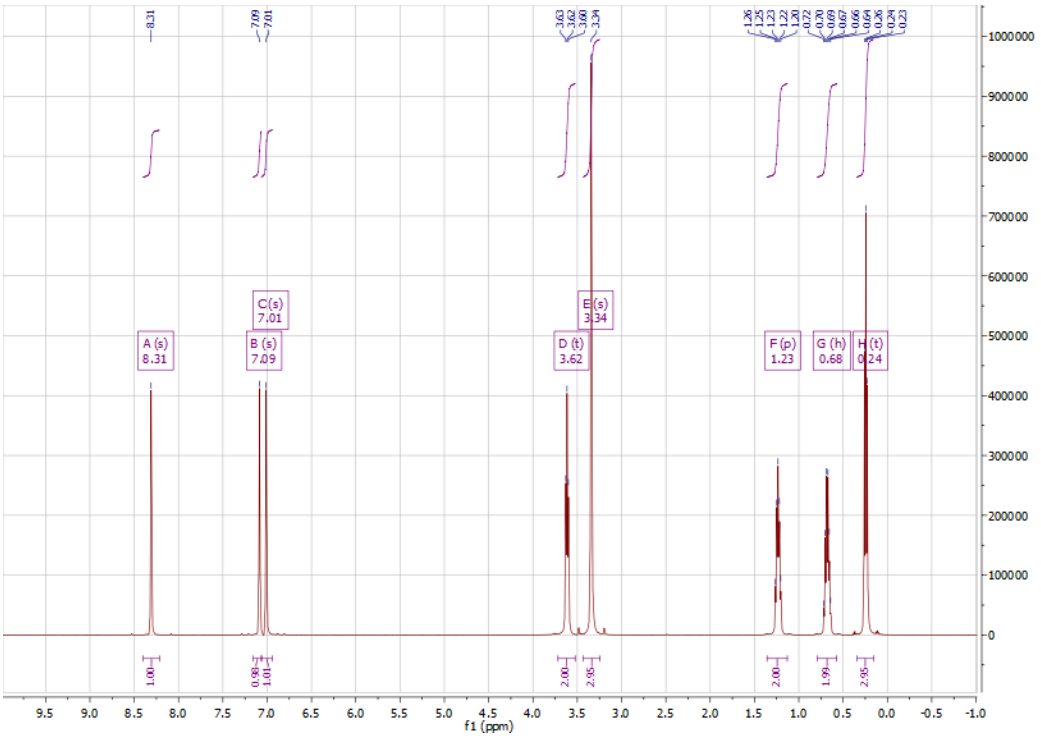

^{13}C NMR [C$_4$C$_1$im][CF$_3$SO$_3$]

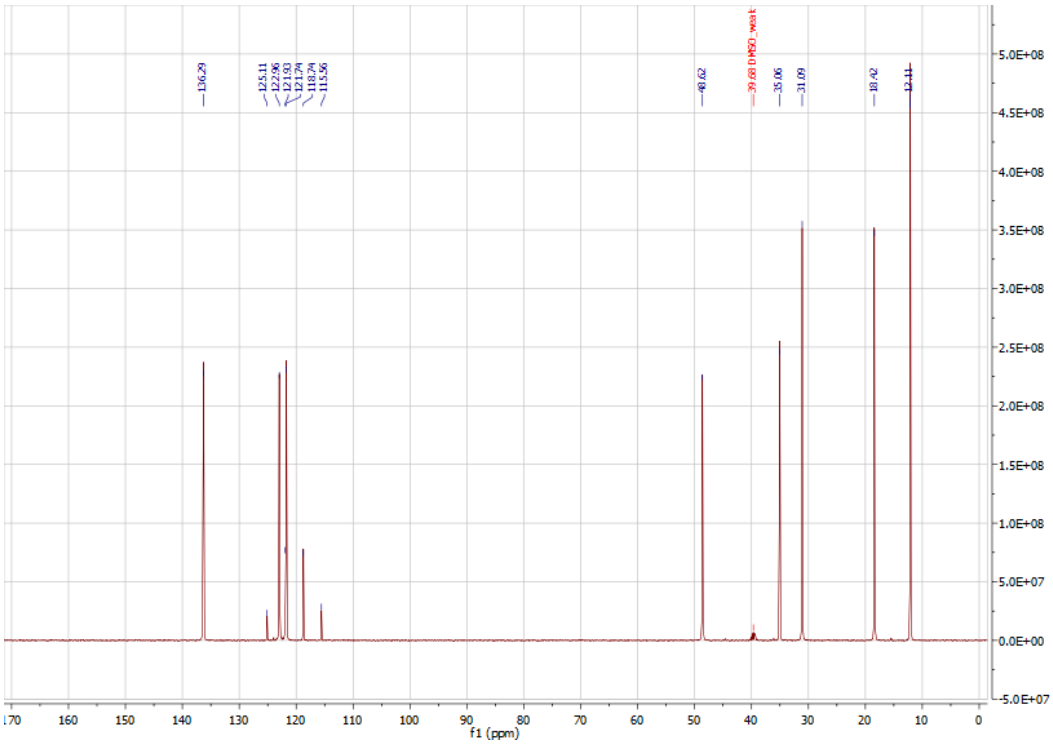

7.3 Mass spectra

Mass spectra of $[C_2C_1im][NTf_2]$

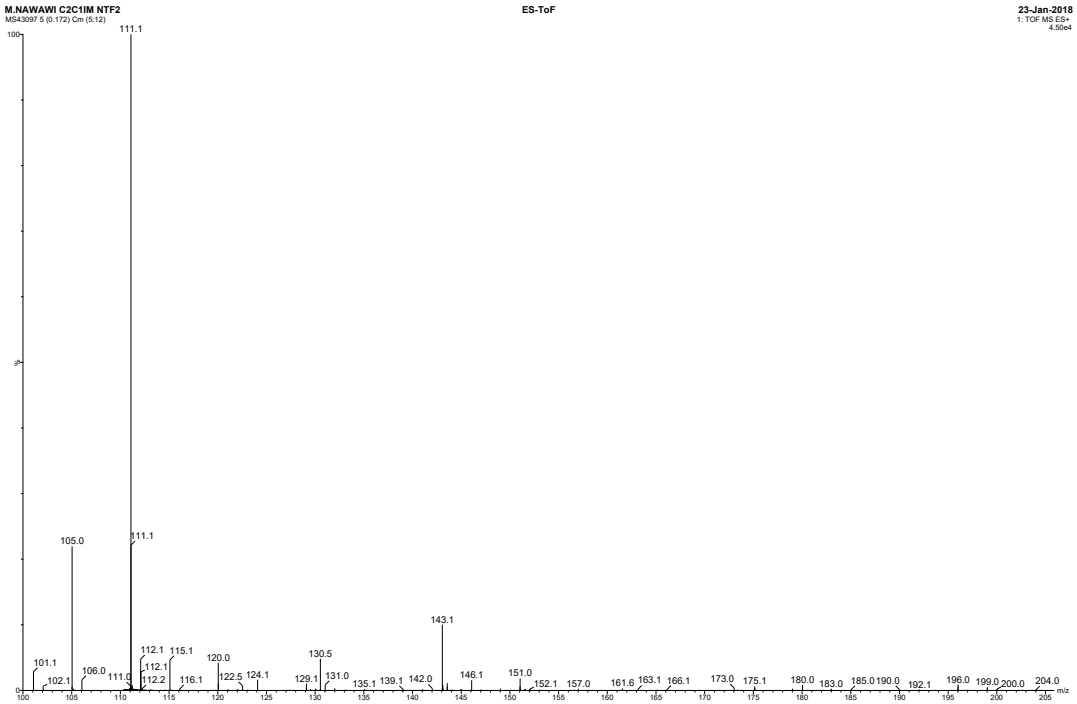

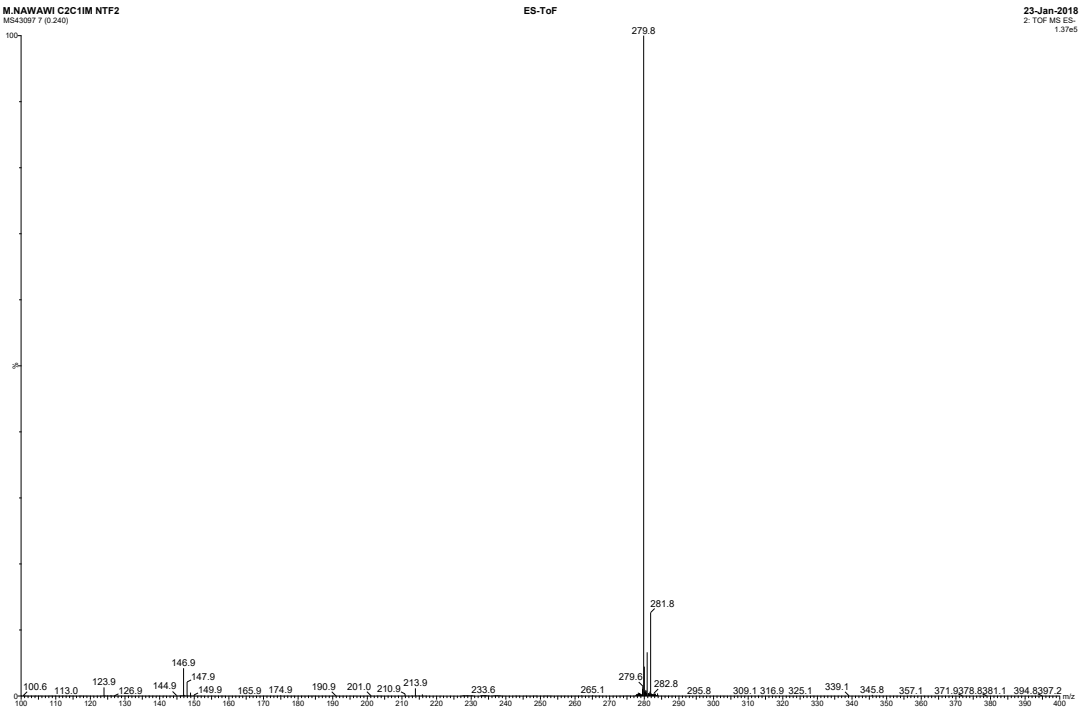

Mass spectra of $[C_3C_1im][NTf_2]$

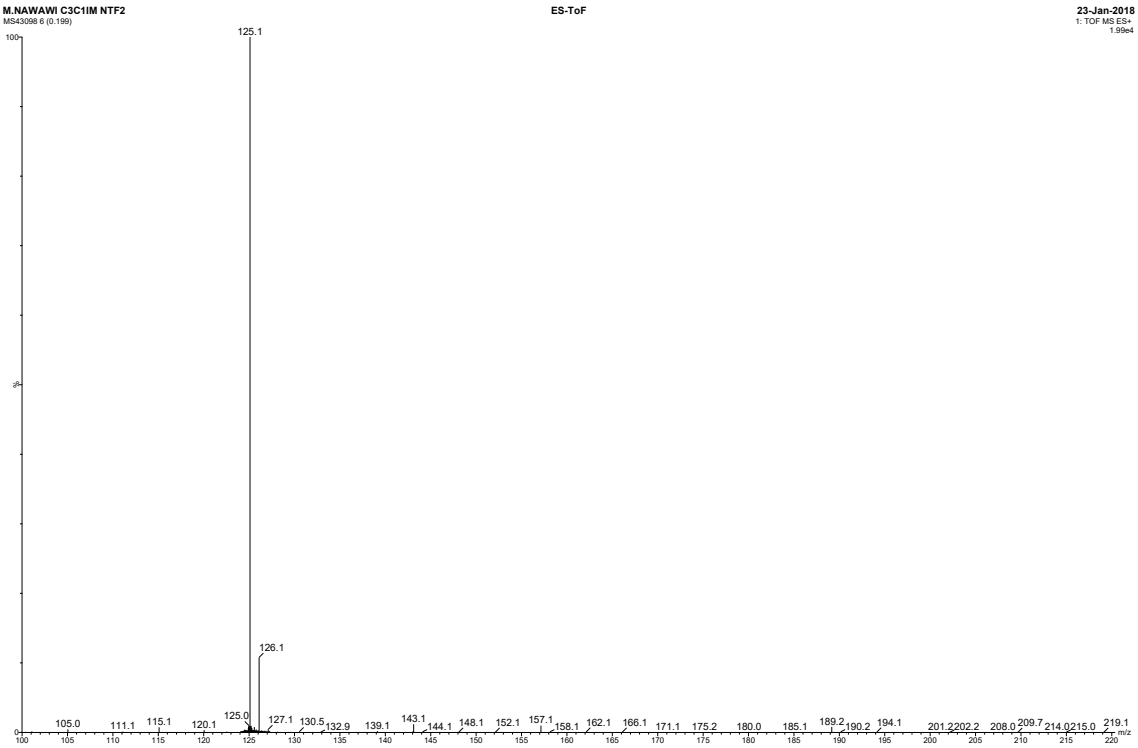

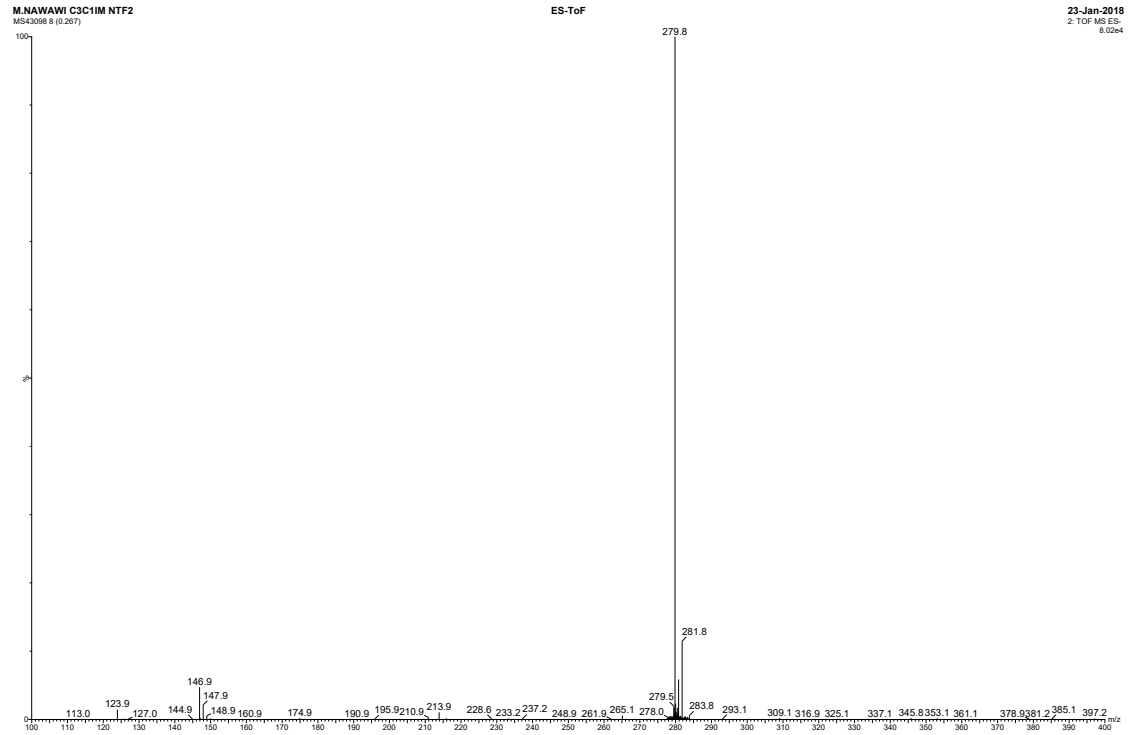

Mass spectra of $[C_4C_1im][NTf_2]$

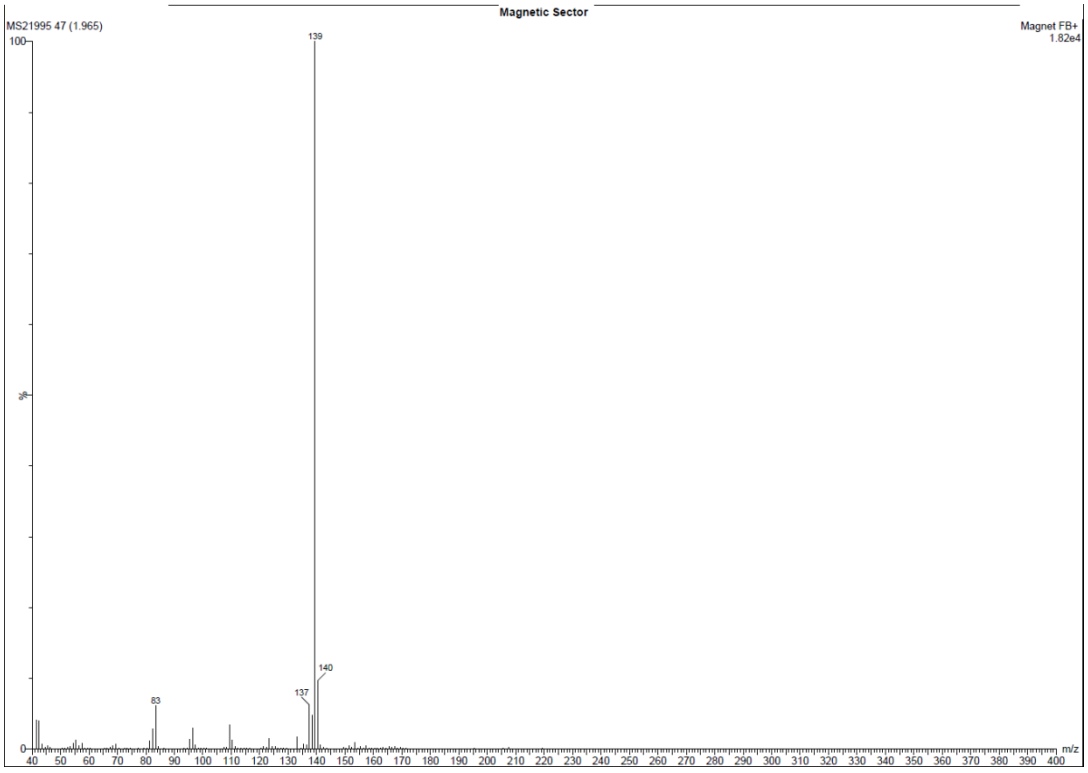

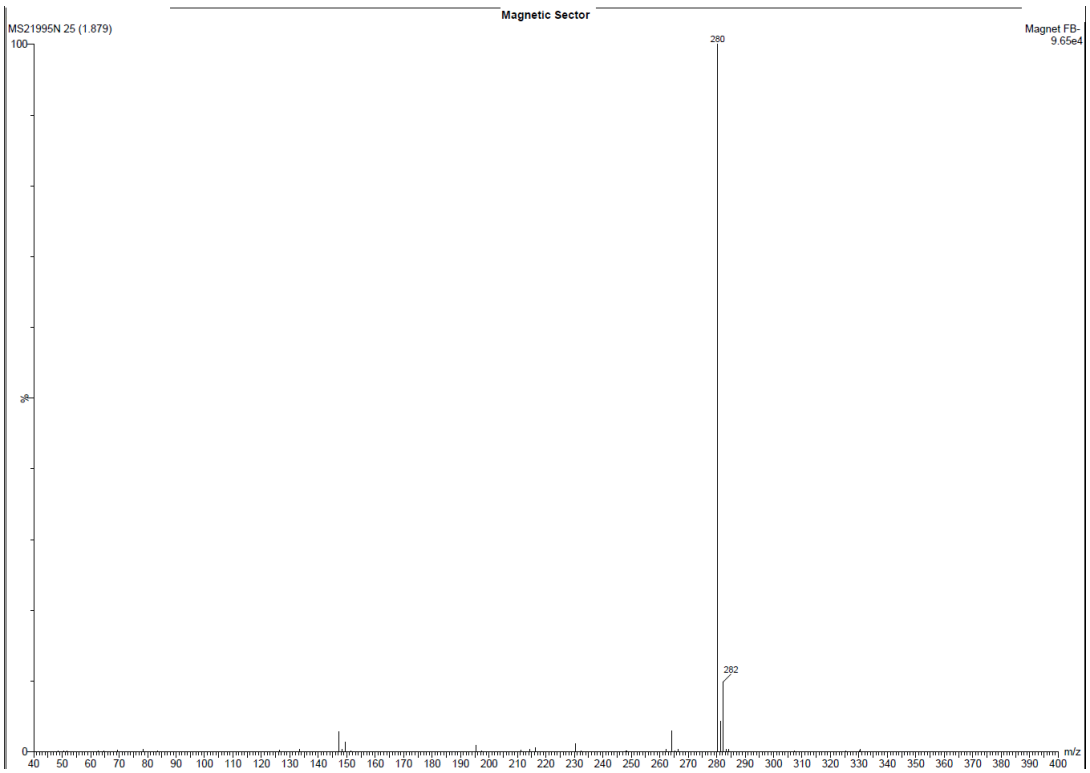

Mass spectra of $[C_6C_1im][NTf_2]$

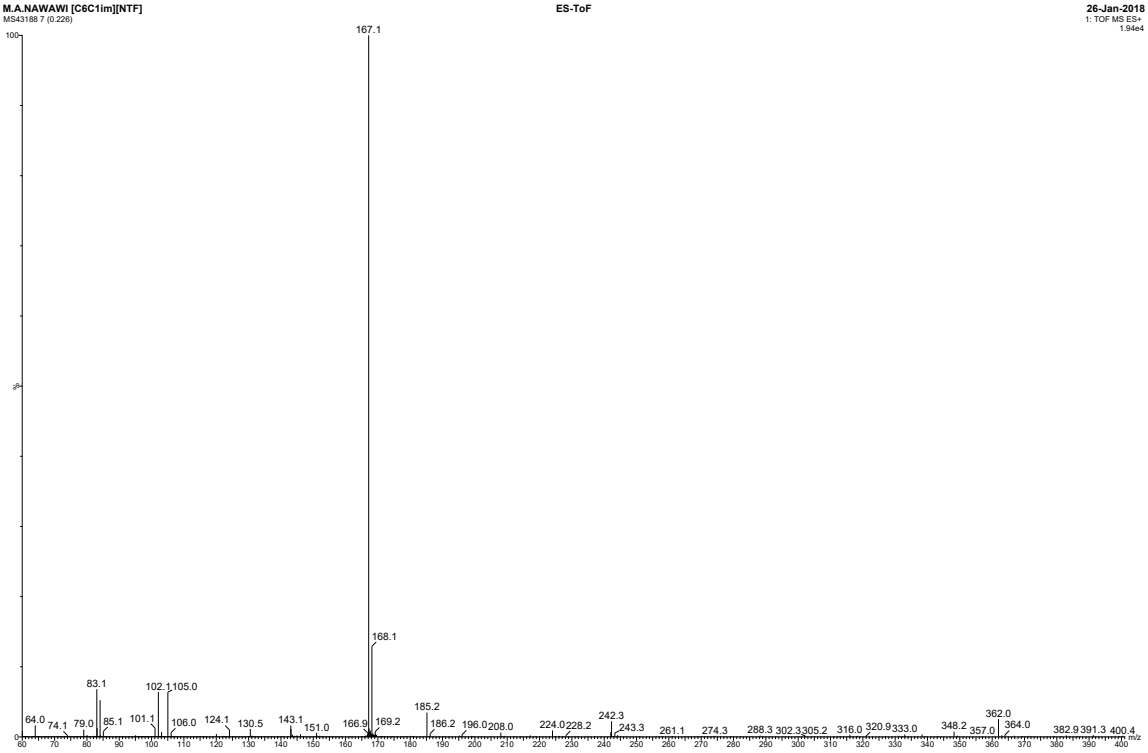

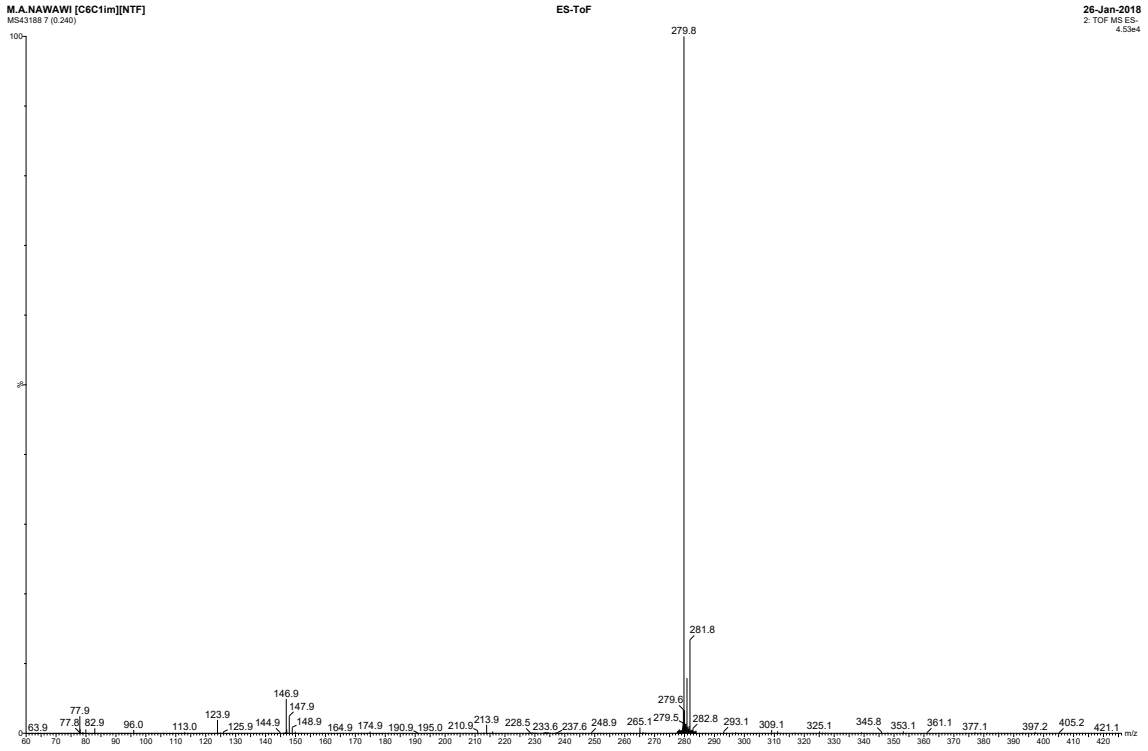

Mass spectra of $[C_8C_1im][NTf_2]$

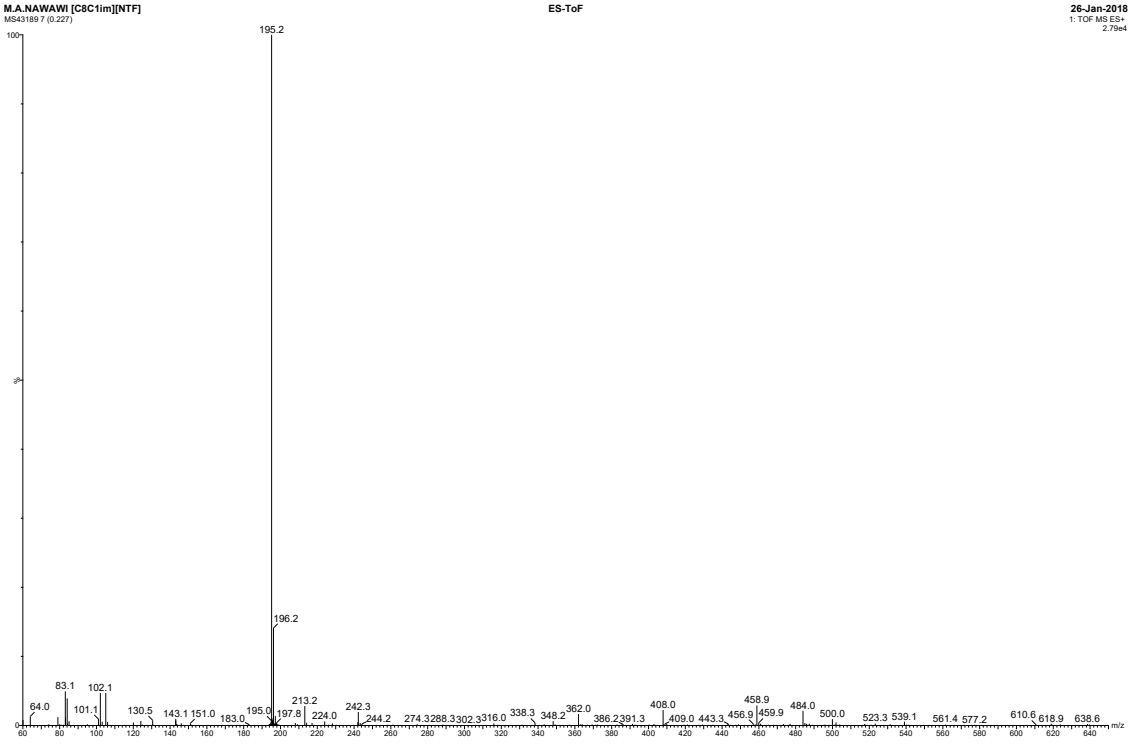

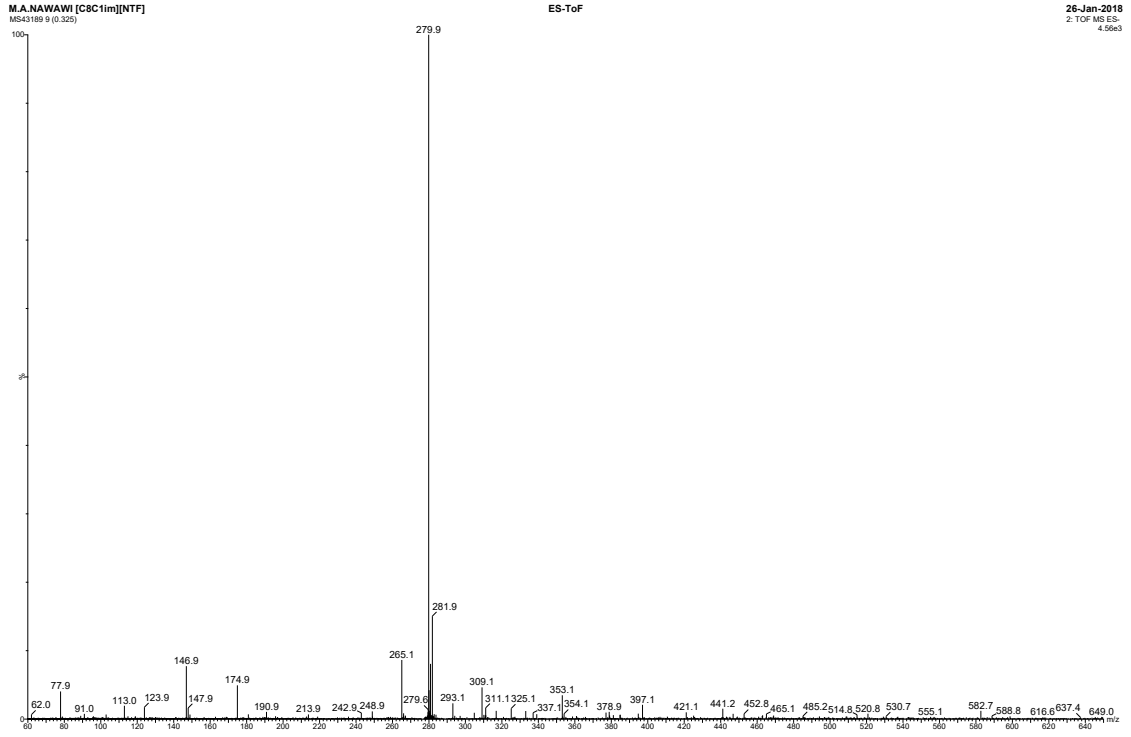

Mass spectra of $[C_{12}C_1im][NTf_2]$

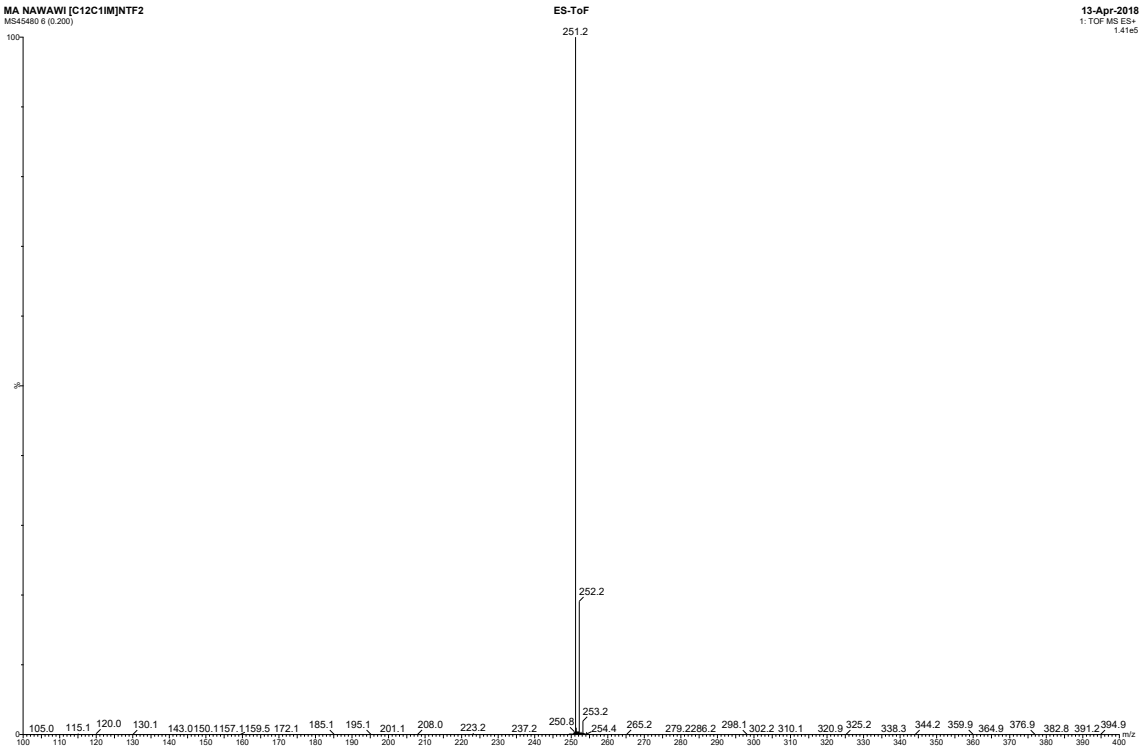

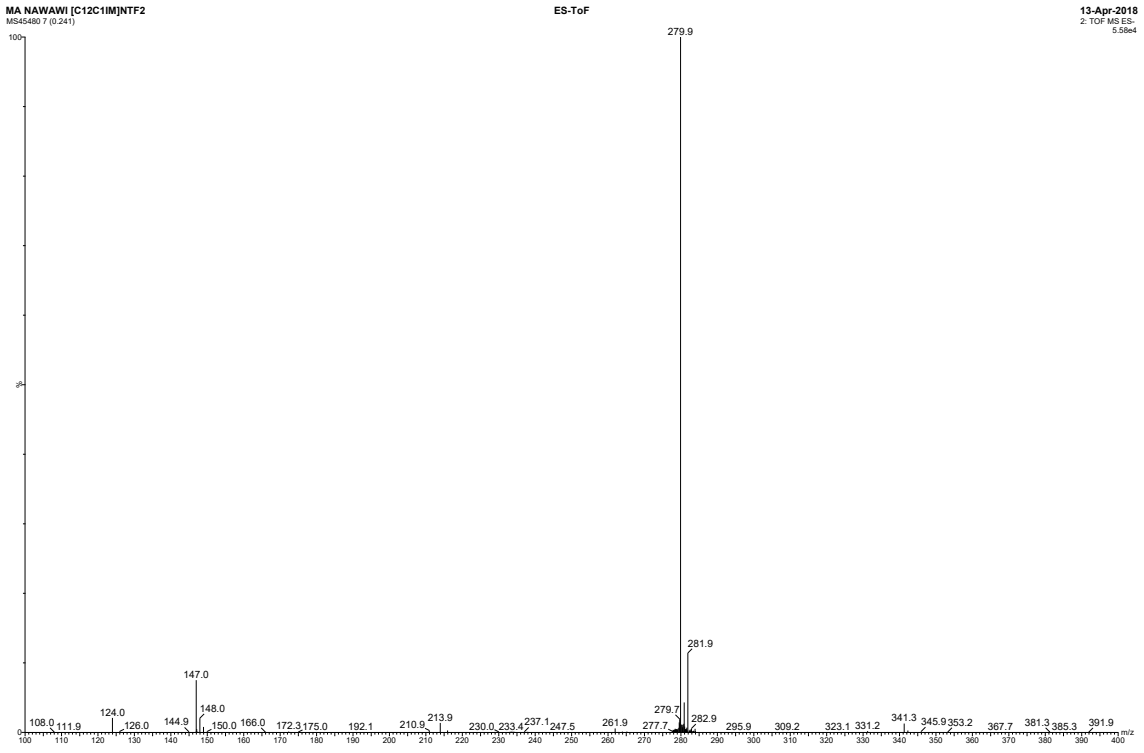

7.4 Decay curves of neat ionic liquids

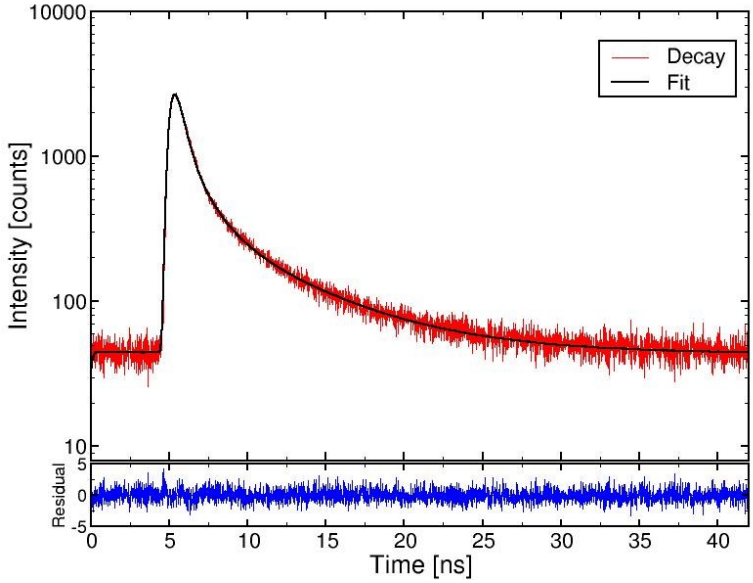

Raw decay data and 3 decay component fit for $[C_2C_1im][NTf_2]$. Bottom graph shows residual values at each point.

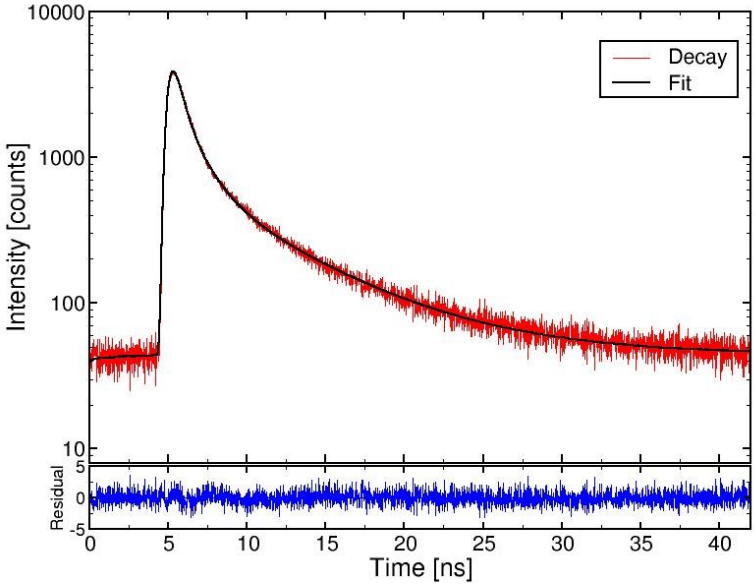

Raw decay data and 3 decay component fit for $[C_3C_1im][NTf_2]$. Bottom graph shows residual values at each point.

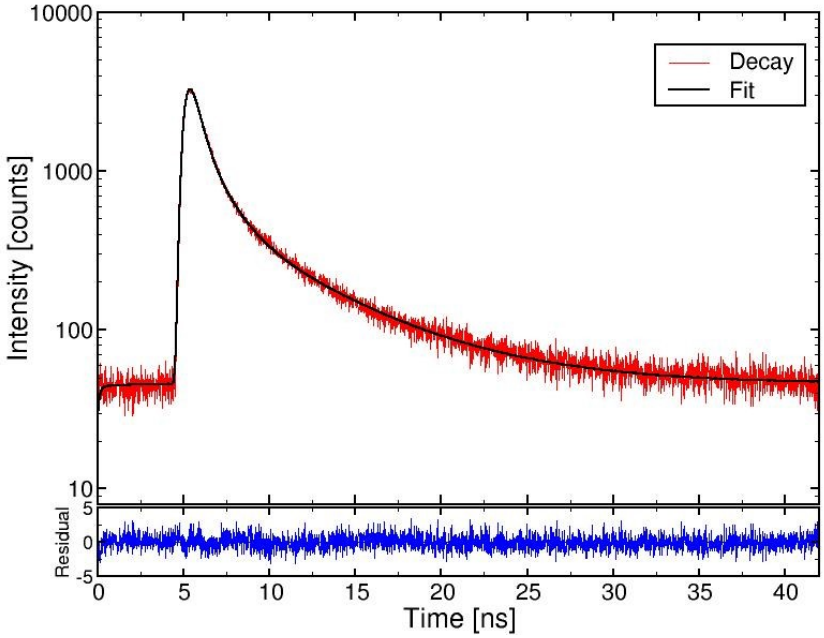

Raw decay data and 3 decay component fit for $[C_4C_1im][NTf_2]$. Bottom graph shows residual values at each point.

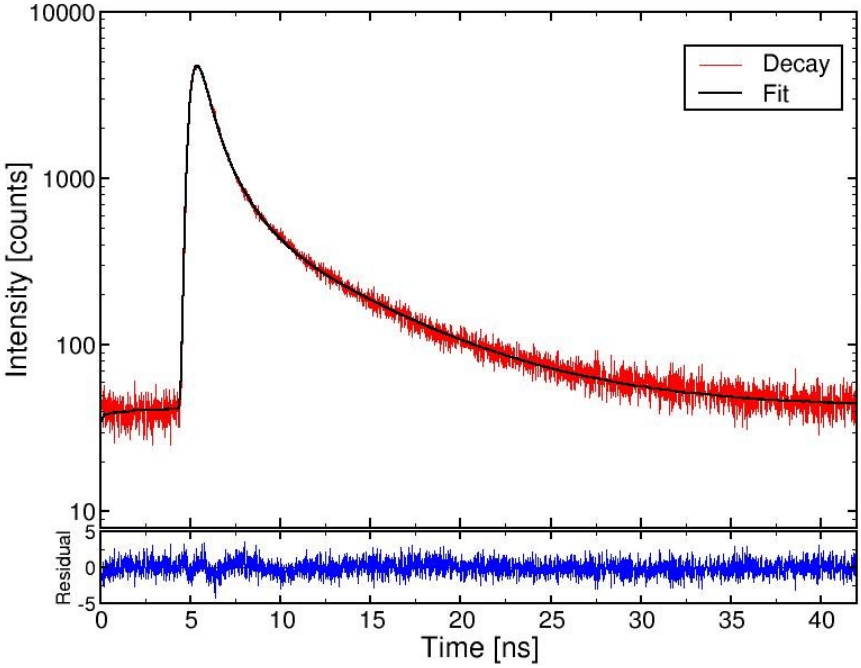

Raw decay data and 3 decay component fit for $[C_6C_1im][NTf_2]$. Bottom graph shows residual values at each point.

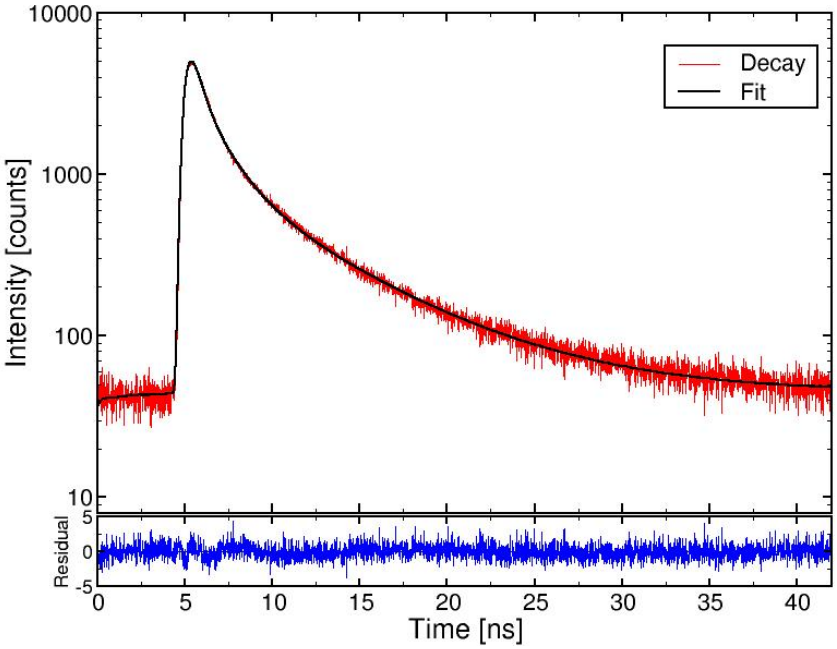

Raw decay data and 3 decay component fit for $[C_8C_1im][NTf_2]$. Bottom graph shows residual values at each point.

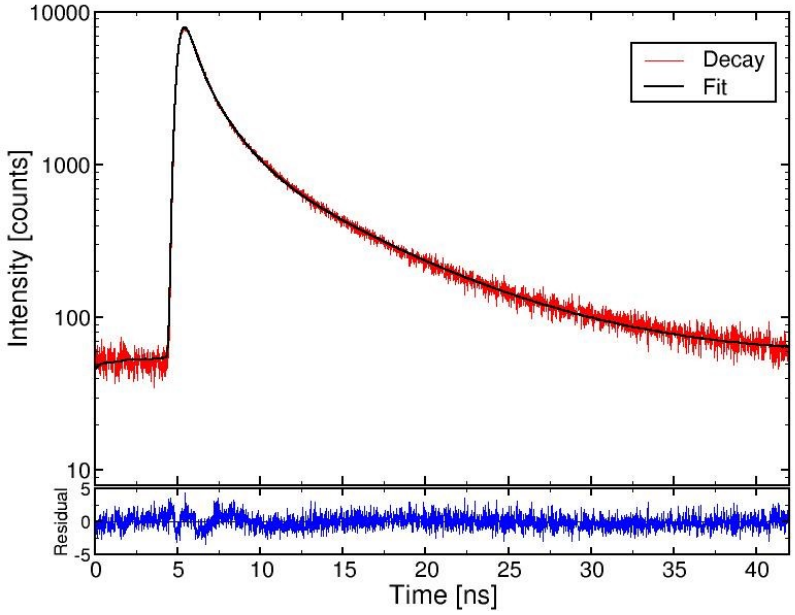

Raw decay data and 3 decay component fit for $[C_{12}C_1im][NTf_2]$. Bottom graph shows residual values at each point.

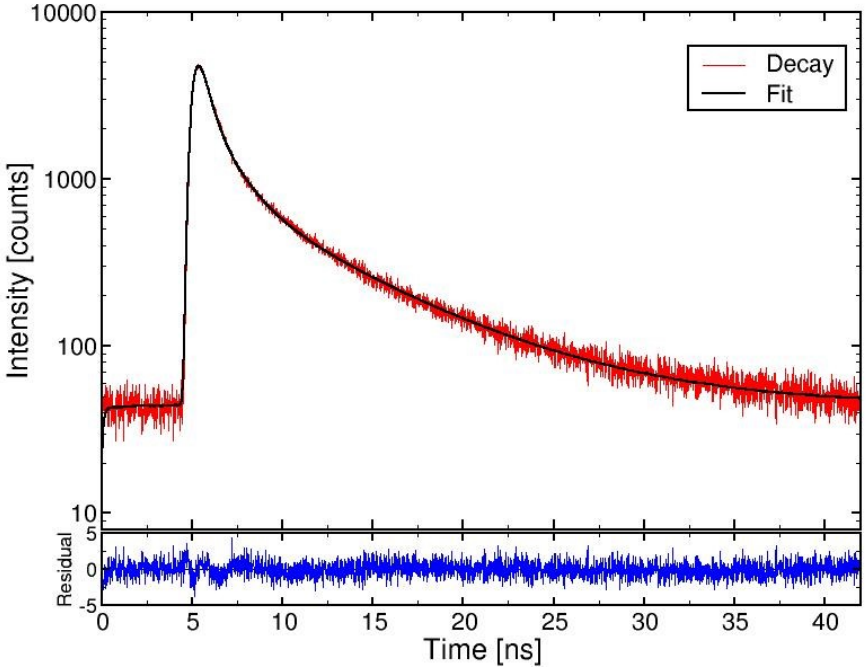

Raw decay data and 3 decay component fit for $[P_{4446}][NTf_2]$. Bottom graph shows residual values at each point.

7.5 Decay curves of 100nM Cy3 in ionic liquids

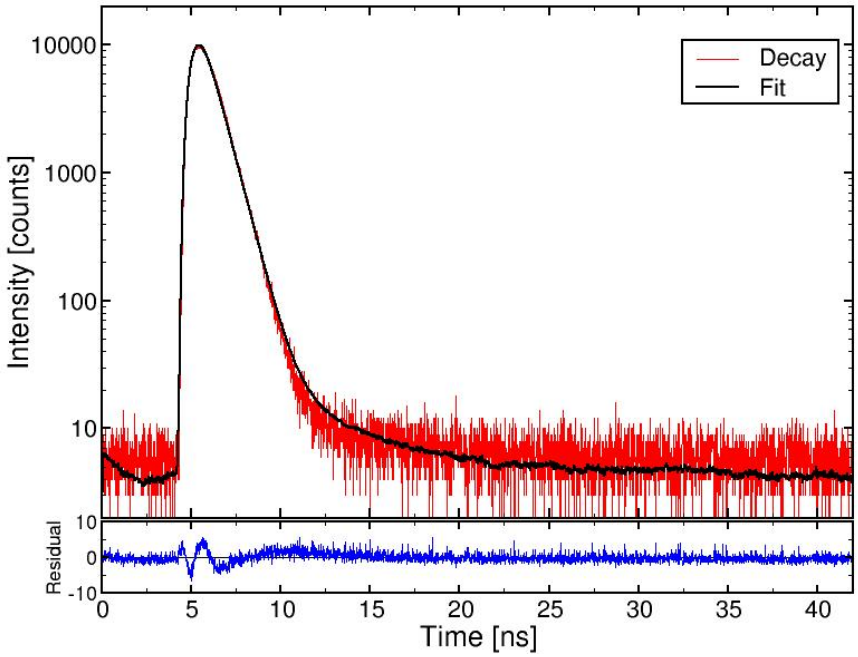

Raw decay data and 2 decay component fit for Cy3 in $[C_2C_1im][NTf_2]$. Bottom graph shows residual values at each point.

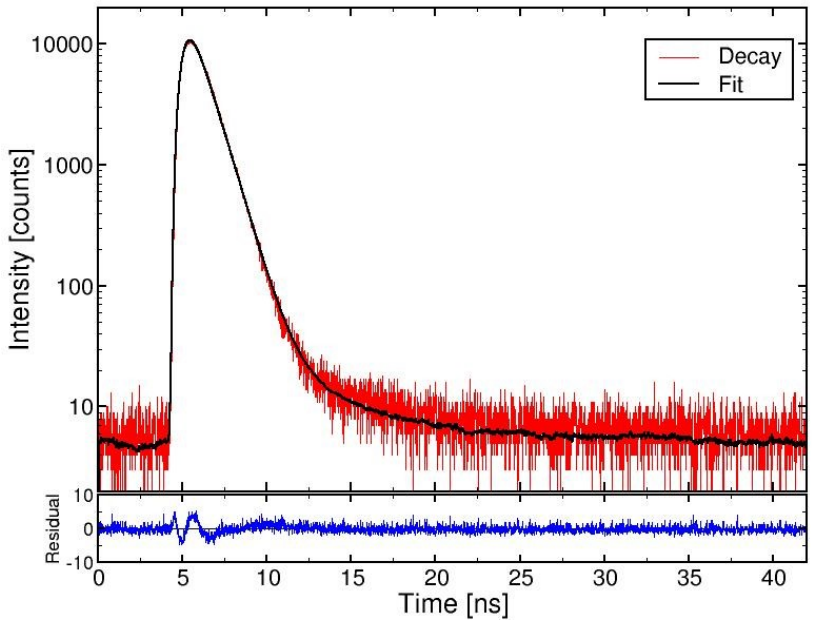

Raw decay data and 2 decay component fit for Cy3 in $[C_3C_1im][NTf_2]$. Bottom graph shows residual values at each point.

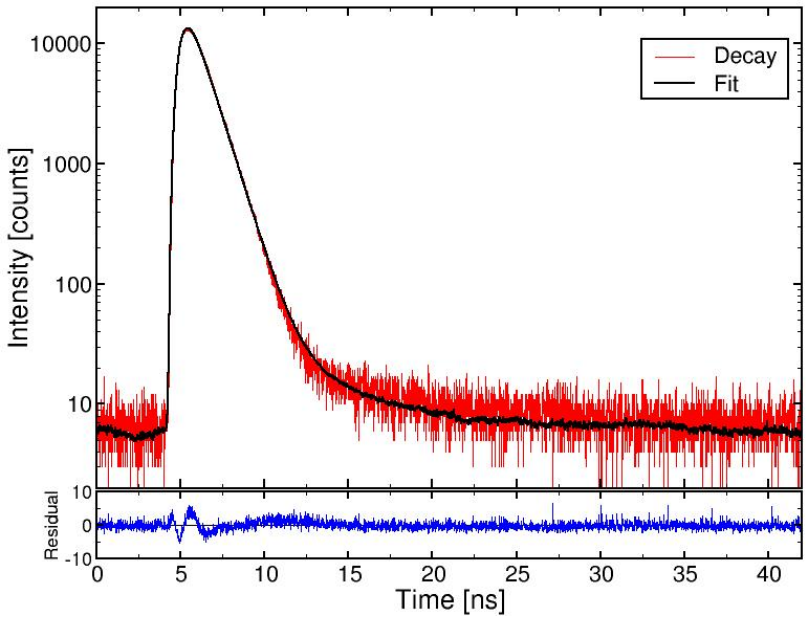

Raw decay data and 2 decay component fit for Cy3 in $[C_4C_1im][NTf_2]$. Bottom graph shows residual values at each point.

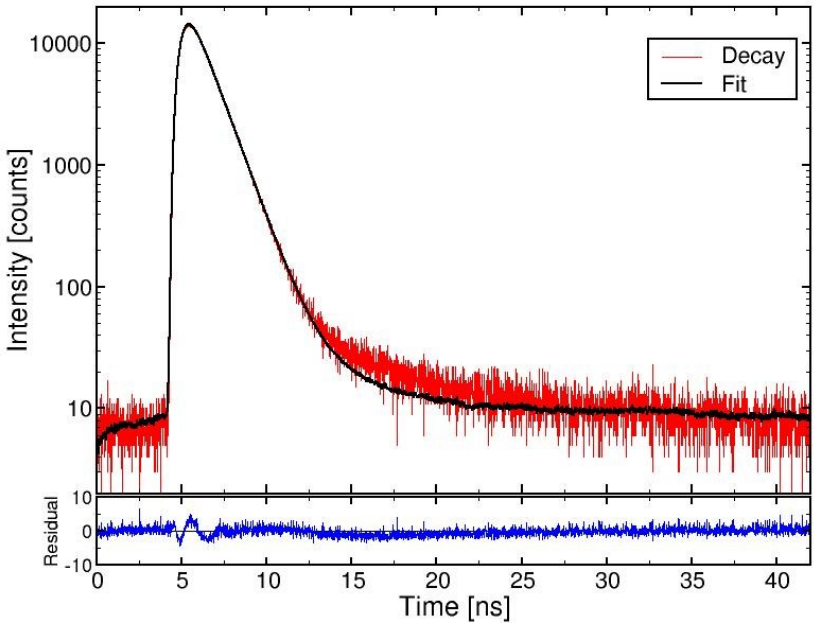

Raw decay data and 2 decay component fit for Cy3 in $[C_6C_1im][NTf_2]$. Bottom graph shows residual values at each point.

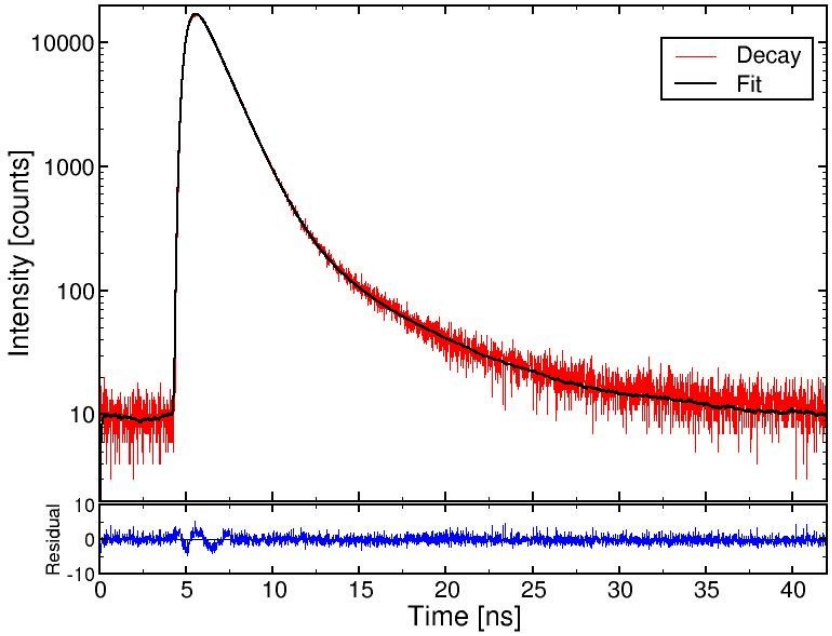

Raw decay data and 3 decay component fit for Cy3 in $[C_8C_1im][NTf_2]$. Bottom graph shows residual values at each point.

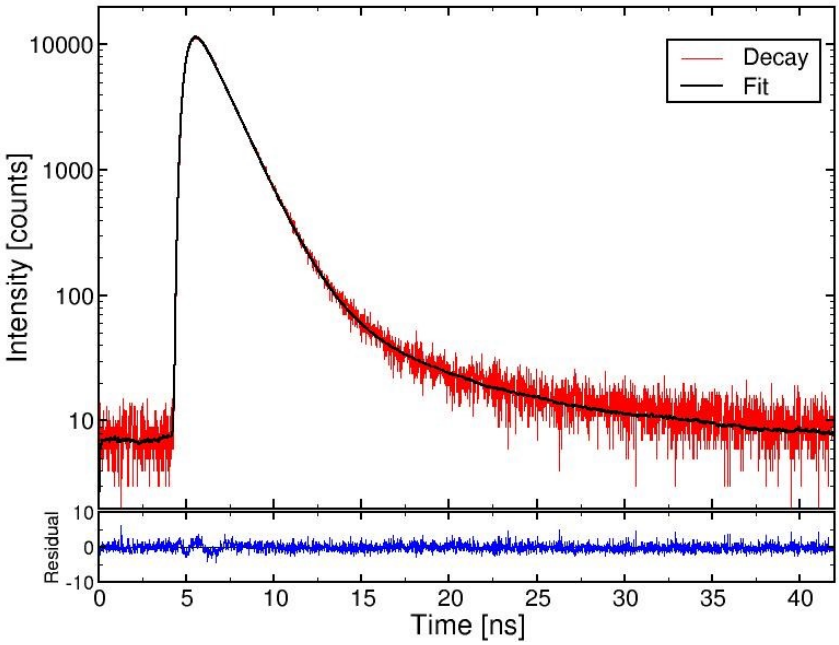

Raw decay data and 3 decay component fit for Cy3 in $[C_{12}C_1im][NTf_2]$. Bottom graph shows residual values at each point.

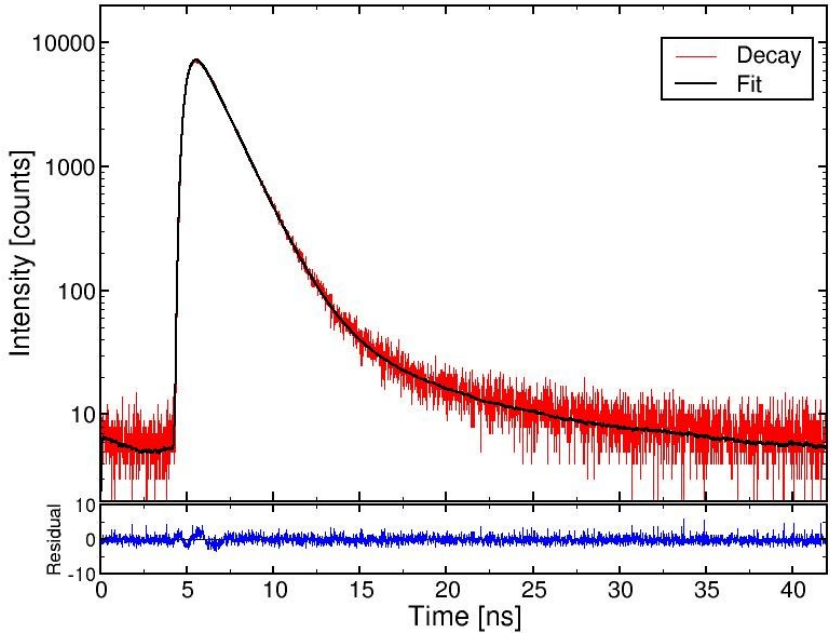

Raw decay data and 3 decay component fit for Cy3 in $[P_{4446}][NTf_2]$. Bottom graph shows residual values at each point.

7.6 Current flow across the cell during application of the potential

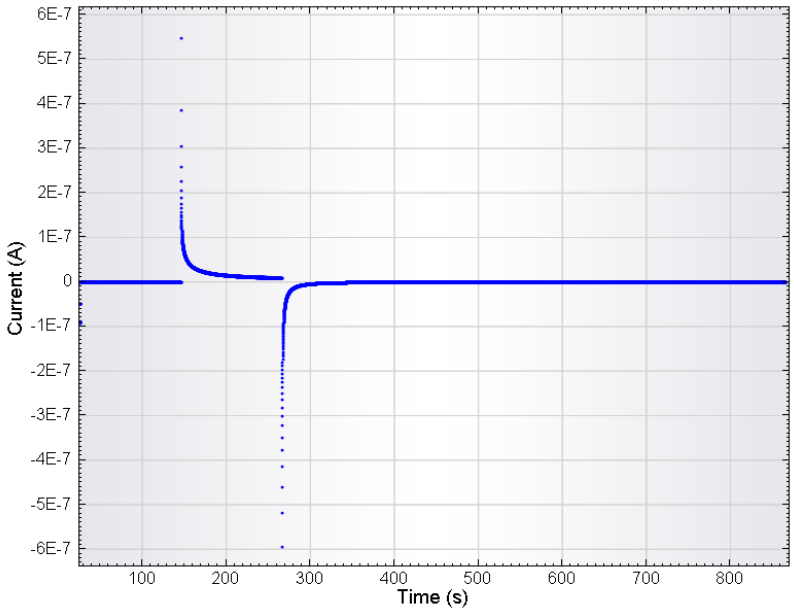

Current flow across the cell in the experiment probing Cy3 1 µm from the electrode

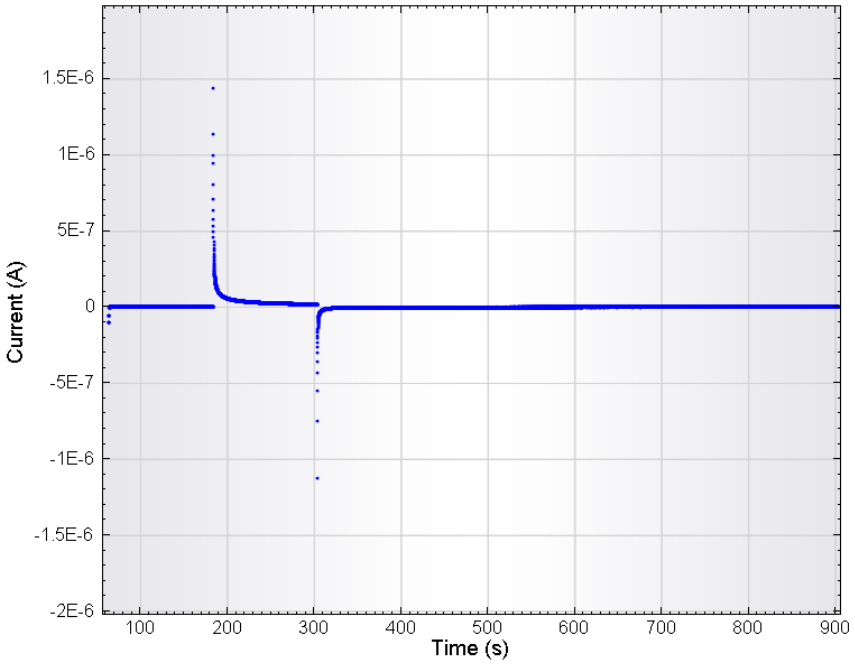

Current flow across the cell in the experiment probing Cy3 10 µm from the electrode.

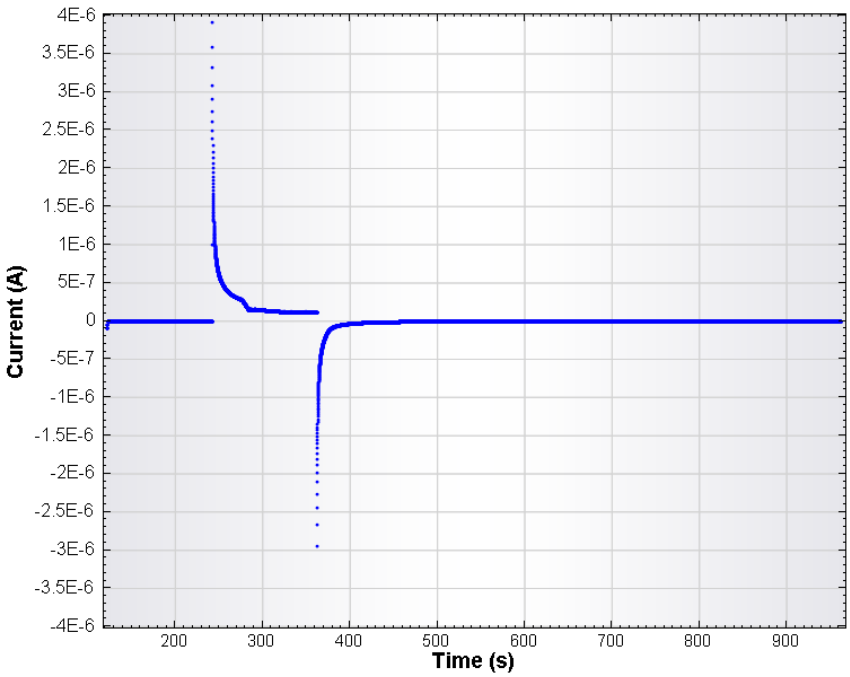

Current flow across the cell in the experiment probing Cy3 25 µm from the electrode.

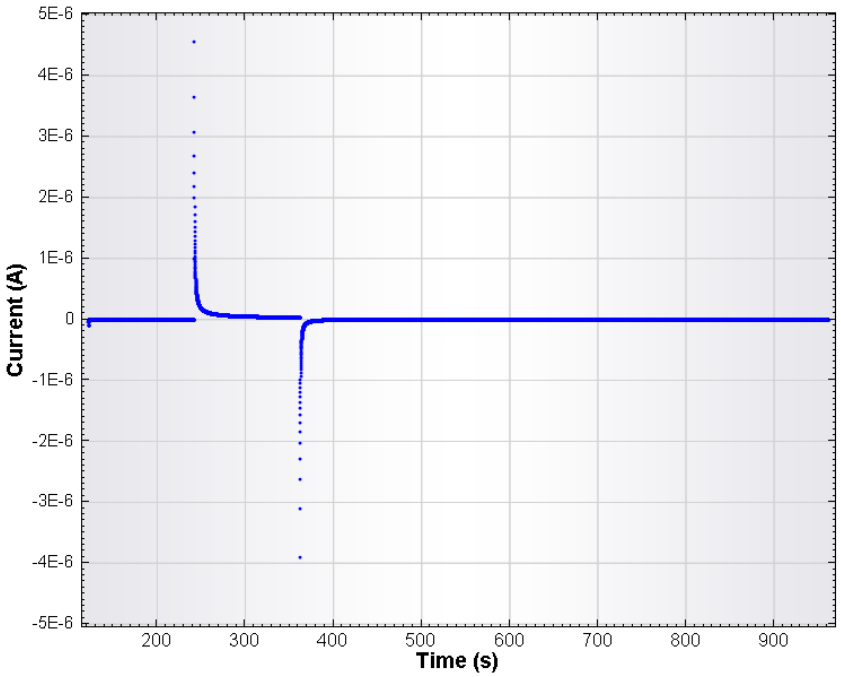

Current flow across the cell in the experiment probing Cy3 50 µm from the electrode.